Magnetic Flux Periodicities and Finite Momentum Pairing in Unconventional Superconductors

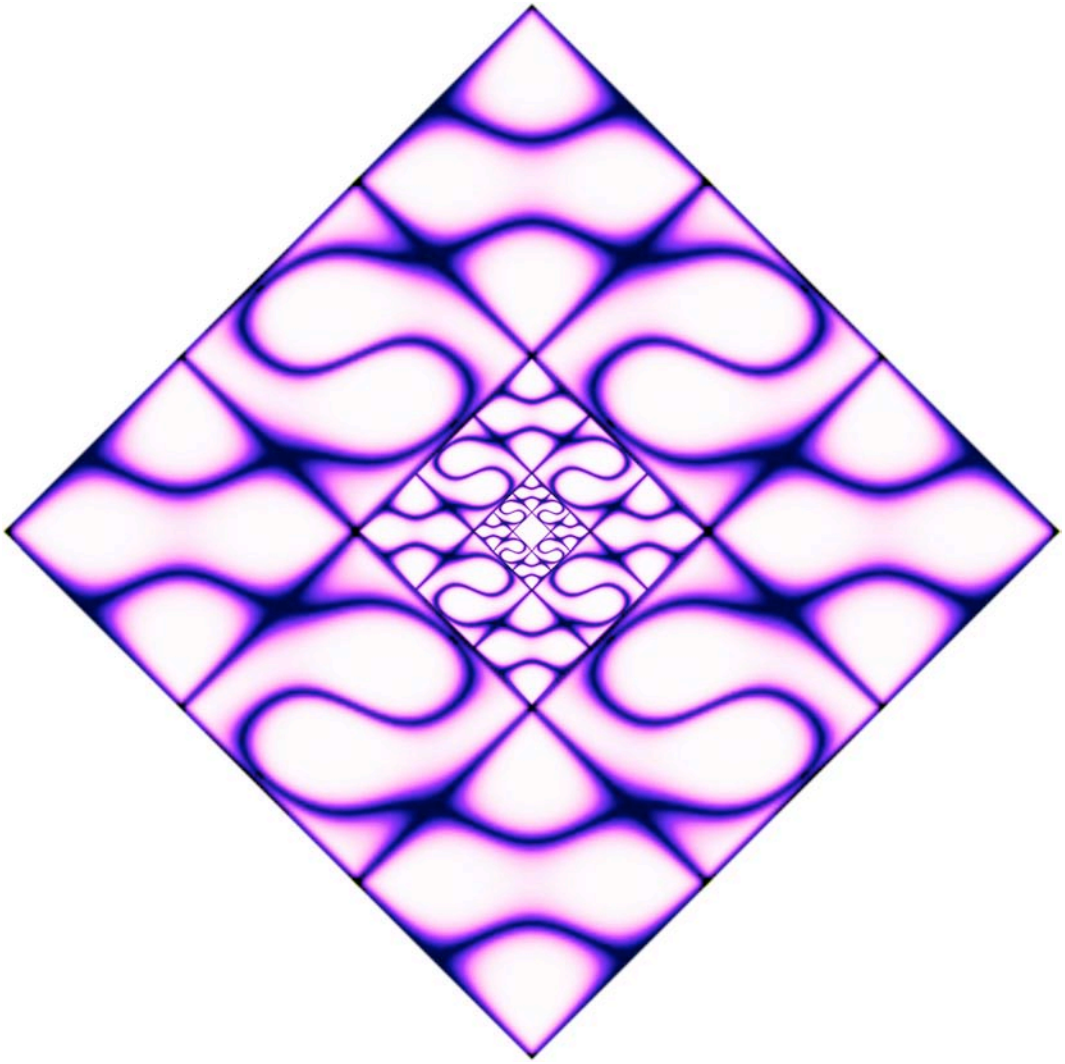

Dissertation zur Erlangung des Doktorgrades der mathematisch-naturwissenschaftlichen Fakultät der Universität Augsburg

vorgelegt von Florian Loder, November 2009

Tag der mündlichen Prüfung: 22.12.2009

Erstgutachter: Thilo Kopp, Universität Augsburg

Zweitgutachter: Dieter Vollhardt, Universität Augsburg

Drittgutachter: Raymond Frésard,

Laboratoire Crismat-ENSICAEN
6, Bld. du Maréchal Juin
F-14050 Caen
Frankreich

Titlepage illustration: Color-coded momentum-space map of the density of states at the Fermi energy in the pair density wave state.

Contents

Introduction

When I first heard about superconductivity, the theory of superconducting quantum interference devices (SQUIDs) had long been established and well understood. At this time, also the theoretical concepts of unconventional superconductivity had been analyzed for years and the consequences of different pairing symmetries had been well known. The fabrication of SQUIDs from high-temperature superconductors with unconventional pairing symmetries was certainly important for applications, but did not arouse huge interest from the theory side. Nevertheless, high-temperature SQUIDs proved to be more challenging than expected, when experiments with $YBa_2Cu_3O_{7-x}$ (YBCO) SQUIDs, conducted mostly by Christof Schneider in 2003 – 2006 in Augsburg, revealed magnetic flux oscillations with a number of periods different from the expected value $hc/2e$.

Flux oscillations in multiply connected geometries are generally highly interesting, because they are a purely quantum mechanical effect and reveal much of the nature of the quantum state of the system. Not only are they characteristic for the fermionic or bosonic nature of the charge carriers, but they contain valuable information about quantum mechanical many-body states of the system, which results from the complex interactions between the charge carriers and the crystal lattice, and between the carriers themselves.

In the case of superconductivity, the observation of flux oscillations with a period of $hc/2e$ was a major proof of the existence of an attractive pairing interaction between electrons in the superconducting state, and thus of the validity of the Bardeen-Cooper-Schrieffer (BCS) theory. The absence of oscillations with other periodicities in conventional superconductors further proved that interactions between the pairs must be negligible in conventional superconductors, which is reasonable for a weakly interacting system. Consequently, the observation of different flux periodicities, as observed in the YBCO SQUIDs, is a sign for correlations between Cooper pairs.

The search for a theoretical description of such correlations, and for the origin of the unconventional flux oscillations, was active when I came to Augsburg for my PhD thesis in 2005 and joined the fascinating research in this field. Because of the complexity in the description of a SQUID, the focus of my attention moved to the analysis of the flux periodicity of simple superconducting loops without Josephson junctions and it soon turned out that the standard theory of such systems is not adequate for loops with unconventional pairing symmetries. Working out the proper extension of the theory

became therefore the main topic of this thesis. It explains why the flux periodicity of loops of nodal superconductors is truly hc/e and not $hc/2e$, as it is in sufficiently large loops of conventional superconductors, and thereby provides an answer to a part of the periodicity problem of the SQUIDs.

A mathematical tool, which turned out to be especially suitable for the description of superconducting loops, is the Green's function formalism and, in particular, the Gor'kov equations describing the superconducting state. In the course of the investigation of flux periodicities, I realized that the Gor'kov equations in their general form can have solutions which are clearly distinct from those of the conventional BCS theory. These solutions are more of the Fulde-Ferrell-Larkin-Ovchnnikov type, but exist in zero magnetic field. Later, I realized that such solutions are currently widely analyzed in connection with charge ordered superconducting states, referred to as "pair density wave" states, which might be realized in some high-temperature superconductors. This connection was quite exciting, and in the following we established a solid microscopic model for the "pair density wave" state on the basis of the Gor'kov equations, which became the second large topic of my thesis and is an on-going project.

This thesis is organized in three parts. Part I and part II are concerned with the flux periodicity of superconducting loops. A general introduction with a historic overview of the development of this field follows in the next two sections of this chapter. Part III contains the model for the "pair density wave" state with a separate introduction at the beginning. Finally, at the end of part III, I give a summary of the complete thesis with an outlook to future projects on the topics of this thesis. In parts I – III, calculations are given as detailed as necessary to follow the discussion. For some most chapters, the methods used and the calculations performed are described more detail in the appendix. At the end of the appendix a collection of the most aesthetic wave functions of free particles in a square frame is assembled, which have been calculated during my thesis.

0.1 A Short History of Flux Periodicities in Conventional Superconductors

The quantum mechanical wave function of particles moving in a multiply connected geometry has to be unique at all positions. This boundary condition leads to a discrete energy spectrum, because the phase difference of the wave function accumulated on a closed path has to be $2\pi k$ for some integer k. For a circular geometry, this phase winding number k represents the angular momentum $\hbar k$ of the particle. In the presence of a magnetic field $\mathbf{B}(\mathbf{r})$, an additional phase $e/hc \int_{\mathbf{r}_0}^{\mathbf{r}} \mathrm{d}\mathbf{r}' \cdot \mathbf{A}(\mathbf{r}')$ adds to the phase of the wave function, where $\mathbf{A}(\mathbf{r})$ is the vector potential generating $\mathbf{B}(\mathbf{r})$, e the electron charge, c the velocity of light, and h is Planck's constant. This leads to a phase difference of $2\pi(k - e\Phi/hc)$ on a closed path C, where $\Phi = \int_C \mathrm{d}\mathbf{r} \cdot \mathbf{A}(\mathbf{r})$ is the magnetic flux inclosed by the path C. Because physical quantities in this system are obtained by summing over all possible k in a thermal average, they are periodic in Φ with a basic period of Φ_0, where

$$\Phi_0 = hc/e \tag{0.1}$$

is the flux quantum in the normal state. In particular, a persistent current $J(\Phi)$ induced by the magnetic flux is zero whenever Φ/Φ_0 is an integer.

The effect described above is present in any system with sufficiently strong phase coherence, and best known in the periodic modulations of the resistance of a microscopic metal loop, predicted first by Ehrenberg and Siday in 1948 [1] and in 1959 by Aharonov and Bohm [2]. Already ten years earlier, London predicted the manifestation of a similar effect in superconducting loops, where the phase coherence is naturally macroscopic [3]: the magnetic flux threading the loop is quantized in multiples of Φ_0, because the interior of a superconductor has to be current free. Although London did not know the existence of $\Phi_0/2$ flux quanta in superconductors, he already speculated that, because the supercurrent might be carried by pairs of electrons with charge $2e$, the superconducting flux quantum, and with it the flux periodicity of the supercurrent, is rather $\Phi_0/2$. This point of view became generally accepted with the publication of the 'Theory of Superconductivity' by Bardeen, Cooper and Schrieffer (BCS) in 1957 [4]. Direct measurements of magnetic flux quanta $\Phi_0/2$ trapped in superconducting rings followed in 1961 by Doll and Näbauer [5] and by Deaver and Fairbank [6], corroborated later by the detection of flux lines of $\Phi_0/2$ in the vortex phase of type II superconductors [7, 8].

For thin superconducting loops with walls thinner than the penetration depth λ, finite currents are flowing throughout the whole superconductor. The magnetic flux is consequently not quantized, but only the quantity $\Phi' = \Phi + \Lambda/c \oint \mathrm{d}\mathbf{r} \cdot \mathbf{J}(\mathbf{r})$ called fluxoid, introduced by London for this purpose by counting the flux induced. The flux Φ is the total flux threading the loop, which contains the current induced flux already.

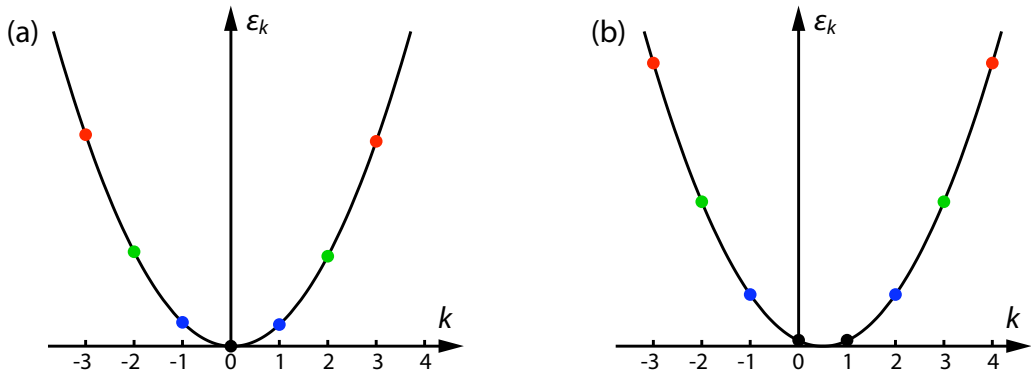

Figure 0.1: Scheme of the pairing of angular-momentum eigenstates in a one-dimensional metal loop for (a) $\Phi = 0$ and (b) $\Phi = hc/2e$, as used by Schrieffer in [9] to illustrate the origin of the $\Phi_0/2$ periodicity in superconductors. Paired are states with equal eigenenergies ε_k, which leads to pairs with a center-of-mass angular momentum $q = 0$ in (a) and $q = 1$ in (b).

Λ is a phenomenological constant parametrizing the strength of the current response of the superconductor to a magnetic field and related to the penetration depth λ as $\Lambda = 4\pi\lambda^2/c^2$ through the London equation [3]. Thin loops react periodically to the continuous variable Φ, and this flux periodicity is the main topic of this work.

It is tempting to explain the $\Phi_0/2$ flux periodicity of superconducting loops by the charge-$2e$ Cooper pairs carrying the supercurrent, but pairing of electrons alone is not sufficient. A theoretical description of the true origin of the half-integer flux quanta was found independently in 1961 by Byers and Yang [10], by Onsager [11], and by Brenig [12] on the basis of the BCS theory. They realized that there are two distinct types of electron pairing, which lead to two classes of superconducting wave functions that are not related by a gauge transformation. An intuitive picture illustrating these two types can be found in Schrieffer's book on superconductivity [9], using the energy spectrum of a one dimensional metal ring: The first class of superconducting wave functions, which London had in mind in his considerations about flux quantization, is related to pairing of electrons with angular momenta $\hbar k$ and $-\hbar k$, which have equal energies in a metal loop without magnetic flux, as schematically shown in figure 0.1 (a). The Cooper pairs in this state have a center-of-mass angular momentum (pair momentum) $q = 0$. The pairing wave functions of the superconducting state for all flux values Φ, which are integer multiples of Φ_0 and correspond to even pair momenta $\hbar q = 2\hbar\Phi/\Phi_0$, are related to the wave function for $\Phi = 0$ by a gauge transformation. The second class of superconducting wave functions occurs for a flux value $\Phi_0/2$ (or odd multiples of this value), where electron states with angular momentum $\hbar k$ and $-\hbar(k+1)$ are paired, which have in this case equal energy [figure 0.1 (b)], and lead to a pair momentum $q = 1$. The corresponding pairing wave function is again related by a gauge transformation to those for flux values

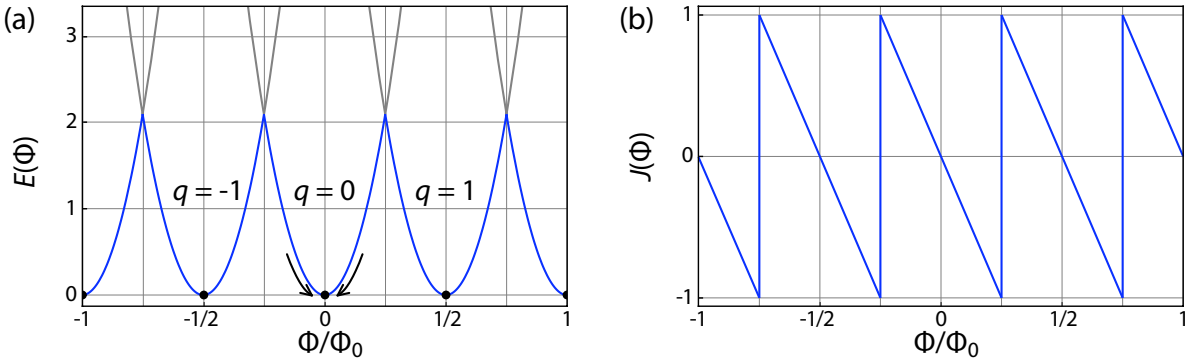

Figure 0.2: (a) Energy $E(\Phi)$ and (b) supercurrent $J(\Phi)$ as a function of flux Φ for a conventional superconducting loop at $T = 0$. The minima in $E(\Phi)$ correspond to superconducting states with different pair momenta q. The screening currents in the superconductor drive the system to the closest minimum for each flux value (black points), if the walls of the loop are thicker than λ.

Φ which are half-integer multiples of Φ_0 and correspond to the odd pair momenta $\hbar q = 2\hbar\Phi/\Phi_0$.

The two types of pairing described above are generally different. For the system to be $\Phi_0/2$ periodic, it is further required that the two pairing types are degenerate, which means that they have the same free energy. Byers and Yang [10], Onsager [11] as well as Brenig [12] showed that this is the case in the thermodynamic limit, which is obtained for a continuous density of states. In this case, the energy $E(\Phi)$ as a function of Φ consists of a series of parabolae with minima at integer multiples of Φ_0 (corresponding to even pair momenta q) and half integer multiples of Φ_0 (corresponding to odd pair momenta q) [figure 0.2 (a)]. If the loop is thicker than λ and the flux is quantized, then the system is in the minimum closest to the value of the external flux (black points). In microscopic systems the degeneracy of the even and odd q minima is lifted, but their position is fixed by the pairing interaction and gauge invariance. The flux periodicity in thin loops is then not necessarily $\Phi_0/2$, but the superconducting flux quantum is always $\Phi_0/2$. (There are mechanisms leading to fractional flux quanta, to which we refer later.) The circulating supercurrent $J(\Phi)$ at temperature $T = 0$ is proportional to $\partial E(\phi)/\partial\Phi$ and forms a $\Phi_0/2$ periodic saw-tooth pattern in the thermodynamic limit, which is shown in figure 0.2 (b).

From the flux periodicity of $E(\Phi)$, it is straightforward to derive the same flux periodicity for all other physical quantities [13]. For $T > 0$, $E(\Phi)$ has to be replaced by the free energy $F(\Phi)$. A clear and unambiguous observation of flux oscillations is possible in the flux dependence of the critical temperature T_c of small superconducting cylinders. Such experiments have been done first by Little and Parks in 1962 [14–16]. They actually measured the resistance R of the cylinder at a fixed temperature T within the finite width

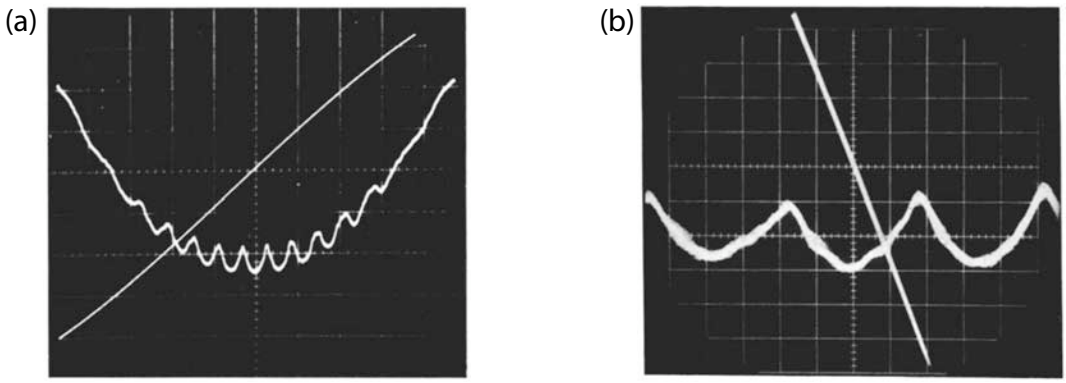

Figure 0.3: (a) Periodic variations of the resistance of a cylinder of indium. (b) Periodic variations for a sample of indium close to the temperature at which it becomes completely superconducting. W. A. Little, Rev. Mod. Phys. **36** 264 (1964).

of the superconducting transition and deduced the oscillation of T_c from the variation of R. Figure 0.3 (a) shows a typical result of R versus Φ for an indium cylinder at a temperature T where the slope of $R(T)$ is steepest. It produced perfect $\Phi_0/2$ periodic oscillations on a parabolic background (for an extended account see [15]).

The discussion of the results by Little and Parks is highly interesting for this work in several points. The simplest theoretical model to predict the amplitude of the oscillations of T_c is the following: For all non-integer or non-half-integer values of Φ, there are screening currents $J(\Phi)$ circulating in the cylinder, as shown in figure 0.2 (b). The kinetic energy $E_{\mathrm{kin}}(\Phi)$ associated with this current is proportional to $J^2(\Phi)$, as is the energy $E(\Phi)$ in figure 0.2 (a). It is therefore suggestive to subtract $E_{\mathrm{kin}}(\Phi)$ from the condensation energy of the superconducting state and deduce the oscillations of T_c from those of $E(\Phi)$. This was done in a first approach by Little and Parks [14] and by Tinkham [13] and Douglass [17] in a Ginzburg-Landau ansatz, although it was shown not to be correct. Parks and Little wrote in a follow-up article [15] that "the microscopic theory [i.e. the BCS theory] shows that it is *not the kinetic energy of the pairs* which raises the free energy of the superconducting phase [...], but rather it is due to *the difference in the energy* of the two members of the pairs". This energy difference arises in the form of a Doppler shift in our analyses and will prove to be the crucial effect which leads to Φ_0 periodicity in unconventional superconductors. It is remarkable that the results of Tinkham and Douglass are nevertheless identical to the microscopic one [18]. The notion whether it is kinetic energy of the screening current that causes the oscillations, or rather an internal cost in energy to form a superconducting state in the presence of a finite flux, is important insofar as it provides an explanation for another problem: In the same way as the pairing of electrons leads to a division of the fundamental flux period Φ_0 into the half-period $\Phi_0/2$, the pairing of pairs to quartets would lead the quarter-period

$\Phi_0/4$. Then the saw-tooth pattern of the supercurrent becomes $\Phi_0/4$ periodic and the maximum current is only half the value for unpaired Cooper pairs. If the oscillation in $E(\Phi)$ came from the current, then the formation of quartets and $\Phi_0/4$ periodicity would be energetically favorable. The fact that it is not so is illustrated by the remark of Little and Parks [15].

There is a second point of particular interest in the results of Little and Parks. After the question of the flux periodicity in superconductors seemed to be settled, they showed that the problem can nevertheless be more complicated. In reference [16] they present results for cylinders of tantalum, for which they cannot detect any flux oscillations in R at all. Even more peculiar are the oscillations observed in an indium cylinder close to the temperature, where R finally vanishes, shown in figure 0.3 (b). There are clearly visible signs of an additional $\Phi_0/8$ periodicity, which is even more surprising because indium is an absolutely conventional superconductor otherwise. These results remained unexplained and drew attention only much later, when flux oscillations of unconventional superconductors were studied.

Finally, there is an interesting remark by Little in [16] concerning the concept of "off-diagonal long-range order" (ODLRO), introduced by Yang as an elegant explanation of flux quantization in a Fermi system [19]. ODLRO occurs if a single off-diagonal element of the reduced density matrix of n-th order, ρ_n, is macroscopically occupied, which for fermions is possible only in the second order density matrix ρ_2, associated with pairs of fermions, or for higher orders. From the existence of ODLRO in ρ_n emerges directly the Meissner effect and flux quantization in units of Φ_0/n, independent of the presence of an energy gap (which is important in our analysis). The crucial part in understanding the long-range order in the superconducting state is therefore, according to Little, why the pairs have the same momentum. Indeed, in BCS theory, it is *assumed* that the pairs have the same momentum, and a more general formulation is necessary to describe the process of condensation in more than one pair momentum. Such a generalized theory was introduced by Gor'kov already in 1958 using the Green's function technique [20], although it is rarely used in its full version. In part III of this work I present solutions of the Gor'kov equations and show that they are closely connected to the emergence of fractional flux oscillations.

The theoretical description of the Little-Parks effect was extended by Bogadchek *et al.* [21] in 1975 to account for the different energies of the even and odd q states in microscopic loops of conventional suerconductors. As a function of Φ, T_c shows then a sequence of longer and shorter oscillations, with an overall periodicity of Φ_0. The difference of long and short oscillations however disappears exponentially for cylinder diameters larger than the superconducting coherence length ξ_0. Subsequently, this was not discussed further and the field of flux oscillations dropped out of focus for a long time.

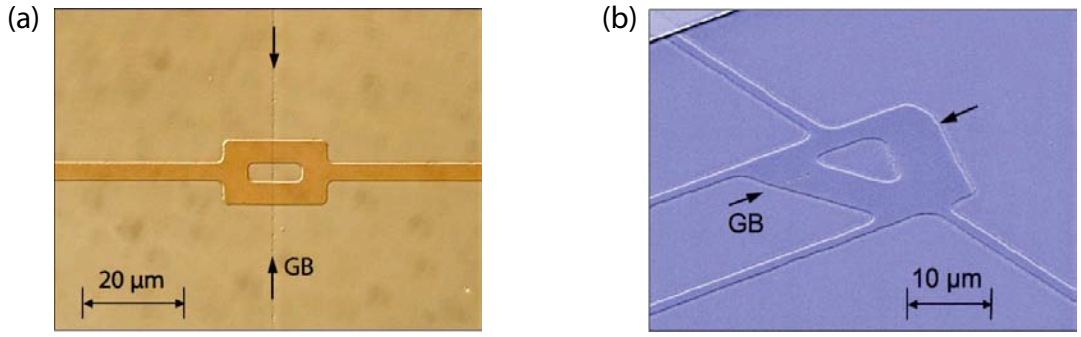

Figure 0.4: Dc SQUIDs fabricated by Ch. Schneider from YBaCuO films with grain-boundary (GB) Josephson junctions. The grain-boundary angle is 90°in (a) and 45°in (b).

0.2 Unconventional Flux Periodicities in Unconventional Superconductors

In the meantime a new type of flux sensitive systems became popular: SQUIDs. The mechanism leading to flux oscillations in SQUIDs is quite similar to that of the Little-Parks experiment, but a finite resistance R is here induced into a superconducting loop not by choosing T close enough to T_c, but by inserting Josephson junctions into the loop. This has the advantage that flux oscillations can be observed at any temperature $T < T_c$, and they are measured most clearly in the flux dependence of the critical current J_c through the SQUID. The oscillations originating from the flux though the SQUID loop are typically overlaid with a Fraunhofer type of oscillations [c.f. figure 0.5 (a)] caused by the magnetic field penetrating the non-superconducting junction area. The effects of the junctions are rather complex and difficult to describe theoretically, but the fast oscillations are a characteristic of the superconducting state in the ring, independent of the nature of the junctions.

SQUIDs fabricated from conventional superconductors have been used in experiments and applications for decades and proved to oscillate perfectly with the expected flux period $\Phi_0/2$. It was therefore a surprise that flux oscillations with different periodicities were found by Lindström *et al.* [22] and Schneider *et al.* [23, 24] in 2003 in SDQUIDs made of films of the unconventional high-T_c superconductor YBCO with Josephson junctions consisting of grain boundaries (figure 0.4). Flux trapping experiments in loops showed that flux quantization in the cuprate class of high-T_c superconductors occurs in units of $\Phi_0/2$ [25], identically to conventional superconductors. Nevertheless Schneider observed a variety of oscillation periods, depending on the geometry of the SQUID loop, the grain-boundary angle, the temperature, and the range of the magnetic field threading the SQUID.

Two distinct types of unconventional oscillations in YBCO SQUIDs have to be dis-

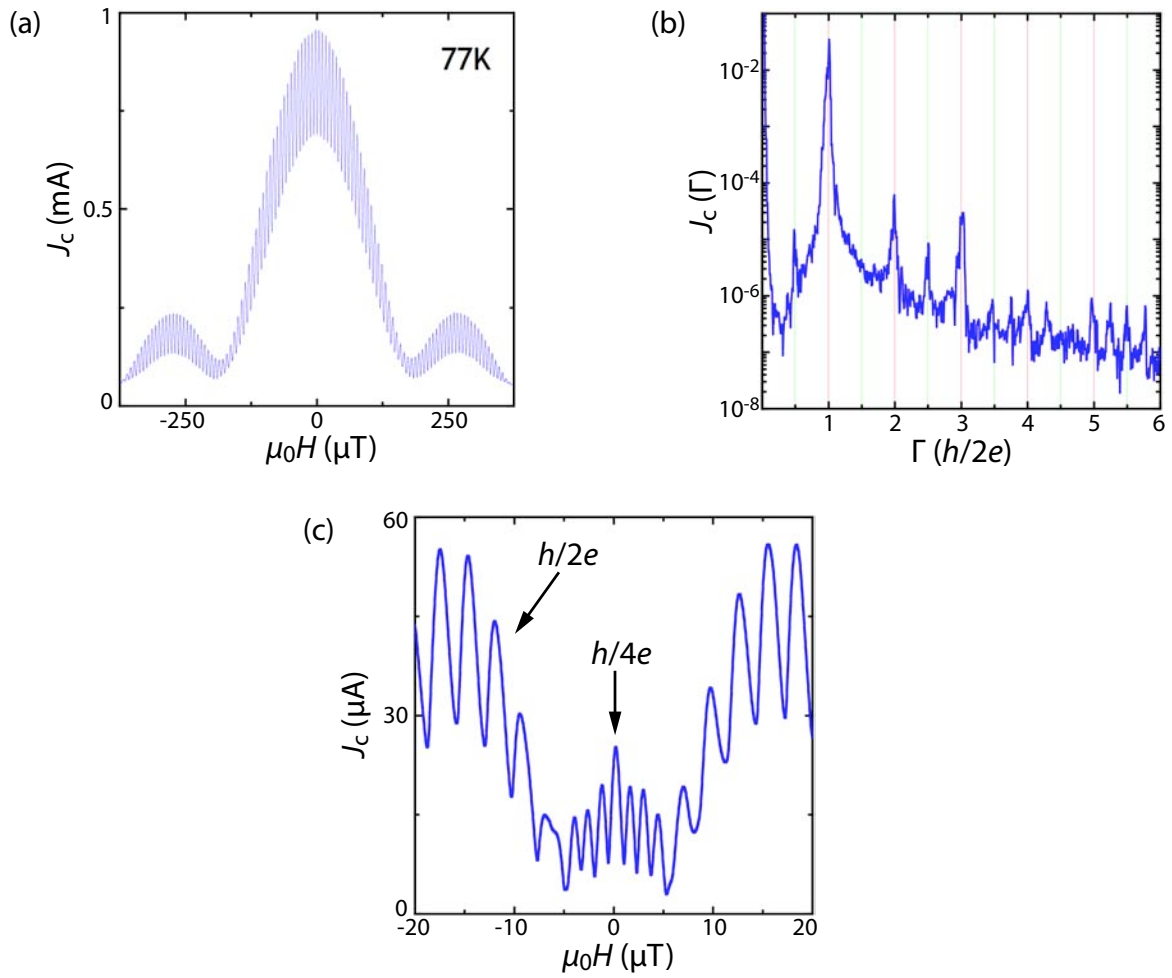

Figure 0.5: (a) Measurement of the critical current $J_c(H)$ done by Ch. Schneider on (a), (b) a 24°grain boundary SQUID at $T = 77$ K as a function of the applied magnetic field where $\Phi_0/2 = 6.7$ μT. (b) Fourier transform Γ of (a). (c) Critical current $J_c(H)$ over a 24°grain boundary SQUID at $T = 4.2$ K, where $\Phi_0/2 = 2.7$ μT. Clearly visible is the abrupt change of periodicity at $\mu_0 H \approx \pm 5$ μT.

cerned. The first type consists of oscillations which have a basic period of $\Phi_0/2$, but are slightly deformed, such that in the Fourier transform peaks appear which do not correspond to the period $\Phi_0/2$ [24]. Such a measurement is shown in figure 0.5 (a) and (b). The peaks in (b) at integer values of Γ (see figure 0.5) are explained as higher harmonics of $\Phi_0/2$ and they are not unusual. But there are clear peaks at $\Gamma = 1/2$ and $\Gamma = 5/2$, which correspond to Φ_0 periodicity and higher harmonics belonging to Φ_0. We will not give a solid explanation for these Fouier peaks, but the idea that the Φ_0 periodicity is an effect of the difference of the even and odd q states in microscopic systems will turn out reasonable in the course of this work, even with a good quantitative

agreement with the experimental result in figure 0.5 (a) and (b).

The second type of unconventional oscillations is more intriguing. In a number of different YBCO SQUIDs made by Schneider, the periodicity of sinusoidal oscillations changes abruptly for increasing magnetic flux. For certain flux ranges, the period is $\Phi_0/4$, as shown in figure 0.5 (c). This was explained by an unusually pronounced second harmonic in the critical current J_c of transparent Josephson junctions, or more fundamentally by interactions between Cooper pairs, leading to the formation of electron quartets, which might be stable in certain flux regimes [23]. The observation of similar abrupt changes to other fractional periodicities like $\Phi_0/6$ and $\Phi_0/8$ make this possibility even more fascinating because it would be a sign of absolutely new, non-BCS types of superconducting states. An experimental way to decide whether all these unconventional oscillations are real characteristics of the superconducting state, or just artifacts of the Josephson junctions, would be Little-Parks experiments with YBCO loops. So far however, such experiments have not been successful, because of technical difficulties in fabricating such loops and the very small amplitude of the flux oscillations in YBCO.

The SQUID experiments described above have caused a revival of theoretical interest in flux oscillations and quantization, this time in connection with unconventional paring symmetries, and was the initial motivation of this work as a direct attempt to find the mechanisms behind the unconventional oscillations. No thorough investigation of the mechanisms determining the flux periodicity in superconductors with gap nodes has existed so far. In particular, no general criterium was known to decide if and when the even and odd q states are equal or not. We give such an analysis for conventional s-wave pairing and for d-wave pairing as an example for unconventional pairing in parts I and II of this work.

We began with the description of a superconducting loop using the Bogoliubov - de Gennes equations on a square frame in real space, which quickly showed that even and odd q states are unequal for d-wave pairing. The difference comes from the Doppler shift of the nodal states, which react paramagnetic to an applied flux and do not appear in the old models. It follows that the supercurrent $J(\Phi)$ is generally Φ_0 periodic. This result, published in reference [26], is described in detail in part II. There we use numerical real-space calculations to further analyze the flux dependence of more complex systems like Josephson junctions and the self-consistent distribution of the screening currents, which generate flux quantization in loops thicker than λ.

Since in a normal metal loop, persistent currents induced by a magnetic flux are typically Φ_0 periodic [2,27], whereas in the superconducting state, they are $\Phi_0/2$ periodic, the question arises how one switches from one regime into the other. Is it a sharp transition at T_c, or a continuous crossover, which is just much broader in a d-wave superconductor? It turns out that it is indeed a crossover, which is rather sharp in conventional superconductors when the coherence length ξ_0 becomes larger than the diameter of the loop [17, 28–32], but extends over the whole parameter range of pairing

interaction strength and loop size for unconventional pairing symmetries. In particular, for d-wave pairing, the Φ_0 periodic part of the supercurrent decreases like $1/R$, where R is the radius of the loop. An intuitive explanation of these effects is much easier in momentum space, which was published in [32] for conventional s-wave pairing symmetry and in [33] for d-wave symmetry. In the latter reference, an analytical approximation is introduced to show that a Fourier component of $J(\Phi)$ corresponding to Φ_0 periodicity persists for all sizes of d-wave loops. In the following, similar results using a quasi one-dimensional model were published by Barash [34], Jurčić *et al.* [35], and Zhu [36].

In this work we describe superconducting loops in a number of different geometries, all of which are especially suitable for demonstrating different aspects of the problem of flux periodicities. Here follows a summary of these models and references for what each of them is used for:

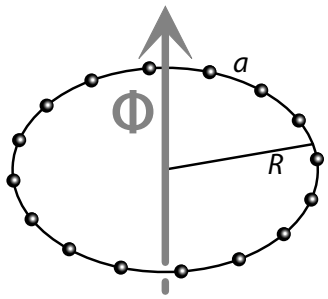

1. A discrete one-dimensional ring is used to illustrate the special properties of the flux induced persistent current in the normal state of a rotational symmetric system and to introduce the physical concepts of the periodicity crossover while entering the superconducting state for increasing order parameter.
[Part I, chapter 1 and 2]

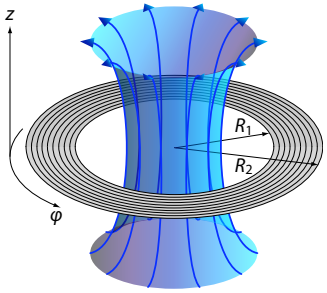

2. For the discussion of the periodicity crossover of a conventional s-wave superconductor within a fully self-consistent multi-channel calculation, we use a two dimensional annulus discretized in radial direction for numerical purpose.
[Part I, chapter 2]

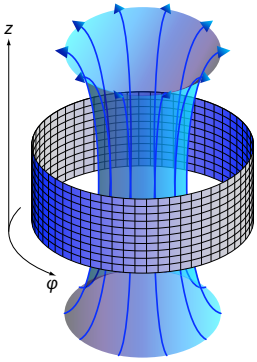

3. For the description of an unconventional d-wave superconductor, a discrete square lattice is needed. Bending this lattice into a thin walled cylinder is a convenient way to obtain a multiply connected geometry for the discussion of the flux periodicity of nodal superconductors. For this geometry, we develop an analytical model for the supercurrent in large cylinders.
[Part I, chapter 3]

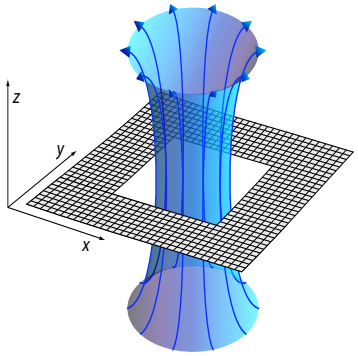

4. To use the powerful method of the Bogoliubov - de Gennes equations in real space, we choose a square frame geometry with a square hole at the center and open boundary conditions. In this geometry, the normal state spectrum is remarkably stable against addition of impurities or small changes of the number of lattice sites, which makes it convenient to study their effects.

[Part II, chapter 5 and 7]

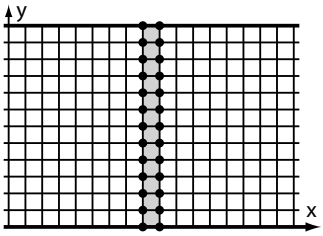

5. We use a square lattice with periodic boundary conditions to model Josephson junctions consisting of rows of impurities, and study the effect of nodal states on the current-phase relation of the junction and on the critical current of flux threaded junctions.

[Part II, chapter 7]

Developing models for the fractional flux periodicities observed in YBaCuO SQUIDs is problematic. The idea of quartet formation is simple, but its mathematical realization is not. Firstly there is no source of a quartet interaction between electrons known, and interactions between Cooper pairs are mathematically extremely complicated [37, 38]. Some starting points have been developed in particle physics for the description of atomic nuclei [39] and as a variational approach analogous to BCS theory, but with a four particle interaction [40–43]. This variational model is solvable under certain circumstances, but since it is a real four-paricle problem, the complexity is overwhelming and solid results are rare. We abandoned the search for fractional flux periods therefore in favor of the Φ_0 periodicity. But unexpectedly, the model used for this purpose, in particular its extended version introduced by Gor'kov, led in the end to a new concept to generate fractional flux periods, and even flux quanta, in a really unconventional superconducting state. This state is called "pair density wave" (PDW) state and has been under investigation for a while in the connection of superconducting stripe phases in some high-T_c cuprates. It emerges naturally from a generalization of the pairing Hamiltonian we used in part I, which allows for the first time to investigate the PDW state in a microscopic theory. In part III we solve and discuss this theory and come finally back to the problem of flux periodicities with a description of how the PDW state leads to a number of fractional flux periods in superconducting loops.

Part I

hc/e Periodicity in Loops of Nodal Superconductors

Introduction to Part I:

In this part, we formulate and solve the BCS theory for conventional and unconventional superconducting loops threaded by a magnetic flux. This is what Byers and Yang [10], Onsager [11] and Brenig [12] have done for conventional superconductors, but here we formulate the theory to capture the differences between the even and odd q states. To derive an analytical expression for the supercurrent in any geometry, one usually takes the limit of large systems and replaces the sum over the eigenstates by a continuous integration over the energy. This was done by BCS in calculating the Meissner effect of the superconducting state, and analogously one obtains the supercurrent induced by the flux through a ring. However, if energy levels exist in close vicinity of the Fermi energy E_F, the discrete nature of the energy spectrum is essential for the description of the current. And that is where the real difference in the behavior of conventional and unconventional nodal superconducting states comes from.

The physical concept of flux induced persistent currents is essentially the same in a normal metal and in a superconducting loop, and it is most clearly presented in a one dimensional ring. In chapter 1 we introduce this concept therefore for the example of a one dimensional ring, analyzing first the normal state, which shows some peculiar characteristics of the persistent current. (For a review on persistent currents see reference [44]). On this basis, we investigate the crossover into a conventional superconducting state controlled by the superconducting order parameter. An elegant formulation of this crossover is possible using Gor'kov equations for the Green's function of the superconducting state.

It is well known that a real long-range ordered superconducting state does not exist in one dimension. However, whereas thermal phase slips might suppress a transition into the superconducting state at finite temperature, quantum phase slips at zero temperature are rare events. Even if phase coherence is broken at certain instants in time and space, the supercurrent does not decay in the ring [45]. We therefore investigate only the zero temperature transition for the one dimensional ring. In chapter 2 we extend the model to self consistent calculations of a conventional s-wave superconducting state in a multichannel system, presented here in the form of a two dimensional annulus. This system also allows also to study the periodicity crossover controlled by temperature while cooling through T_c. The presence of additional channels and the self-consistency condition for the order parameter complicate the numerical calculations, but the mechanisms controlling the flux periodicity of the supercurrent is the same as in one dimension.

Because d-wave pairing is not possible in one dimension, we start the discussion of nodal superconducting loops in chapter 3 in a two dimensional cylinder model, which is a "simple" extension of a one dimensional ring. To analyze the qualitative behavior of large cylinders we introduce an analytical approximation for the supercurrent at $T = 0$ similar to the derivation of the Meissner effect in BCS theory, but refine it to capture the differences of even and odd q states responsible for the Φ_0 periodicity of the supercurrent.

In comparison to a numeric evaluation of the cylinder model we show the excellent agreement with the analytical model for a large cylinder radius.

1 hc/e or $hc/2e$ - The Phenomenon

1.1 Normal State of a One Dimensional Ring

1.1.1 Free Electron in a One Dimensional Ring

The basis for a theoretical understanding of the behavior of a superconducting loop is the knowledge of its normal state. For a many-body system, this can be extremely complex, as the numerous works on the Aharonov-Bohm effect [1, 2, 27, 46] and on normal persistent currents [47–52] prove. A single free electron in a one dimensional ring, represented in the Schrödinger picture, is a simple, but nevertheless instructive, basic example for the normal state in a multiply connected geometry.

Let us consider a single free electron confined on a ring of radius R threaded by a magnetic flux $\Phi = \oint \mathrm{d}\mathbf{l} \cdot \mathbf{A}(R, \varphi)$, where $\mathbf{A}(R, \varphi)$ is the vector potential generating a magnetic field concentrated through, but not touching the ring. The time independent Schrödinger equation describing the wave function $\psi(\varphi)$ of the electron as a function of the angle φ has the form

$$-\frac{\hbar^2}{2m}\left(\frac{\partial}{R\partial\varphi} - \frac{e}{hc}\mathbf{A}(R,\varphi)\right)^2 \psi(\varphi) = E\psi(\varphi). \tag{1.1}$$

We solve equation (1.1) by applying the gauge transformation $\psi(\varphi) \to \tilde{\psi}(\varphi)e^{i\delta(\varphi)}$ on the wave function, where $\delta(\varphi) = e/hc \int_0^\varphi \mathrm{d}\mathbf{l} \cdot \mathbf{A}(R, \varphi)$ is the integral over a segment of the ring with angle φ. The Schrödinger equation for $\tilde{\psi}(\varphi)$ becomes field free and is easily solvable. For a rotational symmetric field distribution, the transformation simplifies to $\delta(\varphi) = e\Phi\varphi/hc = \phi\varphi$, where $\phi = e\Phi/hc$ is the dimensionless magnetic flux. Thus the solutions of equation (1.1) are

$$\tilde{\psi}_k(\varphi) = \frac{1}{\sqrt{2\pi R}} e^{i\varphi(k-\phi)/R} \tag{1.2}$$

with the eigenenergies

$$E_k = \frac{\hbar^2}{2mR^2}(k-\phi)^2. \tag{1.3}$$

The quantum number $k \in \mathbb{Z}$ represents the angular momentum $\hbar k/R$ of the state $\tilde{\psi}_k(\varphi)$.

The crucial observation on the solutions (1.2), (1.3) of the Schrödinger equation is that they depend on the magnetic flux Φ only in the combination $k - \phi$, from which follows directly that the groundstate energy $E_0(\phi)$, given by the minimum of E_k over all k, is a periodic function of Φ with a period of the normal flux quantum $\Phi_0 = hc/e$. The energy of the electron is minimal if Φ is a multiple of Φ_0 (or ϕ an integer) and grows quadratically for increasing Φ until k switches to the next integer at half-integer values of ϕ.

For non-integer values of ϕ, the wave function (1.2) has a finite phase gradient, indicating a current circulating in the ring, which is called a persistent current. It is obtained from the continuity equation [53] as:

$$\begin{aligned} J(\phi) &= \frac{ie\hbar}{2m}\left[\left(\frac{\partial}{R\partial\varphi}\psi_k^*(\varphi)\right)\psi_k(\varphi) - \psi_k^*(\varphi)\left(\frac{\partial}{R\partial\varphi}\psi_k(\varphi)\right)\right] - \psi_k^*(\varphi)\frac{e^2}{mc}\mathbf{A}(R,\varphi)\psi_k(\varphi) \\ &= \frac{ie\hbar}{2m}\left[\left(\frac{\partial}{R\partial\varphi}\tilde{\psi}_k^*(\varphi)\right)\tilde{\psi}_k(\varphi) - \tilde{\psi}_k^*(\varphi)\left(\frac{\partial}{R\partial\varphi}\tilde{\psi}_k(\varphi)\right)\right] \qquad (1.4) \\ &= \frac{e\hbar}{2\pi mR}\frac{k-\phi}{R} = -\frac{e}{h}\frac{\partial E_0(\phi)}{\partial\phi}, \qquad (1.5) \end{aligned}$$

where k is the quantum number of the ground state for each value of ϕ. The persistent current $J(\phi)$ is therefore given by the derivative of the groundstate energy with respect to the magnetic flux, which forms a Φ_0 periodic, piecewise linear function of ϕ: the so-called "saw-tooth pattern", depicted in figure 1.3 (b) and 1.6 (c).

1.1.2 Tight Binding Model

The extension of the single-electron model presented above to a fermionic many-body system is straightforward in the second quantization formalism. For the finite systems we consider here, the tight binding model on a discrete lattice is most convenient for calculations. In this formulation the Hamiltonian is written using the discrete field operators c_{is} and $c_{is}^\dagger$ for the annihilation and creation of an electron with spin s on the lattice site i:

$$\mathcal{H}_0 = t\sum_{\langle ij\rangle,s} e^{\varphi_{ij}} c_{is}^\dagger c_{js} - \mu\sum_{i,s} c_{is}^\dagger c_{is}, \qquad (1.6)$$

where $\langle ij\rangle$ stands for nearest-neighbor sites i and j, $s = \uparrow, \downarrow$ and t is the nearest neighbor hopping amplitude. In analogy to the gauge transformation applied on equations (1.1), the magnetic field enters the Hamiltonian (1.6) through the Peierls phase factor $\varphi_{ij} = e/hc\int_i^j d\mathbf{l}\cdot\mathbf{A}$. We further introduce the chemical potential μ, which controls the number of particles in the system. In the following, we describe the particle-hole symmetric situation with $\mu = 0$, for which the Fermi energy is $E_\mathrm{F} = 0$.

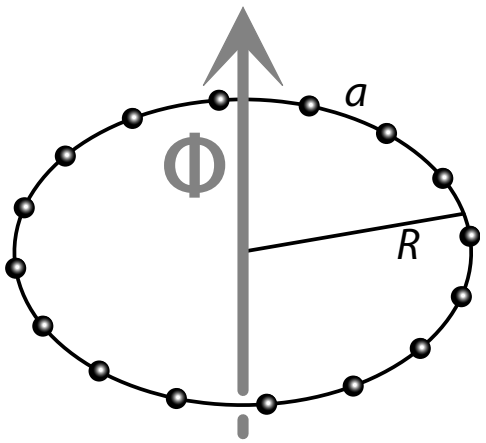

Figure 1.1: To find the most simple description of the many-particle state in a flux threaded loop, we use a tight-binding model on a discrete, one dimensional ring with N lattice sites, lattice constant a and radius $aR = Na/2\pi$. The magnetic flux Φ is concentrated in the interior of the ring and does not touch the ring itself.

In the following, we use a one dimensional ring of radius aR, on which N lattice sites are equally distributed (figure 1.5) at a distance of the lattice constant a. It follows that $R = N/2\pi$ is the dimensionless radius and the Peierls phase factor simplifies to $\varphi_{ij} = 2\pi\phi/N$, which allows to write the Hamiltonian (1.6) in momentum space

$$\mathcal{H}_0 = \sum_{k,s} \varepsilon_k(\phi) c^\dagger_{ks} c_{ks} \tag{1.7}$$

where $c^\dagger_{ks}$ creates an electron described by the wave function $\tilde{\psi}_k(\varphi)$ with angular momentum $\hbar k/aR$, and the energy dispersion is

$$\varepsilon_k(\phi) = -2t \cos\left(\frac{k-\phi}{R}\right) - \mu. \tag{1.8}$$

Physical quantities can now be expressed by the thermal average $n_s(k)$ of the number of electrons with angular momentum k and spin s: $n_s(k) = \langle c^\dagger_{ks} c_{ks} \rangle = f(\varepsilon_k(\phi))$, with the Fermi distribution function $f(\varepsilon) = 1/(1 + e^{\varepsilon/T})$ for the temperature T. Most characteristically, the total energy E of the system is

$$E(\phi) = \langle \mathcal{H}_0 \rangle = \sum_{k,s} \varepsilon_k(\phi) n_s(k), \tag{1.9}$$

which is a piecewise quadratic function of the magnetic flux. The momentum distribution function $n_s(k)$ depends on the magnetic flux, again only in the combination $k - \phi$. From the sum over k in equation (1.9) follows directly the Φ_0 flux periodicity of $E(\phi)$. The

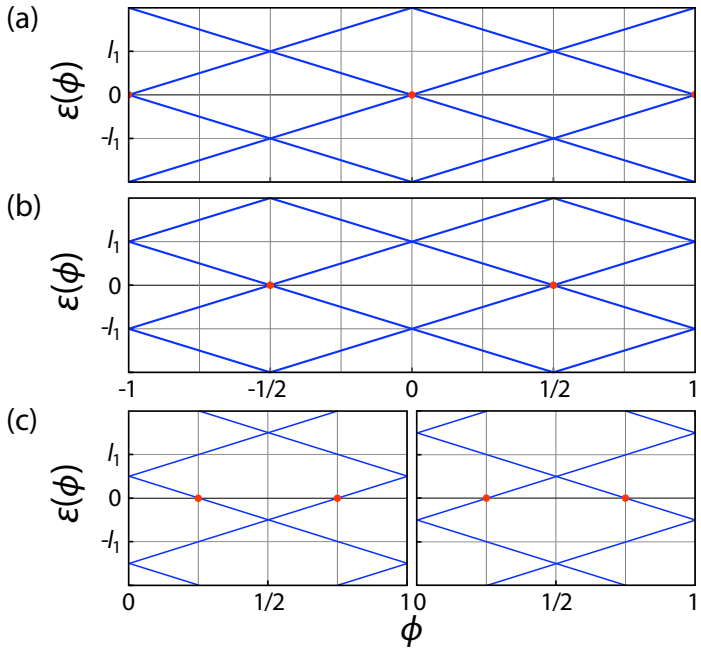

Figure 1.2: Energy spectrum of a discrete one dimensional ring with N lattice sites, $\mu = 0$ and (a) $N/4$ is an integer, (b) $N/4$ a half integer and (c) N an odd number. In (a) and (b), levels cross $E_F = 0$ at integer (a) or half-integer (b) values of ϕ, whereas for odd N, two different spectra are possible [$N = 4n + 1$ (left) and $N = 4n - 1$ (right)], and for both two levels cross E_F in one flux period (red points). I_1 denotes the maximum value of the Doppler shift (see section 3.1).

situation is however much more complicated than for the groundstate energy $E_0(\phi)$ of one single electron; the position of the minima of $E(\phi)$ depends on the total number of electrons, $\sum_{k,s} n_s(k) = N$ for $\mu = 0$, in the ring! This is a consequence of the different structures of the energy spectra for different N, which are shown in figure 1.2. Close to E_F, $\varepsilon_k(\phi)$ shifts linearly with ϕ, which is called Doppler shift, because it is controlled by the angular velocity of the state k. The energy $E(\phi)$ is maximal for those values of ϕ where an energy level reaches E_F (red points) and has minima in between. If N is a multiple of four, then the minima of $E(\phi)$ are at half-integer values of ϕ (light blue curve in figure 1.3), whereas if N is even, but not a multiple of four, the minima are at integer values of ϕ, analogous to the case of one *spinless* electron in section 1.1.1 (dark blue curve in figure 1.3). More special is an odd number of electrons. In this case two different (but physically equivalent) spectra for $N = 4n \pm 1$ are possible, and for both, two levels cross E_F in one flux period. This results in a superposition of the two previous cases and there are minima of $E(\phi)$ for both integer and half-integer values of ϕ and $E(\phi)$ is therefore $\Phi_0/2$ periodic. The persistent current $J(\phi)$ jumps whenever an energy level crosses E_F, because the population of left and right circulating states changes abruptly. In the limit of a continuous density of states, left and right circulating states are always equally

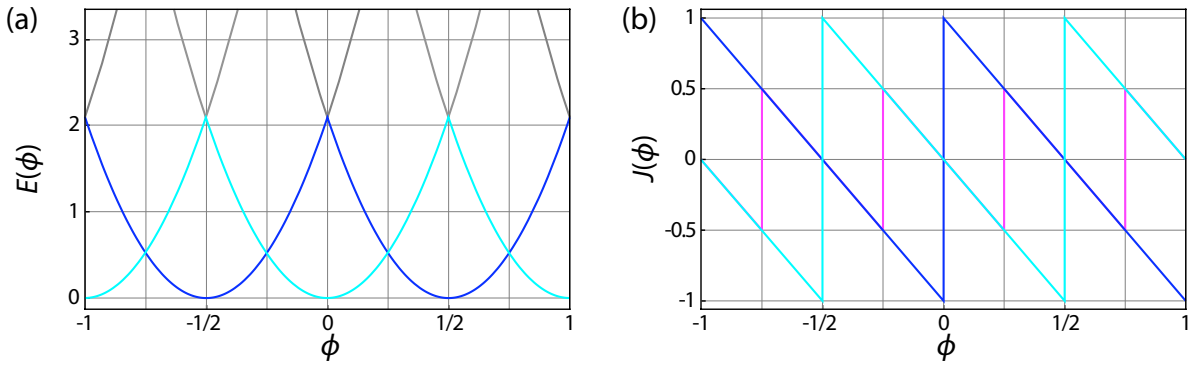

Figure 1.3: (a) Total energy $E(\phi)$ as a function of the magnetic flux ϕ. If the number of electrons on the ring N is a multiple of four, then $E(\phi)$ has minima at integer values of ϕ (turquoise). If N is even but not a multiple of four, then the minima are at half-integer values of ϕ (blue). If N is odd, the system energy switches between the blue and turquoise curves. The gray lines above the crossing points of the parabolae correspond to possible excited states. (b) Persistent current $J(\phi)$ corresponding to the systems described in (a). The purple curve shows the current obtained for odd N.

populated and, consequently, $J(\phi)$ vanishes. The occupied state closest to E_F contributes dominantly to the current, because all other contributions tend to almost cancel in pairs. The Doppler shift decreases with the ring radius like $1/R$ [c.f. equation (1.8)] and the persistent current has the same dependence on the radius. Figure 1.3 (b) shows $J(\phi)$ for the different electron numbers discussed above.

This number dependence is typical for many-body systems with discrete energy levels [48, 49] and not restricted to one dimension. It has no deep physical origin, but cannot be avoided and complicates the characterization of normal metal loops. Because the superconducting state bases on the normal-state spectrum, the number dependence will accompany all the following discussion of flux periodicities.

1.2 Superconducting State

Here we extend the theory of the one dimensional ring to the superconducting state. This system is ideal for studying the crossover from Φ_0 in the normal state to $\Phi_0/2$ periodicity in a conventional superconductor, because it contains all the essential physical concepts, yet remaining simple enough to introduce them clearly. On a first approach, even a non-self-consistent model with fixed superconducting order parameter turns out to contain the periodicity crossover fully. In this section we solve the non-self consistent model using the Gor'kov equations for the superconducting state.

1.2.1 Gor'kov Equations for Finite Momentum Pairing

In conventional BCS theory, Cooper pairs are formed by pairing an electron with its time reversed partner. Applied to a one dimensional ring, this signifies that pairing occurs between the states $|k,\uparrow\rangle$ and $|-k,\downarrow\rangle$ with wave functions as in (1.2), and spin $\uparrow,\downarrow$. In the presence of a magnetic field, or a flux threading the superconductor, the superconducting state is typically not time inversion symmetric. Then the formation of electron pairs with a finite center-of-mass momentum (or angular momentum) can be energetically favorable and it is even necessary for the Φ_0 flux periodicity demanded by gauge invariance.

To account for a finite center-of-mass angular momentum (pair momentum) of a Cooper pair in the ring, we use the BCS type mean-field Hamiltonian

$$\mathcal{H} = \mathcal{H}_0 + \sum_k \left[\Delta^* c_{-k+q\downarrow} c_{k\uparrow} + \Delta c^\dagger_{k\uparrow} c^\dagger_{-k+q\downarrow}\right] \tag{1.10}$$

with a fixed order parameter Δ for pairing with pair momentum $\hbar q/aR$, $q \in \mathbb{Z}$. The quantum number q of the groundstate has to be determined by minimizing the energy $E(\phi)$ over all q. For $T > 0$, one has to minimize the free energy $F(\phi)$, or grand potential $\Omega(\phi)$, to obtain the proper value of q, see appendix A.3. The Hamiltonian (1.10) can readily be diagonalized by a Bogoliubov transformation, leading to a BCS like energy spectrum. This technique is widely discussed in the literature [54–56] and described closer in section 10.2. Here we will introduce the Green's function method for describing a superconducting state, introduced by Gor'kov, which offers a natural and simple treatment of the supercurrent and its flux periodicity.

For spin single pairing, the superconducting state is represented by the spin independent imaginary time Green's function

$$\mathcal{G}(k,k',\tau) = -\langle T_\tau c_{ks}(\tau) c^\dagger_{k's}(0)\rangle, \tag{1.11}$$

and the anomalous Green's functions

$$\mathcal{F}(k,k',\tau) = \langle T_\tau c_{ks}(\tau) c_{-k's'}(0)\rangle, \tag{1.12}$$

$$\mathcal{F}^*(k,k',\tau) = \langle T_\tau c^\dagger_{-ks}(\tau) c^\dagger_{k's'}(0)\rangle \tag{1.13}$$

for $s \neq s'$, where τ is the imaginary time and T_τ the time ordering operator with respect to τ. Using Heisenberg's equations of motion, Gor'kov derived a self-consistent set of equations which links $\mathcal{G}(k,k',\tau)$, $\mathcal{F}(k,k',\tau)$ and $\mathcal{F}^*(k,k',\tau)$ to the superconducting order parameter Δ and is known as the "Gor'kov equations". A detailed treatment of these equations is given in appendix D and in [57,58].

For the purpose of actual calculations, it is advantageous to write the Green's functions in frequency space as functions of the fermionic Matsubara frequency $\omega_n = (2n-1)\pi T$.

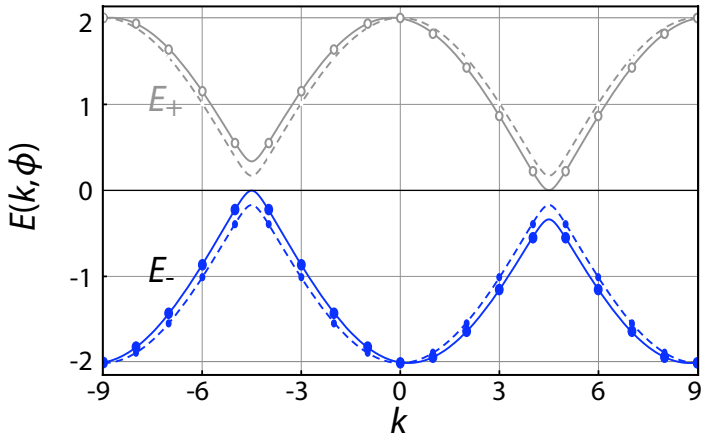

Figure 1.4: Energy dispersion of a ring with an order parameter $\Delta = 0.22t$ for $\phi = 0$ (dashed line) and $\phi = \phi_c \approx 0.24$ (solid line), where the indirect energy gap closes. The filled (empty) circles represent occupied (unoccupied) k-states for a ring with $N = 18$. The asymmetry for $\pm k$ scales with $1/R$.

Because of the isotropy of the ring, the Green's function corresponding to the Hamiltonian (1.10) is diagonal in momentum space, i.e. $\mathcal{G}(k, k', \omega_n) \equiv \mathcal{G}(k, \omega_n)\delta_{kk'}$. Then Gor'kov equations take the form

$$\mathcal{G}(k, \omega_n) = \left[\mathcal{G}_0^{-1}(k, \omega_n) + \Delta^2 \mathcal{G}_0(-k+q, -\omega_n)\right]^{-1}, \tag{1.14}$$

$$\mathcal{F}(k, k-q, \omega_n) = \mathcal{G}_0(k, \omega_n)\Delta\mathcal{G}(-k+q, -\omega_n), \tag{1.15}$$

$$\mathcal{F}^*(k-q, k, \omega_n) = \mathcal{G}_0(-k+q, -\omega_n)\Delta\mathcal{G}(-k, -\omega_n), \tag{1.16}$$

where $\mathcal{G}_0(k, \omega_n) = \left[i\omega_n - \varepsilon_k(\phi)\right]^{-1}$ is the Green's function in the normal state.

The pair momentum q of the superconducting groundstate is a function of the flux ϕ. To ensure the gauge invariance of the Gor'kov equations, they have to be invariant under the replacement $\phi \to \phi \pm 1$ and $q \to \pm 2$. The simplest ansatz for the ϕ dependence of q fulfilling this condition is

$$q(\phi) = \text{floor}(2\phi + 1/2), \tag{1.17}$$

where $\text{floor}(x)$ is the largest integer smaller or equal than x. Exact calculations will show later that this ansatz is essentially correct, but there are small deviations in the value of ϕ where q changes to the next integer.

Factorizing the denominator in (1.14), the Green's function becomes

$$G(k, \omega_n) = \frac{-i\omega_n - \varepsilon_{-k+q}(\phi)}{\left[i\omega_n - E_+(k, \phi)\right]\left[i\hbar\omega_n - E_-(k, \phi)\right]}, \tag{1.18}$$

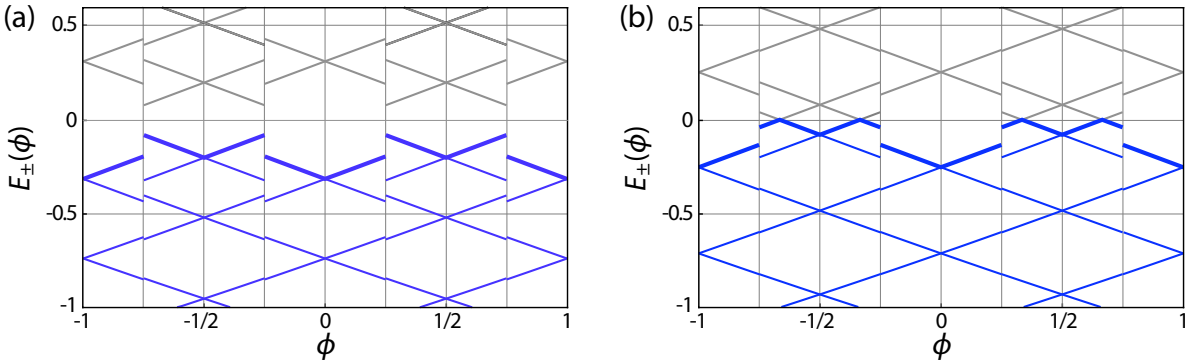

Figure 1.5: Eigenenergies $E_\pm(k, \phi)$ (1.19) as a function of flux for $N = 26$ for a fixed order parameter: (a) "large gap" regime with $\Delta = 0.3t$, (b) "small gap" regime with $\Delta = 0.08t$. Blue lines: occupied states, grey lines: unoccupied states. The bold line marks the highest occupied state for all ϕ.

where the two energy branches $E_\pm(k, \phi)$ are given by

$$E_\pm(k, \phi) = \frac{\varepsilon_k(\phi) - \varepsilon_{-k+q}(\phi)}{2} \pm \sqrt{\Delta^2 + \varepsilon^2(k, \phi)} \tag{1.19}$$

with $\varepsilon(k, \phi) = [\varepsilon_k(\phi) + \varepsilon_{-k+q}(\phi)]/2$. The first term in equation (1.19) in front of the square root describes the shift of the energy levels as a function of the flux. Close to E_F, it is typically (piecewise) linear in ϕ, as shown in figure 1.2 for the normal state and in figure 1.5 for the superconducting state. For $\phi = 0$, and consequently $q = 0$, the Doppler shift vanishes and (1.19) reduces to the usual BCS energy dispersion. For non-zero integer values of ϕ, the quantum numbers k are redistributed among the energy levels, thus ensuring the invariance of the spectrum as a whole.

1.2.2 Crossover from *hc/e* to *hc/2e* Periodicity

To discuss the flux periodicity in a superconducting ring, we choose a number of lattice sites N which is even but not a multiple of four, which gives a unique groundstate for $\phi = 0$ and $\mu = 0$. If N is a multiple of four, the same discussion is valid if ϕ is shifted by 1/2. The case of an odd N will not be discussed here.

The energies $E_\pm(k, \phi)$ are plotted in figure 1.4 as a function of k. For non-integer flux values the dispersion is asymmetric with respect to an inversion in the angular momentum $k \to -k$. This causes an asymmetric population of left and right circulating states and thus leads to a finite supercurrent even in the limit of a continuous density of states, in contrast to the normal state. The asymmetry scales with $1/R$, as does the supercurrent [c.f. equation (1.20)]. The energy gap which separates the upper (E_+) and the lower branch (E_-) is indirect and closes at a critical flux value ϕ_c, if the order

parameter Δ is smaller than a critical value Δ_c. This is illustrated in more detail in figure 1.5 showing a part the spectrum $E_\pm(k,\phi)$ for (a) a "small gap" $\Delta < \Delta_c$ and (b) a "large gap" $\Delta > \Delta_c$ for $N = 26$ and $\mu = 0$. As discussed in section 1.1.2, there are energy levels crossing E_F at half-integer flux values in the normal state. These levels split up into two states with weight 1/2 in the superconducting state. If $\Delta < \Delta_c$, the split levels are still crossing E_F and the crossing points depend on Δ. In this regime, both $E_+(k,\phi)$ and $E_-(k,\phi)$ can be positive or negative. If $\Delta > \Delta_c$, no levels cross E_F and a direct energy gap emerges, i.e. $E_+(k,\phi) > 0$ and $E_-(k,\phi) < 0$ for all k and ϕ and the spectrum is qualitatively independent of Δ. Close to E_F, $E_\pm(k,\phi)$ simplifies to

$$E_\pm(\pm k,\phi) \approx \mp\frac{t}{R}(2\phi - q) \pm \sqrt{\Delta^2 + l(t/R)^2} \tag{1.20}$$

where $k > 0$ and $l = 1$ for even q and $l = 0$ for odd q. The maximum direct energy gap in the even-q sectors is therefore $\Delta_0 = \sqrt{\Delta^2 + (t/R)^2}$, whereas in the odd-$q$ sectors it is $\Delta_1 = \Delta$.

The physical distinction of between the "small gap" and the "large gap" regime is best visible in the supercurrent in the ring, which we obtain from the Green's function as

$$J(\phi) = -\frac{e}{h}\sum_k \frac{\partial\varepsilon_k(\phi)}{\partial\phi} n(k) = \frac{e}{h}\sum_k \frac{\partial\varepsilon_k(\phi)}{\partial k} n(k), \tag{1.21}$$

as shown in appendix A, where $n(k) = T\sum_s\sum_n G(k,\omega_n)$ is the momentum distribution function. The sum over the Matsubara frequency ω_n can be computed analytically by conversion into an integration in the complex plane, leading to

$$n(k) = 2T\sum_n G(k,\omega_n) = \left[u^2(k) f(E_+(k,\phi)) + v^2(k) f(E_-(k,\phi))\right] \equiv n_+(k) + n_-(k), \tag{1.22}$$

with the coherence factors

$$u^2(k) = \left(1 + \frac{\varepsilon(k,\phi)}{E(k,\phi)}\right) \qquad \text{and} \qquad v^2(k) = \left(1 - \frac{\varepsilon(k,\phi)}{E(k,\phi)}\right) \tag{1.23}$$

and $E(k,\phi) = \sqrt{\Delta^2 + \varepsilon^2(k,\phi)}$.

It is instructive to split the supercurrent $J(\phi)$ into a contribution $J_+(\phi)$ from the upper branch of the spectrum and a contribution $J_-(\phi)$ from the lower branch, given by

$$J_\pm(\phi) = \frac{e}{h}\sum_k \frac{\partial\varepsilon_k(\phi)}{\partial k} n_\pm(k). \tag{1.24}$$

Both contributions, as well as the total supercurrent $J(\phi) = J_-(\phi) + J_+(\phi)$, are plotted in figure 1.6. The contribution $J_-(\phi)$ forms a $\Phi_0/2$ periodic saw-tooth pattern, both in

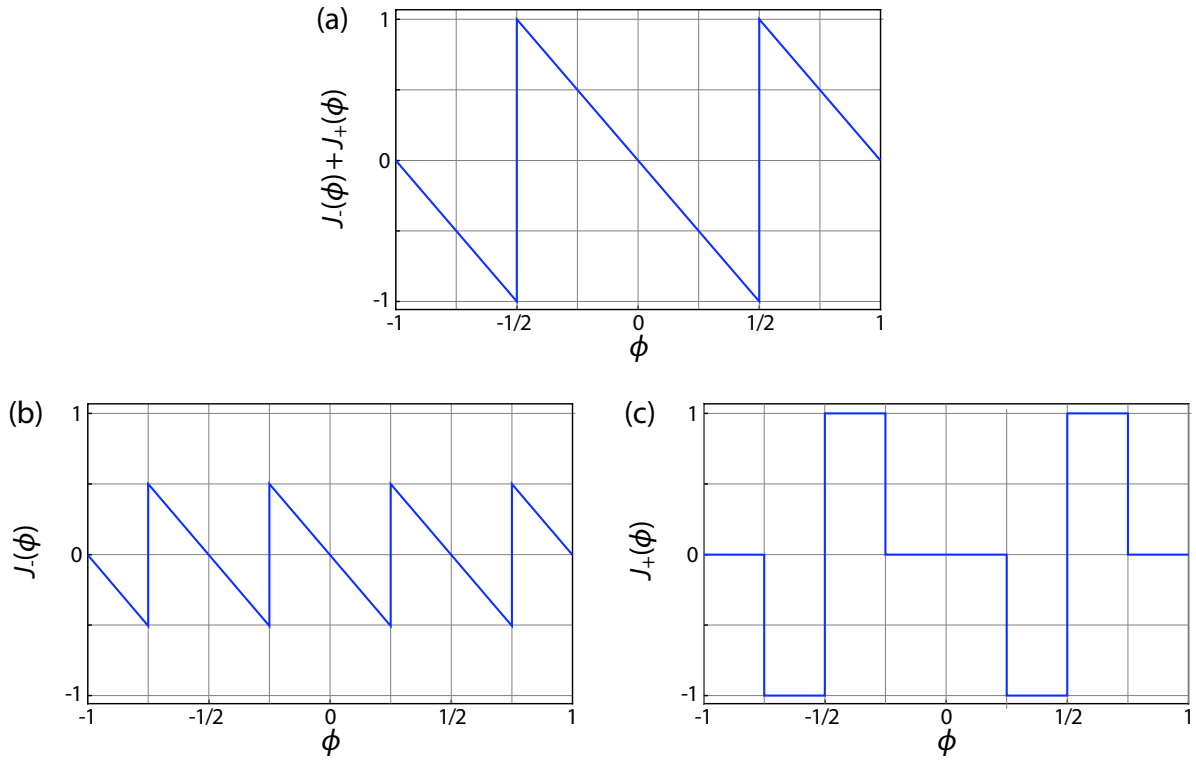

Figure 1.6: (a) The Φ_0 periodic persistent current $J(\phi)$ as obtained from the Green's function formalism in the normal state. (b) The contribution $J_-(\phi)$ is $\Phi_0/2$ periodic and identical in the normal and superconducting state. (c) The Φ_0 periodicity in the "small gap" regime comes exclusively from $J_-(\phi)$, which vanishes in the "large gap" regime.

the normal state and in the superconducting state. The Φ_0 periodic part in the normal state is contained exclusively in $J_+(\phi)$. For increasing Δ, the flux regime where $E_+(k,\phi)$ is partially occupied decreases, until $J_+(\phi)$ vanishes for $\Delta > \Delta_c$. In the "large gap" regime, the supercurrent is carried entirely by $J_-(\phi)$ and is therefore $\Phi_0/2$ periodic and essentially independent of Δ. The discontinuities in $J(\phi)$ are not caused by energy levels crossing E_F, but by the reconstruction of the condensate when the pair momentum q changes to the next integer at the flux values $\phi = (2n-1)/4$. A more detailed analysis of the periodicity crossover is given in section 2.1 together with the self consistency of the order parameter.

We obtain further insight into the mechanisms, which determine the current periodicity, by analyzing Δ_c. According to equation (1.20), close to E_F, the maximum energy shift is $t/(2R)$, and the condition for a direct energy gap [or $E_+(k,\phi) > 0$ for all k, ϕ] and a $\Phi_0/2$-periodic current pattern is therefore $\Delta > \Delta_c = t/(2R)$. The corresponding critical ring radius is $R_c = t/(2\Delta)$. It is instructive to compare R_c with the BCS coherence length $\xi_0 = \hbar v_F/(\pi\Delta)$, where v_F is the Fermi velocity and Δ the BCS order parameter at $T = 0$.

On the lattice we identify $v_F = \hbar k_F/m$ with $k_F = \pm\pi/2a$ and $m = \hbar^2/(2a^2 t)$. Setting the length unit $a = 1$ we obtain $\xi_0 = t/\Delta$ and thus $2R_c = \xi_0$. This signifies that the current response of a superconducting ring whose diameter is smaller than the coherence length is generally Φ_0-periodic [26]. In these rings the Cooper pair wave function is delocalized around the ring.

We have now identified the basic mechanism driving the crossover from Φ_0 periodicity in the normal state to $\Phi_0/2$ periodicity in the superconducting state. It is the crossing of the Fermi energy of energy levels as a function of the magnetic flux that leads to kinks in the energy and to discontinuities in the supercurrent (or normal persistent current in the normal state). If the superconducting gap is large enough to prevent all energy levels from crossing the Fermi energy, the kinks and jumps occur only where the pair momentum of the groundstate changes. The latter is the case if the ring diameter is larger than the coherence length of the superconductor.

2 Crossover from hc/e to $hc/2e$ Flux Periodicity in s-Wave Loops

In this chapter we extend the analysis above to fully self consistent calculations of the order parameter Δ in section 2.1 and to a multi-channel ring (annulus) in section 2.2. We discuss deviations in the flux value where the pair momentum changes, and we analyze the periodicity crossover at finite temperatures.

2.1 One-Dimensional Ring

The self-consistency equation for the s-wave order parameter derives directly from the definition of the anomalous Green's function $\mathcal{F}(k, k-q, \omega_n)$:

$$\Delta(\phi) = T V_0 \sum_k \sum_n \mathcal{F}(k, k-q, \omega_n), \tag{2.1}$$

where V_0 is the s-wave interaction strength and $\Delta(\phi)$ acquires an explicit flux dependence, but is invariant under the replacement $\phi \to \pm 1$ and $q \to \pm 2$. The pair momentum q corresponds to a phase gradient $\Delta(\phi)e^{2\pi i q\varphi}$ in real space (c.f. section 5) and can therefore be interpreted as the phase winding number of the condensate. The states with $q \neq 0$ are closely similar to the finite momentum pairing state introduced by Fulde and Ferrell [59] in a field threaded bulk superconductor. In this section, we take the same ansatz for the

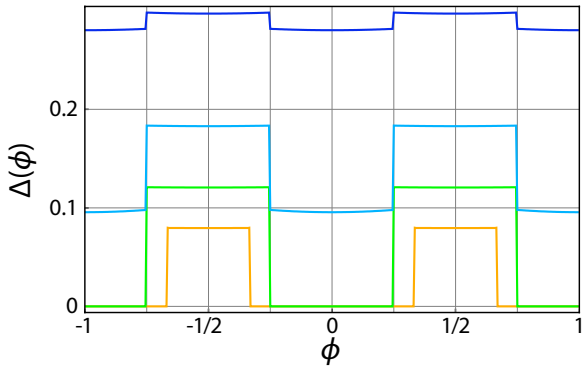

Figure 2.1: Solution of the self-consistency equation (2.3) for different values of the pairing energy V_0 at $T = 0$. From top to bottom: $V_0 = 1.9t,\ 1.6t,\ 1.35t,\ 1.1t$.

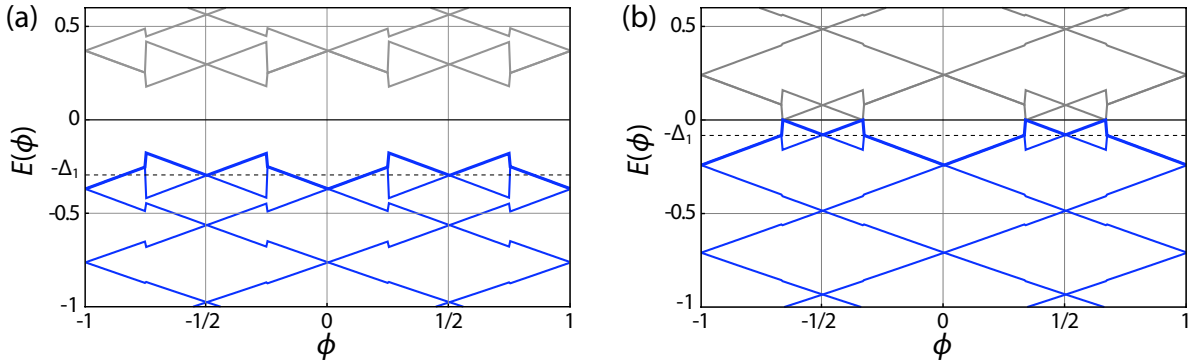

Figure 2.2: Same evaluation of the energy spectrum as in figure 1.5 but for self-consistently calculated order parameter. (a): "large gap" regime ($V_0 = 1.9t$, $\Delta_1 \approx 0.30t$); (b): "small gap" regime ($V_0 = 1.1t$, $\Delta_1 \approx 0.08t$). Superconductivity occurs only in the odd-q sectors for $V_0 = 1.1t$ (see figure 2.1). The bold line marks the highest occupied state for all ϕ. For the definition of Δ_1 see text after equation (1.20).

flux dependence of the groundstate pair momentum number q as in (1.17) in section 1.2.1. The deviations of this form will be discussed in the next section for the annulus.

By inserting $G(k, \omega_n)$ into the Gor'kov equation (1.15), one finds for the anomalous Green's function

$$F(k, k-q, \omega_n) = \frac{\Delta(\phi)}{[i\omega_n - E_+(k,\phi)][i\omega_n - E_-(k,\phi)]}. \tag{2.2}$$

Summing over ω_n and combining equations (2.1) and (2.2) leads to the self-consistency equation for $\Delta(\phi)$:

$$\frac{1}{N}\sum_k \frac{f(E_-(k,\phi)) - f(E_+(k,\phi))}{2\sqrt{\Delta(\phi)^2 + \varepsilon^2(k,\phi)}} = \frac{1}{V_0}. \tag{2.3}$$

Instead of lowering the temperature, we explore below the transition into the superconducting state at zero temperature by increasing the pairing interaction strength V_0.

The flux ϕ affects the solution of the gap equation (2.3) for $\Delta(\phi)$ in two ways. For small-size rings the magnitude of Δ is mainly controlled by the energy of the level closest to E_F. If the quantity $\delta_\phi = \min_k |\varepsilon(k,\phi) - E_F| > 0$, a solution of equation (2.3) exists only above a threshold value of the pairing interaction. In the even-q sectors, this is the case for all values of ϕ, whereas in all odd-q sectors a flux value ϕ exists, for which $\delta_\phi = 0$ and equation (2.3) has a solution for all $V_0 > 0$ (cf. figure 2.1). This is a consequence of the discreteness of the energy levels. In the strong coupling regime $V_0 \gg t$, $\Delta(\phi)$ is modulated only slightly by the flux. For weak coupling $V_0 \approx t$, a solution $\Delta_1 < \Delta_c = t/2R$ is possible in the "small gap" regime, where Δ_1 denotes the order parameter at half-integer

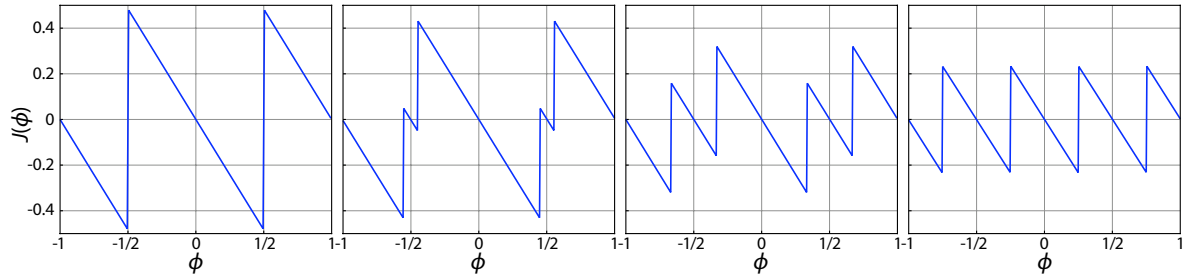

Figure 2.3: Crossover from the Φ_0-periodic normal persistent current to the $\Phi_0/2$-periodic supercurrent in a ring with $N = 26$ at $T = 0$ and $J(\phi)$ in units of $t\Phi_0$. For this ring size $\Delta_c \approx 0.24t$. The discontinuities occur where the ϕ-derivative of the highest occupied state energy changes sign.

flux values. In this case the energy gap closes at a critical flux ϕ_c in the odd-q sectors and $E_+(k, \phi)$ turns negative for the level closest to E_F (see figure 2.2). Thus the dominant term in the sum of equation (2.3) switches sign and the solution for $\Delta(\phi)$ vanishes discontinuously. This is equivalent to a breaking of the Cooper pair closest to E_F, which provides the main contribution to the condensation energy [60, 61]. This feature of the solution of the self-consistency equation is special for strictly one dimensional rings. In these rings superconductivity is destroyed for velocities of circulating Cooper pairs exceeding the Landau critical velocity, which is approached at $\phi = \phi_c$ (cf. reference [62]).

The vanishing of $\Delta(\phi)$ at the flux values where an energy level reaches E_F affects the energy spectrum in the "small gap" regime, as is visible by comparing figure 2.2 (b) to figure 1.5 (b) showing the same spectrum with a fixed Δ. In both figures, the slope of the highest occupied energy level changes at the same flux values. In the "large gap" regime, the small flux dependence of $\Delta(\phi)$ has no visible influence on the spectrum [figures 2.2 (a) and 1.5 (b)]. The current and its flux periodicity is therefore qualitatively the same with and without self consistency.

A self-consistent calculation of the current is shown in figure 2.3 for different values of V_0, illustrating the periodicity crossover. For $V_0 = \Delta(\phi) = 0$ one recovers the Φ_0-periodic saw-tooth pattern for the normal persistent current as discussed in chapter 1. With increasing $\Delta(\phi)$, new linear sections appear continuously. These are the sections where the order parameter is finite in the "small-gap" regime (c.f. [29]). The discontinuities of the current occur where the ϕ derivative of the energy of the highest occupied state switches sign (see figure 2.2). These linear sections increase with increasing $\Delta(\phi)$; once they extend to a range $\Phi_0/2$ upon reaching the "large gap" regime, the current becomes strictly $\Phi_0/2$-periodic.

A second fundamental effect, which manifestly breaks the $\Phi_0/2$-periodicity, is the offset of the transition from even to odd center of mass angular momenta q with respect to evenly spaced flux values $(2n - 1)\,\Phi_0/4$. This small offset was already observed in our

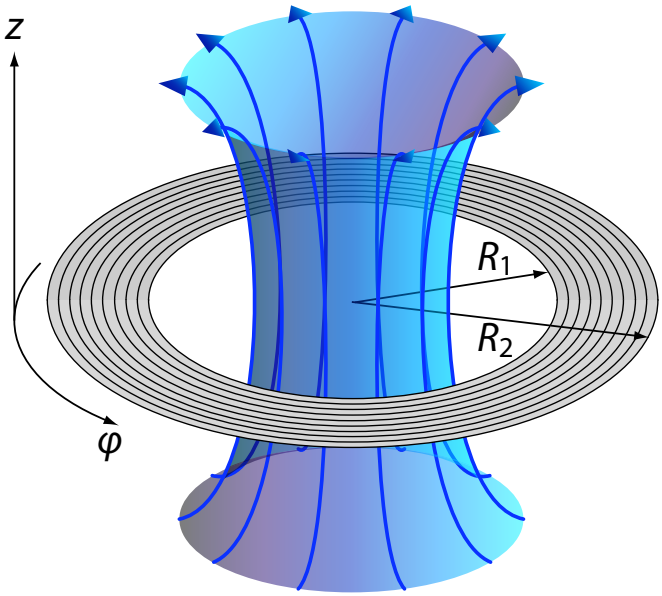

Figure 2.4: Annulus with inner radius R_1 and outer radius R_2. For a magnetic flux threading the interior of the annulus, the radial part of the Bogoliubov - de Gennes equations is solved numerically with a discretized radial coordinate.

previous numerical evaluations for d-wave loops [26]. Vakaryuk [31] has traced this shift to the dependence of the internal energy of Cooper pairs on the center-of-mass state. For a BCS-model superconductor, this effect is fully incorporated in the Bogoliubov - de Gennes evaluation of reference [26] although the quasiparticle-like presentation introduces a different perspective. In the discussion of this section we disregarded the offset for the one dimensional rings in order to focus on the aspects related to the opening of an indirect gap. In section 2.2 we include the offset consistently in the Bogoliubov - de Gennes evaluation of the multi-channel annulus.

It is worthwhile to note that the condition $\Delta > \Delta_c$ (or $R > R_c$) only refers to the periodicity of the supercurrent. It does not guarantee a $\Phi_0/2$-periodicity of the order parameter Δ or the total energy, but only of their derivatives. These quantities need a continuous energy spectrum with degeneracies for flux values which are multiples of $\Phi_0/2$ in order to be $\Phi_0/2$ periodic (cf. references [9,12]).

2.2 Multichannel Ring: Annulus

In this section we investigate a superconducting loop of finite width as shown in figure 2.4 with an inner radius R_1 and an outer radius R_2. For such an annulus, we choose a continuum approach on the basis of the Bogoliubov - de Gennes equations. A detailed discussion of the Bogoliubov - de Gennes equations in a lattice formulation is given in

part II. For integer and half-integer flux values, these equations can be solved analytically, as we show in section 2.2.1. For an arbitrary magnetic flux, we discuss a numerical solution in section 2.2.2.

Consider the Bogoliubov - de Gennes equations for spin singlet pairing

$$\begin{aligned} E_{\mathbf{n}} u_{\mathbf{n}}(\mathbf{r}) &= \left[\frac{1}{2m}\left(i\hbar\nabla + \frac{e}{c}\mathbf{A}(\mathbf{r})\right)^2 - \mu\right] u_{\mathbf{n}}(\mathbf{r}) + \Delta(\mathbf{r})\, v_{\mathbf{n}}(\mathbf{r}) \\ E_{\mathbf{n}} v_{\mathbf{n}}(\mathbf{r}) &= -\left[\frac{1}{2m}\left(i\hbar\nabla - \frac{e}{c}\mathbf{A}(\mathbf{r})\right)^2 - \mu\right] v_{\mathbf{n}}(\mathbf{r}) + \Delta^*(\mathbf{r}) u_{\mathbf{n}}(\mathbf{r}) \end{aligned}, \tag{2.4}$$

with the self-consistency condition (gap equation) for the order parameter $\Delta(\mathbf{r})$:

$$\Delta(\mathbf{r}) = V_0 \sum_{\mathbf{n}} u_{\mathbf{n}}(\mathbf{r}) v^*_{\mathbf{n}}(\mathbf{r}) \tanh\left(\frac{E_{\mathbf{n}}}{2T}\right), \tag{2.5}$$

where V_0 is the local pairing potential. For an annulus of finite width we separate the angular part of the quasi-particle wave functions $u_{\mathbf{n}}(\mathbf{r})$, $v_{\mathbf{n}}(\mathbf{r})$ using polar coordinates $\mathbf{r} = (r, \varphi)$ and the ansatz

$$\begin{aligned} u_{\mathbf{n}}(r, \varphi) &= u_{\mathbf{n}}(r) e^{\frac{i}{2}(k+q)\varphi} \\ v_{\mathbf{n}}(r, \varphi) &= v_{\mathbf{n}}(r) e^{\frac{i}{2}(k-q)\varphi} \end{aligned}, \tag{2.6}$$

where k and q are either both even or both odd integers. Thus $\hbar k$ is the angular momentum as for the one dimensional ring and $\mathbf{n} = (k, \rho)$ with the radial quantum number ρ. The order parameter factorizes into $\Delta(r, \varphi) = \Delta(r) e^{iq\varphi}$ where the radial component

$$\Delta(r) = V_0 \sum_{\mathbf{n}} u_{\mathbf{n}}(r) v^*_{\mathbf{n}}(r) \tanh\left(\frac{E_{\mathbf{n}}}{2T}\right) \tag{2.7}$$

is real. For a magnetic flux Φ threading the interior of the annulus we choose the vector potential $\mathbf{A}(r, \varphi) = \mathbf{e}_\varphi \Phi/(2\pi r)$, where $\mathbf{e}_\varphi$ is the azimuthal unit vector. With

$$\left(-i\nabla \pm \frac{\phi}{r}\mathbf{e}_\varphi\right)^2 = -\frac{1}{r}\partial_r(r\partial_r) + \frac{1}{r^2}(-i\partial_\varphi \pm \phi)^2 \tag{2.8}$$

the BdG equations therefore reduce to radial differential equations for $u_{\mathbf{n}}(r)$ and $v_{\mathbf{n}}(r)$:

$$\begin{aligned} E_{\mathbf{n}}\, u_{\mathbf{n}}(r) &= -\left[\frac{\hbar^2}{2m}\frac{\partial_r}{r}(r\partial_r) - \frac{\hbar^2 l_u^2}{2mr^2} + \mu\right] u_{\mathbf{n}}(r) + \Delta(r) v_{\mathbf{n}}(r) \\ E_{\mathbf{n}}\, v_{\mathbf{n}}(r) &= \left[\frac{\hbar^2}{2m}\frac{\partial_r}{r}(r\partial_r) - \frac{\hbar^2 l_v^2}{2mr^2} + \mu\right] v_{\mathbf{n}}(r) + \Delta(r) u_{\mathbf{n}}(r) \end{aligned}, \tag{2.9}$$

with the canonical angular momenta

$$\hbar l_u = \frac{\hbar}{2}(k + q - 2\phi), \tag{2.10}$$

$$\hbar l_v = \frac{\hbar}{2}(k - q + 2\phi). \tag{2.11}$$

The number q plays the same role as in the previous section. Here we choose q for each value of the flux to minimize the total energy of the system. The flux for which q changes to the next integer can therefore deviate from the values $(2n-1)/4$, where we fixed the switch in q for the one dimensional model.

2.2.1 Hankel-Function Ansatz

A natural choice of an ansatz for the solutions of the coupled differential equations (2.9) are linear combinations of the Hankel functions $H_l^{(1)}$ and $H_l^{(2)}$, since they are individually solutions of the uncoupled equations (2.9) for $\Delta(r) = 0$:

$$\left(\frac{1}{r}\partial_r(r\partial_r) - \frac{l^2}{r^2}\right) H_l^{(1,2)}(\gamma r) = \gamma^2 H_l^{(1,2)}(\gamma r). \tag{2.12}$$

We therefore take $u_{\mathbf{n}}(r)$ and $v_{\mathbf{n}}(r)$ of the form:

$$u_{\mathbf{n}}(r) = u_{\mathbf{n}}\left[H_{l_u}^{(1)}(\gamma_{\mathbf{n}}^u r) + c_{\mathbf{n}}^u H_{l_u}^{(2)}(\gamma_{\mathbf{n}}^u r)\right], \tag{2.13}$$

$$v_{\mathbf{n}}(r) = v_{\mathbf{n}}\left[H_{l_v}^{(1)}(\gamma_{\mathbf{n}}^v r) + c_{\mathbf{n}}^v H_{l_v}^{(2)}(\gamma_{\mathbf{n}}^v r)\right]. \tag{2.14}$$

The equations (2.9) then become

$$\begin{aligned} E_{\mathbf{n}}\, u_{\mathbf{n}}(r)] &= -\left[\frac{\hbar^2}{2m}\left(\gamma_{\mathbf{n}}^u\right)^2 + \mu\right] u_{\mathbf{n}}(r) + \Delta(r) v_{\mathbf{n}}(r) \\ E_{\mathbf{n}}\, v_{\mathbf{n}}(r) &= \left[\frac{\hbar^2}{2m}\left(\gamma_{\mathbf{n}}^v\right)^2 + \mu\right] v_{\mathbf{n}}(r) + \Delta(r) u_{\mathbf{n}}(r) \end{aligned}, \tag{2.15}$$

The coefficients $\gamma_{\mathbf{n}}^\alpha$ and $c_{\mathbf{n}}^\alpha$ with $\alpha = u, v$ are fixed by the open boundary conditions, for which $u_{\mathbf{n}}(r)$ and $v_{\mathbf{n}}(r)$ vanish on the inner and outer boundaries of the annulus: $u_{\mathbf{n}}(R_1) = u_{\mathbf{n}}(R_2) = 0$ and $v_{\mathbf{n}}(R_1) = v_{\mathbf{n}}(R_2) = 0$. This generates the defining equations for $\gamma_{\mathbf{n}}^\alpha$ and $c_{\mathbf{n}}^\alpha$

$$c_{\mathbf{n}}^\alpha = -\frac{H_{l_\alpha}^{(1)}(\gamma_{\mathbf{n}}^\alpha R_1)}{H_{l_\alpha}^{(2)}(\gamma_{\mathbf{n}}^\alpha R_1)} = -\frac{H_{l_\alpha}^{(1)}(\gamma_{\mathbf{n}}^\alpha R_2)}{H_{l_\alpha}^{(2)}(\gamma_{\mathbf{n}}^\alpha R_2)}. \tag{2.16}$$

For all integer and half-integer values of flux, $q = 2\phi$ in the groundstate, thus $l_u = l_v = k/2$. Assuming a constant order parameter $\Delta(r) = \Delta$, the r-dependence drops out from equations (2.15) and we find the eigenvalues and eigenvectors of the usual BCS type

$$E_{\mathbf{n}} = \sqrt{\left(\frac{\hbar^2}{2m}\gamma_{\mathbf{n}}^2 - \mu\right)^2 + \Delta^2} \tag{2.17}$$

with $\gamma_{\mathbf{n}} = \gamma_{\mathbf{n}}^u = \gamma_{\mathbf{n}}^v$ and

$$u_{\mathbf{n}} = \frac{1}{2}\left[1 + \left(\frac{\hbar^2}{2m}\gamma_{\mathbf{n}}^2 + \mu\right)/E_{\mathbf{n}}\right], \tag{2.18}$$

$$v_{\mathbf{n}} = \frac{1}{2}\left[1 - \left(\frac{\hbar^2}{2m}\gamma_{\mathbf{n}}^2 + \mu\right)/E_{\mathbf{n}}\right]. \tag{2.19}$$

These are the two distinct classes of superconducting states as discussed for the $1D$ loop: for integer flux values, Δ is given by summing over all even angular momenta k, whereas for half-integer flux values, Δ is obtained by summing over odd angular momenta.

For general values of magnetic flux, l_u and l_v are different and so are $\gamma_{\mathbf{n}}^u$ and $\gamma_{\mathbf{n}}^v$. The r-dependence of $u_{\mathbf{n}}(r)$ is therefore different from $v_{\mathbf{n}}(r)$ in equations (2.13) and (2.14). In App. A we analyze the solution of the uncoupled equations (2.9) for $\Delta = 0$ and find that the eigenfunctions account for the flux induced Doppler shift by shifting their nodes closer together or further apart—most importantly, $u_{\mathbf{n}}(r)$ shifts its nodes in the opposite direction than does $v_{\mathbf{n}}(r)$. This implies that $u_{\mathbf{n}}(r)$ and $v_{\mathbf{n}}(r)$ with the ansatz of equations (2.13) and (2.14) cannot be solutions of the coupled equations (2.15) for $\Delta(r) \neq 0$.

Moreover, we show in appendix B for the limit of a thin annulus ($R_1 \gg R_2 - R_1$) that both the Doppler shift and the shift of the nodes of $u_{\mathbf{n}}(r)$ and $v_{\mathbf{n}}(r)$ are in leading order linear functions of $q - 2\phi$. It is therefore not possible to find an approximate solution of equations (2.9) that contains the effects of the Doppler shift but neglects the shift of the nodes. Consequently, we have to resort to a numerical solution of the radial component of the BdG equations.

2.2.2 Self-Consistent Numerical Solution

The numerical solution of equations (2.9) is achieved by discretizing the interval $[R_1, R_2]$ for the radial coordinate r into M radii r_i, which defines the grid constant $a = (R_2 - R_1)/M$. In this way we obtain for each angular momentum state k M radial eigenstates (channels), which correspond to the M eigenstates with the lowest eigenenergies $E_{\mathbf{n}}$ of the continuum model. On this set of M radial coordinates, we use the symmetric discrete differential operators $\partial_i f(r_i) = [f(r_{i+1}) - f(r_{i-1})]/a$ and $\partial_i^2 f(r_i) = [f(r_{i+1}) + f(r_{i-1}) - 2f(r_i)]/a^2$.

Inserting these discrete operators into equations (2.9) and using $(1/r)\partial_r r\partial_r = (1/r)\partial_r + \partial_r^2$, one obtains the eigenvalue equation

$$\begin{pmatrix} \hat{t} + \hat{\mu}_k^u & \hat{\Delta} \\ \hat{\Delta} & -\hat{t} - \hat{\mu}_k^v \end{pmatrix} \begin{pmatrix} u_{\mathbf{n}} \\ v_{\mathbf{n}} \end{pmatrix} = E_{\mathbf{n}} \begin{pmatrix} u_{\mathbf{n}} \\ v_{\mathbf{n}} \end{pmatrix} \tag{2.20}$$

where $u_{\mathbf{n}}$ and $v_{\mathbf{n}}$ are real and the operators $\hat{t}$, $\hat{\mu}_k^\alpha$, and $\hat{\Delta}$ are defined through

$$\hat{t}u_{\mathbf{n}}(r_i) = t[u_{\mathbf{n}}(r_{i+1}) + u_{\mathbf{n}}(r_{i-1})] + t\frac{a}{r_i}[u_{\mathbf{n}}(r_{i+1}) - u_{\mathbf{n}}(r_{i-1})], \tag{2.21}$$

and

$$\hat{\mu}_k^\alpha u_{\mathbf{n}}(r_i) = t\left[\frac{a^2}{r_i^2} l_\alpha^2 - 2\right] u_{\mathbf{n}}(r_i), \tag{2.22}$$

$$\hat{\Delta}u_{\mathbf{n}}(r_i) = \Delta(r_i)u_{\mathbf{n}}(r_i), \tag{2.23}$$

where $t = \hbar^2/(2ma^2)$. A self-consistent solution of equation (2.20) and the gap equation

$$\Delta(r_i) = V_0 \sum_{\mathbf{n}} u_{\mathbf{n}}(r_i)v_{\mathbf{n}}(r_i) \tanh\left(\frac{E_{\mathbf{n}}}{2T}\right) \tag{2.24}$$

is found iteratively. The operator $\hat{t}$ consists of a symmetric and an antisymmetric part with respect to r_{i-1} and r_{i+1}. In order to ensure that the eigenvalues of equation (2.20) are real, the prefactor of the second, antisymmetric term in equation (2.21) must be smaller or equal to the prefactor of the symmetric term, which means $M \geq (R_2 - R_1)/2R_1$. This condition is fulfilled since $M = (R_2 - R_1)/a > (R_2 - R_1)/2R_1$.

Once the eigenfunctions of equation (2.20) are known, we obtain the current by evaluating the expectation value of the gauge invariant current operator [60]. The expectation value $J(r)$ of the circulating current is found using a Bogoliubov transformation and the ansatz (2.6) in polar coordinates:

$$J(r) = \frac{\hbar e}{m} \sum_{\mathbf{n}} \left[J_{\mathbf{n}}^u(r) f(E_{\mathbf{n}}) - J_{\mathbf{n}}^v(r) f(-E_{\mathbf{n}})\right], \tag{2.25}$$

with

$$\begin{aligned} J_{\mathbf{n}}^\alpha(r) =& \frac{\hbar e}{m} \mathrm{Im}\left[\alpha_{\mathbf{n}}^*(r,\varphi)\left(-\frac{i}{r}\partial_\varphi - \frac{\phi}{r}\right)\alpha_{\mathbf{n}}(r,\varphi)\right] \\ =& \frac{\hbar e}{m}\frac{l_\alpha}{r}\alpha_{\mathbf{n}}^2(r) \end{aligned} \tag{2.26}$$

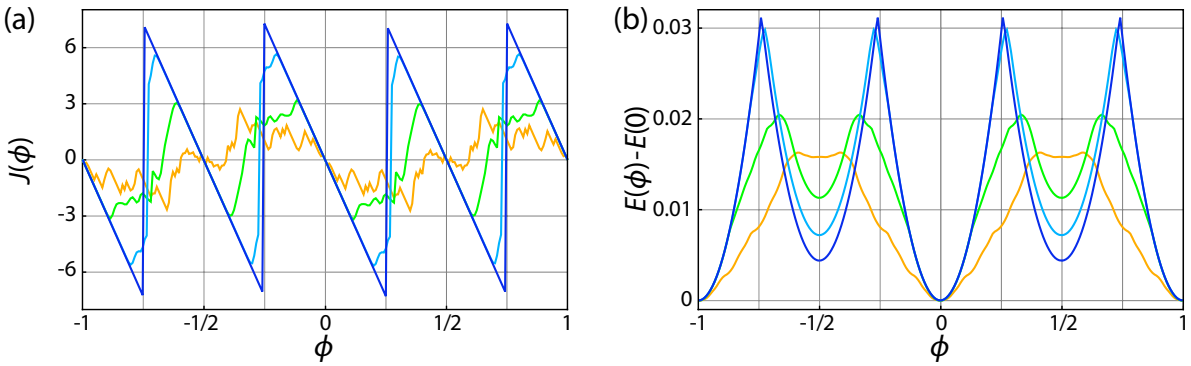

Figure 2.5: Non-self-consistent calculation of current and energy at $T = 0$. The circulating current (a) in an annulus with an inner radius $R_1 = 100a$ and an outer radius $R_2 = 150a$ is shown for fixed, ϕ-independent $\Delta = 0$ (orange), $\Delta = 0.002t$ (green), $\Delta = 0.004t$ (turquoise), $\Delta = 0.006t$ (blue). (b) shows the difference between the total energy of the annulus as a function of ϕ and the total energy at zero flux for the same values for Δ as above.

for $\alpha = u, v$. The contribution of each quasi-particle state to the total current is therefore determined by its angular velocity l_α. The radial quantum number ρ and the Δ-dependence enter only through the occupation probability which is controlled by the eigenenergy $E_{\mathbf{n}}$. Further, the total energy of the system is given by

$$E = \frac{1}{M} \sum_{\mathbf{n}} E_{\mathbf{n}} \sum_i \left[u_{\mathbf{n}}^2(r_i) f(E_{\mathbf{n}}) + v_{\mathbf{n}}^2(r_i) f(-E_{\mathbf{n}}) \right], \tag{2.27}$$

where we neglect a mean-field term of the form $\sum_i \Delta^2(r_i)/V_0$, which is nearly flux independent in the "large gap" regime (see appendix C.2).

2.2.3 Results

The results of the non-self-consistent calculations for the circulating current and the total energy at $T = 0$ and for fixed values of Δ are displayed in figure 2.5. In the normal state ($\Delta = 0$), there are approximately M eigenstates sufficiently close to E_F to cross E_F as a function of ϕ, unlike in small one dimensional rings where only one state crosses E_F. For each crossing, a small jump appears in the current as a function of ϕ. There is a larger jump at the value of ϕ where the energies of the even-q and odd-q states become degenerate and q switches to the next integer. The shape of this function depends on the distribution of eigenenergies close to E_F and therefore on microscopic details of the geometry of the annulus and the Fermi energy E_F. A finite Δ allows for a flux regime with direct energy gap and no crossings of E_F, thus in this regime the current is linear and the total energy quadratic in ϕ. For the largest value ($\Delta = 0.006t$) shown, there is a direct gap for all values of ϕ. Even for this value of Δ, the current and the energy are not

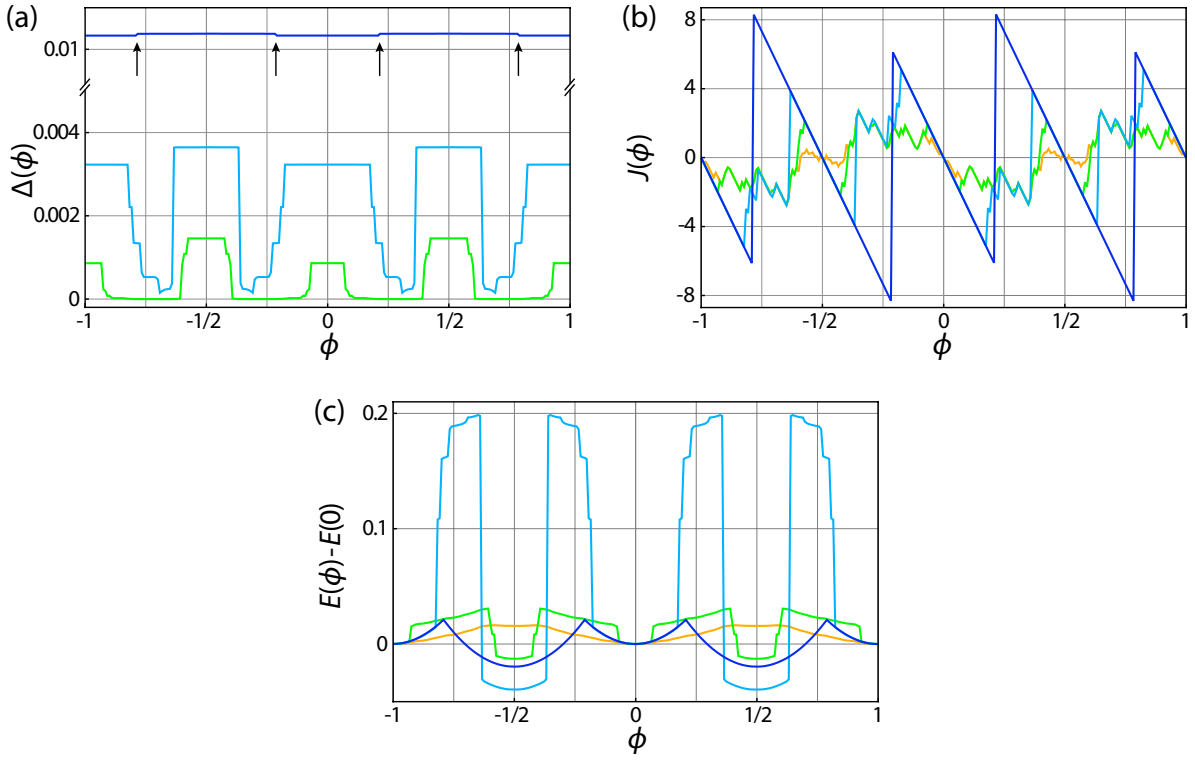

Figure 2.6: Self-consistent calculations for the same annulus as in figure 2.5. In addition, (a) displays the self-consistent order parameter Δ as a function of ϕ. The lines correspond to the pairing interaction $V_0 = 0$ (orange), $V_0 = 0.28t$ (green), $V_0 = 0.32t$ (turquoise), $V_0 = 0.38t$ (blue). The black arrows mark the positions of the q-jump for $V_0 = 0.38t$ and $V_0 = 0.32t$.

exactly $\Phi_0/2$-periodic because of the energy difference of the even and odd q states in finite systems [26, 31].

The introduction of self-consistency for the order parameter does not fundamentally change these basic observations (figure 2.6). One observes that $\Delta(R_1) < \Delta(R_2)$, but if $(R_2 - R_1)/R_1 \gtrsim 1$, the relative difference is small. We denote the average of $\Delta(r)$ over all r with Δ in the following. The crossover is then controlled by the pairing interaction strength V_0, for which we chose such values as to reproduce the crossover from the normal state to a state with direct energy gap for all flux values. The order parameter Δ is now a function of ϕ. If $\Delta(\phi = 0) \lesssim 0.006t$ (cf. figure 2.5), the gap closes with ϕ, and Δ decreases whenever a state crosses E_F. At these flux values we observe a sharp increase in the total energy of the annulus. Unlike in one dimensional rings, Δ does not drop to zero at the closing of the energy gap, but decreases stepwise. In two or three dimensions, Δ remains finite beyond ϕ_c because it is stabilized by contributions to the condensation energy from pairs with relative momenta perpendicular to the direction of the current flow and the closing of the indirect energy gap does not destroy superconductivity [61, 62]. Apart

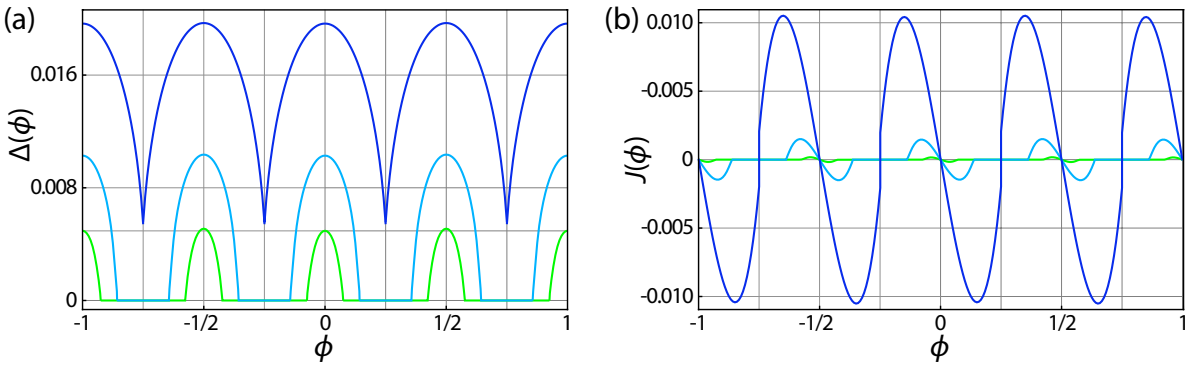

Figure 2.7: The order parameter $\Delta(\phi)$ and the persistent current $J(\phi)$ for the temperature driven transition from the normal to the superconducting state in an annulus with inner radius $R_1 = 30a$ and outer radius $R_2 = 36a$. The pairing interaction is $V_0 = 0.7t$, with a critical temperature of $T_c \approx 0.0523t$ for zero flux. For these parameters $\Delta(T = 0) \approx 0.1t$. The lines (from top to bottom) correspond to the temperatures $T = 0.0513t$ (blue), $T = 0.0520t$ (turquoise), $T = 0.0522t$ (green). Notice that Δ is slightly different for the flux values $\phi = 0$ and $\phi = \pm 1/2$.

from these steps, the current (energy) shows the standard linear (quadratic) behavior.

The offset of the q-jump is only relevant for values of V_0 for which Δ is finite for all ϕ. In figure 2.6, the offset is clearly visible for the largest two values of V_0 (marked with black arrows). Its sign depends on the geometry of the annulus and the pairing interaction V_0— the offset changes sign for increasing V_0 (cf. Ref. [31]).

Experimentally more relevant is to control the crossover through temperature. With the pairing interaction V_0 sufficiently strong to produce a $T = 0$ energy gap much larger than the maximum Doppler shift, the crossover regime is reached for temperatures slightly below T_c. For the annulus of figure 2.7, the crossover proceeds within approximately one percent of T_c. The crossover regime becomes narrower for larger rings, proportional to the decrease of the Doppler shift. In the limit of a quasi one dimensional ring of radius R we can be more precise: If we define the crossover temperature T^* by $\Delta(T^*) = \Delta_c$ and assuming $\Delta_c \ll \Delta$, we can use the Ginzburg-Landau form of the order parameter

$$\frac{\Delta(T)}{\Delta(0)} \approx 1.75\sqrt{1 - \frac{T}{T_c}} \tag{2.28}$$

and obtain

$$\frac{T_c - T^*}{T_c} \approx \frac{\Delta_c^2}{3.1\Delta^2(0)} = \frac{t^2}{12.4\Delta^2(0)R^2} = \frac{E_F^2}{3.1T_c^2R^2}, \tag{2.29}$$

For a ring with a radius of 2500 lattice constants ($\approx 10\,\mu$m) and $\Delta(0) = 0.01t$ (≈ 3 meV) one finds the ratio $(T_c - T^*)/T_c \approx 1.3 \times 10^{-4}$. This is in reasonable quantitative agreement

with the experimental results of Little and Parks [14,15], discussed also by Tinkham [13]. Their theoretical prediction is similar to equation (2.29), up to a factor in which they include a finite mean free path. Moreover, they do not include the difference introduced through even and odd q states. This difference was considered in calculations of T_c by Bogachek *et al.* [21] in the one-channel limit. In equation (2.29) the value of $\Delta(0)$ is in fact different for even and odd q. Although quantitative predictions of $T_c - T^*$ of the theory presented here might be too large compared to the experiment, it serves as an upper limit because it describes the maximum possible persistent current. Scattering processes in real systems will further reduce $T_c - T^*$.

For temperatures close to T_c, the difference of the eigenenergies of even and odd q states is less important than at $T = 0$. Thus the deviation from the Φ_0-periodicity of the current and of the order parameter is smaller. Furthermore, persistent currents in the normal state are exponentially small compared to the persistent supercurrents below T_c. Their respective Φ_0-periodic behavior is therefore essentially invisible for the flux values where $\Delta = 0$. For the annulus of figure 2.7, the difference between $\Delta(\phi = 0)$ and $\Delta(\phi = 1/2)$ is still visible, but the corresponding differences in the current are too small.

We have described the crossover from the Φ_0-periodic persistent currents as a function of magnetic flux in a metallic loop to the $\Phi_0/2$-periodic persistent supercurrent in a one dimensional loop as well as in a multi-channel annulus for conventional s-wave pairing. While a one dimensional superconducting ring is a rather idealized system, it proves valuable for discussing the physics of this crossover, even for a fixed order parameter Δ. The physical concepts, which we illustrated in a simplified form in section 1.2.2, remain thereby valid even in the much more complex context of the self consistent calculations on the annulus. A ring with a radius smaller than half the superconducting coherence length, shows a Φ_0-periodic supercurrent, which reaches the critical current at a critical flux value ϕ_c, determined by the flux dependent closing of the gap. Assuming that this relation remains unchanged on a ring with finite thickness $d \ll R$, as indeed suggested by the multi-channel model, R_c would be of the order of 1 µm for aluminum rings. In two or three dimensions, Δ remains finite beyond ϕ_c. The temperature controlled crossover, while cooling through T_c, appears within a temperature window proportional to $1/R^2$ and thus appears hard to detect in experiment.

At this point, let us clarify the connection of what we showed above to the phenomenon of flux quantization in thick loops. As shown in figure 2.6 (c), the minima of the total energy are in all cases at integer and half-integer values on ϕ. This is a fundamental property of all BCS type superconducting states and the superconducting flux quantum $\Phi_0/2$ is not affected by the Doppler shift of the energy levels. However, the shift of the flux values, where q switches, affects the regimes of external flux, in which the loop quantizes the flux to a certain multiple of the $\Phi_0/2$.

3 Flux Periodicities of Nodal Superconductors

For the discussion of the magnetic flux periodicity of an unconventional superconductor, a multichannel system is a necessary prerequisite. The annulus used in the last chapter is an option, but with some difficulties. The superconducting state of our focus is the d-wave state, which has the symmetry of a square lattice. For a description in momentum space, we need however a rotationally symmetric system. Deforming the lattice to an annulus leads to strong deviations in the order parameter from the desired d-wave symmetry; therefore we choose a second solution: bending a discrete two dimensional $N \times M$ square lattice to a cylinder (figure 3.1) with circumference Na and height Ma.

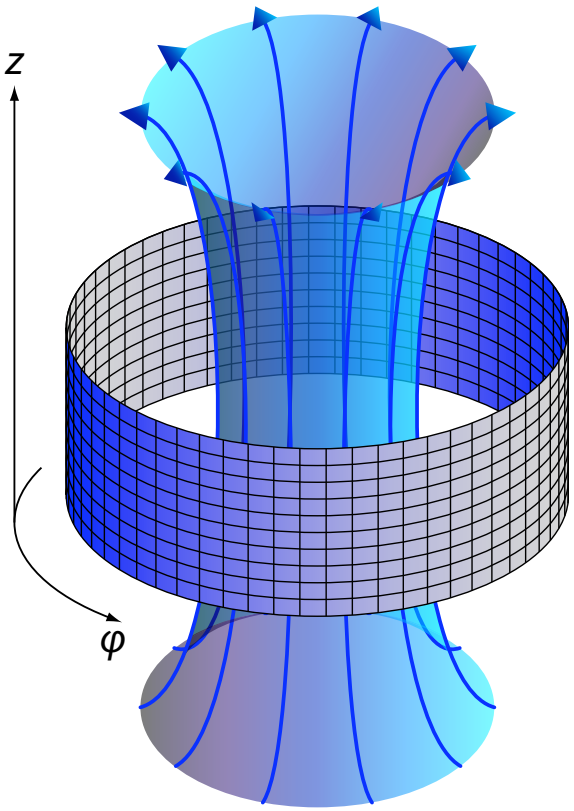

Figure 3.1: As a model system to study persistent supercurrents we use a thin-wall cylinder constructed of a two dimensional discrete lattice. The interior of the cylinder is threaded by a magnetic flux Φ; we assume that the flux does not penetrate into the cylinder wall. In such a system, Φ can be chosen arbitrarily, since quantization applies to the fluxoid and not the flux itself.

For two reasons we expect nodal rather than nodeless superconductors to support a $\Phi_0 = hc/e$ periodicity. The first arises from the discrete nature of the eigenenergies in a finite system. The results of the summation over occupied eigenstates for integer and half-integer flux values differ by an amount proportional to the mean level spacing δ_F in the vicinity of the Fermi energy E_F. In the normal state, $\delta_F \propto 1/V$, where V is the volume of the system. For the thin cylinder shown in figure 3.1 with a circumference Na and a height Ma, the level spacing is $\delta_F \propto 1/(NM)$; in s-wave superconductors with an order parameter $\Delta \gg \delta_F$, δ_F matters little. For superconducting states with gap nodes, the situation is different. For example, in the d-wave superconductors with an order parameter $\Delta_\mathbf{k} \propto k_\varphi^2 - k_z^2$, the nodal states closest to E_F have to fulfill the condition $k_z = k_\varphi$, thus there are fewer possible eigenstates and $\delta_F \propto 1/N$.

The second reason is that for gapless superconductors with a finite density of states close to E_F, the occupation probabilities of these states change with flux. The flux dependence of the occupation enhances the difference of current matrix elements for integer and half-integer flux values [26, 32, 35]. This effect can be understood in terms of the spacial extension of a Cooper pair. In s-wave superconductors, the occupation probability remains constant for all Φ, if the diameter of the cylinder is larger than ξ_0. If this condition is fulfilled, the constituents of a Cooper pair cannot circulate separately; the pair does not "feel" the multiply connected geometry of the cylinder. But for nodal superconducting states, the length scale which characterizes their coherence, diverges in the nodal directions and there are always Cooper pairs which extend around the circumference of the cylinder. Therefore nodal superconductors have no characteristic length scale above which the superconducting state is unaffected by the geometry of the system. These two combined effects are investigated on the basis of an analytical model in section 3.2 and by numerical calculations in section 3.3.

3.1 Superconductivity in a Flux-Threaded Cylinder

The properties of a finite-size multiply connected superconductor depend sensitively on the discrete energy spectrum in the normal state, in particular in circular symmetric geometries. To understand the superconducting spectrum of the discrete $N \times M$ lattice, we therefore have to characterize first its normal state spectrum.

The problem is closely analogous to the one dimensional ring investigated in section 1.1.2. Each energy level of the one dimensional case splits up into M levels, which results in a characteristic flux dependence of the spectral density. For special ratios N/M, the flux values where the levels of the one dimensional ring cross have a high degeneracy; for $N = M$, the degree of degeneracy is M. For the latter case, the differences between the spectrum for integer and half-integer flux values are most pronounced; they are similar to the one dimensional spectrum of figure 1.2 (a), if N and M are even, and similar to the

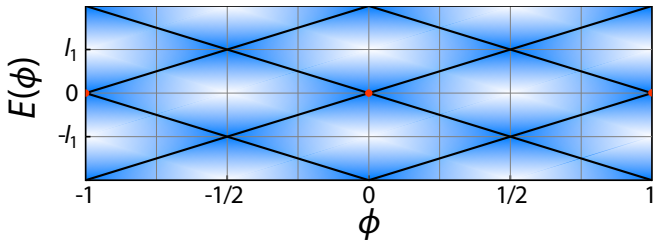

Figure 3.2: The energy spectrum of a cylinder in the normal state depends on the numbers N and M, which parametrize the circumference and height of the cylinder. The black lines represent the energy levels for a one dimensional ring with $M = 1$ and $N/4$ an integer, where level crossings occur for integer values of ϕ (c.f. figure 1.2). I_1 is the maximum Doppler shift for $\phi = 1/2$ (see section 3.2). For $M \gg 1$, the levels split up and form a quasi continuous density of states that depends on the ratio N/M (blue patches).

spectrum of figure 1.2 (b), if N and M are odd. For $N = M \pm 1$, the spectrum is almost $\Phi_0/2$-periodic, which is the extension of the odd N case in the one dimensional ring [figure 1.2 (c)]. Away from these special choices of N and M, the degeneracies are lifted, indicated by the blue shaded "patches" in figure 3.2. The inclusion of a next-nearest neighbor hopping term or a change of μ in equation (3.2) has a similar effect, as shown by Zhu [36]. The size of the normal persistent current circulating around the cylinder is controlled by the change of the density of states near E_F upon increasing ϕ. Since normal persistent currents in clean metallic rings are typically Φ_0 periodic [2,27], we will choose $N = M$ and $\mu = 0$ for our model study, where the Φ_0 periodicity of the spectrum is most clearly established. Whenever an energy level crosses E_F with increasing flux, the current reverses its sign, thus it is Φ_0-periodic for even N and either paramagnetic or diamagnetic in the vicinity of $\phi = 0$, and it is $\Phi_0/2$-periodic for odd N. This lattice-size dependence persists also in rings with electron-electron interactions [50–52, 63] or in mesoscopic superconducting islands [64] and in particular in the superconducting state with small energy gap, as we have shown in chapter 2 for s-wave pairing.

The solution of the BCS theory on the cylinder is similar as in section 2 for a one dimensional ring. We choose in the following N and M even, which leads to a normal state spectrum of the type shown in figure 3.2, in contrast to section 2.1. This is not an obvious choice, but we will see in part III that one obtains this type of spectrum for a square loop, to which we like to compare the results we get for the cylinder geometry.

The starting point for our investigations is the BCS theory formulated on a flux threaded cylinder with circumference $Na = 2\pi Ra$ and height Ma, where R is the dimensionless radius of the cylinder and a the lattice constant. The pairing Hamiltonian

is given by

$$\mathcal{H} = \sum_{\mathbf{k},s} \varepsilon_{\mathbf{k}}(\phi) c^{\dagger}_{\mathbf{k}s} c_{\mathbf{k}s} + \sum_{\mathbf{k}} \left[\Delta^{*}(\mathbf{k},\mathbf{q}) c_{\mathbf{k}\uparrow} c_{-\mathbf{k}+\mathbf{q}\downarrow} + \Delta(\mathbf{k},\mathbf{q}) c^{\dagger}_{-\mathbf{k}+\mathbf{q}\downarrow} c^{\dagger}_{\mathbf{k}\uparrow} \right], \tag{3.1}$$

where $\mathbf{k} = (k_\varphi, k_z)$ with $k_\varphi = n/R$ and $n \in \{-N/2+1, \ldots, N/2\}$. In the z-direction along the axis of the cylinder, we choose open boundary conditions, which allow for even-parity solutions with $k_z = (2m_e - 1)\pi/M$ and odd-parity solutions with $k_z = 2\pi m_o/M$, where $m_e, m_o \in \{1, \ldots, M/2\}$. The operators $c^{\dagger}_{\mathbf{k}s}$ and $c_{\mathbf{k}s}$ are creation and annihilation operators for electrons with angular momentum $\hbar k_\varphi/a$ and momentum $\hbar k_z/a$ in z direction. Note that for convenience, we chose k_φ, $k_z \in [0, 2\pi]$, unlike in chapter 1 and 2. The eigenenergies of free electrons moving on a discrete lattice on the surface of the flux threaded cylinder have the form

$$\varepsilon_{\mathbf{k}}(\phi) = -2t \left[\cos\left(k_\varphi - \frac{\phi}{R} \right) + \cos k_z \right] - \mu. \tag{3.2}$$

For $R \gg 1$, $\varepsilon_{\mathbf{k}}(\phi)$ can be expanded to linear order in ϕ/R and

$$\varepsilon_{\mathbf{k}}(\phi) - \varepsilon_{\mathbf{k}}(0) \approx -2t \frac{\phi}{R} \sin k_\varphi. \tag{3.3}$$

is commonly called the Doppler shift.

The superconducting order parameter in the pairing Hamiltonian (3.1) is defined through

$$\Delta(\mathbf{k},\mathbf{q}) \equiv \Delta_q(\phi) g(\mathbf{k} - \mathbf{q}/2) = \frac{1}{2} \sum_{\mathbf{k}'} V(\mathbf{k},\mathbf{k}',\mathbf{q}) \langle c_{-\mathbf{k}'+\mathbf{q}\downarrow} c_{\mathbf{k}'\uparrow} - c_{-\mathbf{k}'+\mathbf{q}\uparrow} c_{\mathbf{k}'\downarrow} \rangle \tag{3.4}$$

where $V(\mathbf{k},\mathbf{k}',\mathbf{q})$ is the pairing interaction. Here we choose a d-wave interaction in separable form: $V(\mathbf{k},\mathbf{k}',\mathbf{q}) = V_1 g(\mathbf{k} - \mathbf{q}/2) g(\mathbf{k}' - \mathbf{q}/2)$ with the pairing interaction strength V_1. A complete derivation of this type of interaction is given in appendix D.1. The order parameter $\Delta(\mathbf{k},\mathbf{q})$ represents spin-singlet Cooper pairs with pair momentum $\hbar\mathbf{q}/a$. On the cylinder, the coherent motion of the Cooper pairs is possible only in the azimuthal direction, therefore $\mathbf{q} = (q/R, 0)$ with $q \in \{-N/2+1, \ldots, N/2\}$. The quantum number q is chosen to minimize the free energy. The ϕ-dependence of $\Delta_q(\phi)$ enters through the self-consistency condition and has been discussed extensively in [29] and [32] for s-wave pairing, where $g(\mathbf{k}) \equiv$ const. Since $\Delta_q(\phi)$ varies only little with ϕ, we shall postpone the discussion of the flux-dependence of the d-wave order parameter to the numerical evaluations of section 3.3 and start our analytical calculation with a ϕ and q independent order parameter $\Delta(\mathbf{k},\mathbf{q}) \equiv \Delta(\mathbf{k})$ and $\Delta_q(\phi) \equiv \Delta$. As in our preceding work [32], we take $q = \mathrm{floor}(2\phi + 1/2)$ in a first step, such that $\phi - q/2$ is $\Phi_0/2$

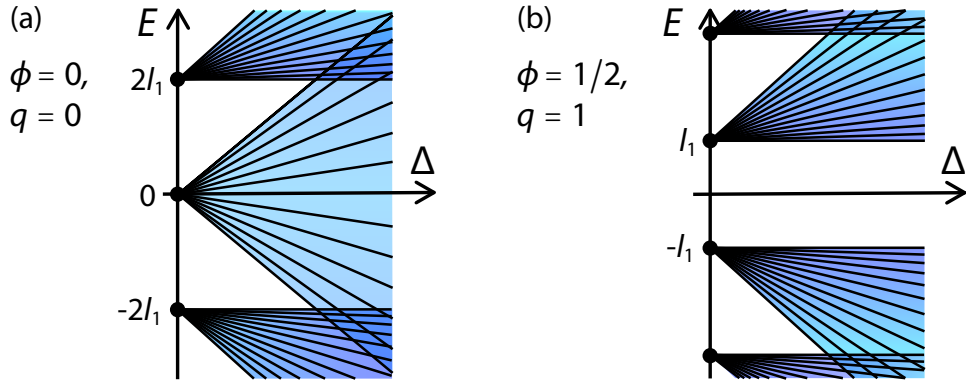

Figure 3.3: Scheme for the evolution of the multiply degenerate energy levels in the normal state with increasing order parameter Δ for the *d*-wave superconducting state. For $\phi = 0$ and $q = 0$ (a), there is a degenerate level $E(\mathbf{k}, 0, 0) = 0$ that splits up for finite Δ into levels spreading between $-\Delta$ and Δ. For $\phi = 1/2$ and $q = 1$ (b), there is an energy gap around $E = 0$ of width $2I_1$, which persists into the superconducting state.

periodic; eventual deviations from this relation will be discussed in section 3.3. Since the Hamiltonian (3.1) is invariant under the simultaneous transformation $\phi \to \phi \pm 1$ and $q \to q \pm 2$, it is sufficient to consider $q = 0$ or 1 and the corresponding flux sectors $-1/4 \le \phi < 1/4$ and $1/4 \le \phi < 3/4$, respectively.

The diagonalization of the Hamiltonian (3.1) leads to the quasi-particle dispersion

$$E_{\pm}(\mathbf{k}, \mathbf{q}, \phi) = \frac{\varepsilon_{\mathbf{k}}(\phi) - \varepsilon_{-\mathbf{k}+\mathbf{q}}(\phi)}{2} \pm \sqrt{\Delta^2(\mathbf{k}) + \varepsilon^2(\mathbf{k}, \mathbf{q}, \phi)}, \tag{3.5}$$

with $\varepsilon(\mathbf{k}, \mathbf{q}, \phi) = [\varepsilon_{\mathbf{k}}(\phi) + \varepsilon_{-\mathbf{k}+\mathbf{q}}(\phi)]/2$. Expanding $E_{\pm}(\mathbf{k}, \mathbf{q}, \phi)$ to linear order in both ϕ/R and q/R gives

$$E_{\pm}(\mathbf{k}, \mathbf{q}, \phi) \approx -e_q(\mathbf{k}) \pm \sqrt{\Delta^2(\mathbf{k}) + \left[\varepsilon_{\mathbf{k}}(0) - l_q(\mathbf{k})\right]^2}, \tag{3.6}$$

where

$$e_q(\mathbf{k}) = \frac{\phi - q/2}{R} 2t \sin k_\varphi \qquad \text{and} \qquad l_q(\mathbf{k}) = \frac{tq}{R} \sin k_\varphi. \tag{3.7}$$

In the normal state $\Delta = 0$, the additive combination of $e_q(\mathbf{k})$ and $l_q(\mathbf{k})$ leads to the $\mathbf{q}$-independent spectrum equation (3.2). For $\Delta > 0$, the spectrum (3.6) differs for even and odd q, except for special ratios of N and M, as discussed above. This difference is crucial for nodal superconducting states, as shown schematically in figure 3.3 (and especially for *d*-wave pairing in figure 3.9): The condition $k_\varphi \approx k_z$ for levels close to E_F causes a level spacing $\delta_F \approx 2l_1(\mathbf{k}_F)$ for small Δ, where $\mathbf{k}_F$ is the Fermi momentum. For N

and M even and $q = 0$, the degenerate energy level at $E = E_\mathrm{F} = 0$ splits into M levels for increasing Δ, which spread between $-\Delta$ and Δ. For $q = 1$, the degenerate levels closest to E_F are located at $E = \pm|l_1(\mathbf{k}_F)|$, thus a gap of $2l_1(\mathbf{k}_F)$ remains in the superconducting spectrum. If N and M are odd, the spectra for even and odd q (figure 3.3 (a) and (b)) are exchanged, and if either N or M is odd, the spectrum is a superposition of (a) and (b).

The gauge invariant circulating supercurrent is given by

$$J(\phi) = \frac{e}{h} \sum_{\mathbf{k},s} v_\mathbf{k} n_s(\mathbf{k}), \tag{3.8}$$

where $v_\mathbf{k} = \partial\varepsilon_\mathbf{k}(\phi)/\partial(Rk_\varphi)$ is the group velocity of the single-particle state with eigenenergy $\varepsilon_\mathbf{k}(\phi)$. The spin independent occupation probability of this state is

$$n_s(\mathbf{k}) = \langle c^\dagger_{\mathbf{k}s} c_{\mathbf{k}s} \rangle = u^2(\mathbf{k},\mathbf{q},\phi) f(E_+(\mathbf{k},\mathbf{q},\phi)) + v^2(\mathbf{k},\mathbf{q},\phi) f(E_-(\mathbf{k},\mathbf{q},\phi)). \tag{3.9}$$

The Bogoliubov amplitudes are

$$u^2(\mathbf{k},\mathbf{q},\phi) = \frac{1}{2}\left[\frac{\varepsilon(\mathbf{k},\mathbf{q},\phi)}{E(\mathbf{k},\mathbf{q},\phi)} + 1\right] \quad \text{and} \quad v^2(\mathbf{k},\mathbf{q},\phi) = \frac{1}{2}\left[\frac{\varepsilon(\mathbf{k},\mathbf{q},\phi)}{E(\mathbf{k},\mathbf{q},\phi)} - 1\right]. \tag{3.10}$$

From equations (3.8) and (3.9), the supercurrent in the cylinder is obtained by evaluating either the sum numerically, as discussed in section 3.3, or from the approximative analytic solution in section 3.2, which allows insight into the origin of the Φ_0-periodicity in nodal superconductors.

3.2 Analytic Solution and Qualitative Discussion

An analytic evaluation of the supercurrent is possible only in the thermodynamic limit where the sum over discrete eigenstates is replaced by an integral. For a multiply connected geometry, this limit is not properly defined because the supercurrent or the Doppler shift vanish in the limit $R \to \infty$. Care is needed to modify the limiting procedure in a suitable way to access the limit of a large but non-infinite radius of the cylinder. In this limit it is mandatory to consider the supercurrent density $j(\phi) = J(\phi)/M$ rather than the supercurrent $J(\phi)$. In this scheme, we treat the density of states as a continuous function in any energy range where the level spacing is $\propto 1/NM$, but we keep the finite energy gap of width $2l_q(\mathbf{k}_F) \propto 1/R \propto 1/N$ around E_F in the odd-q sectors.

For a tight binding energy spectrum as defined in equation (3.2), the density of states is a complete elliptic integral of the first kind. For the purpose of an analytic calculation, a quadratic spectrum with a constant density of states in two dimensions is a more appropriate starting point. We use the expanded form of equation (3.2):

$$\varepsilon_\mathbf{k}(\phi) = t\left[\left(k_\varphi - \frac{\phi}{R}\right)^2 + k_z^2\right] - \mu', \tag{3.11}$$

where $\mu' = \mu + 4t$. The quadratic spectrum (3.11) has no upper bound and the sum in equation (3.8) correspondingly extends from $-\infty$ to ∞ for both k_φ and k_z.

Some algebraic steps are needed to rearrange the sum in equation (3.8) suitably to convert it into an integral. For finite ϕ, $\varepsilon_{\mathbf{k}}(\phi) \neq \varepsilon_{-\mathbf{k}}(\phi)$, and consequently the sum has to be decomposed into a component with $k_\varphi \geq 0$ and a second one with $k_\varphi < 0$. We therefore take $k_\varphi \geq 0$ and write $v_{\mathbf{k}}$ as

$$v_{\pm\mathbf{k}} = \frac{2t}{R}\left(\pm k_\varphi - \frac{\phi}{R}\right) = v_d(\mathbf{k}) \pm v_p(\mathbf{k}), \tag{3.12}$$

where $v_d(\mathbf{k}) = -2t\phi/R^2$ is the diamagnetic contribution and $v_p(\mathbf{k}) = 2tk_\varphi/R$, a paramagnetic contribution, respectively [65].

In a continuous energy integration, the Doppler shift is noticeable only in the vicinity of E_F. On the Fermi surface, k_φ and k_z are related by:

$$k_{\varphi,F}(k_z) = \sqrt{\frac{\mu'}{t} - k_z^2}. \tag{3.13}$$

In this spirit we approximate $e_q(\mathbf{k})$ and $l_q(\mathbf{k})$ by $e_q(k_z) \approx 2t(\phi - q/2)k_{\varphi,F}(k_z)/R$ and $l_q(k_z) \approx tqk_{\varphi,F}(k_z)/R$, respectively. The eigenenergies (3.6) near E_F are thereby rewritten as

$$E_+(\pm k_\varphi, k_z, \mathbf{q}, \phi) = \mp e_q(k_z) + \sqrt{\Delta_{\mathbf{k}}^2 + \left(\varepsilon_{\mathbf{k}}(0) \mp l_q(k_z)\right)^2} \tag{3.14}$$

$$E_-(\pm k_\varphi, k_z, \mathbf{q}, \phi) = \mp e_q(k_z) - \sqrt{\Delta_{\mathbf{k}}^2 + \left(\varepsilon_{\mathbf{k}}(0) \mp l_q(k_z)\right)^2} \tag{3.15}$$

For the evaluation of the supercurrent $J(\phi)$ in equation (3.8), the sum over $\mathbf{k}$ is now replaced by an integral over k_φ and k_z, which is then performed by integrating over the normal state energy ε and an angular variable θ. According to our scheme for replacement of discrete energy levels by a continuous spectrum, the density of states becomes gapless in the limit $M \to \infty$ for $q = 0$, although N is kept finite. For $q = 1$ instead, a k_z-dependent gap $2|l_1(k_z)|$ remains. Thus we replace $\varepsilon_{\mathbf{k}}(0) \mp |l_q(k_z)|$ by the continuous quantity $\varepsilon \pm |l_q(E_\mathrm{F}, \theta)|$. In summary, the procedure is defined by the following steps:

$$\sum_{\mathbf{k}} \xrightarrow{R,M\to\infty} \frac{RM}{2\pi}\int_0^\infty \mathrm{d}k_\varphi \mathrm{d}k_z = \frac{RM}{2\pi}\int_0^\infty \mathrm{d}k k \int_{-\pi/2}^{\pi/2}\mathrm{d}\theta = M\mathcal{N}\int_{-\mu'}^{\mu'}\mathrm{d}\varepsilon\int_{-\pi/2}^{\pi/2}\mathrm{d}\theta, \tag{3.16}$$

where we use the parametrization

$$\begin{pmatrix} k_\varphi \\ k_z \end{pmatrix} = \begin{pmatrix} k\cos\theta \\ k\sin\theta \end{pmatrix} = \sqrt{\frac{\varepsilon + \mu'}{t}}\begin{pmatrix} \cos\theta \\ \sin\theta \end{pmatrix}, \tag{3.17}$$

with $\varepsilon = tk^2 - \mu'$ and where $\mathcal{N} = R/4\pi t$ is the constant density of states in the normal state. The energy integral runs over the whole tight-binding band width $8t$ with the Fermi energy $E_\mathrm{F} = 0$ in the center of the band. Correspondingly, we integrate from $-\mu'$ to μ'. Furthermore, the Doppler shift is parametrized for $\varepsilon \approx E_\mathrm{F}$ as

$$e_q(\theta) = \frac{\phi - q/2}{R} 2t\sqrt{\mu'/t}\cos\theta \qquad \text{and} \qquad l_q(\theta) = \frac{tq}{R}\sqrt{\mu'/t}\cos\theta, \tag{3.18}$$

where the function $l_q(\theta)$ is positive for all allowed values of θ. The supercurrent thus becomes

$$\begin{aligned} j(\phi) &= \frac{1}{M}\frac{e}{h}\left[\sum_{k_\varphi>0,k_z,s} v_\mathbf{k} n_{\mathbf{k}s}(\mathbf{q}) + \sum_{k_\varphi<0,k_z,s} v_\mathbf{k} n_{\mathbf{k}s}(\mathbf{q})\right] \\ &\approx 2\mathcal{N}\frac{e}{h}\int_{-\pi/2}^{\pi/2}\mathrm{d}\theta \int_{-\mu'}^{\mu'}\mathrm{d}\varepsilon\big[n_{q+}(\varepsilon,\theta)v_+(\varepsilon,\theta) + n_{q-}(\varepsilon,\theta)v_-(\varepsilon,\theta)\big], \end{aligned} \tag{3.19}$$

where $n_{q\pm}(\varepsilon,\theta) = n_{\pm\mathbf{k}(\varepsilon,\theta)}(\mathbf{q})$ and $v_\pm(\varepsilon,\theta) = v_{\pm\mathbf{k}(\varepsilon,\theta)}$. The factor 2 in equation (3.19) originates from the spin sum. We collect the terms proportional to $v_d(\varepsilon,\theta) = -2t\phi/R^2$ into a diamagnetic current contribution j_d and the terms proportional to $v_p(\varepsilon,\theta) = 2tk_{\varphi,F}(\varepsilon,\theta)/R$ into a paramagnetic contribution j_p. Using $f(-E) = 1 - f(E)$, equation (3.19) simplifies to

$$j_\mathrm{d} = 4\mathcal{N}\frac{e}{h}\int_{-\pi/2}^{\pi/2}\mathrm{d}\theta \int_{l_q(\theta)}^{\mu'}\mathrm{d}\varepsilon\, v_d(\varepsilon,\theta)\frac{\varepsilon}{\sqrt{\Delta^2+\varepsilon^2}}\big[f(E+e_q(\theta)) - f(-E+e_q(\theta))\big], \tag{3.20}$$

$$j_\mathrm{p} = 4\mathcal{N}\frac{e}{h}\int_{-\pi/2}^{\pi/2}\mathrm{d}\theta \int_{l_q(\theta)}^{\mu'}\mathrm{d}\varepsilon\, v_p(\varepsilon,\theta)\big[f(-E-e_q(\theta)) - f(-E+e_q(\theta))\big], \tag{3.21}$$

where $j_\mathrm{d} = j_\mathrm{d}(q,\phi)$ and $j_\mathrm{p} = j_\mathrm{p}(q,\phi)$. Here, the integration is over positive values of ε only and the lower boundaries of the integration over ε are controlled by $l_q(\theta)$. Since $l_q(\mathbf{k}) = 0$ at the minimum of the band ($\varepsilon = -\mu'$), the upper integral boundary remains μ'. We used the abbreviations $\Delta = \Delta(\theta)$ and $E = E(\varepsilon,\theta) = \sqrt{\Delta^2(\theta)+\varepsilon^2}$. The current j_d turns out to be diamagnetic in the even-q flux sectors and paramagnetic in the odd-q sectors. For even q, it is equivalent to the diamagnetic current obtained from the London equations [55, 66]. The current j_p has always the inverse sign of j_d and is related to the quasi-particle current as shown below. As presented in section 3.1, E displays distinct spectra in the even-q and odd-q flux sectors. To analyze the flux dependent properties of the spectra and the current, we distinguish the case of s-wave pairing (or any other superconducting state with a complete energy gap) and the case of unconventional pairing with nodes in the gap function. For the latter, we focus on d-wave pairing.

3.2.1 *s*-Wave Pairing Symmetry

For s-wave pairing, $\Delta(\varepsilon, \theta) \equiv \Delta$ is constant. Therefore, if we assume that $\Delta \geq e_q(\theta)$ for all θ, the lower energy integration boundaries in equations (3.20) and (3.21) are equal to Δ. Thus $j(\phi)$ is equal in both the even-q and odd-q flux sectors and the flux periodicity is $\Phi_0/2$. However, if $\Delta < \max_\theta e_q(\theta)$, equation (3.8) has to be evaluated exactly, the procedure and results of which have been presented in [32].

With $\varepsilon = \sqrt{E^2 - \Delta^2}$, equations (3.20) and (3.21) transform into integrals over E with $\mathrm{d}\varepsilon = D_s(E)\,\mathrm{d}E$, where

$$D_s(E) = \frac{\partial \varepsilon}{\partial E} = \begin{cases} E\,(E^2 - \Delta^2)^{-1/2} & \text{for} \quad E \geq \Delta \\ 0 & \text{for} \quad E < \Delta \end{cases} \tag{3.22}$$

is the superconducting density of states for s-wave pairing. This leads to

$$j_\mathrm{d} = 4\mathcal{N}\frac{e}{h}\int_{-\pi/2}^{\pi/2}\mathrm{d}\theta\int_\Delta^{\mu'}\mathrm{d}E v_d\left(\sqrt{E^2-\Delta^2},\theta\right)\left[f(E+e_q(\theta)) - f(-E+e_q(\theta))\right], \tag{3.23}$$

$$j_\mathrm{p} = 4\mathcal{N}\frac{e}{h}\int_{-\pi/2}^{\pi/2}d\theta\int_\Delta^{\mu'}dE D_s(E) v_p\left(\sqrt{E^2-\Delta^2},\theta\right)\left[f(-E-e_q(\theta)) - f(-E+e_q(\theta))\right]. \tag{3.24}$$

At $T = 0$, we find

$$j_\mathrm{d} = -4\mathcal{N}\frac{e}{h}\int_{-\pi/2}^{\pi/2}\mathrm{d}\theta\int_\Delta^{\mu'}\mathrm{d}E\,2t\frac{\phi - q/2}{R^2} = -2(\mu' - \Delta)\frac{e}{h}\frac{\phi - q/2}{R}, \tag{3.25}$$

$$\begin{aligned} j_\mathrm{p} &= 4\mathcal{N}\frac{e}{h}\int_{-\pi/2}^{\pi/2}\mathrm{d}\theta\int_\Delta^{e_q(\theta)}\mathrm{d}E D_s(E)\frac{2t}{R}\sqrt{\frac{\varepsilon+\mu'}{t}}\cos\theta \\ &= \frac{8t\mathcal{N}}{R}\frac{e}{h}\sqrt{\frac{\mu'}{t}}\int_{-\pi/2}^{\pi/2}\mathrm{d}\theta\cos\theta\int_\Delta^{e_q(\theta)}\mathrm{d}E D_s(E) + O\left(\frac{\varepsilon}{t}\right)^2. \end{aligned} \tag{3.26}$$

In the integral of j_p, the inequality $\varepsilon/t \ll 1$ applies, and terms of order $O(\varepsilon/t)^2$ are negligible.

The current j_d becomes independent of the superconducting density of states. Its size is essentially proportional to E_F, as long as $\mu' \gg \Delta$ holds. The paramagnetic current j_p depends on the absolute value of the order parameter and on its symmetry.

If $\Delta > e_q(\theta)$ for all values of θ, then $j_\mathrm{p} = 0$ and the supercurrent $j(\phi) = j_\mathrm{d}$ consists of the diamagnetic part only. For $T > 0$, j_d decreases slightly, but remains of the same order of magnitude. The current j_p increases with increasing T and reaches its maximum value at T_c. For finite temperatures j_p is usually denoted as the quasi-particle current.

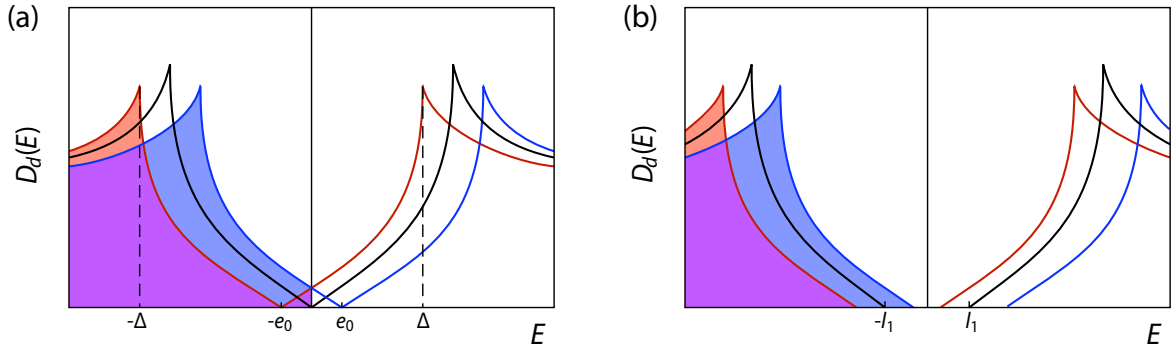

Figure 3.4: Scheme for the density of states of a *d*-wave superconductor for $\phi = 1/4$, where $e_q(1/4) = l_1/2$. The center of mass angular angular momentum $\hbar q/aR$ of the Cooper pairs is (a) $q = 0$ and (b) $q = 1$. The energies are Doppler shifted to higher (red) or lower energies (blue). This results in a double-peak structure and for $q = 0$ in an overlap of the upper and lower "band" in the region $-e_0 < E < e_0$ [68] and states in the upper band become partially occupied. For $q = 1$ there is a gap l_1 of the size of the maximum Doppler shift at $\phi = 1/4$. The black line represents the density of states (a) for $\phi = 0$ and (b) for $\phi = 1/2$.

The entire supercurrent is always the sum of the diamagnetic current j_d and the quasi-particle current j_p, and therefore decreases with temperature and vanishes at T_c [67]. The quasi-particle current has the same flux periodicity as the supercurrent, even though it is carried by single quasiparticle excitations. In the normal state ($\Delta = 0$),

$$\begin{aligned} j_\mathrm{p} &= \frac{8t\mathcal{N}}{R}\frac{e}{h}\sqrt{\frac{\mu'}{t}}\int_{-\pi/2}^{\pi/2} \mathrm{d}\theta \cos\theta \int_0^{e_q(\theta)} \mathrm{d}E = 4\mu'\frac{e}{h}\frac{\phi - q/2}{R\pi}\int_{-\pi/2}^{\pi/2}\mathrm{d}\theta\cos^2\theta \\ &= 2\mu'\frac{e}{h}\frac{\phi - q/2}{R}, \end{aligned} \tag{3.27}$$

which cancels j_d exactly in the limit $M \to \infty$. [1]

3.2.2 Unconventional Pairing with Gap Nodes

For a more general order parameter $\Delta(\theta)$, an analytic solution of equations (3.20) and (3.21) is hard to obtain. For *s*-wave symmetry, j_d depends only weakly Δ; j_d is indeed maximal for $\Delta = 0$. Equation (3.25) for j_d is valid also for unconventional order parameter symmetries. Physically, j_d reflects the difference in the density of states of quasi-particle states with orbital magnetic moment parallel and anti-parallel to the external magnetic field. The first group of states is Doppler shifted to lower energies, whereas the latter

[1] In this procedure, the normal persistent current vanishes, but this is unproblematic here because the normal current above T_c is exponentially small for $T_\mathrm{c} \gg \delta_F$.

is Doppler shifted to higher energies. This is schematically shown in figure 3.4 for d-wave pairing (c.f. [68]). In this picture, j_d is proportional to the difference between the area beneath the red and and blue curves representing the density of states arising of bands $E_-(\pm|\mathbf{k}|, \mathbf{q}, \phi) < 0$ (underlaid red and blue). Therefore we approximate j_d for $\Delta(\theta) \ll \mu' = E_\mathrm{F} + 4t$ by

$$j_\mathrm{d} = -2\mu' \frac{e}{h} \frac{\phi - q/2}{R}, \tag{3.28}$$

as given by equation (3.25) with $\Delta = 0$. On the other hand, j_p is represented by the occupied quasi-particle states in the overlap region of $E_+(\mathbf{k}, \mathbf{q}, \phi)$ and $E_-(\mathbf{k}, \mathbf{q}, \phi)$ with width $2e_q(\mathbf{k}_F)$. It is therefore strongly dependent on the characteristic density of states in the vicinity of E_F. In figure 3.4 (a), which refers to even q, the current j_p is determined by the small triangular patch where the upper and lower bands overlap. For odd q, the two bands do not overlap, therefore $j_\mathrm{p} = 0$.

We will now analyze such a scenario for d-wave pairing. With an order parameter $\Delta_\mathbf{k} = \Delta(k_\varphi^2 - k_z^2) \approx \Delta \cos 2\theta$. Again, we assume $\Delta > e_q(\theta)$ for all θ; then the integral in equation (3.21) contains only the nodal states closest to E_F, for which the d-wave symmetry demands $k_\varphi \approx k_z$. Jointly with equation (3.13) this condition fixes the Doppler shift at E_F to the $\mathbf{k}$-independent value $e_q = (\phi - q/2)\sqrt{2t\mu'}/R$ and $l_q = (q/R)\sqrt{t\mu'/2}$. With the density of states in the d-wave superconducting state

$$D_d(E) = \frac{1}{\sqrt{E^2 - \Delta^2 \cos^2 2\theta}}, \tag{3.29}$$

equation (3.21) for the paramagnetic current j_p at $T = 0$ then takes the form

$$j_\mathrm{p} = 4\mathcal{N} \frac{e}{h} \int_{l_q}^{e_q} \mathrm{d}E \int_{-\pi/2}^{\pi/2} \mathrm{d}\theta D_d(E) \frac{2t}{R} \sqrt{\frac{\varepsilon + \mu'}{t}} \sin\theta. \tag{3.30}$$

In the odd-q flux sectors, $l_q \geq e_q$ for all values of ϕ, therefore $j_\mathrm{p} = 0$. In the $q = 0$ sector, $l_q = 0$ and

$$\begin{aligned} j_\mathrm{p} &\approx \frac{2e}{h\pi} \sqrt{\frac{\mu'}{t}} \int_0^{e_q} \mathrm{d}E \int_{-\pi/2}^{\pi/2} d\theta \sin\theta \frac{1}{\sqrt{E^2 - \Delta^2 \cos^2 2\theta}} \approx \frac{2e}{\pi h} \sqrt{\frac{\mu'}{t}} \int_0^{e_q} \mathrm{d}E \frac{E}{\Delta} \\ &= \frac{e}{\pi h \Delta} \sqrt{\frac{\mu'}{t}} e_q^2 = \frac{2}{\pi\Delta} \sqrt{t\mu'^3} \frac{e}{h} \left(\frac{\phi - q/2}{R} \right)^2, \end{aligned} \tag{3.31}$$

where the same approximations as in the s-wave case are applied. The dominant contribution to the angular integral over θ originates from the nodal parts, where the integrand

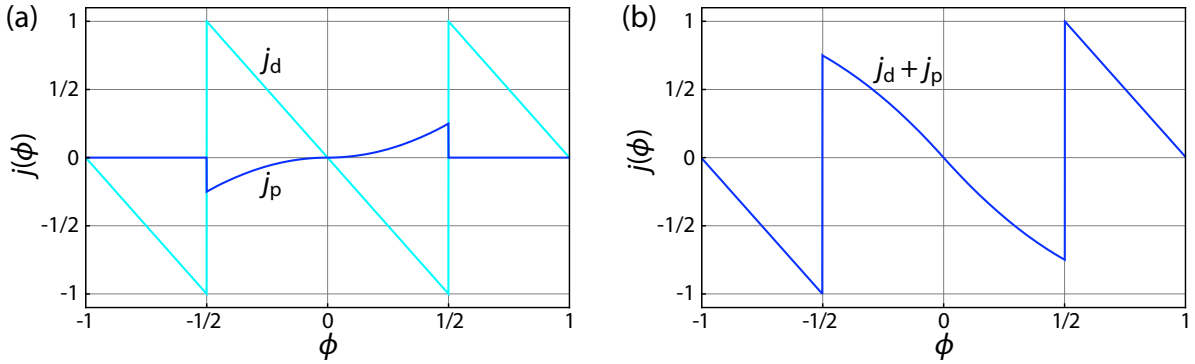

Figure 3.5: The supercurrent density $j(\phi) = j_d + j_p$ in a thin d-wave cylinder as a function of flux ϕ (arbitrary units). Shown is the result of the analytical model [equation (3.34)] for the characteristic value $b = 0.4$. For $-1/4 < \phi < 1/4$, where $q = 0$, the current is reduced by a contribution proportional to ϕ^2, whereas it is linear in ϕ otherwise. This gives rise to an overall flux periodicity of Φ_0.

can be linearized in θ, such that the integral can be performed approximately (see e.g. [58]).

In the even-q sectors, the total current $j(\phi) = j_d + j_p$ finally becomes

$$j(\phi) = -2\mu' \frac{e}{h} \frac{\phi}{R} \left[1 - \frac{\sqrt{t\mu'}}{\pi\Delta} \frac{\phi}{R} \right], \tag{3.32}$$

which results in the ratio

$$\frac{j_p}{j_d} = \frac{\sqrt{t\mu'}}{\pi\Delta} \frac{\phi}{R} \equiv b\phi \tag{3.33}$$

of the two current components.

In the odd-q flux sectors, $j_p = 0$ and the supercurrent is $j(\phi) = j_d$. As a function of ϕ, $j(\phi)$ is consequently Φ_0 periodic; within one flux period from $-1/2$ to $1/2$ we represent it as

$$j(\phi) = -2\frac{\mu'}{R}\frac{e}{h} \begin{cases} \phi + 1/2 & \text{for } -1/2 \le \phi < -1/4, \\ \phi(1 - b\phi) & \text{for } -1/4 \le \phi < 1/4, \\ \phi - 1/2 & \text{for } 1/4 \le \phi < 1/2, \end{cases} \tag{3.34}$$

(c.f. figure 3.5). The amount by which the supercurrent differs in the even-q and odd-q flux sectors is represented best in the form of Fourier components: the n-th Fourier component of $j(\phi)$ is $j_n = \int_{-1/2}^{1/2} d\phi\; j(\phi) e^{2\pi i n \phi}$. Here, we denote the first Fourier component by j_1, and the second Fourier component by j_2 and obtain

$$j_1 = -2\frac{\mu'}{R}\frac{e}{h} b \frac{8 - \pi^2}{16\pi^3} \qquad \text{and} \qquad j_2 = -2\frac{\mu'}{R}\frac{e}{h}\frac{4\pi i - b}{16\pi^2}. \tag{3.35}$$

To leading order in $1/R$, the ratio of the Φ_0 and the $\Phi_0/2$ Fourier component therefore is

$$\left|\frac{j_1}{j_2}\right| = \frac{\pi^2 - 8}{4\pi^2}\frac{\sqrt{2t\mu'}}{\Delta R} \xrightarrow{\mu=0} \approx 0.07\frac{2t}{\Delta R} \tag{3.36}$$

and scales with the inverse ring diameter. This $1/R$ law is the direct consequence of the d-wave density of states $D_d(E) \propto E$. For some other unconventional superconducting states with $D(E) \propto E^n$ in the vicinity of E_F, the decay of the j_1 Fourier component results in a $1/R^n$ law. Using equation (3.36) to estimate this ratio for a mesoscopic cylinder with a circumference $Ra = 2600a \approx 1\,\mu\mathrm{m}$ and a ratio $\Delta/t = 0.01$, we obtain $j_1/j_2 \approx 0.03$.

3.3 Numerical Solution for d-Wave Pairing at $T = 0$

In this section we evaluate numerically the supercurrent in equation (3.8) together with the self-consistency condition

$$\frac{1}{V_1} = \frac{1}{NM}\sum_{\mathbf{k}'}\frac{g^2(\mathbf{k}-\mathbf{q}/2)}{2\sqrt{\Delta_q^2(\phi)g^2(\mathbf{k}-\mathbf{q}/2)+\varepsilon^2(\mathbf{k}',\mathbf{q},\phi)}}\left[f(E_-(\mathbf{k}',\mathbf{q},\phi)-f(E_+(\mathbf{k}',\mathbf{q},\phi)\right], \tag{3.37}$$

where the d-wave pairing symmetry follows from

$$g(\mathbf{k}) = \cos(k_\varphi - q/2R) - \cos k_z \tag{3.38}$$

and the order parameter is $\Delta(\mathbf{k},\mathbf{q}) = \Delta_q(\phi)g(\mathbf{k}-\mathbf{q}/2)$. Here we take into account the full q- and ϕ-dependence of $\Delta_\mathbf{k}(\mathbf{q},\phi)$. The q-dependence of $g(\mathbf{k}-\mathbf{q}/2)$ is essential to ensure the invariance of the gap equation (3.37) under the replacement $\phi \to \phi \pm 1$ and $q \to q \pm 2$ (see appendix D.1). At those flux values for which the total energies (derived in appendix D.3)

$$E(\phi) = \sum_{\mathbf{k},s}\varepsilon_\mathbf{k}(\phi)n_s(\mathbf{k}) + \frac{\Delta_q(\phi)}{V_1}. \tag{3.39}$$

are equal, q advances to the next integer. This flux value may deviate from the values $\phi = (2n-1)/4$, for which we fixed the q-sector transitions in section 3.1.

Loops of d-wave superconductors can be arranged in two different ways. In a first choice for the geometry the order parameter winds jointly with the lattice around a hole such that the phase of the order parameter remains constant on the selected path. The cylinder geometry described here is an example for this choice. The second option is to fix the orientation of the lattice and to cut out a hole. Then the phase of the order parameter

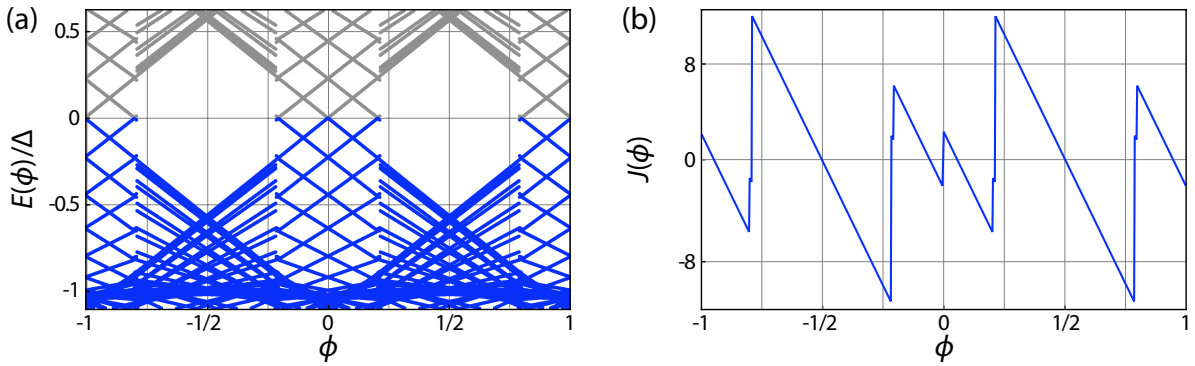

Figure 3.6: Energy spectrum and supercurrent $J(\phi)$ in a cylinder with circumference of $N = 56$ and height of $M = 28$ and $\Delta = \Delta_q(\phi = 0) \approx 0.1t$. The blue lines represent occupied states which form the condensate, whereas the grey lines represent empty states. The spectrum (a) is similar to the one obtained in [26] for a square frame geometry. Clearly visible is the energy gap in the odd-q flux sectors, whereas in the even-q flux sectors states cross the Fermi energy upon changing the flux. At these crossing points, a jump in the supercurrent is observed (b). Compare to figures 5.4 and 5.5 showing the spectrum and supercurrent in a square frame.

rotates by 2π on any closed path encircling the hole once. This will be investigated with a square frame in part II and was also considered in the one dimensional model in [34]. These two arrangements are in fact physically equivalent. The square frame geometry ensures the right number of lattice sites for the maximum difference in the spectrum of the even-q and odd-q flux sectors, as discussed in section 3.1. For a direct comparison to the cylinder geometry, we chose a cylinder with $N = 56$ and $M = 28$, which has the same hole diameter as the square frame in [26], and the ratio $N/M = 2$ produces qualitatively the same energy spectrum. The resulting spectrum is shown in figure 3.6 (a). It has indeed the same characteristic features as in the square frame geometry. An energy gap of the same order of magnitude exists in the odd-q flux sectors, and the density of states in the even-q flux sectors is gapless. There are no hybridization effects in the spectrum of the cylinder, since it preserves the full rotational symmetry. The features mentioned above are also in agreement with the qualitative discussion of section 3.2. Clearly visible in figure 3.6 (b) are the jumps in the supercurrent whenever an energy level crosses E_F, and the offset in the flux value for which q switches (large jumps). This offset depends in a complex way on the system size and the pairing potential strength, but generally decreases for larger values of N, M, and V_1.

The spectrum and the supercurrent in figure 3.6 display the expected signatures of discreteness which are not captured by the analytic analysis of section 3.2. The important parameter is obviously the size of the level spacing. Explicitly we take a closer look at a cylinder with $N = M = 2600$, and thus a circumference of the order of 1 µm. The

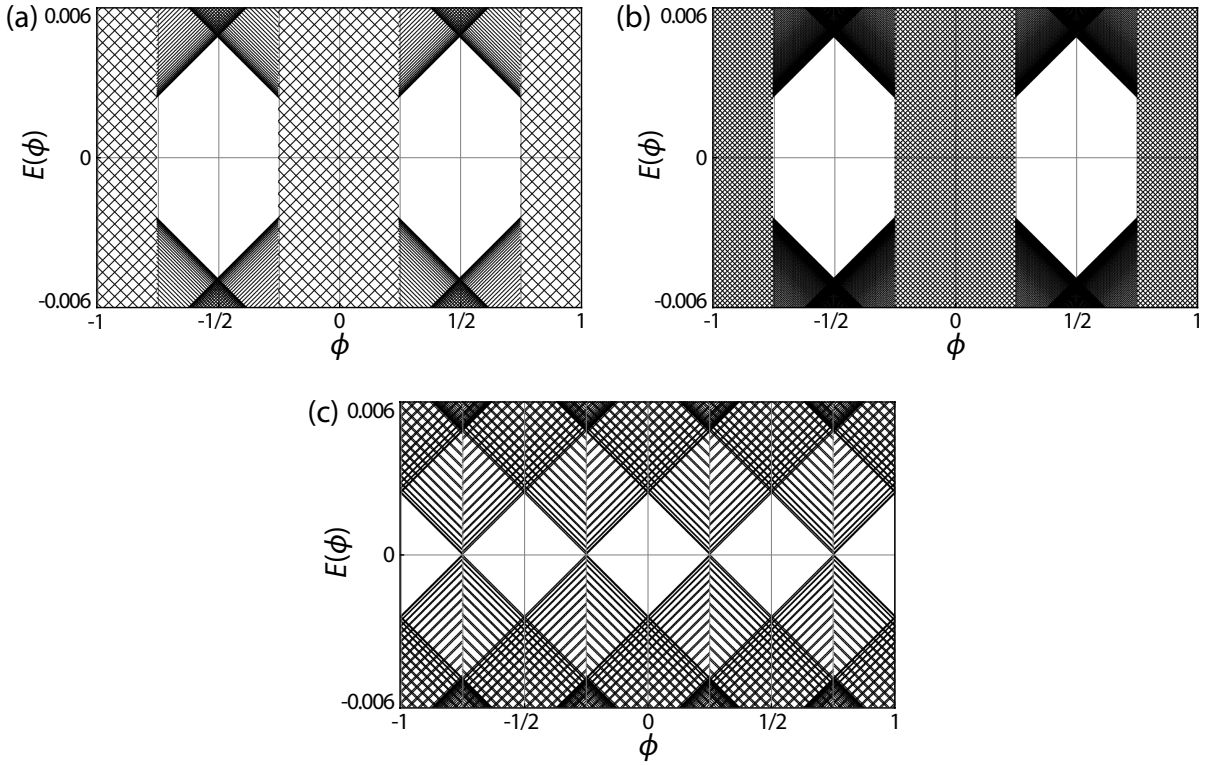

Figure 3.7: A section of the energy spectrum around E_F. (a) and (b) show the spectra of a cylinder with $N = M = 2600$. (a) $V_1 = 0.4t$ and $\Delta \approx 0.05t$; (b) $V_1 = 0.2t$ and $\Delta \approx 0.02t$. The energy gap $l_1 \ll \Delta_q(\phi)$ for these systems and all the states shown have the same Doppler shift (all lines are parallel / perpendicular). The density of states is quasi continuous in the even-q flux sectors and grows linearly with decreasing $\Delta_q(\phi)$. (c) shows the $\Phi_0/2$-periodic spectrum of a cylinder with $N = 2600$ and $M = N + 1$.

calculated spectra are shown in figure 3.7 (a) and (b) for different pairing potentials, resulting in (a) $\Delta_q(\phi) \approx 0.05t$ and (b) $\Delta_q(\phi) \approx 0.02t$. The qualitative features ot the much smaller cylinder remain, but the gap l_1 in the odd-q flux sectors is smaller, because l_1 decreases with $1/N$. In the even–q flux sectors, there are M levels spread out between $-\Delta_q(\phi)$ and $\Delta_q(\phi)$, which leads to an increase in the density of states around E_F with decreasing $\Delta_q(\phi)$ for fixed N and M. The representation with a continuous density of states is therefore appropriate for $\Delta_q(\phi) \ll t$, which is fulfilled well in figure 3.7 (b). Figure 3.7 (c) shows the spectrum for $M - 1 = N = 2600$, which is almost identical in even-q and odd-q flux sectors. There is still a gap for non-integer (or half-integer) values of ϕ, but it is equally distributed in the even-q and odd-q sectors. Other choices of N and M produce mixed features of the spectra in figure 3.7 (a) and 3.7 (c). All the energy levels shown in each part of figure 3.7, which belong to nodal states, have apparently the same derivative with respect to ϕ.

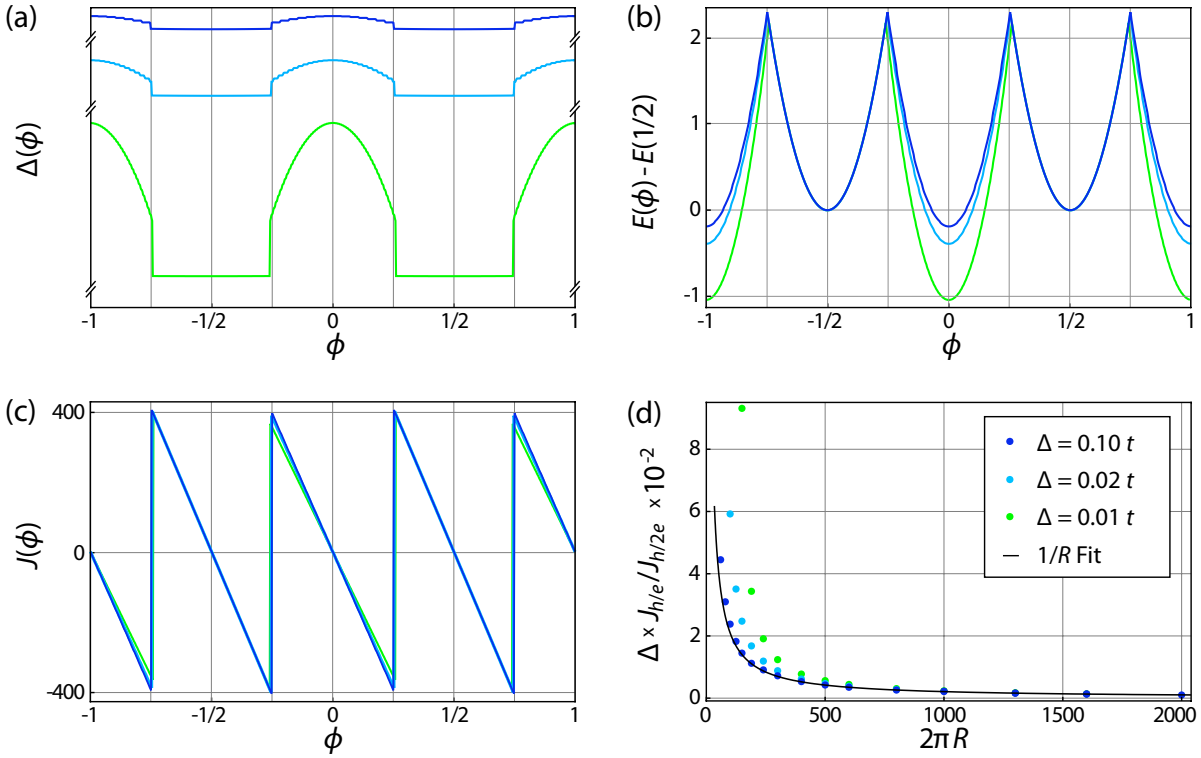

Figure 3.8: (a-c) Self-consistent order parameter $\Delta_q(\phi)$, energy $E(\phi)$ and supercurrent $J(\phi)$ plotted as a function of flux ϕ for $V_1 = 0.25t$ (blue), $V_1 = 0.2t$ (turquoise), and $V_1 = 0.15t$ (green). $\Delta_q(\phi)$ and $E(\phi)$ are shown in units of t and $J(\phi)$ in units of t/Φ_0. The oscillations of all quantities are $\propto 1/R$ and of the order of t for $E(\phi)$. The amplitude of the oscillations in $\Delta_q(\phi)$ are rather small. For $V_1 = 0.25t$, $\Delta_q(\phi) \approx 0.036t$ with an oscillation amplitude $\delta\Delta = [\Delta_0(0) - \Delta_1(1/2)]/\Delta_0(0) \approx 10^{-8}$, $\Delta_q(\phi) \approx 0.02t$ and $\delta\Delta \approx 5 \times 10^{-6}$ ($V_1 = 0.2t$), and $\Delta_q(\phi) \approx 0.009t$ and $\delta\Delta \approx 4 \times 10^{-5}$ ($V_1 = 0.15t$). (d) Ratio of the first and second Fourier components of the supercurrent as a function of the cylinder radius R for fixed values of Δ. The height M of the cylinder is equal to $N = 2\pi R$, which yields the maximum values for J_1. For N larger than some Δ-dependent number (see main text), the results of the exact evaluations fit very well to the prediction of equation (3.36) (black line).

The small level spacing in the μm sized cylinders results in solutions $\Delta_q(\phi)$ of the gap equation (3.37), which are nearly constant [figure 3.8 (a), note the vertical scale discussed in the figure caption]. The ϕ-dependence of the energy $E(\phi)$ also becomes small, whereas the small difference for even-q and odd-q remains important for the supercurrent $J(\phi)$. Since $J(\phi) \propto \partial E(\phi)/\partial\phi$, the differences in $E(\phi)$ imply different current amplitudes in the even and odd q sectors [see figure 3.8 (b) and (c)]. This effect is larger for smaller $\Delta_q(\phi)$, because the number of energy levels crossing E_F increases with decreasing $\Delta_q(\phi)$. For the chosen pairing potentials V_1, the difference of the amplitudes of $J(\phi)$ for even and odd q are of the order of a few percent. Per contra, the current

jumps within a q-sector are tiny for the large radius of the μm-size cylinders. However, the resulting $\Delta_q(\phi)$ is considerably larger than in the d-wave cuprate superconductors.[2] Consequently, the upper limit for the difference of $J(\phi)$ in the even-q and odd-q sectors would be larger in the cuprate superconductors than in the model system calculated here. The offset in the jump of $J(\phi)$ from the flux values $\phi = (2n-1)/4$ is resolved for the smallest V_1 in figure 3.8. However, at low temperatures the superconducting state for each q becomes metastable for those flux values, for which it is not the groundstate. At which flux values such a metastable state decays into the groundstate is not clear and the position of the jump in the supercurrent can vary in experiments.

We now compare the R-dependence of the ratio of the first and second Fourier components J_1/J_2 analogous to section 3.2. This is shown in figure 3.8 (d) for different values of V_1. The ratio is in excellent agreement with equation (3.36) for system sizes larger than a few hundred lattice constants. For smaller systems, J_1 becomes larger than predicted by the $1/R$ size dependence. The scale which decides about the validity of the approximations used in section 3.2 is the ratio of the level spacing and $\Delta_q(\phi)$. Equation (3.36) therefore holds, if the prefactor of ϕ in equation (3.33) is small, that is, if $\sqrt{8}\,t \ll \pi\Delta R$, because t/R is proportional to the level spacing of the nodal states. For a cylinder with radius $Ra = 2600a \approx 1\mu\text{m}$ and $\Delta_q(\phi)/t \approx 0.01$, we obtain the ratio $J_1/J_2 \approx 0.04$, which is almost identical with the result of section 3.2.

3.4 Periodicity Crossover for small Δ

So far we always assumed that $\Delta_q(\phi) \gg e_q(\phi)$ and concluded that variations in $\Delta_q(\phi)$ are negligible. But if $\Delta_q(\phi)$ is of the same order as the Doppler shift $e_q(\phi)$, the situation changes dramatically. This is the case, if either the radius R of the cylinder is very small, or the pairing potential V_1 is small or the temperature T is close to T_c. Here, we analyze the flux periodicity and the crossover from a "small-gap" to a "large gap" regime by increasing V_1 from zero to higher values at $T = 0$, and by lowering T through T_c for fixed V_1. As mentioned above, the amplitude of the oscillations, especially those of $\Delta_q(\phi)$, become very small for increasing R. For very large R, the periodicity crossover takes place within a tiny range of V_1 or T, respectively. To observe the crossover more comfortably in a larger window of V_1 or T, we use smaller systems here.

The mechanism of the periodicity crossover at $T = 0$, controlled by V_1, is best discussed by analyzing the total energy $E(\phi)$ [figure 3.9 (b)]. It differs little from the crossover in s-wave superconductors, for which it was investigated in [32]. In the normal state ($V_1 = 0$), $E(\phi)$ is q-independent and consists of an Φ_0 periodic series of parabolae. For

[2] Angle-resolved photoemission spectroscopy on various cuprates suggests a tight-binding $t \approx 200$ meV – 400 meV. The gap at the antinodes, obtained from tunneling spectra, varies between 10 meV and 50 meV [69,70], therefore $\Delta \approx 0.002t - 0.01t$.

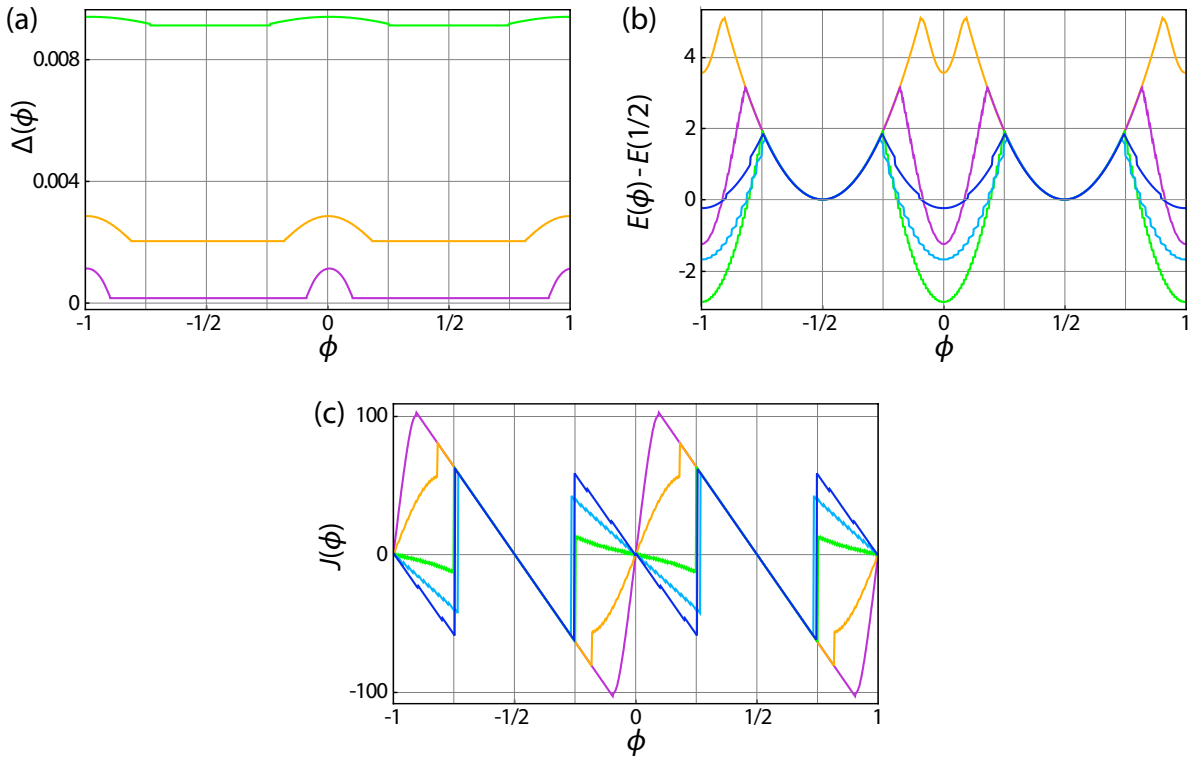

Figure 3.9: Periodicity crossover at $T = 0$ in a cylinder with $N = M = 400$ for $V_1 = 0.40t$ (blue), $V_1 = 0.2t$ (turquoise), $V_1 = 0.15t$ (green), $V_1 = 0.1t$ (orange) and $V_1 = 0.07t$ (purple). For $V = 0.1t$ and $V = 0.07t$, $\Delta_q(\phi)$ is smaller than the Doppler shift for all ϕ, thus $J(\phi)$ approaches the Φ_0-periodic normal persistent current.

increasing V_1, a new minimum in $E(\phi)$ forms at the crossing points of two parabolae. This minimum moves downward in energy until this new parabolic arc crosses the neighboring parabolae at the flux values $\phi = (2n-1)/4$. The energies of the old and the new minima are generally different for any finite system, but they approach each other when $\Delta_q(\phi) \gg \delta_F$. In the odd-$q$ flux sectors, $\Delta_q(\phi)$ is nearly constant because no energy levels cross E_F, whereas in the even-q sectors, levels cross E_F for all values of V_1. This causes the wiggles in $E(\phi)$ and the decrease of $\Delta_q(\phi)$ with increasing ϕ [figure 3.9 (a)]. For the smallest two values shown in figure 3.9 (a), $\Delta_q(\phi)$ approaches zero as a function of ϕ for even q; for this reason the odd-q states extend far into the even-q flux sectors. With increasing V_1, the nearly $\Phi_0/2$ periodic sawtooth pattern of the supercurrent evolves from the Φ_0 periodic normal persistent current [figure 3.9 (c)].

The temperature controlled crossover at T_c is analogous to the crossover controlled by V_1, but the finite temperature has quenched all the effects of discreteness as well as the gap in the odd-q flux sectors. This means that the deviations from the $\Phi_0/2$ periodicity are invisible in figure 3.10. Deviations appear with decreasing temperature as

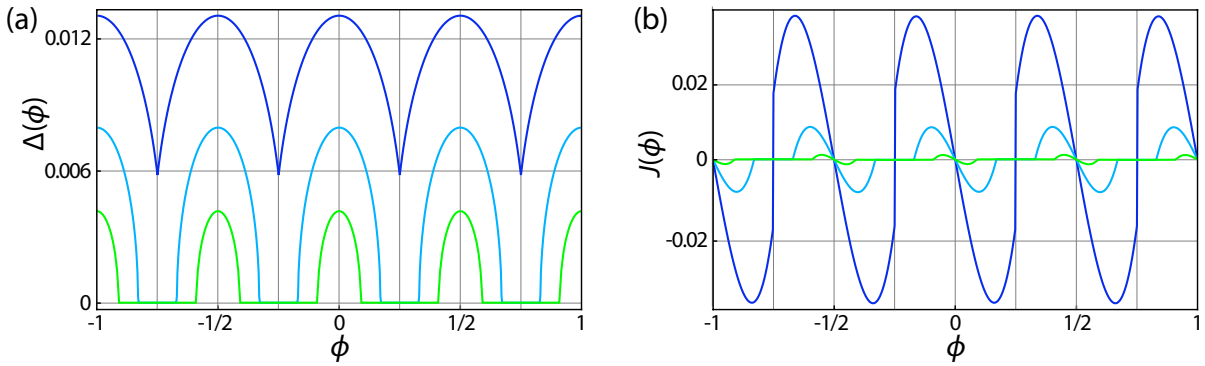

Figure 3.10: Temperature driven periodicity crossover for fixed $V_1 = 0.4t$ in a cylinder with $N = M = 100$ for $T = 0.1863t$ (blue), $T = 0.1870t$ (turquoise) and $T = 0.1873t$ (green). The amplitude of the normal persistent current in the sectors with $\Delta_q(\phi) = 0$ is much smaller than for $\Delta_q(\phi) > 0$ and is invisible on this plot scale.

T approaches l_1. The supercurrent decreases linearly with increasing T until it reaches the exponentially small value of the normal persistent current at $T = T_c$ [figure 3.10 (b)] [67]. This suppression as well as the suppression of $\Delta_q(\phi)$ with temperature [figure 3.10 (a)] differ only little from those of s-wave superconductors. The only qualitative difference is, that a characteristic temperature T^* exists for s-wave superconductors, below which $\Delta(\phi = 0)$ is larger than the maximum Doppler shift. This is equivalent to a coherence length $\xi(T^*) = 2Ra$ [32]. Below T^*, $\Delta(\phi) > 0$ for all ϕ in s-wave superconductors, and the thermodynamic quantities are therefore not affected by the Doppler shift. The relation $\Delta(\phi = 0, T = 0) \approx 1.75 T_c$ leads to the estimate

$$\frac{T_c - T^*}{T_c} \approx \frac{E_F^2}{3.1 T_c^2 R^2}. \tag{3.40}$$

For d-wave pairing, there is no such characteristic temperature because of the nodal states, but in analogy we can define T^* as the crossover temperature below which $\Delta_q(\phi) > 0$ for all ϕ. Analogously to the s-wave case, we denote this situation as the "large-gap" regime. For temperatures $T^* < T < T_c$, $\Delta_q(\phi)$ approaches zero for certain values of ϕ, which we call the "small-gap" regime. Since for a d-wave superconductor with nearest neighbor hopping $\Delta(\phi = 0, T = 0) > 1.75 T_c$ [71], one expects that $T_c - T^*$ is also larger and the crossover broader than for s-wave pairing.

3.5 Conclusions

We have shown that in rings of unconventional superconductors with gap nodes, there is a paramagnetic, quasi-particle-like contribution $j_p > 0$ to the supercurrent at $T = 0$.

This current is generated by the flux induced "reoccupation" of nodal quasiparticle states slightly below and above E_F. Formally a coherence length $\hbar v_F/\Delta(\mathbf{k},\mathbf{q}) > 2R$ can be ascribed to these reoccupied states, which are therefore affected by the symmetry of the system, however large the number of lattice sites is. If the normal state energy spectrum has a flux periodicity of Φ_0, than the superconducting spectrum is Φ_0 periodic, too. The normal state spectrum of a cylinder with a discrete lattice strongly depends on the number of lattice sites on the cylinder. This problem is characteristic for rotationally symmetric systems and is much less pronounced in geometries with lower symmetry, such as the square frame discussed in part II. In such systems, the addition or removal of a small number of lattice sites or impurities do not change the spectrum qualitatively. For an experimental arrangement where the difference in even and odd flux values is as large as possible, a square loop would be preferable. Our results obtained in section 3.2 and section 3.3 for the periodicity of the physical quantities $\Delta_q(\phi)$, $E(\phi)$, and $J(\phi)$ provide therefore an upper limit for the Φ_0 periodic components.

The Φ_0 periodicity is best visible in the current component j_p at $T = 0$. For d-wave-pairing $j_\mathrm{p} \propto 1/R^2$, and the Φ_0 periodic Fourier component decays like the inverse radius of the cylinder, relative to the $\Phi_0/2$ periodic Fourier component. The lack of a characteristic length scale in nodal superconductors, such as the coherence length for s-wave pairing, generates this algebraic decay with increasing R. Although j_p is larger for small Δ, it almost vanishes close to T_c, if $\Delta \gg \delta_F$, and variations of T_c with flux, as in the Little-Parks experiment [14,15], do not differ for s- and d-wave superconductors.

A possible set-up for the experimental detection of the Φ_0 periodicity of the supercurrent is the insertion of Josephson junctions onto the cylinder, thereby creating a SQUID. The oscillations of the SQUID's critical current have the same flux periodicity as the circulating supercurrent. The relation to the effect described here however is not established yet, because of the unknown influence of the Josephson junctions. A step in this direction is provided in chapter 7, where the current-phase relation of Josephson junctions is analyzed in real space.

A different approach to study the crossover from the normal persistent current to the supercurrent in a ring was proposed by Büttiker and Klapwijk [72] and later by Cayssol *et al.* [73]. They analyzed a normal metal ring with an s-wave superconducting segment of variable length l. The energy spectrum, which they found, depends on l in a similar way as it does in our analysis on the radius R. In this set-up, Φ_0 periodicity should be found if $l < \xi_0$, although the ring diameter is much larger than ξ_0. Analogously, we expect the ratio j_1/j_2 of the first and second Fourier component the supercurrent to be proportional to $1/l$ for a d-wave superconducting segment. This might be of advantage for experimental detection.

Part II

Real Space: The Bogoliubov - de Gennes Equations

Introduction to Part II:

So far we have presented the principles of the crossover from Φ_0 to $\Phi_0/2$ flux periodicity in conventional and unconventional superconductors and the mechanisms that leads to the persistence of Φ_0 periodicity in large loops of nodal superconductors. Here we present an approach to this topic in real space: the Bogoliubov - de Gennes equations, which we introduce in chapter 4. The information we obtain from this technique is in some sense complementary to that obtained in part I from the momentum space formulation. The latter proved useful to understand the physical concepts and the description of large systems, even the derivation of an analytical model. The prize paid was the restriction to highly symmetric systems with their intriguing energy spectra in the normal state. Is the Φ_0 periodicity detectable in realistic system setups, or is it rather an artifact of the high degeneracy of energy levels in clean and highly symmetric systems? On the other hand, using the Bogoliubov - de Gennes equations in real space, we can easily determine the spectrum of "natural" system geometries with reduced symmetry or systems containing lattice defects, impurities, magnetic fields or further correlations in real space. Computational power however restricts the system size, and therefore the particular effects introduced by discreteness are strongly present.

The combination of momentum and real space methods can provide answers to the questions above. In the following, we first discuss the natural multi-channel loop for a square lattice: a square frame, as shown in figure 5.1, with a square hole at the center, threaded by a magnetic flux ϕ. We use this system in chapter 5 to study the flux periodicity of the total energy or the persistent current in clean symmetric square frames, analogously to part I. In chapter 7, we investigate a slightly different system reacting periodically to a magnetic field: Josephson junctions. These can easily be modeled in real space by inserting potential barriers, e.g. into a square or into a cylinder. In this context, we further investigate the effect of impurities and lattice defects on the energy spectrum of the square frame.

Another issue, which we neglected in the momentum space calculations in part I, is the self-consistency of the magnetic field. The persistent current flowing in a flux threaded loop generates a magnetic moment parallel or antiparallel to the external magnetic flux, which tends to complement the external flux to the closest multiple of the superconducting flux quantum $\Phi_0/2$. In the thin walled cylinder, the self consistency of the field is uninteresting, but in the annulus or the square frame, flux quantization should principally be observable for suitable parameters. We investigate this topic in chapter 6.

4 The Bogoliubov - de Gennes Equations

As "Bogoliubov - de Gennes equations" one usually denotes a matrix equation defining the Bogoliubov transformation for diagonalizing the BCS Hamiltonian (4.1) in real space, together with a self-consistency equation for the order parameter. This chapter is an introduction to the Bogoliubov - de Gennes equations; a detailed derivation of the the mean-field Hamiltonian and the calculation of observables is given in appendix C. The Hamiltonian which we use in this part has the form

$$\mathcal{H} = \sum_{\langle ij\rangle,s} t_{ij} c_{is}^{\dagger} c_{js} + \sum_{i} \left[\Delta_i^{*} c_{i\downarrow} c_{i\uparrow} + \Delta_i c_{i\uparrow}^{\dagger} c_{i\downarrow}^{\dagger}\right] + \sum_{\langle ij\rangle} \left[\Delta_{ji}^{*} c_{j\downarrow} c_{i\uparrow} + \Delta_{ij} c_{i\uparrow}^{\dagger} c_{j\downarrow}^{\dagger}\right] + \sum_{i,s} (U_i - \mu) c_{is}^{\dagger} c_{is}, \tag{4.1}$$

where $c_{is}^{\dagger}$, c_{is} are creation and annihilation operators for an electron on lattice site i with spin s, and μ is the chemical potential. The sum $\sum_i$ runs over all lattice sites and the sum $\sum_{\langle ij\rangle}$ runs over all nearest neighbor sites i and j, and $t_{ij} = te^{\varphi_{ij}}$ with the nearest neighbor hopping amplitude t and a Peierls phase factor

$$\varphi_{ij} = \frac{e}{\hbar c} \int_i^j \mathrm{d}\mathbf{r} \cdot \mathbf{A}(\mathbf{r}). \tag{4.2}$$

Additionally, we can include an impurity term consisting of potential scatterers with repulsive potentials $U_i > 0$, which we use to model tunnel junctions. A Hamiltonian of the form (4.1) has been used mainly for the numeric investigation of vortices in d-wave superconductors and the technique is described in a number of articles [74–81].

Two types of spin singlet pairing are used. The order parameter Δ_i is defined on lattice site i and represents conventional s-wave pairing originating from an on-site interaction. The order parameter Δ_{ij} originating from a nearest-neighbor interaction is defined on the bond between the two nearest neighbor sites i and j. They are defined through

$$\Delta_i = V_0 \langle c_{i\downarrow} c_{i\uparrow}\rangle \tag{4.3}$$

$$\Delta_{ij} = \frac{V_1}{2} \left[\langle c_{j\downarrow} c_{i\uparrow}\rangle - \langle c_{i\downarrow} c_{j\uparrow}\rangle\right]. \tag{4.4}$$

with the interaction strengths V_0 and V_1. The definition (4.4) is equivalent to $\Delta_{ij} = V\langle c_{j\downarrow} c_{i\uparrow}\rangle$ if $\mathcal{H}$ contains only spin-singlet interaction. To diagonalize the Hamiltonian

(4.1) we use the Bogoliubov transformation

$$c_{i\uparrow} = \sum_n \left[u_{ni} a_{n\uparrow} - v_{ni}^* a_{n\downarrow}^\dagger \right] \tag{4.5}$$

$$c_{i\downarrow} = \sum_n \left[u_{ni} a_{n\downarrow} + v_{ni}^* a_{n\uparrow}^\dagger \right], \tag{4.6}$$

where the coefficients u_{ni} and v_{ni} are obtained from the eigenvalue equation

$$\begin{pmatrix} \hat{t} & \hat{\Delta} \\ \hat{\Delta}^* & -\hat{t}^* \end{pmatrix} \begin{pmatrix} \mathbf{u}_n \\ \mathbf{v}_n \end{pmatrix} = E_n \begin{pmatrix} \mathbf{u}_n \\ \mathbf{v}_n \end{pmatrix} \tag{4.7}$$

and the sum runs over all positive eigenvalues E_n and their corresponding eigenvectors. The action of the operators $\hat{t}$ and $\hat{\Delta}$ on the vectors $\mathbf{u}_n$ and $\mathbf{v}_n$ is given by

$$\hat{t} u_{ni} = \sum_j t_{ij} u_{nj} + (U_i - \mu) u_{ni}, \tag{4.8}$$

$$\hat{\Delta} v_{ni} = \Delta_i v_{ni} + \sum_j \Delta_{ij} v_{nj}, \tag{4.9}$$

where j labels the nearest neighbor sites of site i. Inserting the transformation (4.6) into Eq. (4.3) and (4.4) leads to the self-consistency equations

$$\Delta_i = V_0 \sum_n u_{ni} v_{ni}^* \tanh\left(\frac{E_n}{2T}\right), \tag{4.10}$$

$$\Delta_{ij} = \frac{V_1}{2} \sum_n \left[u_{ni} v_{nj}^* + u_{nj} v_{ni}^* \right] \tanh\left(\frac{E_n}{2T}\right). \tag{4.11}$$

Equations (4.10) and (4.11) together with Eq. (4.7) are called the Bogoliubov - de Gennes equations. The eigenvalue equation (4.7) can be interpreted as a kind of time independent Schrödinger equation for the superconducting wave functions $(\mathbf{u}_n, \mathbf{v}_n)$ [82]. The standard technique to solve them is to choose suitable initial values for Δ_i or Δ_{ij}, then calculate $\mathbf{u}_n$ and $\mathbf{v}_n$ through solving the eigenvalue equation (4.7) and recalculate the order parameters until convergence is achieved. This takes typically around twenty loops, if the order parameters have a uniform phase. In the presence of a vector potential leading to a phase gradient in Δ_i or Δ_{ij}, complete convergence may take hundreds, even thousands of loops.

The bond order parameters Δ_{ij} can be projected onto a d-wave component and an extended s-wave component defined on site i as

$$\Delta_i^s = \frac{1}{4} \left[\Delta_{i,i+\hat{x}} e^{i\varphi_{i,i+\hat{x}}} + \Delta_{i,i-\hat{x}} e^{i\varphi_{i,i-\hat{x}}} + \Delta_{i,i+\hat{y}} e^{i\varphi_{i,i+\hat{y}}} + \Delta_{i,i-\hat{y}} e^{i\varphi_{i,i-\hat{y}}} \right], \tag{4.12}$$

$$\Delta_i^d = \frac{1}{4} \left[\Delta_{i,i+\hat{x}} e^{i\varphi_{i,i+\hat{x}}} + \Delta_{i,i-\hat{x}} e^{i\varphi_{i,i-\hat{x}}} - \Delta_{i,i+\hat{y}} e^{i\varphi_{i,i+\hat{y}}} - \Delta_{i,i-\hat{y}} e^{i\varphi_{i,i-\hat{y}}} \right]. \tag{4.13}$$

In a uniform system with nearest neighbor pairing, the self-consistency equation (4.11) selects a pure d-wave superconducting state, i.e. $\Delta_i^s = 0$. Impurities, potentials or boundary conditions breaking the uniformity generate an extended s-wave contribution $\Delta_i^s > 0$ [76]. Further sources of an extended s-wave order parameter can be finite momentum pairing leading to a phase gradient in Δ_{ij}, or the inclusion of a strong next-nearest neighbor hopping term altering the kinetic energy.

The expectation value of the current J_{ij} (cf. reference [60]) from site i to j is given by

$$J_{ij} = -\frac{8t}{\Phi_0} \sum_n \mathrm{Im}\left(u_{nj} u_{in}^* e^{-i\varphi_{ij}}\right) f(E_n). \tag{4.14}$$

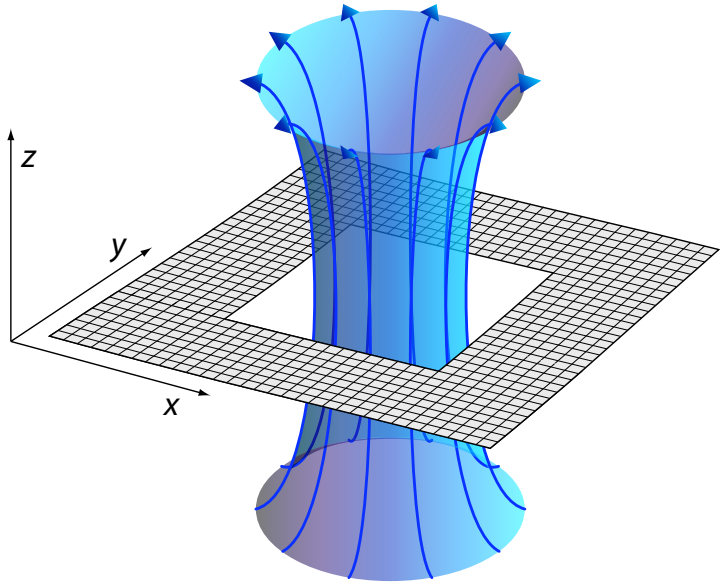

Figure 5.1: For the investigation of the flux periodicity of *d*-wave superconductors using the Bogoliubov - de Gennes equations in real space, we use a discrete square lattice with open boundary conditions and a square hole in the center the frame, which is pierced by the magnetic flux Φ.

5 Flux Periodicity in Superconducting Square Frames

The Bogoliubov - de Gennes equations introduced above are now applied to the square frame geometry shown in figure 5.1, consisting of a discrete $N \times N$ lattice with a centered $L \times L$ square hole threaded by a magnetic flux ϕ, and the edges of which are oriented in x- and y-direction. Since the flux threading the hole is supposed not to penetrate into the frame, we describe it by a magnetic field concentrated in the center of the hole, which is generated by a vector potential of the form $\mathbf{A}(\mathbf{r}) = 2\pi\phi/|\mathbf{r}|^2(y, -x, 0)$. The corresponding Peierls phase factor φ_{ij} measures the angle between the sites i and j and the center of the lattice. The phase factors are in this case given by

$$\varphi_{ij} = \phi \arctan\left[\frac{\mathrm{i_x j_y} - \mathrm{j_x i_y}}{\mathrm{i_x j_x} + \mathrm{i_y j_y}}\right], \tag{5.1}$$

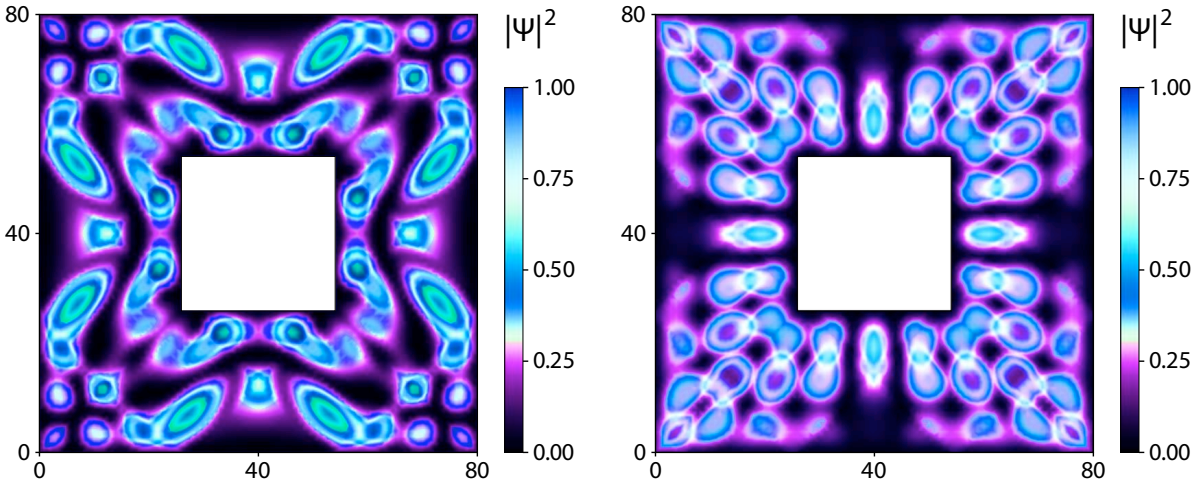

Figure 5.2: Real-space representation of a square loop with a typical electronic probability density $|\Psi|^2$ of a single state in the condensate. The figure displays an eigenstate of the d-wave pairing Hamiltonian, calculated for a square-loop with 80×80 lattice sites with a pairing interaction $V_1 = 0.3t$. The hole in the center has a size of 28×28 unit cells. To enhance the contrast of the complicated pattern, the special color code shown on the right is used and the discrete lattice points are smoothly interpolated.

where we chose the origin of the coordinate system at the center of the lattice (see appendix C.1).

In the normal state with $\Delta_{ij} = 0$, the Bogoliubov - de Gennes equations reduce to the discrete Laplace equation, the solutions of which are plane "square frame waves". While the low-energy states do not differ much from free plane waves, the high-energy "square frame waves" near E_F develop some peculiar, frame specific features. The wave length of a state near E_F is close to two lattice constants, therefore the probability density divides into two sublattices. In the square frame, structures on different sublattices can overlap, which results in the characteristic real space density profiles, which persist in the nodal states of a d-wave superconductor. Figure 5.2 shows two such examples, and further figures for the normal state are given in appendix E. The d-wave loop eigenstates are obviously far more complex than the angular momentum eigenstates of a one-dimensional circular ring (cf. Ref. [9]), and the current flow in the frame can only be evaluated numerically. Nevertheless, a qualitative discussion allows the same insight into the underlying physics as in part I.

The characterization of the superconducting solutions of the Bogoliubov - de Gennes equations in the square frame is analogous to the momentum space. The absolute value of the d-wave order parameter $|\Delta_i^d|$ is shown in figure 5.3 (a) for $\phi = 0$. The open boundary conditions cause a decrease on the boundaries and are responsible for Friedel oscillations visible along the diagonal of the frame. For $\phi \neq 0$, $|\Delta_i^d|$ is slightly diminished, an effect

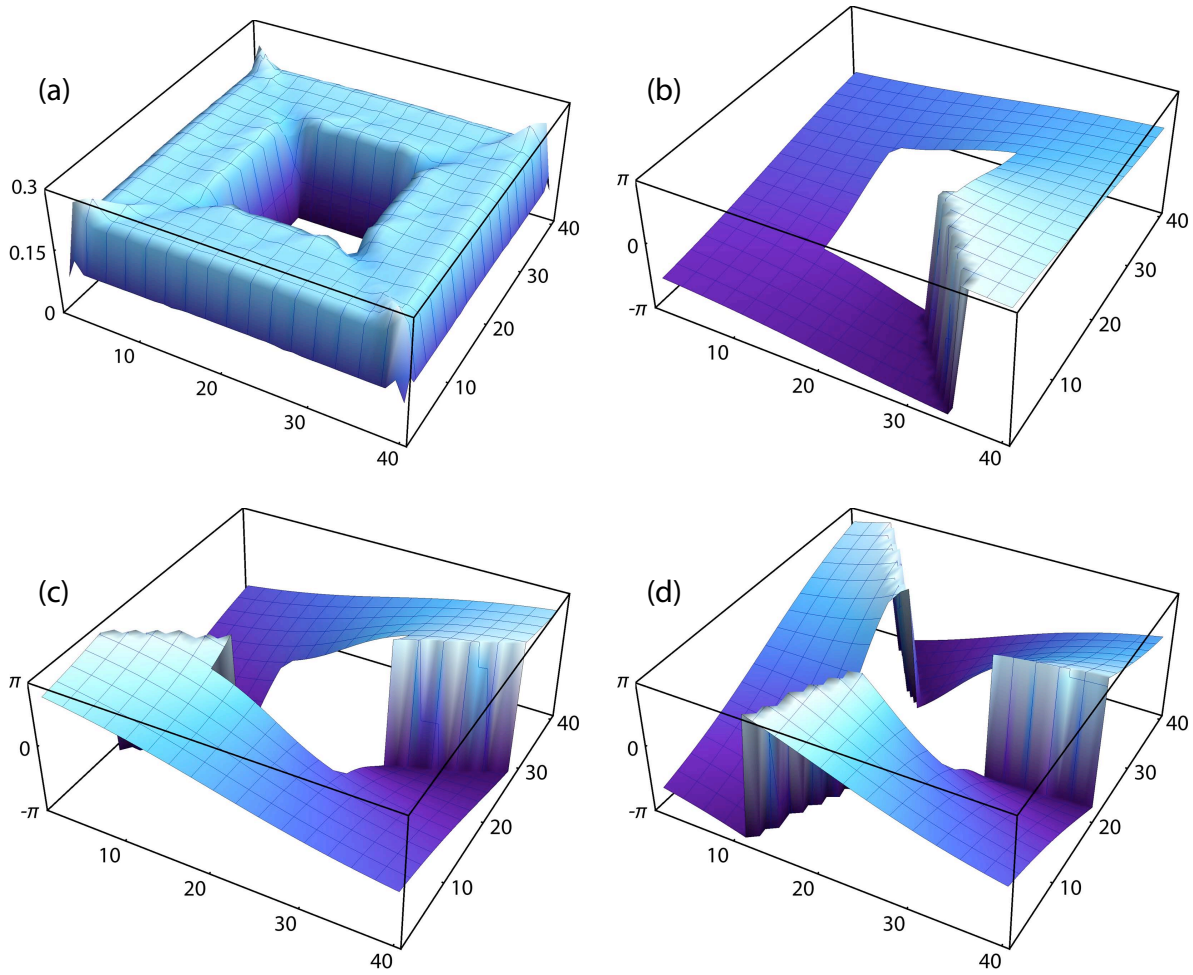

Figure 5.3: (a) Absolute value of the d-wave order parameter Δ_i^d in a 40 × 40 square frame with a 14 × 14 hole at the center for $q = 0$, $\phi = 0$, and $V_1 = 0.3t$. For this interaction strength, the suppression of Δ_i^d for $\phi \neq 0$ is small and not visible in this kind of plot. The phase of Δ_i^d is shown for winding numbers $q = 1, 2, 3$ in (b), (c) and (d), respectively.

qualitatively analogous to the one discussed in section 3.3 and almost invisible for the parameters chosen in figure 5.3. In multiply connected geometries, the Bogoliubov - de Gennes equations generally allow for solutions where Δ_i^d has a phase gradient such that the phase difference on a closed path around the hole is $2\pi q$ with an integer q. As in part I, this phase winding number q represents the center-of-mass movement of a Cooper pair, although it cannot be identified with the angular momentum in the square geometry. The different solutions are numerically obtained by choosing appropriate initial values for the phase of Δ_i^d, and the phases of the self-consistent results are shown in figure 5.3 (b), (c) and (d) for $q = 1$, 2 and 3 and flux values $\phi = 1/2$, 1 and $3/2$, respectively. The winding number q of the groundstate has the same flux dependence as given in

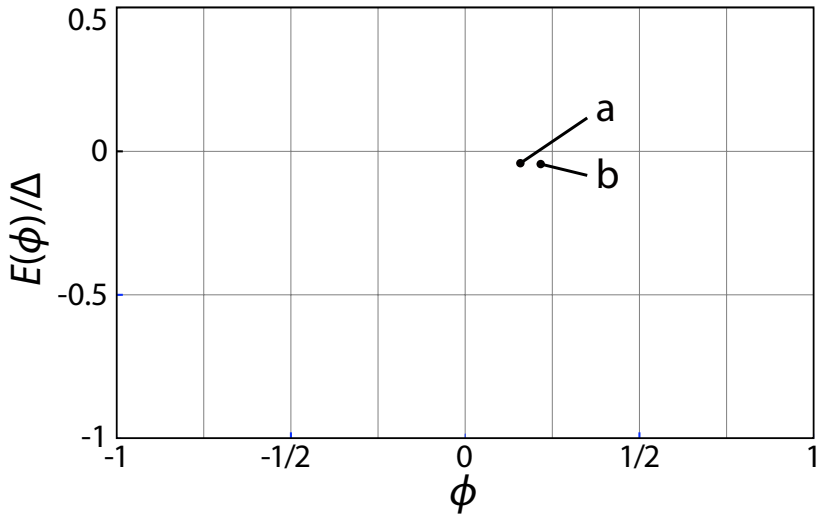

Figure 5.4: Energy spectrum of the *d*-wave BCS model. The eigenenergies in the gap region are shown for a square 40×40 loop with a hole of 14×14 unit cells and pair interaction $V_1 = 0.3t$ as a function of flux ϕ (in units of Φ_0). The energies are given in units of the superconducting order parameter Δ at $\phi = 0$ ($\Delta \approx 0.22t$). The superconducting condensate consists of the states below $E_F = 0$ (blue lines). Reconstruction of the condensate takes place near $\phi = \pm(2n + 1)/2$, where the eigenenergies jump abruptly. The labels 'a' and 'b' refer to the current patterns shown in figure 4.

equation (1.17) in section 1.2.1 for the one dimensional ring, apart from the small shift of the flux value where the condensate reconstructs (c.f. figure 5.4).

To assess the global quantities, viz. energy $E(\phi)$ and current $J(\phi)$, the evolution of the eigenenergies with magnetic flux has to be calculated. The eigenstates with energies below E_F form the ground-state condensate (figure 5.4). Here we discuss only flux values ϕ between 0 and 1/2, because all quantities are either symmetric or antisymmetric with respect to flux reversal $\phi \to -\phi$. The spectrum for a square frame with $N = 40$ and $L = 14$ is shown in figure 5.4 for half filling, i.e. $\mu = 0$. Because the number of lattice sites on straight paths around the hole is a multiple of four in a square frame, the spectrum is almost identical to the one calculated in section 3.3 for a cylinder with an even number of lattice sites and the same number $N - L = 26$ of transverse channels [figure 3.6 (a)]. For the square frame, the energy levels do not actually cross E_F, because the lack of a rotational symmetry leads to hybridization of the levels and level repulsion. Nevertheless, the same clearly distinct flux regimes are found: the flux intervals between 0 and 1/4 and from 1/4 to 1/2.

Up to $\phi \simeq 1/4$ the $J(\phi)$ generates a magnetic field which tends to reduce the applied field. This is achieved by a continuous shift of the eigenenergies in the condensate. At $\phi = 0$, pairs of states with opposite circulation compensate their respective currents, thus

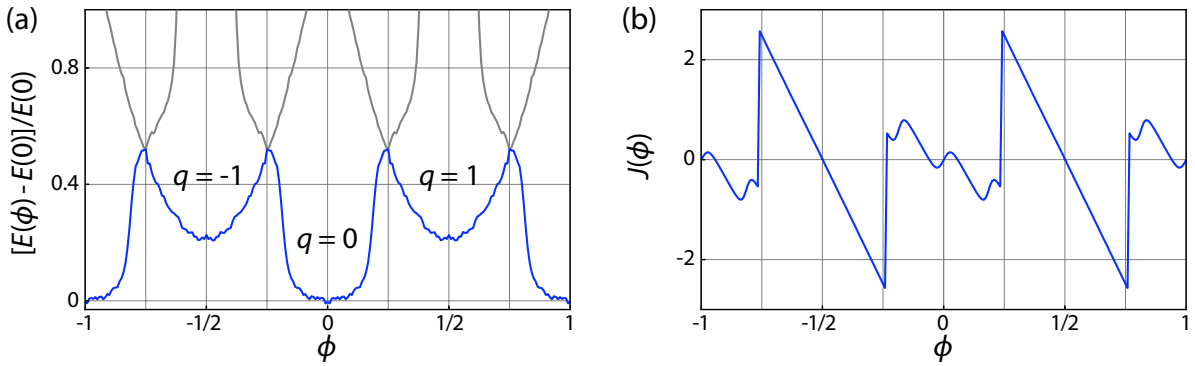

Figure 5.5: Flux dependence of energy and current. Total energy $[E(\phi) - E(0)]/E(0)$ (a) and total circulating current $J(\phi)$ (b) for a square 40×40 loop with a hole of 14×14 unit cells and pair interaction $V_1 = 0.3t$ as a function of flux ϕ in units of Φ_0. $J(\phi)$ is given in units of $t/\Phi_0 = 6 \times 10^{-5} A$ for a typical choice of $t = 250$ meV. There is a clear distinction between condensate states with an even and an odd winding number q of the order parameter, reflected e.g. in the deformation of the $q = 0$-parabola. The overall ϕ periodicity for $E(\phi)$ and $J(\phi)$ is Φ_0.

$J = 0$. The well separated states at $\phi = 0$ in figure 5.4 are the states in the vicinity of the nodes of the mesoscopic d-wave superconductor. At energies further away from E_F, the density of states is higher; these are the states near the maximum energy gap Δ that provide most of the condensation energy. For $\phi > 0$, the energy of the states with orbital magnetic moment anti-parallel (parallel) to the magnetic field is increased (decreased). Correspondingly the supercurrent, which is carried by these states, depends on the details of level crossings and avoidings. The main contribution to the supercurrent arises from the occupied levels closest to E_F, because the contributions from the lower-lying states tend to cancel in adjacent pairs.

As the highest occupied state shifts with increasing flux to lower energies, the current in the square loop first increases for small ϕ (figure 5.5), then decreases, when the highest occupied level with an orbital moment opposite to the applied magnetic field starts to dominate. With increasing flux this state approaches E_F. For s-wave rings this "Doppler shift energy" (cf. Ref. [54]) corresponds to the critical value of the superfluid velocity, for which the indirect energy gap closes. For d-wave loops, the order parameter is protected by the numerous states that form the "lobes" of the d-wave gap parameter.

For loops with d-wave and other unconventional order parameter symmetries, the states in the vicinity of the nodes evolve with increasing flux as for s-wave rings in the "small gap" regime. They do not necessarily cross E_F (figure 5.4) due the hybridization of the respective states above and below E_F. Nevertheless, a state with one direction of current is replaced by a state of opposite direction (figure 5.6). The current carrying states of the condensate are thereby continuously changing near the extrapolated crossing

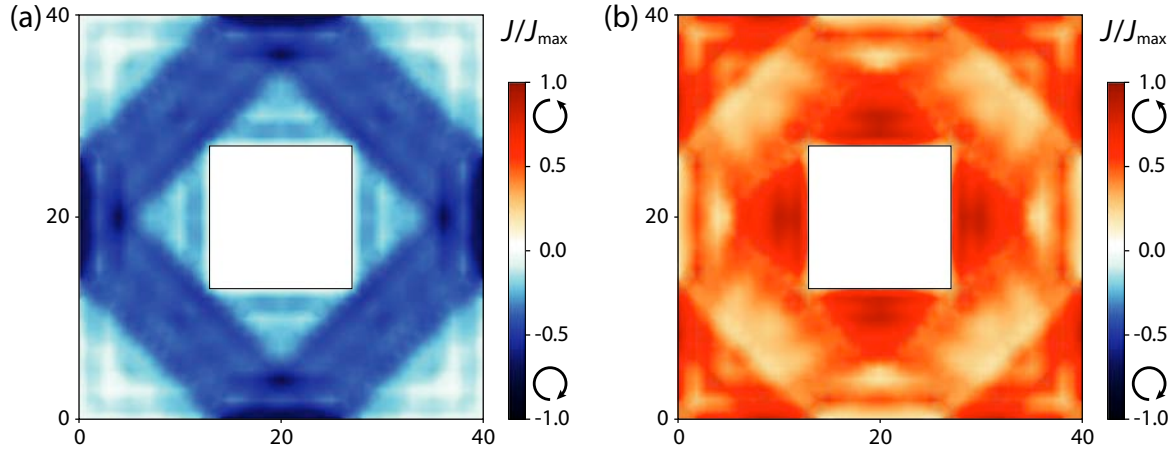

Figure 5.6: Current distribution in a square loop of 40×40 lattice sites. The current expectation value of the occupied state closest to $E_F = 0$ is shown for flux $\phi = 0.17$ (top panel, the state is marked with 'a' in figure 5.4) and for $\phi = 0.21$ (bottom panel, marked with 'b' in figure 5.4). The color encodes the projection of the current onto a square path around the loop whereby red presents a counterclockwise and blue a clockwise circulation. The maximal current is $J_{max} = 0.15t/\Phi_0$ for (a) and $0.13t/\Phi_0$ for (b). The current distribution of each of the two states has strong spatial variations and does not fulfill the continuity condition which, however, is restored for the total current.

points. As a consequence, the energy "parabola" centered at zero flux is different from the ground-state energy parabola centered at $\phi = 1/2$ [figure 5.5 (a)]. The deviation from a parabolic shape near zero flux is due to the evolution of the near-nodal states; the vertical offset of the energy minima at $\phi = n$ results mostly from the flux dependence of the states near the maximum value of the anisotropic gap.

For a flux value near $\phi = 1/4$ the condensate reconstructs. The superconducting state beyond 1/4 belongs to the class of wavefunctions introduced by Byers and Yang [10] in which, for a circular geometry, each pair acquires a center of mass angular momentum $\hbar$ [9]. Remarkably, in the flux interval from near 1/4 to 1/2, a full energy gap exists also for d-wave superconductors (figure 5.4). Such a gap is characteristic for mesoscopic structures and observed also in nano wires with d-wave pairing symmetry [83, 84]. Here the circulating current enhances the magnetic field; the paramagnetic moment of the current is parallel to the field. The resulting energy gain is responsible for the field-induced energy gap. This reconstruction of the condensate is the origin of the Φ_0 periodicity in energy and current.

Our calculations based on the Bogoliubov de Gennes equations show that a d-wave superconducting loop in square geometry has almost identical properties to a flux threaded cylinder. This is remarkable, because on a closed path in the square frame, the phase of the d-wave order parameter Δ_i^d rotates by 2π, whereas in the cylinder, the order

parameter rotates with the lattice. The results demonstrate therefore that while changes in geometry, the number of transverse channels and elastic scattering by impurities modify the spectrum and the $J(\phi)$ characteristics in detail, they do not eliminate the Φ_0 periodic component. Such calculations will be discussed in section 7.1.2 in connection with Josephson junctions. As long as the single particle states are well defined, also electronic correlation effects, which are responsible for the renormalization of states and of coupling parameters, are not expected to bear a strong influence on the discussed phenomena. The geometrical reduction of the symmetry, here to a four fold rotational symmetry, stabilizes therefore the spectrum compared to the cylinder geometry, which may enhance the measurability of the Φ_0 periodic current contributions in experiment.

6 Self-Consistent Treatment of the Magnetic Field

In the literature on superconductivity, the quantization of the magnetic flux is usually discussed in two limits [85]: Rings, or cylinders, with wall thickness $D \gg \lambda$ or quasi one dimensional rings with $D \ll \lambda$. In the first case, one deals with a penetration layer of width λ where the supercurrent flows and assumes that the interior of the superconductor is field and current free, which leads directly to the quantization of the magnetic flux in multiples of $\Phi_0/2$. In the second case, one neglects the screening field generated by the supercurrent itself. Then the total magnetic flux is a continuous variable and only the fluxoid is quantized.

The crossover between the two regimes is not so easily accessible. The way to analyze this problem is to use the Maxwell equation connecting magnetic field and current (Biot-Savart) as a self-consistency equation for the supercurrent, and to solve it iteratively jointly with the Bogoliubov - de Gennes equations in real space. This is a complete description free of further parameters and approximations, but numerically demanding, as described in section 6.2. One obtains a simpler model assuming an ideal superconducting annulus showing a $\Phi_0/2$ periodic, piece-wise linear current-flux relation (saw-tooth pattern). This model is equivalent to solving London's equations on the annulus and leads to an implicit integral equation, which we solve in section 6.1 below.

6.1 Vector-Potential in an Annulus

A conventional superconducting annulus with inner radius $R_1 > \xi_0$ has a linear current-flux relation in the flux regime $-1/4 < \phi_0 < 1/4$, where ϕ_0 is the external magnetic flux threading the annulus. The external vector potential generating ϕ_0 has the form (in polar coordinates): $\mathbf{A}^0(r,\varphi) = (0, A^0_\varphi(r))$ with $A^0_\varphi(r) = 4\pi\phi_0/r$ and generates a current of the form $\mathbf{j}(r,\varphi) = (0, j_\varphi(r))$. The external flux ϕ_0 is supposed to be generated by currents flowing far away from the annulus outside the system and therefore do not enter the description. In the flux regime $-1/4 < \phi_0 < 1/4$, supercurrent and total vector potential $\mathbf{A}(\mathbf{r}) = \mathbf{A}^0(\mathbf{r}) + \mathbf{A}^{\mathrm{i}}(\mathbf{r})$ are linked through a kind of London equation:

$$j_\varphi(r) = -\frac{A_\varphi(r)}{\Lambda c}, \tag{6.1}$$

where $\mathbf{A}^{\mathrm{i}}(\mathbf{r})$ is the potential induced by the supercurrent and Λ is an external parameter measuring the response of the superconductor to the magnetic flux [3]. In London's theory, it is identified as $\Lambda = m/n_s e^2 = 4\pi\lambda^2/c^2$ where n_s is the density of electrons in the superconducting condensate and λ the London penetration depth. In other flux regimes, London's equation is analogous with the flux replaced as $\phi \to \phi - q/2$. The formula of Biot-Savart provides an equation for the induced vector potential $\mathbf{A}^{\mathrm{i}}(\mathbf{r})$ as a function of $\mathbf{j}(\mathbf{r})$:

$$\mathbf{A}^{\mathrm{i}}(\mathbf{r}) = \frac{1}{c}\int \mathrm{d}^3\mathbf{r}'\,\frac{\mathbf{j}(\mathbf{r}')}{|\mathbf{r}-\mathbf{r}'|}. \tag{6.2}$$

Inserting equation (6.1) into (6.2) defines $A^{\mathrm{i}}_{\varphi}(r)$ in polar coordinates:

$$\begin{aligned} A^{\mathrm{i}}_{\varphi}(r) &= \frac{1}{c}\int_0^{\infty}\mathrm{d}r'\,r'\int_{-\pi}^{\pi}\mathrm{d}\varphi'\,\frac{j_{\varphi}(r')}{\sqrt{r^2+r'^2-2rr'\cos(\varphi-\varphi')}} \\ &= \Lambda\int_{R_1}^{R_2}\mathrm{d}r'\,r'A_{\varphi}(r')\int_{-\pi}^{\pi}\mathrm{d}\varphi'\,\frac{1}{\sqrt{r^2+r'^2-2rr'\cos(\varphi-\varphi')}} \qquad (6.3) \\ &= \Lambda\int_{R_1}^{R_2}\mathrm{d}r'\,r'A_{\varphi}(r')\chi(r,r'), \qquad (6.4) \end{aligned}$$

where

$$\chi(r,r') = \frac{4r'}{r+r'}F\left(\frac{\pi}{2},\frac{2\sqrt{rr'}}{r+r'}\right) \tag{6.5}$$

and $F(a,k) = \int_0^a \mathrm{d}t\left(1-k^2\sin^2 t\right)^{-1/2}$ is the incomplete elliptic integral. Equation (6.4) is an implicit equation for the induced potential $A^{\mathrm{i}}(r)$ from which we can derive the self consistent field and current distribution in the annulus. To solve equation (6.4) numerically, we replace the integral over r' by a Riemann sum with N terms:

$$A^{\mathrm{i}}_n = \Lambda d\sum_m \left[A^{\mathrm{i}}_m + A^0_m\right]\mathcal{X}_{nm} \tag{6.6}$$

with $A^{\mathrm{i},0}_n = A^{\mathrm{i},0}_{\varphi}(r_n)$, $\mathcal{X}_{nm} = \chi(r_n,r_m)$ and $d = (R_2-R_1)/N$. This can be written as a linear matrix equation

$$\left(\mathcal{X} - \frac{\mathbb{1}}{d\Lambda}\right)\mathbf{A}^{\mathrm{i}} + \mathcal{X}\mathbf{A}^0 = 0. \tag{6.7}$$

This equation is not generally solvable, because it has no solution if $\mathcal{X}\mathbf{A}^0$ is not an eigenvector of the matrix $(\mathcal{X} - \mathbb{1}/d\Lambda)$. The closest approximation to a solution, which

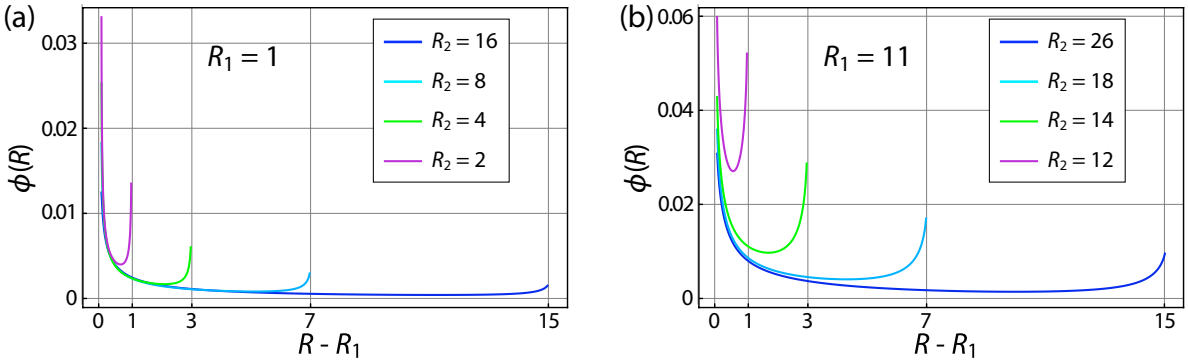

Figure 6.1: Self consistent solution for the total magnetic flux $\phi(R)$ inside a circle with radius R in untits of $1000a$. The external flux concentrated through the annulus is $\phi_0 = 0.1$ and $\Lambda = 0.4\Phi_0$.

becomes a solution in the limit $N \to \infty$, can be found with the help of a standard LAPACK routine which finds the minimum

$$\min_{\mathbf{A}^{\mathrm{i}}} \left\| \left(\mathcal{X} - \frac{\mathbb{1}}{d\Lambda} \right) \mathbf{A}^{\mathrm{i}} + \mathcal{X}\mathbf{A}^{0} \right\| . \tag{6.8}$$

The solution of equation (6.8) is plotted in figure 6.1 for an external flux $\phi_0 = 0.1$ and different parameters, showing the crossover from the "thin-ring" to the "thick-ring" limit. One clearly sees that the total magnetic flux $\phi = \phi_0 + \phi_{\mathrm{i}}$ is shielded and decreases sharply inside the annulus from its initial value of $\phi_0 = 0.1$ to almost zero in the thickest annulus. The penetration depth is essentially equal for all annuli, but the value, to which ϕ decreases, becomes larger for larger inner radius R_1 and the shielding is therefore less effective. It is interesting to observe that the flux, and with it the circulating supercurrent, does not actually vanish exponentially inside the annulus, as it does in an infinitely extended superconductor, but it saturates at a certain value and increases again close to the outer boundary. Thus there are surface currents flowing on the inner as well as on the outer boundary of the annulus.

In the further flux regimes, ϕ approaches the value of the corresponding flux quantum in the same way as it approaches zero in figure 6.1. The model solved above displays how the current and the induced vector potential lead to the quantization of the magnetic flux and how discrete flux quanta emerge from the continuous variable ϕ in thin loops.

6.2 Lattice Formulation

Here we describe the scheme to solve the Bogoliubov - de Gennes equations numerically including the formula for Biot-Savart (6.2) as an additional self-consistency equation for

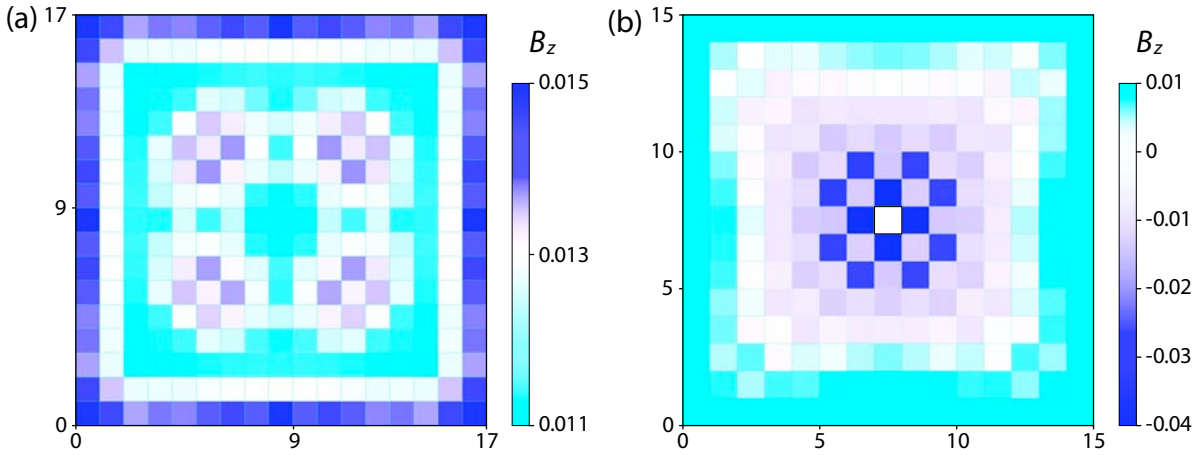

Figure 6.2: Self-consistent solution of the magnetic field B_z in a square lattice with open boundary conditions. (a) A 18 × 18 lattice penetrated by a homogeneous magnetic flux $\Phi = 4\Phi_0$, generating four vortices with $\Phi_0/2$ flux lines, and boundary currents. The amplitude between the vortex cores and the minimum magnetic field is ~ 5%. (b) A 16 × 16 lattice with a flux $\phi = 0.2$ threading the central plaquette (white plaquette in the center). This calculation is done for $\kappa = 0.3$ (see main text) and not fully converged at the outer boundaries.

the induced vector potential. The corresponding discrete Peierls phase factors are

$$\varphi^{\mathrm{i}}_{ij} = \frac{1}{2}\left[\sum_{k\neq i} J_{k,k-i+j}\left|\frac{\mathbf{r}_i+\mathbf{r}_j}{2}-\mathbf{r}_{\mathbf{k}}\right|^{-1} - \sum_{k\neq j} J_{k,k+i-j}\left|\frac{\mathbf{r}_i+\mathbf{r}_j}{2}-\mathbf{r}_{\mathbf{k}}\right|^{-1}\right], \tag{6.9}$$

where J_{ij} is the current flowing from site i to site j and it is recalculated from equation (4.14) in each self-consistency loop. The total Peierls phase factors are $\varphi_{ij} = \varphi^0_{ij} + \varphi^{\mathrm{i}}_{ij}$, where φ^0_{ij} are the external phase factors.

In this way we obtain a fully self-consistent description of the supercurrent J_{ij} in arbitrary systems, which accounts for the non-linearities in the current-flux relation in nodal superconductors and provides in principle a direct way to calculate the penetration depth λ for complex geometries. When doing the actual numerical calculations, one encounters however several and severe problems: The additional self-consistency condition slows down the convergence dramatically. The maximum lattice sizes for which this technique worked was therefore restricted to about 40 × 40 sites. For reasonable pairing interaction strength V, this is not large enough for frames which shield the magnetic flux properly. For the description of flux quantization, our technique is consequently not yet good enough. Unfortunately, to increase V_1 in order to decrease λ does not help either. The shorter λ is, the larger the phase gradients in the frame become, which hinders again the convergence of the supercurrent.

A possibility to show that the proposed scheme works in principle is to control the current response of the square frame to a magnetic flux through a parameter κ: $\varphi_{ij} = \varphi^0_{ij} + \kappa\varphi^{\mathrm{i}}_{ij}$. By increasing κ from zero to one, we can turn on the self-consistency condition for the supercurrent slowly from loop to loop. This trick works quite well to calculate the self-consistent magnetic flied in the vortex-lattice phase of a d-wave superconductor in a constant external magnetic field B_z perpendicular to the lattice. In a discrete lattice, B_z is defined on each plaquette of the lattice as the flux threading the plaquette, which is explained in detail in appendix C.1. Figure 6.2 (a) shows the distribution of B_z in a 18×18 lattice with open boundary conditions, threaded by a homogeneous external magnetic flux $4\Phi_0$, i.e. eight superconducting flux quanta. Clearly visible are four $\Phi_0/2$-flux lines through the lattice, at the cores of which the magnetic field is enhanced. The second half of the magnetic flux does not penetrate the lattice through vortices, but generates boundary currents circulating at the edge of the lattice. The amplitude of the increase of B_z at the vortex cores is $\sim 5\%$, which is in qualitative agreement with exact calculations of the field distribution around a vortex core [86].

While the modulations in B_z are rather small in the vortex lattice, the field gradients in a flux threaded square frame are much larger. Because of this, the scheme to achieve convergence doesn't work so excellently for the square frame. So far convergence was achieved only for $\kappa \lesssim 0.3$. For this value, λ is still much larger than the size of our test systems. Nevertheless, we can draw a qualitative picture of the shielding of the flux from the calculations with $\kappa = 0.3$ and compare it to the results obtained for the annulus. Figure 6.2 (b) shows the distribution of B_z for a 16×16 frame with an exrenal flux $\Phi = 0.2\Phi_0$ threading the central plaquette (the white plaquette in the center). The induced supercurrent generates a magnetic field in the frame pointing in the opposite direction. It decreases sharply –away from the inner edge– and reverses it sign close to the outer edge of the frame. This behavior is closely similar to the results in section 6.1 for thin annuli, where the total flux also increases at the outer edge. The existence of the boundary currents which cause this increase, as well as the boundary currents in figure 6.2 (a), are not primarily due to the self consistency of the current, but they are rather a consequence of the open boundary conditions. They are observed similarly for a fixed vector potential. Tth total induced magnetic field in figure 6.2 (b) is considerably too small to compensate the external flux. Neglecting the induced field as we have assumed in the previous sections is therefore an accurate approximation for systems of comparable size.

7 Flux Periodicity of Josephson Junctions

Apart from flux threaded superconducting loops, the energy levels are Doppler shifted in any current carrying system like wires or the surface of bulk superconductors. In these systems, the phase gradient of the superconducting order parameter usually never reaches the value necessary to drive the superconductor into a finite momentum pairing state with $q \neq 0$, therefore no flux periodicity is usually discussed. An exception are systems with strong inhomogeneities of the order parameter, which act as Josephon junctions. In the presence of Josephson junctions, the phase gradient accumulates at the junctions and they react periodically to the phase gradient, as described by the first Josephson relation. Junctions react also periodically to transverse magnetic fields renormalizing the phase gradient over the junction. From what we learned about the flux periodicity in multiply connected geometries, it looks natural that the Doppler shift of nodal states might also influence the periodicity of Josephson junctions.

A Josephson junction is intrinsically a much more complicated system as a pure superconducting loop, with a number of parameters characterizing the junction itself and the superconducting states on each side of the junction. Most junctions can be classified either as transparent junctions or as tunnel junctions, regardless of the setup of the junction: geometrical constriction, potential barrier, normal metal bridge and so on. This classification is closely related to the Doppler shift of single energy levels in the system, as will be explained below. In the following we will therefore discuss the first and second Josephson relations in both the tunnel and the transparent regime.

7.1 Current-Phase Relation

In this section we analyze the current-phase relation (first Josephson relation), which describes the supercurrent J over a Josephson junction as a function of the phase difference $\delta\varphi$ of the order parameters on both sides of the junction:

$$J = J_c \sin(\delta\varphi), \tag{7.1}$$

where J_c is the critical current over the junction, above which the supercurrent breaks down. This was predicted by Josephson 1962 [87] and derives directly from the Ginzburg-Landau description of the Josephson junction [88]. In the case of transparent junctions, the $\sin(\delta\varphi)$ in equation (7.1) deforms into a saw-tooth pattern analogous to the one we found for the current-flux relation in superconducting loops [89]. It is crucial to

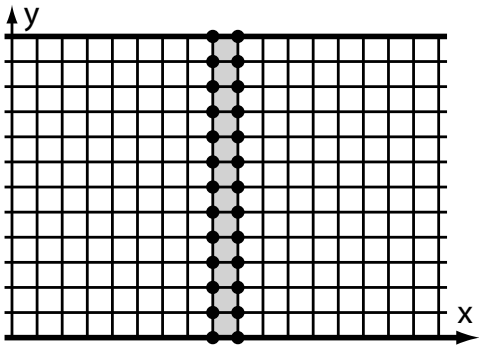

Figure 7.1: To model a Josephson junction we choose a discrete square lattice with N sites and periodic boundary conditions in x-direction, and M sites and open boundary conditions in y-direction. The junction itself is modeled by one or two lines of potential scatterers (black points) with a repulsive potential $U > 0$.

remember that the phase gradient of the order parameter is twice that of the superconducting wave function (compare with the ansatz for $u_{\mathbf{n}}(r)$ and $v_{\mathbf{n}}(r)$ in section 2.2). If the phase difference of the order parameter on both sides of the junction is $\delta\varphi$, then the phase difference of the wave function is $\delta\varphi/2$. Because the system has to be 2π periodic in $\delta\varphi/2$, the periodicity in $\delta\varphi$ of the energy spectrum of a finite system is 4π, and the current contributions of each energy level add up to a 2π periodic supercurrent only in the thermodynamic limit. The assumption that the Doppler shift of the energy levels might lead to the same doubling of the periodicity in $\delta\varphi$ of a junction as is it does for the flux periodicity of loops is therefore obvious. This we analyze in detail in this section.

While for the tunnel regime we rely on a simple linear junction model, we will analyze transparent junctions by inserting a Josephson junction into a square frame as discussed above. This has the advantage of a remarkable stability of the energy spectrum against the insertion of impurities and lattice defects, as will be seen in section 7.1.2.

7.1.1 Tunnel Junctions

A simple model of a tunnel junction is a square lattice with N sites and periodic boundary conditions in x-direction, and M sites and open boundary conditions in y-direction. The junction itself is modeled by one or two lines of potential scatterers (black points) with a repulsive potential $U > 4t$ in the tunnel regime (figure 7.1). In the absence of a magnetic field, this system is homogeneous in y-direction. It is therefore possible to Fourier transform it with respect to the y-coordinate, which allows the diagonalization of much larger systems [90, 91].

The Bogoliubov - de Gennes equations introduced in section 4 are slightly modified in this case: The eigenvalue equation (4.7) for nearest neighbor interaction is here defined

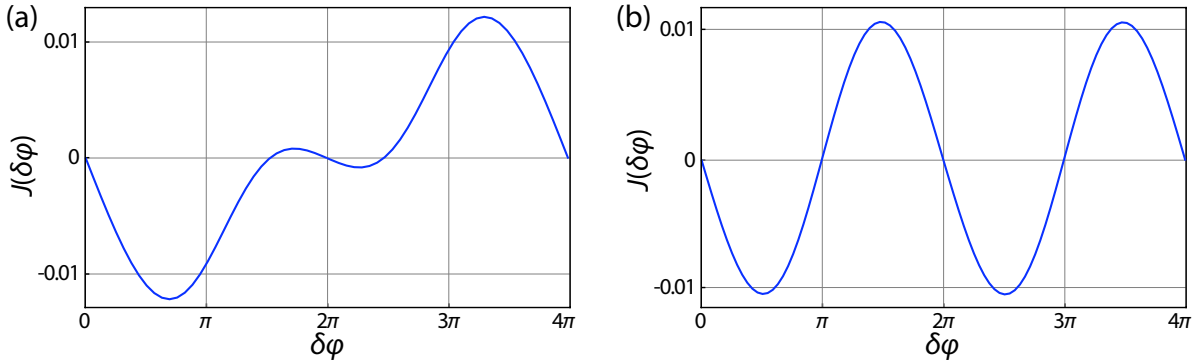

Figure 7.2: Current-phase relation for Josephson junctions in the tunnel regime. (a): $N = 18$, $M = 12$, $V_1 = 0.3t$ and $U = 4.5t$. The usual $\sin(\delta\varphi)$ relation is considerably deformed, which is typical for thin junctions with very few channels. (b): $N = 20$, $M = 200$, $V_1 = t$ and $U = 5t$. This junction has sufficiently many channels to exhibit the usual current-phase relation.

through the actions

$$\hat{t}u_{ni_xk_y} = \sum_{j_x} t_{ij}u_{nj_xk_y} + (\varepsilon_{k_y} + U_{i_x})u_{ni_xk_y}, \tag{7.2}$$

$$\hat{\Delta}v_{ni_xk_y} = \sum_{j_x} \Delta_{ij}v_{nj_x,k_y} + \Delta_{k_y}v_{ni_xk_y}, \tag{7.3}$$

where $\varepsilon_{k_y} = -2t\cos k_y - \mu$ and $\Delta_{k_y} = \Delta_y \cos k_y$. The index of the eigenvectors $\mathbf{u}_n$ and $\mathbf{v}_n$ is here the site i_x in x-direction and the wave number k_y in y-direction. The corresponding self-consistency equations are

$$\Delta_{ij} = \frac{V_1}{2}\sum_{nk_y}\left[u_{ni_xk_y}v^*_{nj_xk_y} + u_{nj_xk_y}v^*_{ni_xk_y}\right]\tanh\left(\frac{E_n(k_y)}{2k_BT}\right) \tag{7.4}$$

if $j = i \pm \hat{x}$, and

$$\Delta_y = V_1\sum_{nk_y} u_{ni_xk_y}v^*_{ni_xk_y}\cos k_y \tanh\left(\frac{E_n(k_y)}{2k_BT}\right). \tag{7.5}$$

The self-consistency equation for the s-wave order parameter Δ_i with on-site interaction is analogous to (7.5), but without the factor $\cos k_y$.

To induce a finite phase gradient of the order parameter and thus a supercurrent, we introduce a phase jump $\delta\varphi$ in the matrix elements t_{ij} for hopping from $i_x = N-1$ back to $i_x = 0$, and a jump $-\delta\varphi$ for the corresponding hopping in the opposite direction. An alternative, but physically equivalent choice for the phase of t_{ij} is a constant phase shift $e^{i\varphi_{ij}}$ with $\varphi_{ij} = \delta\varphi/N$ for all hopping processes along the x-direction, which is mathematically

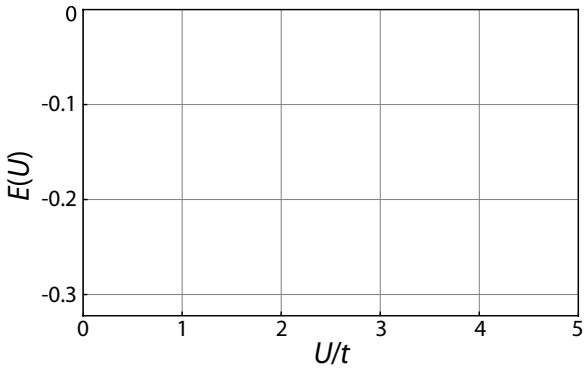

Figure 7.3: The highest occupied energy levels of a linear Josephson juntion with $N = 18$, $M = 12$ and $V_1 = 0.6t$ as a function of the repulsive potential U on the junction.

identical to a cylinder threaded by a flux $\phi = \delta\varphi/4\pi$. In the fully transparent case with $U = 0$, this leads to a homogeneous phase gradient of $\Delta_i^d = (\Delta_{i,i+\hat{x}} + \Delta_{i,i-\hat{x}})/2 + \Delta_y$ (or of Δ_i, respectively), whereas far in the tunnel regime $U > 4t$, the phase drops fully over the junction. The current flowing over the junction is calculated as in equation (4.14). The results for two typical situations are shown in figure 7.2. (a) shows the current-phase relation of a thin Josephson junction with a width of $M = 12$ sites. The usual current-phase relation is considerably deformed in this case, as is typical for junctions with very few channels [89]. The exact form of the current-phase relation is characteristic for each junction; it depends on the structure of the energy spectrum, which changes strongly upon increasing or decreasing the system size or adding impurities. For increasing M, the current-phase relation approaches (7.1), as the level spacing becomes negligible. This is the regime of wide junctions, shown in figure 7.2 (b), which is described well by the Ginzburg-Landau model.

Our numerical analysis shows that deviations from the first Josephson relation (7.1) become completely invisible for wide junctions in the tunnel regime. There is no doubling of the period detected, even for d-wave superconductors with small energy gap. The reason for this is that, along with the suppression of the maximum current J_c over the junction, the Doppler shift decreases strongly with increasing repulsive potential U. In the tunnel regime $U > 4t$, J_c decreases by a factor 10^3 and more as compared to $U = 0$. Because of that, no energy levels (or extremely few in very large systems) approach E_F as a function of $\delta\varphi$ and consequently, the effect of single particle currents reversing their current direction does not take place. In other words: for tunnel junctions, the thermodynamic Ginzburg-Landau limit is reached also for d-wave superconductors if the density of states close to E_F becomes quasi continuous, in contrast to the case of a flux treaded loop. The deformation of the current-phase relation in figure 7.2 (a) in thin junctions is not due to levels reaching E_F, but because the main current is carried by very

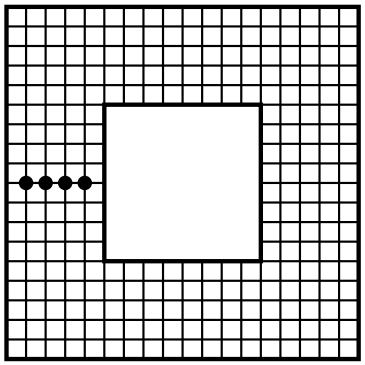

Figure 7.4: For the description of transparent junctions, we choose again the square frame geometry and model the junction with potential scatterers arranged on a line crossing one arm on the frame (black points). The current is driven by a magnetic flux threading the frame.

few energy levels, of which each has a period of 4π.

7.1.2 Transparent Junctions

The situation in transparent junctions is much more confusing than it is for tunnel junctions. The first reason for this is the fact that the superconducting states on both sides of the junction are strongly coupled. It is therefore impossible to choose the phase of the corresponding order parameters independently, and consequently the phase difference $\delta\varphi$ is not an adequate variable for describing the current over the junction. Strictly speaking, there is no second Josephson relation for transparent junctions. The second reason is that, as mentioned before, the energy spectrum in a linear junction changes dramatically upon changing microscopic details of the system, such as the strength of the repulsive potential U on the impurity sites in this case. This is illustrated vividly by figure 7.3 showing the wild behavior of the highest occupied energy levels as a function of U.

The problems referred to above can be resolved largely by using a square frame geometry as in section 5. Here the Josephson junction is modeled by adding potential scatterers on a line cutting the frame, as shown in figure 7.4, and the current is driven by a magnetic flux ϕ threading the frame. For a tunnel junction, this would induce a phase jump of $4\pi\phi$ in the order parameter over the junction and thus a $\sin(2\phi)$ current-flux relation. In transparent junctions, the jump is smaller and vanishes completely in a clean frame.

For strong enough U, here we take $U = 100t$, these impurities act as a geometrical constriction. Figure 7.5 finally shows explicitly that the spectrum of a square frame remains qualitatively invariant upon inserting impurities, even sufficiently strong to block the current over the impurity site completely. (b) and (c) show the spectra as

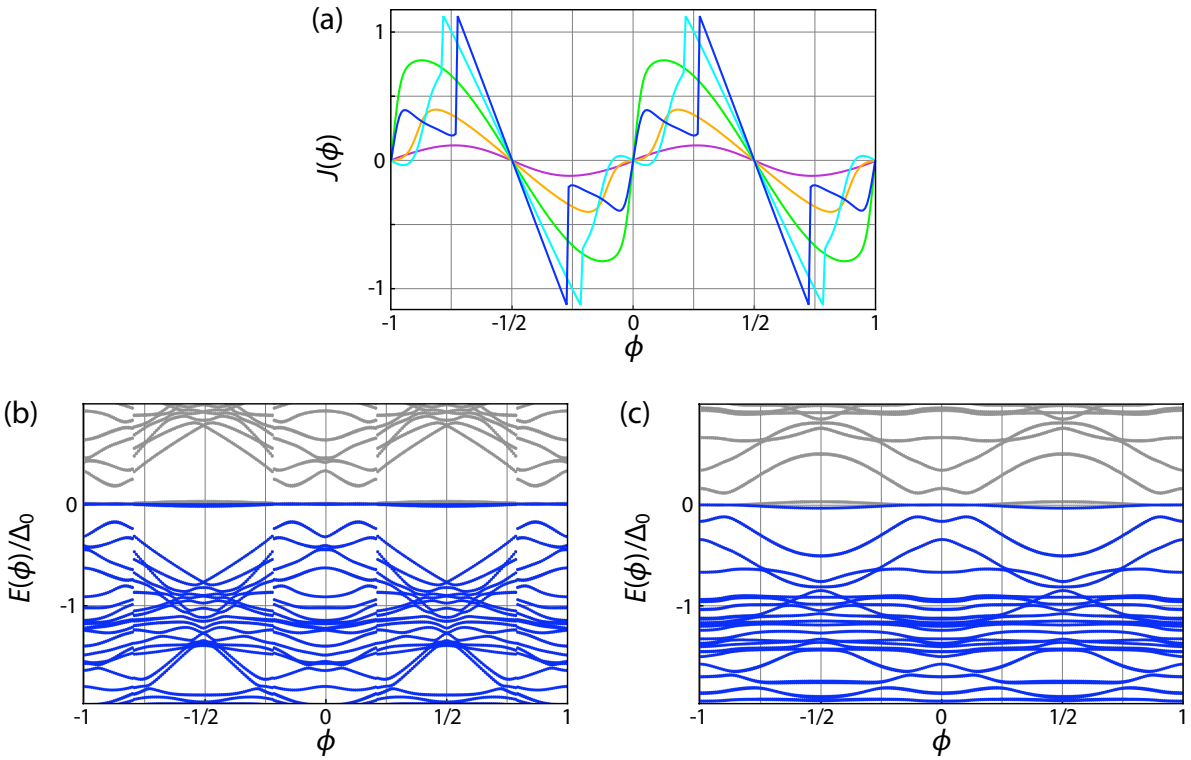

Figure 7.5: Supercurrent $J(\phi)$ and energy spectrum of a 20 × 20 square frame with a 8 × 8 hole containing a Josephson junction as a function of flux . The width of the arms for the frame is six sites. The impurity potential is $U = 100t$. (a) $J(\phi)$ for one (blue), two (turquoise), three (green), four (orange) and five (purple) impurity sites. (b) Energy spectrum for two impurity sites. (c) Energy spectrum for four impurity sites.

function of ϕ for (b) two impurities and (c) four impurities for a 20 × 20 square frame with a 8 × 8 square hole. In the presence of impurities, bound states arise at E_F in a d-wave superconductor [76, 78], which are nearly flux independent. Otherwise, the spectrum in (b) is very similar to that of the clean frame discussed in section 5 (figure 5.4). Clearly visible is the discontinuity of the spectrum where the condensate reconstructs to a superconducting state with different winding number q. The relevance of q is a characteristic property of transparency and is directly connected to a discontinuity of the supercurrent, which is visible in figure 7.5 (a) for one and two impurities.

For three to five impurities, the supercurrent is continuous, as is the spectrum shown in (c) for four impurities. Nevertheless, the typical features of the square frame spectrum are still present in (c), in particular the gap in the odd flux regimes and one energy level approaching E_F in the even q regime. This level causes the wiggle in the supercurrent around $\phi = 0$; its slope and that of a few others remain almost as steep as in a clean frame, which indicates the existence of channels with free current flow. The Doppler shift of

nodal states is therefore not negligible in calculating the supercurrent over transparent Josephson junctions, and it may cause deviations from the $\sin(4\pi\phi)$ current-flux relation even in the limit of large junctions.

We finally remark that in the case of five impurities, only one channel through the junction remains, which is almost blocked by the bound state. Thus the spectrum becomes nearly flux independent, leading to a junction in the tunnel regime. The supercurrent does not reproduce the predicted $\sin(4\pi\phi)$ current-phase relation, but rather a $\sin(2\pi\phi)$ relation. This is due to the point-contact like character of the junction and the extreme limit of the deformation of the current-flux relation as shown in figure 7.2.

7.2 Field Threaded Junctions

A magnetic field threading a Josephson junction adds to the phase difference of the order parameters of the superconductors on both sides of the junction in a characteristic way, and thus alters the supercurrent over the junction as a function of the field. This behavior is known as the second Josephson relation and understood well on the basis of a Ginzburg-Landau description. For a fixed external phase difference $\delta\varphi$, the current-flux relation of a linear junction homogeneous in y-direction forms a Fraunhofer diffraction pattern [88]. The current-flux relation is known under this name, although it deviates from the Fraunhofer form for all other junction geometries, but it has a characteristic flux periodicity of $\Phi_0/2$ for conventional Josephson junctions. The Fraunhofer pattern of flux threaded junctions is therefore a further relation where the Doppler shift might cause a doubling of the flux period.

Here we use again the linear junction model of section 7.1.1 and fix the phase difference to $\delta\varphi = \pi/2$, for which the absolute value of the current over a junction in the tunnel regime is maximal. In order to introduce a magnetic field threading the junction, we construct the junction from single plaquettes with potential scatterers with a repulsive potential U on each site of the plaquette. Each plaquette l belonging to the junction is threaded by a magnetic flux ϕ^l, generating Peierls phase factors φ^l_{ij} as described in appendix C.1. Here, we restrict our discussion to a homogeneous field distribution inside the junction: $\phi^l = \phi$ for all l. In the presence of a magnetic field, the system is not homogeneous in y-direction, and we have to diagonalize it fully in real space. This restricts again the maximum system size which we can analyze.

7.2.1 Current-Flux Relation of Tunnel Junctions

The simplest model of a field threaded Josephson junction consists of two lines of impurity sites as used in section 7.1.1 (figure 7.1). The current-flux relation of such a junction, as obtained from the Bogoliubov - de Gennes equations, is shown in figure 7.6 for s and

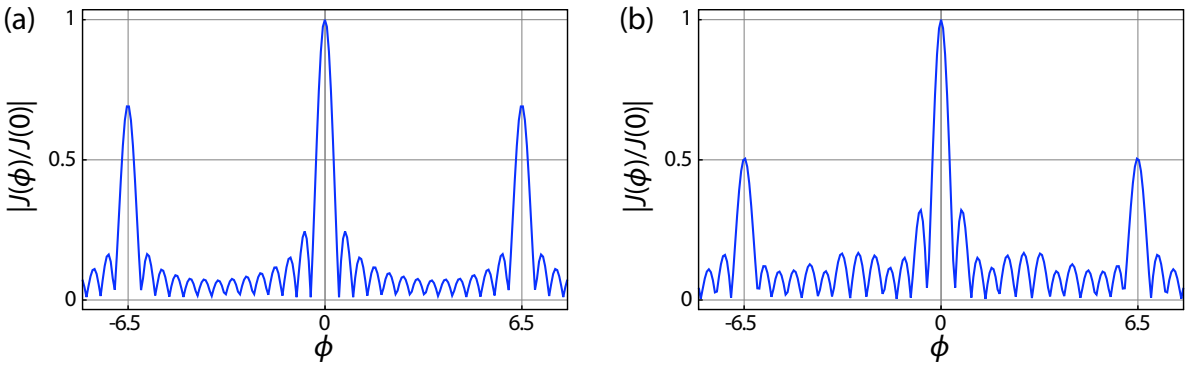

Figure 7.6: Absolute value of the maximum current over a tunnel junction as a function of the total magnetic flux , obtained from the Bogoliubov - de Gennes equations solved on a lattice with $N = 16$, $M = 14$, $U = 5t$, and $\delta\varphi = \pi/2$ in units of $J(0)$. (a) s-wave pairing with $V_0 = t$. (b) d-wave pairing with $V_1 = 0.7t$. Here ϕ is the flux within the junction, generated by an external magnetic field.

d-wave junctions with a length of 14 sites, or 13 plaquettes. Upon first glance, the current-flux relation of the s-wave junction [figure 7.6 (a)] looks indeed like the Fraunhofer pattern known from the Ginzburg-Landau model of linear Josephson junctions [88], as does the current-flux relation with slight deviations for the d-wave junction [figure 7.6 (b)]. The characteristics are a central peak around $\phi = 0$ of width Φ_0 and side peaks of decreasing height of width $\Phi_0/2$. They display the expected global periodicity of $13\Phi_0$, enforced by gauge invariance if each plaquette is threaded by an integer multiple of Φ_0. A closer look on figure 7.6 (a) shows however, that the s-wave junction has one maximum too many in one period of $13\Phi_0$, whereas the d-wave junction has not. The width of the peaks in (a) is therefore a bit smaller than the expected value Φ_0. We explain this effect jointly with an investigation of the current-flux relation of inhomogeneous junctions in the following by analyzing the Ginzburg-Landau model for junctions in lattices.

We consider a two dimensional superconductor which is divided by a thin, quasi one-dimensional Josephson junction of width d oriented along the y-direction with $d \ll \lambda$, such that screening currents are negligible. If the junction is threaded by a constant magnetic field $B_z(x, y) = B_z$, the supercurrent over the junction derived from the Ginzburg-Landau equations is

$$J = \int \mathrm{d}y\, j_c(y) \sin(ky), \tag{7.6}$$

where $k = \pi B_z d/\Phi_0$. The critical current density $j_c(y)$ is an arbitrary function of y controlled by the microscopic structure of the junction. If $j_c(y)$ is constant, one obtains

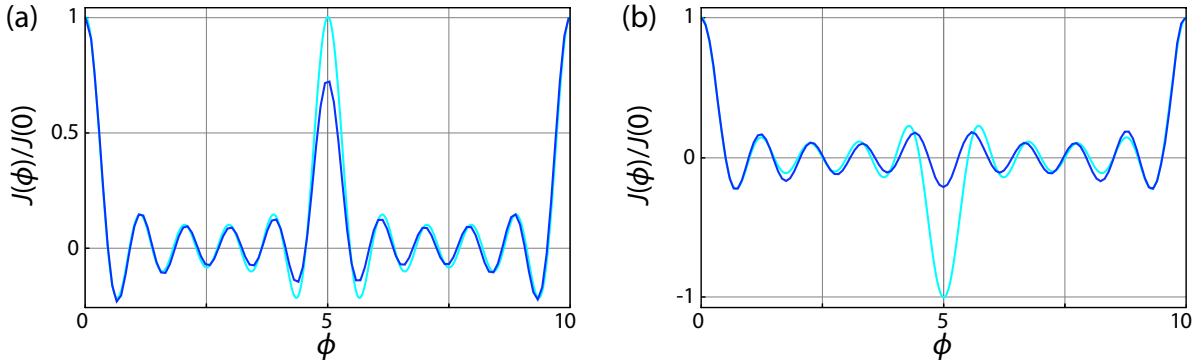

Figure 7.7: Current-flux relation of a Josephson junction as in figure 7.6 but with $M = 11$ (10 plaquettes) as obtained from the Bogoliubov - de Gennes equations (blue) and from the discrete Ginzburg-Landau model (turquoise). (a) s-wave pairing: The peak at $\phi = (M-1)/2$ of the current-flux relation (7.9) has the same sign as the peak at $\phi = 0$. (b) d-wave pairing: The peak at $\phi = (M-1)/2$ of the current-flux relation (7.11) has the opposite sign as the peak at $\phi = 0$.

the well known Fraunhofer pattern

$$\left|\frac{J(\Phi)}{J(0)}\right| = \left|\frac{\sin(\pi\Phi/\Phi_0)}{\pi\Phi/\Phi_0}\right| \tag{7.7}$$

for the current over the junction, where Φ is the total magnetic flux through the area of the junction.

On a discrete square lattice with M lattice sites in y-direction and an order parameter defined on the lattice sites (s-wave), equation (7.6) becomes

$$J = \sum_{i=1}^{M} j_{c,i} \sin(k y_i). \tag{7.8}$$

If $j_{c,i}$ is equal for all i, one obtains a flux dependence similar to the Fraunhofer pattern:

$$\frac{J(\phi)}{J(0)} = \sum_{i=1}^{M} \sin(k y_i)/(M+1) = \frac{\sin\left(k(M+1)/M\right)}{(M+1)\sin\left(k/M\right)}. \tag{7.9}$$

This formula reproduces the flux dependence of the supercurrent as obtained from the Bogoliubov - de Gennes equations (shown in figure 7.7), apart from slight deviations in the amplitude around the middle peak at $\phi = (M-1)/2$. It explains naturally the deviation from $\Phi_0/2$ periodicity: it is an effect of discreteness, caused by the fact that there is a lattice site more in y-direction than the number of plaquettes.

From what we just learned about an s-wave junction, we construct a simple Ginzburg-Landau analogon for a d-wave junction: in a d-wave superconductor, the order parameter

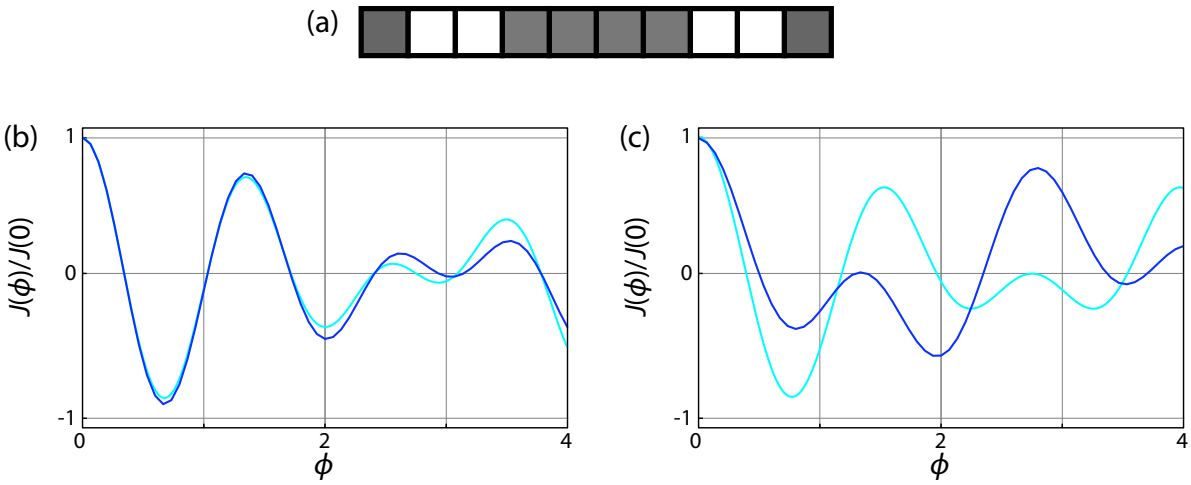

Figure 7.8: Current-flux relation for a Josephson junction with $M = 11$ and a inhomogeneous impurity distribution. The gray plaquettes in the profile of the junction (a) have a scattering potential $U = 100t$, while the white plaquettes have $U = 2t$, thus leaving two transparent channels through which almost the entire current flows. Blue: Bogoliubov - de Gennes equations and turquoise: Ginzburg-Landau model for (b) *s*-wave pairing and (c) *d*-wave pairing.

is defined on the bonds between two neighboring lattice sites. We define the corresponding supercurrent therefore as a current flowing in the middle between two sites, which leads to

$$J = \sum_{i=1}^{M-1} j_{c,i} \sin(k(y_i + 1/2)). \tag{7.10}$$

In the case of a constant $j_{c,i}$, we get

$$\frac{J(\phi)}{J(0)} = \sum_{i=1}^{M-1} \sin(k(y_i + 1/2))/M = \frac{\sin(k)}{M \sin(k/M)}, \tag{7.11}$$

which indeed reproduces almost the $\Phi_0/2$ periodic Fraunhofer pattern obtained from the Bogoliubov - de Gennes equations with nearest-neighbor pairing. The deviations in the amplitude are larger than for the *s*-wave junction, which signifies that the Ginzburg-Landau conditions are not fulfilled as well as by the *s*-wave junction.

The Ginzburg-Landau formulae (7.8) and (7.10) are suitable also to calculate the supercurrent over junctions with an inhomogeneous impurity distribution. It is instructive to compare it again to results obtained from the Bogoliubov - de Gennes equations. Figure 7.8 shows such a comparison for a junction with $M = 11$ and current flowing only through the two gaps between the white plaquettes in figure 7.8 (a). In the microscopic model, this is achieved by setting strong repulsive potentials $U = 100t$ on the

sites of the gray plaquettes and a small potential $U = 2t$ on the white plaquettes. In the Ginzburg-Landau model, we set $j_{c,i} = 0$ except for the two transparent channels. This system looks quite far from fulfilling the conditions of the Ginzburg-Landau equations. Nevertheless, for the s-wave junction, the results obtained from the Bogoliubov - de Gennes and Ginzburg-Landau equations are remarkably close. Even for the d-wave junction, the simple construction using the Ginzburg-Landau equations reproduces the same features as the Bogoliubov - de Gennes equations, in particular it has maxima for the same flux values, but the amplitudes of the single oscillations deviate strongly.

All these considerations together lead to the final conclusion that, even for small junctions where discreteness is pronounced, we do not find any indications that the Doppler shift has an effect on the current-flux relation of Josephson junctions in the tunnel regime. The essential characteristics of the current-flux relation, especially the position of the current maxima, agree well with the Ginzburg-Landau model, where these effects are not included.

7.2.2 Current-Flux Relation of Transparent junctions

A magnetic field threading a Josephson junction generates a supercurrent circulating around the junction, similar to a vortex in a type II superconductor, but with the complete flux in the junction. If the junction is sufficiently transparent, the order parameter reacts to the current loop with a phase winding as in a flux threaded ring, with a winding number q that minimizes the total energy. The superconducting state in a transparent junction is therefore characterized similarly as a loop by the quantum number q related to a center-of-mass movement of the Cooper pairs and consequently, the supercurrent over the junction changes sign discontinuously when the condensate reconstructs to another q.

Remarkably, if the transparency is reduced, the discontinuities vanish smoothly, the current-flux relation of the superconducting state with fixed q becomes periodic in ϕ, and in the tunnel regime, all states with different q become equivalent. This behavior is illustrated by figure 7.9, which shows $E(\phi)$, $J(\phi)$ and the spectrum as a function of ϕ for a uniform junction with nearest-neighbor pairing and $U = 2t$. The total energy consists of a series of parabolae, which correspond to different phase winding numbers. The kinks in $E(\phi)$ and in the flux dependence of the spectrum are sharp for small values of ϕ, but the finite repulsion on the junction smoothes out the discontinuities in the supercurrent. Although the Doppler shift of the energy levels is not strongly pronounced in the example of figure 7.9, the physical phenomena typical for multiply connected geometries govern the field dependence of the supercurrent over a Josephson junction, if its transparency is sufficiently high.

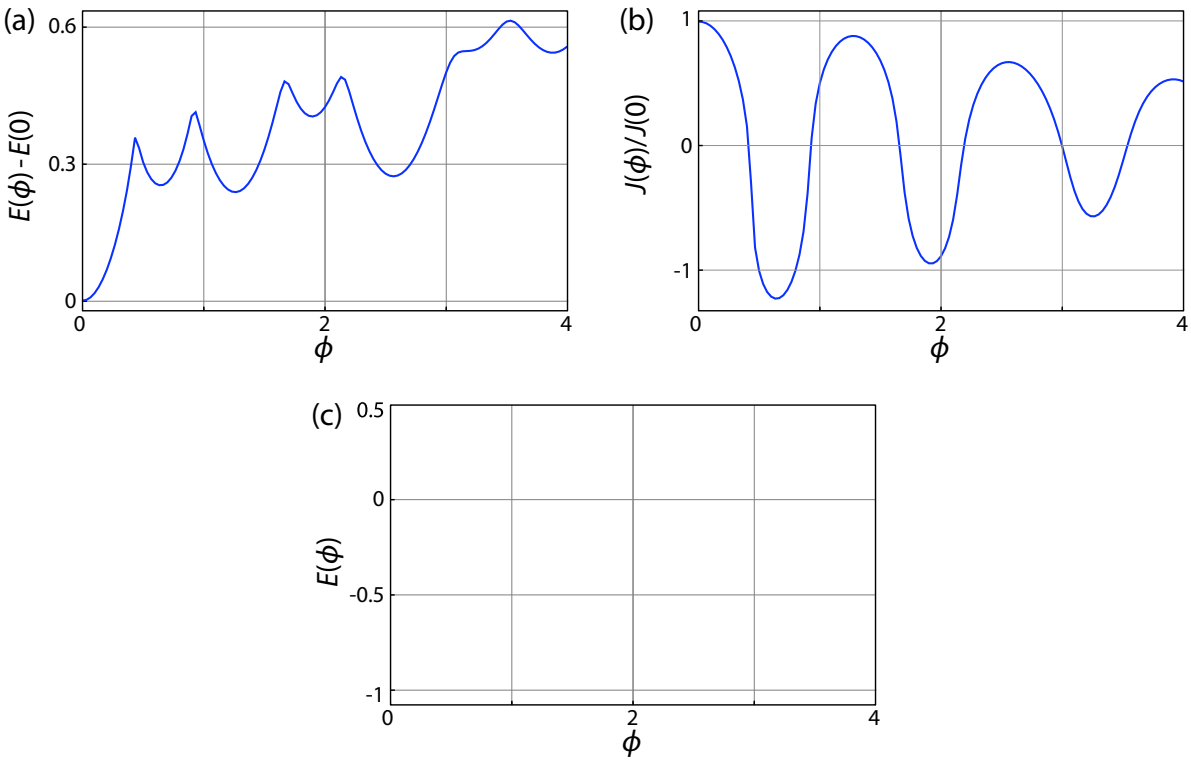

Figure 7.9: Characteristics of a transparent junction as obtained from the Bogoliubov - de Gennes equations in a system with $N = 14$ and $M = 12$ and a homogeneous impurity distribution with repulsive potential $U = 2t$.

8 Conclusions

In part I we established the theory of the crossover from Φ_0 periodic persistent currents in normal metal loops to the $\Phi_0/2$ periodic supercurrent in conventional superconducting loops. We showed in a momentum-space formulation that for unconventional pairing symmetry, this crossover is extended to infinite loop sizes, and that the Φ_0 periodic current component decays algebraically in the loop size.

The calculations in momentum space were restricted to rotational symmetric systems like a cylinder, whose energy spectrum depends sensitively on microscopic details. In section 5 we have provided an analysis of the flux periodicity in a square frame with d-wave pairing symmetry analogous to the one in part I for a cylinder geometry. The results are amazingly similar, as the energy spectra in figures 3.6 and 5.4 show. Nevertheless, the real-space calculations contributed decisively to the understanding of the problem of the flux periodicity. Firstly, we could prove that the characteristic flux dependence of the d-wave energy spectrum is not geometry dependent. Even more, the reduction of the symmetry stabilizes this features, as calculations on frames containing impurities or rough boundary conditions showed.

Secondly, within the real-space formulation, we have the freedom to construct and analyze more complex systems than just loops, in particular we investigated the periodicity of Josephson junctions with and without magnetic fields for quite a while. The idea that the Doppler shift drives energy levels through the Fermi energy in junctions between d-wave superconductors, and thereby doubles the periodicity of the current-phase relation, seemed natural, but it turned out to be more complicated. Thin junctions with only a few channels have always a period in the phase difference of 4π even for s-wave superconductors, and the Doppler shift in tunnel junctions is too small to influence the current-phase relation. Only for transparent junctions, the Doppler shift becomes important; in this regime the supercurrent over a Josephson junction behaves similar to the persistent supercurrent in a loop.

These observations are valid in the same way for the current-flux relation of field threaded junctions. The long and rather laborious investigation therefore did not produce any new and exciting physics. Nevertheless, it was necessary to realize the connection between the transparence of a system and the Doppler shift of the energy levels, and it provided many improvements in the technique of solving the Bogoliubov - de Gennes equations. It is notable that the microscopic theory reproduced the results from the Ginzburg-Landau description of Josephson junctions in such a good agreement, even

for nanoscopically small systems with d-wave pairing.

Finally, within the real-space framework of the Bogoliubov - de Gennes equations, a self consistent treatment of the magnetic field and the induced supercurrent is possible. Within a simplified annulus model we succeeded to analyze the crossover from fluxoid to flux quantization while increasing the thickness of the annulus. The microscopic calculations in a square frame tended to confirm this method, but the technique used was not good enough to obtain fully converged solutions in large enough systems.

Part III

Finite Momentum Pairing

9 Introduction

In the description of superconducting loops using the BCS Hamiltonian (1.10) of section 1.2.1, we chose the pair momentum, or phase winding number, q by minimizing the energy of the system with respect to all q. This is necessary not only to determine the groundstate, but also to ensure gauge invariance of the Hamiltonian. The requirement to adjust the Hamiltonian "by hand" for each specific value of the magnetic flux ϕ is a consequence of the BCS ansatz in which all Cooper pairs have the same center of mass (angular) momentum q. This assumption is not a strict requirement for the solvability of the theory, although it simplifies the solution tremendously. It is therefore evident to look for a more general pairing Hamiltonian which naturally conserves gauge invariance and selects the appropriate pair momenta of the groundstate.

The BCS ansatz in real space, described by the Bogoliubov - de Gennes equations, provides such a generalization in principle. The Fourier transformation of the real-space BCS Hamiltonian leads to a momentum-space Hamiltonian containing a sum over all pair momenta [equations (10.1) and (10.18)], providing exactly the model required above. A mathematical formalism to deal with such a model is the set of Gor'kov equations in their general form. Applying them on an s-wave loop, we found that indeed the self-consistency condition selects reliably the pair momentum of the groundstate, while the order parameters for all other pair momenta vanish; the Cooper pairs condensate as expected into a macroscopic quantum state characterized by the quantum number q.

The same equations applied on a superconducting loop with d-wave pairing brought a surprising result: For sufficiently strong pairing interaction strength V_1, not only one pair momentum was selected, but typically two different pair momenta q and $-q$ simultaneously, both for zero and finite magnetic flux. This result is special for two reasons: firstly because finite momentum pairing without a magnetic field is unusual and secondly because the coexistence of more than one pair momentum contradicts the established picture of the superconducting condensate. We have found a clearly non-BCS solution of the Gor'kov equations, which is rather a relative of the inhomogeneous Larkin-Ovchinnikov state [92], but in our case without a time-inversion breaking magnetic field.

A superconducting state, in which the pair momenta q and $-q$ coexist, has been investigated intensively in the last few years in a quite different connection: the "pair density wave" (PDW) state, which is regarded as a candidate for the superconducting state observed in some high-T_c cuperates, especially Nd-doped $La_{2-x}Sr_xCuO_4$ [93, 94] and

$La_{2-x}Ba_xCuO_4$ for $x = 1/8$ [95–99]. These systems show a charge stripe order, typically with a wave length of four lattice constants, that coexists with spin order with a wave length of eight lattice constants, and superconductivity at sufficiently low temperatures. The PDW state is defined as a multi-component Ginzburg-Landau order parameter in real space, in the most common form with two components as $\Delta(\mathbf{r}) = \Delta_{\mathbf{q}} e^{i\mathbf{q}\cdot\mathbf{r}} + \Delta_{-\mathbf{q}} e^{-i\mathbf{q}\cdot\mathbf{r}}$. It is accompanied by a charge-stripe order with wave vector $\mathbf{K} = 2\mathbf{q}$, and charge stripes perpendicular to $\mathbf{q}$. There are more complex forms of the PDW state with, e.g., four pair momenta in x- and y-direction and a checkerboard charge order, or even a state with eight pair momenta. The PDW state is a zero field equivalent of the Larkin-Ovchinnikov state and explicitly constructed to conserve time-inversion symmetry.

So far the PDW state is a pure phenomenological model, analyzed in most detail by Agterberg *et al.* [100–102] and Berg *et al.* [97, 103, 104] in the last few years. Their investigations do not incorporate the pairing symmetry of electron pairs, and a theory which yields the PDW as the groundstate of a microscopic Hamiltonian is lacking. Developments in this direction were made by several authors, mostly in connection with the Larkin-Ovchinnikov state [105–107] or in a multi-band system [108]. Here the new superconducting solutions of the Gor'kov equations come into the focus. We will see that these solutions are the momentum space equivalents of PDW states, and they emerge in our model as the groundstate of the extended pairing Hamiltonian, if the pairing symmetry allows for gap nodes. In this way, the finite momentum pairing theory for superconducting loops, which we described in parts I and II, develops in a new exciting direction completely independent of multiply connected geometries and magnetic fields; it leads to a microscopic model for the PDW state.

The connection between the PDW state and the charge-stripe order observed in the cuprates is not clearly established yet. Our model does not contain spin correlations, which are essential for the emergence of the stripe order in $La_{2-x}Sr_xCuO_4$ for $x = 1/8$ and the characteristic wave length of four lattice constants. Spin-ladder models in the framework of the t–J model, either site or bond centered, proved quite successful in the description of the spin properties of the striped cuprates [109–114]. The inclusion of spin correlations into our microscopic theory is therefore a desirable extension and a project within the real space formulation of our model. The solution as presented here is therefore not meant as a theory for the stripe phase in the cuprates, but it is a proof of principle that a microscopic pairing Hamiltonian can exhibit a time-inversion symmetric finite momentum pairing groundstate in zero magnetic field.

In chapter 10, we introduce the formalism of the Gor'kov equations and their solution. We further show that the model is equivalently solvable by diagonalizing a mean-field pairing Hamiltonian using the Bogoliubov transformation method, or by extending the Bogoliubov - de Gennes equations adequately in real space. A detailed analysis of the solutions of the model is given in section 11 with focus on the striped PDW state with pair momenta $\mathbf{q}$ and $-\mathbf{q}$. In section 12 we eventually return to the problem of flux

periodicities of superconducting loops, which we investigate with focus on the new effects emerging from the possibility of coexisting pair momenta. We show that the realization of PDW states in loops allows for a number of new flux periodicities, in particular $\Phi_0/4$ periodicity, and even the emergence of fractional flux quanta.

10 Formalism

In the following we introduce the mathematical formalism necessary for the theoretical description of the coexistence of different pair momenta. We concentrate on the Green's function technique for the description of superconductivity, relying on the Gor'kov equations. This technique is treated as detailed as necessary for the description of the characteristic effects arising from the coexistence of different pair momenta in section 10.1. A derivation of the Gor'kov equations and a collection of formulae for the description of the PDW state is given in appendix D. In analogy to the solution of the Gor'kov equations, it is straightforward to extend the well-established Bogoliubov transformation method for superconductivity with finite momentum pairing, or the Bogoliubov - de Gennes equations in real space to allow for different pair momenta. We introduce these latter techniques in section 10.2 and more detailed in appendix D.3 and D.4.

10.1 Gor'kov Equations

We start from a tight binding Hamiltonian on a square lattice with N sites and periodic boundary conditions

$$\mathcal{H} = \sum_{\mathbf{k},s} \varepsilon_{\mathbf{k}} c^\dagger_{\mathbf{k}s} c_{\mathbf{k}s} + \frac{1}{N} \sum_{\mathbf{q}} \sum_{\mathbf{k},\mathbf{k}'} \sum_{s,s'} V(\mathbf{k},\mathbf{k}',\mathbf{q}) c^\dagger_{\mathbf{k}s} c^\dagger_{-\mathbf{k}+\mathbf{q}s'} c_{-\mathbf{k}'+\mathbf{q}s'} c_{\mathbf{k}'s}. \tag{10.1}$$

with an attractive interaction $V(\mathbf{k},\mathbf{k}',\mathbf{q})$ and k_x, k_y, q_x, and $q_y \in [-\pi,\pi]$. With a nearest and next-nearest neighbor hopping amplitude t and t', respectively, the single-electron dispersion has the form

$$\varepsilon_{\mathbf{k}} = -2t\left[\cos k_x + \cos k_y\right] + 4t' \cos k_x \cos k_y - \mu. \tag{10.2}$$

For the superconducting state with singlet pairing, we use the BCS type mean-field decoupling scheme and approximate $\langle c^\dagger_{\mathbf{k}\uparrow} c^\dagger_{-\mathbf{k}+\mathbf{q}\downarrow} c_{-\mathbf{k}'+\mathbf{q}\downarrow} c_{\mathbf{k}'\uparrow}\rangle \to \langle c^\dagger_{\mathbf{k}\uparrow} c^\dagger_{-\mathbf{k}+\mathbf{q}\downarrow}\rangle \langle c_{-\mathbf{k}'+\mathbf{q}\downarrow} c_{\mathbf{k}'\uparrow}\rangle$. The system is then represented by the spin independent imaginary time Green's function $\mathcal{G}(\mathbf{k},\mathbf{k}',\tau) = -\langle T_\tau c_{\mathbf{k}s}(\tau) c^\dagger_{\mathbf{k}'s}(0)\rangle$, and the anomalous propagators $\mathcal{F}(\mathbf{k},\mathbf{k}',\tau) = \langle T_\tau c_{\mathbf{k}s}(\tau) c_{-\mathbf{k}'s'}(0)\rangle$ and $\mathcal{F}^*(\mathbf{k},\mathbf{k}',\tau) = \langle T_\tau c^\dagger_{-\mathbf{k}s}(\tau) c^\dagger_{\mathbf{k}'s'}(0)\rangle$ for $s \neq s'$. The Hamiltonian (10.1) allows for other mean-field terms which correspond to charge order and do not appear in standard BCS theory. These we neglect in the present formalism and introduce them in section 10.2 in a formalism more convenient for this purpose.

The Heisenberg equations of motion for the normal and anomalous Green's functions lead to the Gor'kov equations [58]:

$$\mathcal{G}(\mathbf{k},\mathbf{k}',\omega_n) = \mathcal{G}_0(\mathbf{k},\omega_n)\left[\delta_{\mathbf{k}\mathbf{k}'} - \sum_{\mathbf{q}} \Delta(\mathbf{k},\mathbf{q})\mathcal{F}^*(\mathbf{k}-\mathbf{q},\mathbf{k}',\omega_n)\right], \tag{10.3}$$

$$\mathcal{F}(\mathbf{k},\mathbf{k}',\omega_n) = \mathcal{G}_0(\mathbf{k},\omega_n)\sum_{\mathbf{q}} \Delta(\mathbf{k},\mathbf{q})\mathcal{G}(-\mathbf{k}',-\mathbf{k}+\mathbf{q},-\omega_n), \tag{10.4}$$

$$\mathcal{F}^*(\mathbf{k},\mathbf{k}',\omega_n) = -\mathcal{G}_0(-\mathbf{k},-\omega_n)\sum_{\mathbf{q}} \Delta^*(\mathbf{k},\mathbf{q})\mathcal{G}(\mathbf{k}+\mathbf{q},\mathbf{k}',\omega_n). \tag{10.5}$$

where $\mathcal{G}_0(\mathbf{k},\omega_n) = \left[i\omega_n - \varepsilon_{\mathbf{k}}\right]^{-1}$ is the Green's function in the normal state. The order parameter $\Delta(\mathbf{k},\mathbf{q})$ is determined by the self-consistency condition

$$\Delta(\mathbf{k},\mathbf{q}) = -\frac{T}{N}\sum_{n}\sum_{\mathbf{k}'} V(\mathbf{k},\mathbf{k}',\mathbf{q})\mathcal{F}(\mathbf{k}',\mathbf{k}'-\mathbf{q},\omega_n). \tag{10.6}$$

$$\Delta^*(\mathbf{k},\mathbf{q}) = -\frac{T}{N}\sum_{n}\sum_{\mathbf{k}'} V(\mathbf{k},\mathbf{k}',\mathbf{q})\mathcal{F}^*(\mathbf{k}'-\mathbf{q},\mathbf{k}',\omega_n). \tag{10.7}$$

The normal and anomalous Green's functions have finite values only under the following conditions:

$$\mathcal{G}(\mathbf{k},\mathbf{k}',\omega_n) \neq 0 \text{ if} \begin{cases} \mathbf{k}' = \mathbf{k}, \\ \mathbf{k}' = \mathbf{k}+\mathbf{q}-\mathbf{q}' \text{ and} \Delta(\mathbf{k},\mathbf{q}) \neq 0,\ \Delta(\mathbf{k}',\mathbf{q}') \neq 0 \end{cases} \tag{10.8}$$

$$\mathcal{F}(\mathbf{k},\mathbf{k}',\omega_n) \neq 0 \text{ if } \ \mathbf{k}' = \mathbf{k}-\mathbf{q} \text{ and } \Delta(\mathbf{k},\mathbf{q}) \neq 0 \tag{10.9}$$

$$\mathcal{F}^*(\mathbf{k},\mathbf{k}',\omega_n) \neq 0 \text{ if } \ \mathbf{k}' = \mathbf{k}+\mathbf{q} \text{ and } \Delta(\mathbf{k},\mathbf{q}) \neq 0 \tag{10.10}$$

Inserting Eq. (10.4) into Eq. (10.3) leads to a system of coupled equations for the Green's function:

$$\begin{aligned}\mathcal{G}(\mathbf{k}+\mathbf{q}_1,\mathbf{k}+\mathbf{q}_2,\omega_n) &= \mathcal{G}_0(\mathbf{k}+\mathbf{q}_1,\omega_n)\Delta(\mathbf{k}+\mathbf{q}_1,\mathbf{q}_1)\mathcal{G}_0(-\mathbf{k},-\omega_n) \\ &\times\left[\Delta^*(\mathbf{k},\mathbf{q}_1)\mathcal{G}(\mathbf{k}+\mathbf{q}_1,\mathbf{k}+\mathbf{q}_2,\omega_n) + \Delta^*(\mathbf{k},\mathbf{q}_2)\mathcal{G}(\mathbf{k}+\mathbf{q}_2,\mathbf{k}+\mathbf{q}_2,\omega_n)\right]^{-1}.\end{aligned} \tag{10.11}$$

In principle, equation (10.11) can be solved numerically for all $\mathbf{k}$ and ω_n to obtain exact solutions of Gor'kov's equations, but this is a rather extensive task. Assuming that $\sum_n \mathcal{G}(\mathbf{k},\mathbf{k}',\omega_n) \ll \sum_n \mathcal{G}(\mathbf{k},\mathbf{k},\omega_n)$ for $\mathbf{k} \neq \mathbf{k}'$, which will be verified a posteriori, $\mathcal{G}(\mathbf{k}+\mathbf{q}_1,\mathbf{k}+\mathbf{q}_2,\omega_n)$ is approximated by keeping only the term proportional to $\mathcal{G}(\mathbf{k}+\mathbf{q}_2,\mathbf{k}+\mathbf{q}_2,\omega_n)$ in the denominator in Eq. (10.11) and the sum over $\mathbf{q}$ in (10.3) – (10.5) drops out. Within this approximation the Gor'kov equations are solved analytically, as shown below.

To find explicit solutions of the Gor'kov equations we choose an ansatz for a self consistent solution consisting of Q trial vectors $\mathbf{q}_1, \ldots, \mathbf{q}_Q$ and set $\Delta(\mathbf{k}, \mathbf{q}) = 0$ for all other values of $\mathbf{q} \neq \mathbf{q}_i$. Thereby we test selected combinations of $\mathbf{q}$-vectors for self consistent solutions. The Green's function can then be rearranged as

$$\mathcal{G}(\mathbf{k}, \mathbf{k}, \omega_n) = \frac{\prod_i (-i\omega_n - \varepsilon_{-\mathbf{k}+\mathbf{q}_i})}{(i\omega_n - \varepsilon_{\mathbf{k}}) \prod_i (-i\omega_n - \varepsilon_{-\mathbf{k}+\mathbf{q}_i}) + \sum_i \Delta(\mathbf{k}, \mathbf{q}_i) \Delta^*(\mathbf{k} - \mathbf{q}_i, \mathbf{q}_i) \prod_{j \neq i} (-i\omega_n - \varepsilon_{-\mathbf{k}+\mathbf{q}_j})}, \tag{10.12}$$

where the products and sums over i and j run from 1 to Q. The denominator of $\mathcal{G}(\mathbf{k}, \mathbf{k}, \omega_n)$ is a polynomial in ω_n of degree $Q + 1$, whose zeros $E_\alpha(\mathbf{k})$, $\alpha = 0, \ldots, Q$, constitute the energy spectrum of the system. If $Q \leq 3$, one can obtain algebraic expressions for $E_\alpha(\mathbf{k})$, which are given in appendix D.2.4 for $Q = 2$. One obtains the momentum occupation probability function $n(\mathbf{k})$ by summing over ω_n, which leads to

$$n(\mathbf{k}) = 2T \sum_n \mathcal{G}(\mathbf{k}, \mathbf{k}, \omega_n) = 2 \sum_\alpha u_\alpha^2(\mathbf{k}) f(E_\alpha(\mathbf{k})), \tag{10.13}$$

where

$$u_\alpha^2(\mathbf{k}) = \frac{\prod_i [E_\alpha(\mathbf{k}) - \varepsilon_{-\mathbf{k}+\mathbf{q}_i}]}{\prod_{\beta \neq \alpha} [E_\alpha(\mathbf{k}) - E_\beta(\mathbf{k})]}. \tag{10.14}$$

and the products and sums over α and β run from 0 to Q. The factor 2 in Eq. (10.13) comes from the sum over spin $\uparrow$ and $\downarrow$. Analogously one finds the anomalous probabilities

$$\tilde{n}(\mathbf{k}, \mathbf{q}_i) = T \sum_n \mathcal{F}(\mathbf{k}, \mathbf{k} - \mathbf{q}_i, \omega_n) = \Delta(\mathbf{k}, \mathbf{q}_i) \sum_\alpha w_\alpha^2(\mathbf{k}, \mathbf{q}_i) f(E_\alpha(-\mathbf{k} + \mathbf{q}_i)) \tag{10.15}$$

with

$$w_\alpha^2(\mathbf{k}, \mathbf{q}_i) = -\frac{\prod_{j \neq i} [E_\alpha(-\mathbf{k} + \mathbf{q}_i) - \varepsilon_{-\mathbf{k}+\mathbf{q}_i-\mathbf{q}_j}]}{\prod_{\beta \neq \alpha} [E_\alpha(-\mathbf{k} + \mathbf{q}_i) - E_\beta(-\mathbf{k} + \mathbf{q}_i)]}. \tag{10.16}$$

The conventional BCS solution is realized for $Q = 1$ with just two quasiparticle bands and $\mathbf{q} = \mathbf{0}$. Generally, one obtains a set of $2Q$ coupled self-consistency equations for $\Delta(\mathbf{k}, \mathbf{q}_i)$:

$$\frac{\Delta(\mathbf{k}, \mathbf{q}_i)}{V_{0,1}} = -\frac{T}{N} \sum_{\mathbf{k}'} \Delta(\mathbf{k}', \mathbf{q}_i) \tilde{n}(\mathbf{k}, \mathbf{q}_i), \tag{10.17}$$

for an on-site interaction strength V_0 or a nearest-neighbor interaction strength V_1.

10.2 Extended Bogoliubov Transformation

The mean-field decoupling scheme used above leads to an extended BCS-type Hamiltonian of the form

$$\mathcal{H} = \sum_{\mathbf{k},s} \varepsilon_{\mathbf{k}} c^\dagger_{\mathbf{k}} c_{\mathbf{k}} + \sum_{\mathbf{k}} \sum_{\mathbf{q}} \left[\Delta^*(\mathbf{k},\mathbf{q}) c_{-\mathbf{k}+\mathbf{q}\downarrow} c_{\mathbf{k}\uparrow} + \Delta(\mathbf{k},\mathbf{q}) c^\dagger_{\mathbf{k}\uparrow} c^\dagger_{-\mathbf{k}+\mathbf{q}\downarrow} \right] \tag{10.18}$$

Taking the same ansatz for a set of Q pair momenta as for the solution of the Gor'kov equations, the Hamiltonian (10.18) can be written in matrix form using a hermitian $(Q+1)\times(Q+1)$ matrix. Because the structure of this formalism is evident already for $Q = 2$, we present here all equations for $Q = 2$. The generalization to an arbitrary Q is given in appendix D.3 and D.4. Thus we obtain the Hamiltonian

$$\mathcal{H} = \sum_{\mathbf{k}} \left(c^\dagger_{\mathbf{k}\uparrow}, c_{-\mathbf{k}+\mathbf{q}_1\downarrow}, c_{-\mathbf{k}+\mathbf{q}_2\downarrow} \right) \begin{pmatrix} 2\varepsilon_{\mathbf{k}}/3 & \Delta(\mathbf{k},\mathbf{q}_1) & \Delta(\mathbf{k},\mathbf{q}_2) \\ \Delta^*(\mathbf{k},\mathbf{q}_1) & -2\varepsilon_{-\mathbf{k}+\mathbf{q}_1}/3 & 0 \\ \Delta^*(\mathbf{k},\mathbf{q}_2) & 0 & -2\varepsilon_{-\mathbf{k}+\mathbf{q}_2}/3 \end{pmatrix} \begin{pmatrix} c_{\mathbf{k}\uparrow} \\ c^\dagger_{-\mathbf{k}+\mathbf{q}_1\downarrow} \\ c^\dagger_{-\mathbf{k}+\mathbf{q}_2\downarrow} \end{pmatrix}. \tag{10.19}$$

To diagonalize (10.19), we use a Bogoliubov transformation of the form

$$a_\alpha(\mathbf{k}) = u_{0\alpha}(\mathbf{k}) c_{\mathbf{k}\uparrow} + u_{1\alpha}(\mathbf{k}) c_{-\mathbf{k}+\mathbf{q}_1\downarrow} + u_{2\alpha}(\mathbf{k}) c_{-\mathbf{k}+\mathbf{q}_2\downarrow} \tag{10.20}$$

for $\alpha = 0, 1, 2$, where we construct fermionic quasi-particle operators $a_\alpha(\mathbf{k})$ from one electron-creation operator and two hole-creation operators and the three coherence factors $u_{1,2,3}(\mathbf{k})$ that we derive from diagonalzing the 3×3 matrix in (10.19). The Hamiltonian (10.19) then becomes

$$\mathcal{H} = \sum_{\mathbf{k}} \left[E_0(\mathbf{k}) a^\dagger_0(\mathbf{k}) a_0(\mathbf{k}) + E_1(\mathbf{k}) a^\dagger_1(\mathbf{k}) a_1(\mathbf{k}) + E_2(\mathbf{k}) a^\dagger_2(\mathbf{k}) a_2(\mathbf{k}) \right] \tag{10.21}$$

with the three bands of eigenenergies $E_0(\mathbf{k})$, $E_1(\mathbf{k})$ and $E_2(\mathbf{k})$. For $Q = 2$ one can diagonalize the Hamiltonian (10.19) analytically. The eigenenergies $E_\alpha(\mathbf{k})$ are thereby given by the zeros of a polynomial identical to that in the denominator of the Green's function in (10.12), and are therefore identical to the ones obtained from the Gor'kov equations. Further, one finds that $u^2_\alpha(k) = u^2_{0\alpha}(\mathbf{k})$ and $w^2_\alpha(\mathbf{k},\mathbf{q}_i) = u_{i\alpha}(\mathbf{k}) u_{0\alpha}(\mathbf{k})$. Thus the Bogoliubov transformation method is equivalent to the approximated Gor'kov equations.

The three energy bands $E_{0,1,2}(\mathbf{k})$ are ploted in figure 10.1 for the parameters used for the PDW solution in chapter 11.2 and (a) $\mathbf{q}_1 = \mathbf{q}_2 = 0$ and (b) $\mathbf{q}_1 = (\pi/3, 0)$ together with $\mathbf{q}_2 = (-\pi/3, 0)$. In the standard d-wave state (a), $E_0(\mathbf{k})$ and $E_2(\mathbf{k})$ are identical to the upper and lower band in standard BCS theory, while $E_1(\mathbf{k}) = \varepsilon_{\mathbf{k}}$ is identical to the normal state dispersion. The coherence factors $u_{\alpha 1}(\mathbf{k})$ vanish in this case, therefore the band $E_1(\mathbf{k})$ is unoccupied and physically irrelevant. For finite $\mathbf{q}_1 \neq \mathbf{q}_2$, $E_1(\mathbf{k})$ becomes

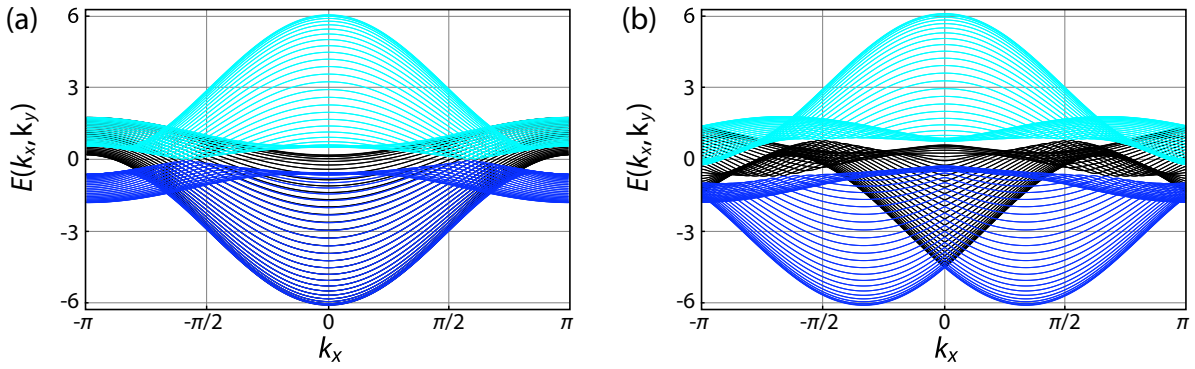

Figure 10.1: Eigenenergies $E_0(k_x, k_y)$ (blue), $E_1(k_x, k_y)$ (black) and $E_2(k_x, k_y)$ (turquoise) of the Hamiltonian (10.19) with nearest-neighbor pairing as a function of k_x for 60 equidistant values of k_y in $[-\pi, \pi]$, $t' = 0.3t$ and $V_1 = t$. (a) Standard d-wave state with $\mathbf{q}_1 = \mathbf{q}_2 = 0$. (b) Finite momentum pairing state with $\mathbf{q}_1 = (\pi/3, 0)$ and $\mathbf{q}_2 = -\mathbf{q}_1$.

populated and the three bands intertwine around E_F. In (b), $E_0(\mathbf{k})$ has minima for $k_x = \pm\pi/3$ for certain values of k_y, while the minima of the other k_y are at $k_x = \pm\pi$. The minima of $E_2(\mathbf{k})$ are at $k_x = 0$ and $k_x = 2\pi/3$. This indicates a charge density modulation in real space in x-direction with wave vector $\mathbf{K} = (2\pi/3, 0)$ and a corresponding wave length $3a$. The folding of the Brillouin zone is however not complete, because there is no k_x where the derivative $\partial E_\alpha(\mathbf{k})/\partial k_x = 0$ for all k_y.

By the transformation (10.20) the anomalous probability function $\tilde{n}(\mathbf{k}, \mathbf{q}_i)$ becomes

$$\tilde{n}(\mathbf{k}, \mathbf{q}_i) = \langle c_{-\mathbf{k}+\mathbf{q}_i\downarrow} c_{\mathbf{k}\uparrow} \rangle = \sum_\alpha u_{i\alpha}(\mathbf{k}) u_{0\alpha}(\mathbf{k}) f(E_\alpha(\mathbf{k})) \tag{10.22}$$

for $i = 1, 2$, which leads to the same self-consistency equation for the order parameters $\Delta(\mathbf{k}, \mathbf{q}_i)$ as in equation (10.17).

An advantage of the Bogoliubov transformation method is that it is simple to extend the pairing Hamiltonian (10.19) to include a mean-field charge order parameter $\eta(\mathbf{q})$ for charge order with wave vector $\mathbf{q}$. It appears naturally as the matrix elements where the matrix in (10.19) has zeros. A detailed derivation of $\eta(\mathbf{q})$ is given in appendix D.3.3 together with a corresponding self-consistency equation similar to the one for $\Delta_{s,d}(\mathbf{q})$.

In real space, the analogon of the Hamiltonian (10.19) is

$$\mathcal{H} = \left(\mathbf{c}_\uparrow^\dagger, \mathbf{c}_\downarrow, \mathbf{c}_\downarrow\right) \begin{pmatrix} 2\hat{t}/3 & \hat{\Delta}_1 & \hat{\Delta}_2 \\ \hat{\Delta}_1^* & -\hat{t}^*/3 & 0 \\ \hat{\Delta}_2^* & 0 & -2\hat{t}^*/2 \end{pmatrix} \begin{pmatrix} \mathbf{c}_\uparrow \\ \mathbf{c}_\downarrow^\dagger \\ \mathbf{c}_\downarrow^\dagger \end{pmatrix}. \tag{10.23}$$

It constitutes together with the self-consistency equation

$$\Delta_{l,ij} = V_1 \sum_n \sum_\alpha u_{l\alpha ni} u_{0\alpha nj}^* f(E_{\alpha n}), \tag{10.24}$$

the set of extended Bogoliubov - de Gennes equations, derived in appendix D.4. With an order parameter $\Delta_{l,ij} = \Delta_{ij} e^{i\mathbf{q}_l (i+j)/2}$, one obtains solutions with pair momenta $\mathbf{q}_l$, equivalent to the ones from the Hamiltonian (10.19) in momentum space.

11 The Pair Density Wave Solution

In section 11.1 we analyze under which conditions different pair momenta can coexist, and in particular, which specific pair momenta coexist. The answer depends on a number of parameters. Most important is the result that stable solutions with $Q \geq 2$ exist only for unconventional pairing symmetries, here generated by a nearest-neighbor interaction. For a large range of parameters, one distinct solution is the most stable one: the striped PDW state with $Q = 2$ and pair momenta $\mathbf{q}_1 = -\mathbf{q}_2 = (q, 0)$. The characteristic properties and stability range of this state are investigated in section 11.2, together with an analysis of why finite momentum pairing can energetically be favorable.

11.1 Solutions of the Self-Consistency Equation

At this stage we have to decide what subsets of pair momenta are interesting candidates for stable solutions of the self-consistency equation (10.17). The order parameters for different pair momenta compete against each other for the available electrons at the Fermi surface. Consequently, the chances for finding a stable solution are better the smaller Q is. Further, because of the competition, no $\mathbf{q}$ should be distinguished from the others in a particular solution of the Gor'kov equations, and therefore all $\mathbf{q}$ should have the same absolute value in this particular solution, which gives time reversal invariant combinations of pair momenta. On a square lattice, this leaves only a small number of possible sets with $Q \geq 2$:

$$
\begin{aligned}
Q = 2: &\quad \{(q,0),(-q,0)\},\{(0,q),(0,-q)\},\{(q,q),(-q,-q)\},\{(q,-q),(-q,q)\},\\
Q = 4: &\quad \{(q,0),(-q,0),(0,q),(0,-q)\},\{(q,q),(-q,-q),(q,-q),(-q,q)\},\\
Q = 8: &\quad \{(q,0)\pm(0,d),(-q,0)\pm(0,d),(0,q)\pm(d,0),(0,-q)\pm(d,0)\},
\end{aligned}
$$

for some d fulfilling the lattice-vector condition. These are the sets of pair momenta that have been considered in the Ginzburg-Landau model for the PDW state [101]. From the considerations above we expect the first two combinations with $Q = 2$ to be the most stable ones and the one with $Q = 8$ to be the least stable one, i.e., it requires the strongest pairing interaction strength to be stabilized.

For the solution of the self-consistency equation (10.17), the exact form of the pairing interaction is crucial. We describe conventional pairing, originating from an on-site interaction, by a constant interaction $V(\mathbf{k}, \mathbf{k}', \mathbf{q}) = V_1$ in momentum space and a corresponding conventional s-wave order parameter $\Delta(\mathbf{q}_i)$. As the simplest ansatz that

allows for unconventional pairing, we choose an attractive interaction between electrons on neighboring sites. In the singlet channel this is equivalent to the interaction $V(\mathbf{k},\mathbf{k}',\mathbf{q}) = V_s(\mathbf{k},\mathbf{k}',\mathbf{q}) + V_d(\mathbf{k},\mathbf{k}',\mathbf{q})$ in momentum space, with factorizable extended s-wave and d-wave components $V_s(\mathbf{k},\mathbf{k}',\mathbf{q})$ and $V_d(\mathbf{k},\mathbf{k}',\mathbf{q})$, where

$$V_{s,d}(\mathbf{k},\mathbf{k}',\mathbf{q}) = V_1 g_{s,d}(\mathbf{k}-\mathbf{q}/2)\, g_{s,d}(\mathbf{k}'-\mathbf{q}/2). \tag{11.1}$$

$V > 0$ is the attractive pairing interaction strength and $g_s(\mathbf{k}) = \cos k_x + \cos k_y$ and $g_d(\mathbf{k}) = \cos k_x - \cos k_y$. Thus the order parameter for nearest-neighbor interaction is

$$\Delta(\mathbf{k},\mathbf{q}) = \Delta_s(\mathbf{q}) g_s(\mathbf{k}-\mathbf{q}/2) + \Delta_d(\mathbf{q}) g_d(\mathbf{k}-\mathbf{q}/2). \tag{11.2}$$

The vector $\mathbf{q}$ labels mean-field solutions which correspond to order parameters in real space with phase winding numbers q_x and q_y in x- and y-direction, respectively. Inserting $V(\mathbf{k},\mathbf{k}',\mathbf{q})$ into (10.17) gives the simplified self-consistency equation for $\Delta(\mathbf{q}_i)$

$$\frac{\Delta(\mathbf{q}_i)}{V_0} = -\frac{1}{N}\sum_{\mathbf{k}'} \tilde{n}(\mathbf{k},\mathbf{q}_i) \tag{11.3}$$

and for $\Delta_s(\mathbf{q})$ and $\Delta_d(\mathbf{q})$, respectively:

$$\frac{\Delta_{s,d}(\mathbf{q}_i)}{V_1} = -\frac{1}{N}\sum_{\mathbf{k}'} g_{s,d}(\mathbf{k}'-\mathbf{q}_i/2)\tilde{n}(\mathbf{k},\mathbf{q}_i). \tag{11.4}$$

Equation (11.3) or (11.4) is solved iteratively for each $\mathbf{q}$ in a given set. If the interaction strength $V_{0,1}$ exceeds a certain threshold value, all of the symmetric sets above provide time reversal invariant solutions with identical $\Delta(\mathbf{q}_i) > 0$ or $\Delta_{s,d}(\mathbf{q}_i) > 0$, respectively, for all i and a wide range of different pair momenta q. But, and that is crucial, only for nearest-neigbor pairing can these solutions be stable against deviations in the initial values of the order parameters. Namely, for s-wave pairing with constant V_0, they decay into the BCS state with the pair momentum $\mathbf{q}_i$ that had the largest initial order parameter. The PDW solutions in fact correspond to energy maxima of the s-wave pairing Hamiltonian. The situation is different for the nearest-neighbor interaction: Above a critical interaction strength V_{c1}, the time-reversal invariant PDW solutions become stabilized against unequal initial values, i.e., they represent local minima in $E = \langle \mathcal{H} \rangle$ [equation (11.6)] and become the groundstate for a V_1 larger than a further critical interaction strength V_{c2}. As anticipated, V_{c1} is smallest for the stripe state with pair momenta $(\pm q, 0)$ or $(0, \pm q)$ parallel to an axis of the lattice. For the diagonal stripe state, V_{c1} is larger, and it is much larger (around three times the value of the stripe state) for the checkerboard states with $Q = 4$ and the $Q = 8$ state, because for smaller V_1, these states lie on saddle points of E and decay into a PDW state with smaller Q. Another interesting

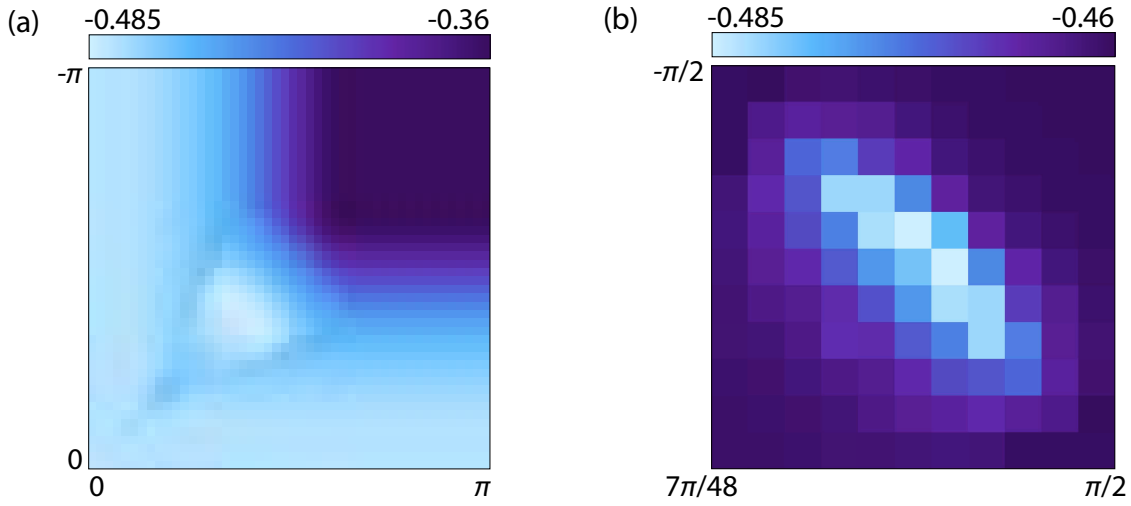

Figure 11.1: (a) Total energy $E/N = \langle \mathcal{H} \rangle / N$ for different values of q_1 (x-axis) and q_2 (note that the y-axis shows $-q_2$) for $\rho = 0.8$, $V_1 = 2.4t$ and $t' = 0.3t$. For most combinations of q_1 and q_2, the order parameter for the pair momentum with larger absolute value is zero, except within the structure emerging from the diagonal where $q_1 = -q_2$. The global minimum lies in this structure, where q_1 and q_2 coexist. (b) A finer resolution of the minimum reveals that there are actually two minima for two pair momenta on both sides of the diagonal.

observation is that for the nearest-neighbor interaction, asymmetric stable solutions of the PDW type are possible, where $\Delta_{s,d}(\mathbf{q})$ is different for different $\mathbf{q}$. These states break time-inversion symmetry and represent current carrying states. Such solutions appear in the selfc-onsistency loop preferably for exactly zero temperature and vanish for small temperatures $0 < T \ll T_c$. These solutions belong to tiny local minima in E resulting from the discrete formulation of the tight-binding model (c.f. figure 11.1).

The physical properties of the different PDW states are similar. The presence of more than one pair momentum leads to spacial inhomogeneity, which gives rise to an extended s-wave component $\Delta_s(\mathbf{q})$ of the superconducting order parameter that rises from zero for $q = 0$ to typically around 10% percents of $\Delta_d(\mathbf{q})$ for $q = \pi/2$. The PDW state develops a charge order defined by the superposition of all linear charge density waves with wave vectors $\mathbf{K} = \mathbf{q}_i - \mathbf{q}_j$, for which the Green's function $G(\mathbf{k}, \mathbf{k} + \mathbf{K}, \omega_n)$ is finite [c.f. (10.8) and equation (11.7) below]. These properties and their consequences will be analyzed in the following on the most common PDW solutions: the symmetric stripe state with $\mathbf{q} = (\pm q, 0)$ along the x-direction and $\Delta_{s,d}(\mathbf{q}) = \Delta_{s,d}(-\mathbf{q})$.

11.2 The Superconducting Charge-Stripe State

To analyze the properties of the stripe state, we choose parameters typical for the description of high-T_c superconductors, i.e. $t' = 0.3t$ and a mean-charge density $\rho = 0.8$. The qualitative behavior of the solution of the Gor'kov equations is however independent of these choices. To further test the stability of the charge-stripe solution, we solved Eq. (10.17) iteratively for various selected combinations of pair momenta and different initial values of the corresponding order parameters. In particular, we investigated the stability of the above solution against decay into the $\mathbf{q} = \mathbf{0}$ state by using an ansatz with the three center of mass momenta $\{(q,0),(-q,0),(0,0)\}$, but for $V_1 > V_{c1}$, the finite momentum pairing proves stable.

So far we have verified that stable finite momentum pairing solutions of the self-consistency equation exist. They refer to local minima of the free energy. To determine the groundstate at $T = 0$, the global minimum of the total energy

$$E = \langle \mathcal{H} \rangle = \sum_{\mathbf{k}} \varepsilon_{\mathbf{k}} n(\mathbf{k}) + \frac{1}{V_1} \sum_i \left[\Delta_s^2(\mathbf{q}_i) + \Delta_d^2(\mathbf{q}_i) \right] \tag{11.5}$$

$$\equiv E_{\text{kin}} + E_{\text{pot}} \tag{11.6}$$

has to be determined with respect to all q. Figure 11.1 (a) shows the energy $E/N = \langle \mathcal{H} \rangle / N$ for the two pair momenta $(q_1, 0)$ (x-axis) and $(q_2, 0)$ (note that the y-axis shows $-q_2$). On the diagonal are the time inversion symmetric PDW states. For most combinations of q_1 and q_2, the order parameter for the pair momentum with larger absolute value is zero (i.e. no coexistence of different pair momenta), except within the structure emerging from zero on the diagonal. In this structure the pair momenta q_1 and q_2 coexist, and the global minimum lies in its center, which, for the parameters of figure 11.1, is close to $q_1 = -q_2 = \pi/3$. A finer resolution of the minimum [figure 11.1 (b)] reveals that for finite system sizes and $T = 0$, there are actually two minima for two neighboring discrete pair momenta on both sides of the diagonal. This spontaneous symmetry breaking might be the reason for the emergence of asymmetric solutions at $T = 0$. At small but finite T, the two minima blur and merge to a single minimum at $q_1 = -q_2$. In the deep purple regime of (a), the system is in the normal state.

At cut along the diagonal given by $q_1 = -q_2 = q$ of E is shown in figure 11.2 (a) for different V_1. The typical q-dependence of E has a minimum at $q = 0$ and a further minimum for $q > 0$. The minimum at $q = 0$ corresponds to the standard d-wave superconducting state. With increasing V_1, the energy of the minimum at finite q decreases, accompanied by a shift to larger q. This implies the existence of a critical interaction strength V_{c2}, depending on t' and the mean electron density $\rho = 1/N \sum_{\mathbf{k}} n(\mathbf{k})$, above which the finite momentum pairing state is the groundstate. The optimal q depends sensitively on V_1, t' and ρ, but it is typically found in between $q \approx \pi/8$ and $q \approx \pi/2$ for a wide parameter

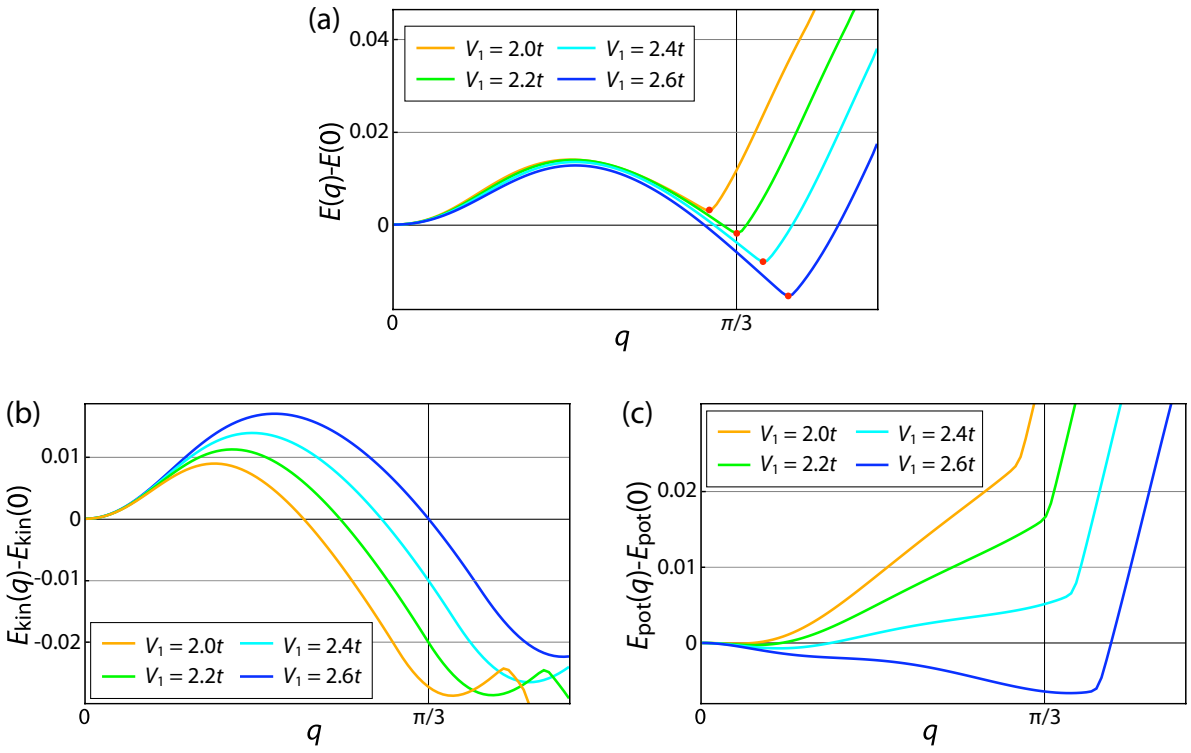

Figure 11.2: (a) Energy $E = \langle \mathcal{H} \rangle$ as a function of the pair momentum $\mathbf{q} = (q, 0)$ for different pairing interaction strengths V_1. Calculations were performed for a 384×384 lattice with fixed electron density $\rho = 0.8$ and $t' = 0.3t$. For these parameters, the finite momentum pairing state becomes the groundstate for $V_1 > V_{c2} \approx 2.2t$ with $q = \pi/3$. (b) Kinetic energy E_{kin} and (c) potential energy E_{pot} for the same system.

range. Typically, V_{c2} increases for deceasing ρ and is minimal for $t' \approx 0.25t$. Whereas for the parameters chosen above, $V_{c2} \approx 2.2t$, one finds for $\rho = 1$ and $t' = 0$ a $V_{c2} \approx 4t$. For even larger values of V_1 ($\sim 6t$), our calculations identified the groundstate to be of a checkerboard type with $Q = 4$ and with pair momenta $\{(\pm q, 0), (0, \pm q)\}$, or of the type containing eight pair momenta ($V_1 \approx 9t$).

At first glance, the appearance of an energy minimum at finite q without a magnetic field is surprising and even irritating, because of the cost in kinetic energy inevitable in the formation of Cooper pairs with finite pair momentum. A clue for the origin of the energy gain is provided by the fact that the finite-q minimum is absent for conventional pairing and by an analysis of the kinetic energy E_{kin} and the potential energy E_{pot} [see equation (11.6)] separately. Figure 11.2 (b) shows E_{kin} as a function of q. As expected, it has a minimum at $q = 0$ and increases for increasing q. But at a certain value of q, E_{kin} decreases again. This decrease is caused by a decrease of the order parameter $\Delta_d(\pm\mathbf{q})$ and thus by a decrease of the number of paired electrons. This behavior is normal, even

for a conventional BCS superconducting state, because it occupies electron states which are above E_F. In conventional superconductors, the decrease of E_kin is dominated by an increase of E_pot, thus the total energy E grows for a shrinking order parameter. This is not so for the PDW state with unconventional pairing symmetry! As shown in figure 11.2 (c), E_pot increases barely, or even decreases for increasing q, if V_1 is strong enough. The reason for this behavior is that for finite q, the nodes of the order parameters $\Delta_d(\mathbf{q})$ and $\Delta_d(-\mathbf{q})$ shift relative to each other in momentum space, and this shift is maximal for $q = \pi/2$. The condensate represented by $\Delta_d(\mathbf{q})$ contains therefore electrons with momenta that lie at the nodes of $\Delta_d(-\mathbf{q})$ and cannot be paired in this second condensate, and vice versa. In this way, more potential energy can be gained from the pairing interaction. Because this mechanism to increase the gain of potential energy is only possible in the presence of gap nodes, it becomes evident why on-site pairing cannot sustain a PDW state with coexisting different pair momenta.

For the finite-q groundstate solutions the charge density $\rho(\mathbf{r}) = \sum_s \langle c^\dagger_{\mathbf{r}_i s} c_{\mathbf{r}_i s} \rangle$ has an oscillatory part arising from the off-diagonal terms of the Green's function:

$$\rho(\mathbf{r}) = \frac{1}{N} \sum_{\mathbf{k}} \left[n(\mathbf{k}) + 2 \sum_{i \neq j} e^{i(\mathbf{q}_i - \mathbf{q}_j)\cdot \mathbf{r}} T \sum_n \mathcal{G}(\mathbf{k} + \mathbf{q}_i, \mathbf{k} + \mathbf{q}_j, \omega_n) \right]. \tag{11.7}$$

For the $\mathbf{q} = (\pm q, 0)$ state the charge density forms a sinusoidal stripe pattern with wave number $2q$. Correspondingly, the charge density varies as

$$\rho(\mathbf{r}) = \rho + \rho_1 \cos(2qx), \tag{11.8}$$

with an amplitude $\rho_1/\rho \approx 2\%$ for the parameters used in this section. This justifies the assumption of small charge modulations in the approximation for $\mathcal{T}(\mathbf{k}, \mathbf{k}', \omega_n)$ in section 10.1. For $q = \pi/3$, the wavelength of the stripe pattern is therefore three lattice constants. For larger ρ and consequently larger V_1, the wave length is shorter and the amplitude ρ_1/ρ typically larger.

The charge modulation in the superconducting state suggests to include a self-consistent charge density wave order parameter $\eta(\mathbf{k})$ in the mean-field decoupling scheme of the Hamiltonian (10.1). This is achieved easiest within the extended Bogoliubov transformation, as shown in appendix D.3.3, and $\eta(\mathbf{k})$ has to be calculated self consistently for each $\mathbf{k}$. We have analyzed this extension with coexisting order parameters for superconducting and charge density wave order for selected cases. The presence of $\eta(\mathbf{k})$ in (10.1) lowers the total energy E a few tenth of a percent and thus "tends" to stabilize the PDW state. Compared to $\Delta_d(\mathbf{q})$, $\eta(\mathbf{k})$ remains small for all $\mathbf{k}$ and does not change the solutions qualitatively.

The PDW state has further characteristic properties that are at variance with a BCS like d-wave superconductor (with $q = 0$). The density of states $D(E) = \sum_{\mathbf{k}} \mathrm{Im}\, G(\mathbf{k}, \mathbf{k}, E - i0^+)$,

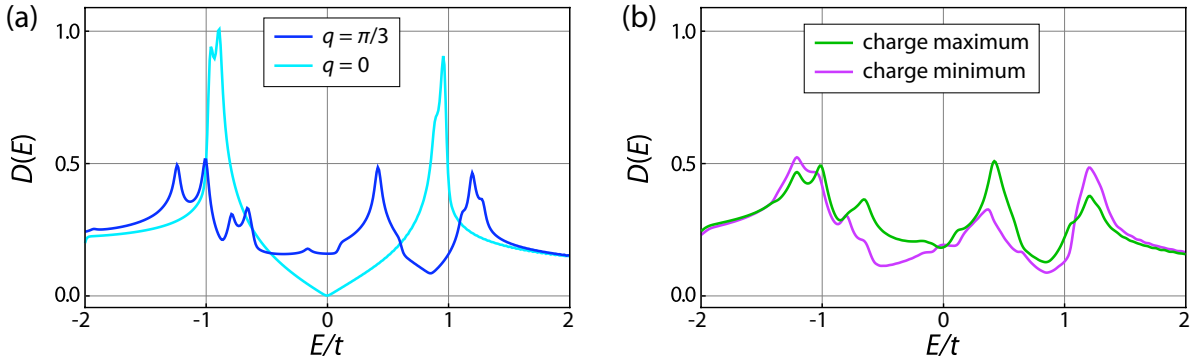

Figure 11.3: (a) Density of states $D(E)$ of the groundstate solutions for interaction strength $V_1 = 2t$ and $V_1 = 2.2t$, corresponding to $q = 0$ and $q = \pi/3$, respectively. The other parameters are the same as in Fig. 11.2. The coherence peaks of the $\mathbf{q} = \mathbf{0}$ state are split due to the van Hove singularity of the two dimensional tight-binding dispersion. (b) Local density of states for $q = \pi/3$ on a site with higher density (green) and on a site with lower density (purple).

where Im G is the imaginary part of the analytical continuation of $\mathcal{G}$ to the real frequency axis, is shown in Fig. 11.3 (a). For $q = \pi/3$, the density of states bears little resemblance to a d-wave like gap. It is finite for all energies, even at E_F, and there are four coherence peaks, originating from the edges of the three bands $E_{1,2,3}(\mathbf{k})$ (compare with figure 10.1 and figure D.1 in appendix D.2.4). A similar splitting is observed for current carrying d-wave states [33, 68] which originates from the Doppler shift of the finite momentum eigenstates. The two peaks at energies $E < 0$, as well as one coherence peak for $q = 0$, are themselves split because of the van Hove singularity which is found at approximately $E \approx t$ in the normal state. Because the charge stripes are three lattice constants wide, there is a site in the center of the stripe with higher density and on both sides of this a site with lower density. The local density of states on these sites is slightly different, as shown in figure 10.2 (b).

Figure 11.4 displays the characteristic momentum space properties of the PDW state for the same parameter set as before and, for comparison, of the d-wave superconductor with $q = 0$. The same plots, but for a particle-hole symmetric system with $\rho = 1$ and $t' = 0$, and for the checkerboard state are shown in figure 11.5. In the PDW state, the momentum distribution function $n(\mathbf{k})$ develops structures with sharp boundaries. These boundaries consist of lines in momentum space where $E_\alpha(\mathbf{k}) = 0$, for $\alpha = 0, 1$ or 2 and indicate a Fermi-surface reconstruction. The occupation probability of the zero-energy states is finite only within a certain range around the points in momentum space, where the nodes of the d-wave superconductor lie, and thereby they generate the Fermi-arc like structures in figure 11.4 (d). For $t' = 0$, the results are similar to those obtained in reference [105]. The pair density $P(\mathbf{k}) = \sum_i P(\mathbf{k}, \mathbf{k} - \mathbf{q}_i)$, where $P^2(\mathbf{k}, \mathbf{k}') = 2\langle c^\dagger_{\mathbf{k}\uparrow} c^\dagger_{-\mathbf{k}'\downarrow}\rangle\langle c_{-\mathbf{k}'\downarrow} c_{\mathbf{k}\uparrow}\rangle$, clearly shows that the fingershaped momentum-space structures of $n(\mathbf{k})$ contain unpaired

electrons only. These structures close and form Fermi pockets for suitable parameters, as in figure 11.5 (a), (c) and (e). The overall number of pairs is smaller in the PDW state than in the $q = 0$ state. This seems to contradict the fact that it has the lower energy. The latter, however, consists of both the kinetic energy, which rises in the SC state and acts against the formation of pairs, and the gain of condensation energy. The optimal balance between these two contributions depends on details of the single particle kinetic energy $\varepsilon_{\mathbf{k}}$ and the interaction potential $V(\mathbf{k}, \mathbf{k}', \mathbf{q})$ and does not generally favor a larger number of paired electrons.

11.3 Conclusions

We have shown that the extended BCS theory with attractive nearest-neighbor interaction provides self-consistent solutions with the simultaneous formation of electron pairs with center-of-mass momenta $\mathbf{q}$ and $-\mathbf{q}$, or, for larger interaction strength V_1, four or eight different pair momenta with equal absolute value. It is a microscopic solution which constitutes a stable macroscopic state of the PDW type which was proposed to describe the striped SC phase in hole doped 214 cuprates. This finite momentum pairing state is the groundstate beyond a critical interaction strength V_{c2}. V_{c2} depends sensitively on the band filling ρ and ranges from $V_{c2} \approx 1.4t$ for $\rho = 0.6$ to $V_{c2} \approx 4t$ for $\rho = 1$. This is consistent with the result in reference [103] that only the uniform phase with fixed $\mathbf{q}$ can be the groundstate of the BCS Hamiltonian in the weak coupling limit.

Our results demonstrate as a proof of principle that stable groundstate solutions of the pairing Hamiltonian (10.1) exist with coexisting finite momentum pairing amplitudes for center-of-mass momenta $\mathbf{q} = (q, 0)$ and $-\mathbf{q}$; these solutions are absent for an attractive contact interaction. Due to the concomitant striped charge density modulation with wave vector $\mathbf{K} = 2\mathbf{q}$, a connection to the striped superconductor $La_{15/8}Ba_{1/8}CuO_4$ appears tempting. However, in these materials spin correlations are essential because of the presence of spin-order patterns, and as a source of the characteristic 1/8 doping anomaly [112] and the charge order wave length of four lattice constants.

Because the most relevant correlations are not diagonal in momentum space, an extension of the present model in this direction is most convenient in the third approach described in section 10.2: the extended Bogoliubov - de Gennes equations in real space. The inclusion of correlations leading to spin order in the Bogoliubov - de Gennes equations has been used widely in the connection of magnetization appearing around impurities or in vortex cores [75, 78, 80, 81] of high-T_c cuprates. Of particular interest is the inclusion of an on-site repulsion term of the form $U \sum_i (n_{i\uparrow} c^\dagger_{i\downarrow} c_{i\downarrow} + n_{i\downarrow} c^\dagger_{i\uparrow} c_{i\uparrow})$ into the real-space Hamiltonian (10.23), which is known to generate spin order for large potential U [115], or a mean-field order parameter for the magnetization: $J \sum_{\langle ij \rangle, s} s\, m_j c^\dagger_{is} c_{is}$, where $m_i = (n_{i\uparrow} - n_{i\downarrow})/4$ [75, 79, 80]. The formalism is well established in the description

of d-wave superconductors. However, the generation of a PDW state by an iterative solution of the Bogoliubov - de Gennes equations is nontrivial, even in the absence of spin correlations. While in momentum space the pair momentum of the order parameter $\Delta_{s,d}(\mathbf{q}_l)$ is fixed, in real space $\mathbf{q}_l$ is selected only by the initial phase gradient $e^{i\mathbf{q}_l\cdot(i+j)/2}$ of $\Delta_{l,ij}$. There is a tendency, which grows for larger values V_1 and $\mathbf{q}_l$, that the system does not converge into the PDW state, but into the homogeneous d-wave state. Nevertheless, we have confirmed the existence of the energy minimum for finite $\mathbf{q}$ above a critical interaction strength V_{c2} in the same range as obtained in momentum space. Also the general dependence on the mean-charge density ρ has been confirmed, but we have not yet succeeded to reproduce the results from momentum space systematically over a large parameter range. The establishment of a solid microscopic description of the PDW state including spin correlations is an ongoing and future project, which should explore the parameter space $V_1 - U - J$ and hopefully provides a basic understanding of the superconducting stripe state in cuprates.

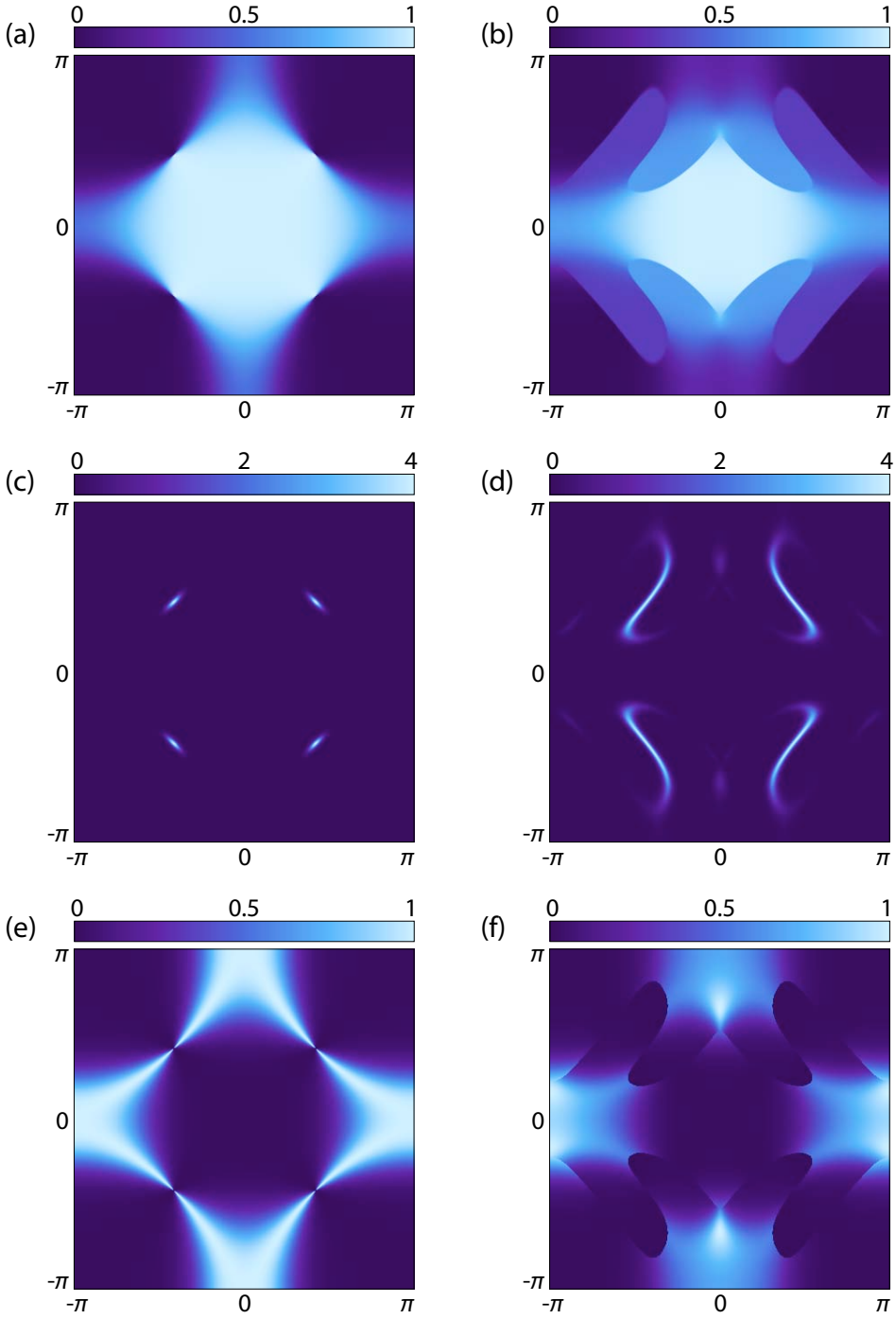

Figure 11.4: Momentum space properties of the finite momentum pairing state with $q = \pi/3$ and the same parameters as in Fig. 11.3 (right panels) and for comparison the d-wave superconductor for $q = 0$ (left panels). (a), (b): Occupation probability function $n(\mathbf{k})$. (c), (d): Density of states with zero energy $\mathrm{Im}\, G(\mathbf{k}, \mathbf{k}, 0 - i\delta)$ (here: $\delta = 0.04t$). (e), (f): Pair density $P(\mathbf{k})$.

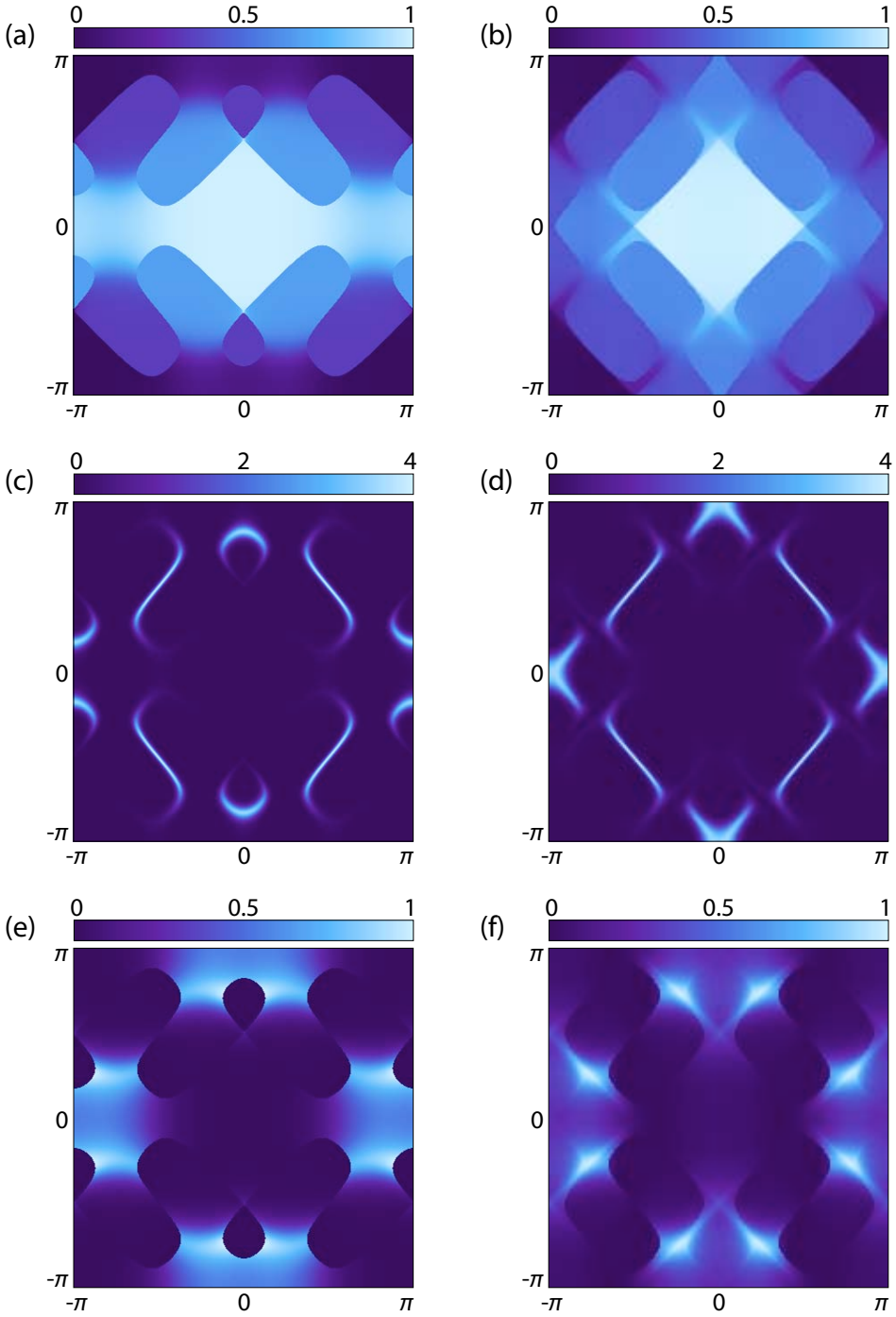

Figure 11.5: Same as in figure 11.4, but for different parameters. Left panels: $q = \pi/2$, $V_1 = 4t$ $\rho = 1$ and $t' = 0$. Right panels: Checkerboard state with the same parameters as above, except $V_1 = 6t$.

12 Unusual Flux Periodicities in Superconducting Loops

At this point it is worthwhile to return to back to "the" initial problem which originally motivated this work: What mechanism might be responsible for the appearance of flux oscillations with periodicities other than $\Phi_0/2$ in SQUIDs, or generally in superconducting loops made of unconventional superconductors? We have discussed thoroughly the origin of a Φ_0 Fourier component arising in d-wave loops, but the observed oscillations with shorter wave length remained unexplained, apart from the somewhat unsatisfactory models for the formation of electron quartets or droplets mentioned in the introduction.

Here we introduce a much simpler ansatz for a theory of higher flux periodicities that bases exclusively on the pairing Hamiltonian (10.1) of the extended BCS theory. Although it is far from being an established theory, it shows that allowing the coexistence of different pair momenta gives rise to a rich variety of possible flux periodicities in superconducting loops.

There are actually two distinct mechanisms leading to higher flux periodicities. The first ansatz follows from the Ginzburg-Landau model of the PDW state [100–102,104], and provides a possibility for a $\Phi_0/4$ flux periodicity. In these publications it was shown that the Ginzburg-Landau functional for a composite order parameter of the form $\Delta(\mathbf{r}) = \Delta_{\mathbf{q}}(\mathbf{r})e^{i-\mathbf{q}\cdot\mathbf{r}} + \Delta_{-\mathbf{q}}e^{-i\mathbf{q}\cdot\mathbf{r}}$ contains terms of the form $\Delta_{4e}(\mathbf{r}) = \Delta_{\mathbf{q}}(\mathbf{r})\Delta_{-\mathbf{q}}(\mathbf{r})$, which corresponds to a charge-4e superconductor where electron quartets emerge from nonlinear coupling between the order parameters for pair momenta $\mathbf{q}$ and $-\mathbf{q}$. The pure charge-4e superconducting state, where only Δ_{4e} contributes, shows flux quantization in $\Phi_0/4$, but exists only in special circumstances [104]. A more realistic scenario seems to be the emergence of $\Phi_0/4$ vortices, which occur naturally at dislocations of charge stripes in the PDW state [101]. In this context, the combination of more than two different pair momenta (such as the checkerboard state with four pair momenta or a state with three pair momenta in a triangular lattice) can lead to other fractional flux quanta. Our microscopic model contains the coupling between the order parameters for different pair momenta and should therefore be able to describe $\Phi_0/4$-vortices, e.g., by generating stripe dislocations in the solution of the extended Bogoliubov - de Gennes equations in real space.

The second ansatz is a straightforward extension of the cylinder model we used in part I. By solving the generalized pairing Hamiltonian (10.1) on a cylinder geometry, we investigate which combination of pair momenta is the groundstate for different values

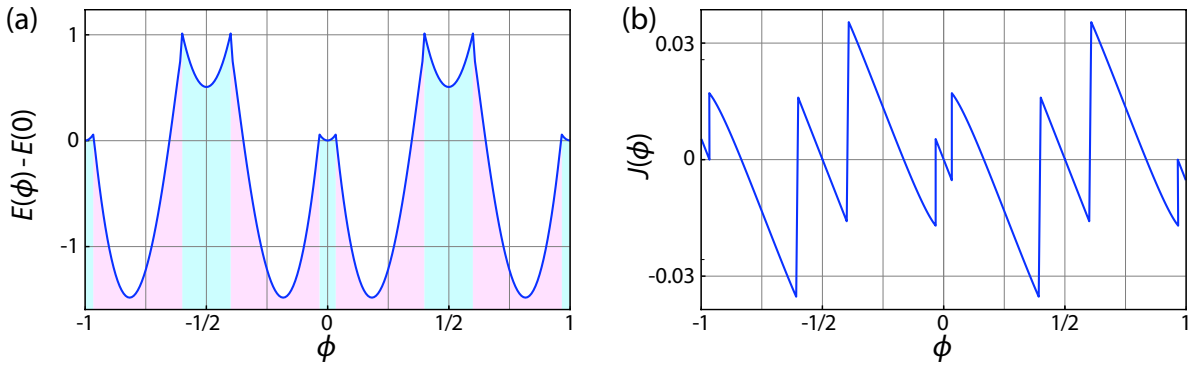

Figure 12.1: Total groundstate energy $E(\phi)$ and supercurrent $J(\phi)$ calculated in a 40×40 lattice with $V_1 = 3t$ and half band filling. In (a), in the flux regimes underlaid in blue, the groundstate is a d-wave superconductor, whereas in the regimes underlaid in pink, it is a mixed state with the two pair momenta of the neighboring d-wave states. The supercurrent shown in (b) has four jumps in one flux period at the flux values, where the groundstate changes the pairing type.

of the magnetic flux ϕ threading the cylinder. In particular, one might guess that for $\phi = 1/4$, where in the BCS superconductor changes the pair momentum q from zero to one, the coexistence of $q = 0$ and $q = 1$ could be the groundstate. This mechanism would produce an additional minimum around flux values $(2n+1)/4$, $n \in \mathbb{Z}$ and thus generate an $\Phi_0/4$ flux periodicity.

To test this idea, we take the simplest possible kinetic energy $\varepsilon_{\mathbf{k}}(\phi)$ with $t' = 0$, and half filling with $\mu = 0$. To verify the possibility of the coexistence of different pair momenta in certain flux regimes, we select the groundstate energy $E(\phi)$ out of two candidates: the d-wave superconductor with pair momentum $q(\phi)$ as in part I, and the mixed state with pair momenta q and $q+1$. The result is shown in figure 12.1 for pairing interaction strength $V_1 = 3t$. For integer and half-integer values of ϕ, the groundstate is the d-wave superconductor with pair momentum $q = 2\phi$. But between these flux values, there appear additional minima in $E(\phi)$ which belong to the q and $q+1$ mixed state, where q is the pair momentum of the neighboring d-wave regime to the left. For increasing V_1, these new minima are lowered considerably in energy and the flux regime where the mixed state is favored grows. For $V_1 \gg 4t$, we expect the groundstate to be of the PDW type for all values of ϕ. It is interesting to notice that the mixed state minima appear not at flux values $(2n+1)/4$, but are shifted a notch towards the nearest integer. The flux regimes with a d-wave groundstate are underlaid n blue in figure 12.1 (a) and the flux regimes of the mixed state in pink.

At the flux values where the condensate reconstructs to a different pairing type, the supercurrent $J(\phi)$, shown in figure 12.1 (b), is discontinuous. The four jumps in one flux period of Φ_0 are not distributed equally, which might be an effect of small system

size. Nevertheless this kind of saw-tooth pattern has a dominant Fourier component corresponding to $\Phi_0/4$ periodicity.

Of course a much more thorough analysis is required to predict the effective ground-state of nodal superconducting loops for all flux values and parameters. But this one example proves that additional minima in the total energy can emerge in the groundstate of an extended pairing Hamiltonian with nearest-neighbor pairing, which leads to higher flux periodicities in flux threaded superconducting loops and even generate fractional flux quanta – a concept that deserves further analysis in a future project.

13 Summary and Outlook

In this thesis, we investigated novel properties of unconventional superconductors, which arise from nodal states for electron pairing with finite center-of-mass momentum. In the following we summarize the two fields which developed in the course of this thesis, present an outlook on the questions that remained unsolved, and suggest future projects to tackle them

Flux periodicities in superconducting loops:

The initial motivation of this work was to find the origin of unusual flux oscillations observed in YBCO SQUIDs, which cannot be explained by the standard theory of superconducting loops and Josephson junctions. The reason why these findings are important may be traced to a large part to the historical development of the theory of superconductivity and more generally to the gauge invariance of quantum mechanics. The observation of flux oscillations with periodicities different from $hc/2e$ in unconventional superconductors proved the incompleteness of the initial evaluations of the flux periodicity in the BCS theory, or even the presence of a non-BCS type of superconducting state in the case of fractional flux periodicities.

The focus of our analysis turned mostly on the phenomenon of hc/e periodic oscillations of the supercurrent in loops with d-wave pairing symmetry. This periodicity is typical for the flux dependence of persistent currents in clean normal metal loops, as we have discussed in chapter 1 and is fundamental for all multiply connected systems with electronic charge carriers. We introduced a one dimensional model in momentum space for the supercurrent which intuitively describes the crossover from the hc/e periodic normal metal loop to the $hc/2e$ periodic superconducting loop. From this model we learned in particular that a superconducting loop is strictly $hc/2e$ periodic only in the limit of an infinite loop radius. However, for a conventional s-wave superconductor, the hc/e periodic part of the supercurrent vanishes exponentially if the loop radius is larger than the superconducting coherence length ξ. If this condition is fulfilled, the energy spectrum is fully gaped for all values of the magnetic flux threading the loop. Consequently, the occupation probability of each quasi-particle state is independent of the flux, which is the decisive condition for the supercurrent to be $hc/2e$ periodic.

In superconducting loops with a nodal gap structure, there is no characteristic length scale for the loop size like the coherence length ξ, above which the occupation probability is flux independent. The density of states is finite arbitrarily close the Fermi energy E_F for

nodal superconductors, and allows for a flux dependent occupation probability. Because the number of energy levels close to E_F is different for even and odd multiples of the superconducting flux quantum $hc/2e$, the number of states reoccupied as a function of the flux is also different in the corresponding flux regimes, leading to a hc/e periodic contribution to the supercurrent. The fraction of reoccupied states becomes smaller the larger the radius of the loop is, but it does not vanish. To calculate the exact dependence of the hc/e periodic part of the supercurrent in large loops, we therefore developed an analytical model using a continuum approximation for the density of states of a superconducting cylinder. The model calculation reveals that the relation between the first Fourier component J_1 of the supercurrent and the second Fourier component J_2, corresponding to hc/e and $hc/2e$ periodicity, respectively, is $J_1/J_2 \propto 1/R$, where R is the loop radius. This behavior is a direct consequence of the linear density of states in a d-wave superconductor close to E_F.

An analysis of the flux dependence of the supercurrent is possible also in a real space description by solving the Bogoliubov - de Gennes equations in a square frame geometry. The results are identical to the ones obtained for small systems in momentum space, but the square geometry has an energy spectrum that is much more stable against variations in the number of lattice sites, or the addition of impurities. This allowed us to verify the stability of the hc/e periodic supercurrent in systems with impurities and systems with lower symmetries.

The real space formulation is suitable to investigate also the influence of the gap nodes on the periodicity of the current-phase relation of Josephson junctions. This turned out to be a rather complex analysis for several reasons. The analysis of the results of different types of junctions led to the conclusion, that for the current-phase relation of Josephson junctions in the tunnel regime, the reoccupation of energy levels is negligible, because the Doppler shift of the levels as a function of the flux is proportional to the current over the junction and therefore too small. Transparent junctions however behave similar as superconducting loops and consequently, the nodal states are relevant for the current-phase relation. The same behavior is found in the current-flux relation of Josephson junctions penetrated by a transverse magnetic flux. Although the current-flux relation of d-wave junctions in the tunnel regime deviates from the simple Fraunhofer pattern, these deviations originate only from the order parameter symmetry and are explainable within a Ginzburg-Landau model. In the transparent regime, the effects observed in loops are present once more, this time in the form of supercurrents circulating in a vortex structure around the center of the junction.

We conclude that the emergence of hc/e periodicity in nodal superconductors is a property of systems which react periodically to a magnetic field also in the normal state. It is caused by the reoccupation of nodal states, which belong to the superconducting condensate, and is therefore not an effect of normal conducting quasi-particle excitations!

We have presented a detailed analysis of the origin of hc/e oscillations and consider

the problem as solved. Nevertheless, there remain open questions:

1. The flux-dependent minima of the groundstate energy depend on the center-of-mass angular momentum q of the Cooper pairs – where q may be identified with the winding number of the order parameter phase around the superconducting loop. The shift of the energy minima of the even and odd q superconducting states relative to each other depends on microscopic details of the energy spectrum and we have not identified the physical factors controlling the shift. Juričić *et al.* [35] gave a solution on the basis of a quasi one-dimensional model, but the fully self-consistent problem is more complicated.

2. We introduced a procedure to find a self consistent treatment of the magnetic field in superconducting loops. An extension of this technique is obviously necessary to succeed to calculate, e.g., the difference of the penetration depth λ for even and odd q states or differences in the current distribution for varying magnetic fields as in SQUIDs.

3. For the direct comparison of our findings with the experimental results obtained from SQUIDs, the numeric simulation of a dc SQUID containing two Josephson junctions is necessary. Apart from the difficulties arising in the description of an isolated junction, calculating the groundstate of the SQUID from the Bogoliubov - de Gennes equations is a problem. In the dc SQUID geometry, the phase gradient of the order parameter of the superconducting state in both parts of the SQUID can be different, which leads to almost degenerate states of the system with different current flow. To calculate these states and classify them correctly is the challenge in determining the flux periodicity of a d-wave SQUID.

4. All the calculations, which we described in this thesis were performed in the grand canonical ensemble, in which the BCS theory is originally formulated. It is known that in nanoscopic systems, conservation of the particle number has an influence on the superconducting state [116,117]. A formalism to test the periodicity crossover described in chapter 2 in a canonical ensemble was developed and a conclusion of this analysis might be possible in the future.

The outset of this work was motivated mostly by the attempt to explain the fractional flux periodicities observed in YBCO SQUIDs, which pointed in the direction of electron quartets and interaction between Cooper pairs. This attempt has not been pursued far within this thesis, because more fundamental problems had to be solver first. In chapter 12 we introduced a novel concept of fractional flux periodicities and quanta, which relies exclusively on a pair interaction and unconventional pairing symmetry. In connection with further investigations of the PDW state, this concept shall be further analyzed and it

is expected to give an insight into the amazing variety of the flux periodicities in d-wave SQUID experiments.

Finite momentum pairing in zero magnetic field:

In the couse of the analysis of superconducting loops, we developed an extension of the BCS theory using a pairing Hamiltonian which allows for the simultaneous formation of different pair momenta. This was originally motivated by the desire to construct an explicitly gauge invariant theory for the loops that automatically selects the ground state pair momentum for all flux values. For conventional s-wave pairing, this theory provided the expected results, but for a d-wave pairing type, we found unexpected solutions: for sufficiently large pairing interaction strength, different pair momenta coexist in the ground state with zero magnetic flux!

These findings for unconventional pairing symmetries proved highly relevant, independent of multiply connected geometry, because they provide a solution for several fundamental problems in superconductivity, namely a microscopic theory for the "pair density wave" state. In the PDW state, the pair momenta $\mathbf{q}$ and $-\mathbf{q}$ coexist, which leads to a stripe pattern of the pair density with wave vector $\mathbf{q}$ and a striped charge order with wave vector $2\mathbf{q}$, and it is phenomenologically equivalent to the Larkin-Ovchinnikov state.

Once this connection was realized, the development and analysis of our PDW model became the main focus of this thesis. We introduced distinct formulations of the model, even a real-space formulation on the basis of extended Bogoliubov - de Gennes equations, and analyzed, the stability of the PDW solution for a number of different parameters. It was reconfirmed that a conventional on-site interaction cannot sustain a stable PDW solution independent of the interaction strength. However, for a nearest-neighbor interaction, the ground state of our model is the PDW state with pair momentum $\mathbf{q} = (q, 0)$, if the interaction strength exceeds a critical value V_{c2}, which typically decreases with decreasing mean charge density ρ. For $\rho = 0.8$, we find $V_{c2} \approx 2.4t$, and a ground state pair momentum $q = \pi/3$, leading to a charge order with a wave length of three lattice constants and an amplitude of $\sim 2\%$ of ρ. If the interaction strength is smaller than V_{c2}, the ground state is the d-wave superconductor with $q = 0$. Some characteristic momentum-space properties of our model are worth mentioning: Whereas the d-wave superconductor has four nodal points in momentum space, the PDW solution has a partially reconstructed Fermi surface, which leads to Fermi surface arc-like structures and a finite density of states at the Fermi energy. The regions of momentum space enclosed by the arcs contain only unpaired electrons and they close to Fermi pockets in a certain parameter range.

As the source of the energy gain in the PDW state with finite pair momentum, we identified the shift of the nodes in the order parameters for $\mathbf{q}$ and $-\mathbf{q}$, which increases

the potential energy gain from the creation of electron pairs. The existence of gap nodes is therefore a crucial precondition for the formation of a finite momentum pairing state.

Our theory does not have a characteristic value for q in the ground state; it changes smoothly as a function of the system parameters. It does not show any anomalies for certain band fillings either. To establish a connection of the charge ordered state emerging from our model and the charge stripe state observed in some high-T_c cuprates, in particular in $La_{15/8}Ba_{1/8}CuO_4$, the model is still lacking crucial ingredients. Most importantly we have not included yet spin correlations, which seem to be essential for the observed width of four lattice constants of the charge stripes. This sets the direction for the future development of the theory.

The inclusion of spin correlations into our model is most convenient in real space, as discussed in section 11.2. The technique for the solution of the extended Bogoliubov - de Gennes equations for finite momentum pairing is not fully established yet and more work has to be done. To focus on real-space calculations is necessary also to analyze the influence of impurities or further charge correlations on the PDW state. An intermediate goal is the determination of a phase diagram with respect to the nearest-neighbor pairing interaction strength V_1 and an on-site repulsion U, which is known to support spin and charge order in connection with impurities.

We conclude that so far we have shown as a poof of principle, that different pair momenta can coexist for nearest-neighbor pairing in the ground state of a BCS type mean-field theory. This result is important for the on-going research in the field charge ordered superconductors and provides a natural basis for the continuation of work in this direction.

We have shown that novel phenomena emerge from combining unconventional electron pairing with the formation of electron pairs with finite center-of-mass momentum. Such phenomena are found in nature in rich varieties and have become a major field in the experimental and theoretical research on superconductivity.

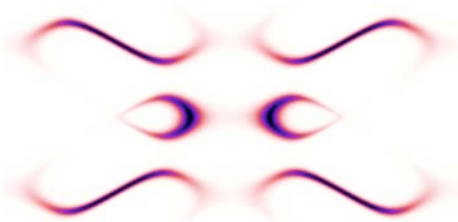

Appendix

A Current

A.1 Continuity Equation

Here we derive an expression for the gauge invariant current operator on a discrete square lattice from the continuity equation. Since the total current in two dimensions is a simple linear combination of the current in x- and y-direction, it is sufficient to use the one dimensional continuity equation

$$\frac{d}{dt}\rho_i + \nabla_i J_i = 0, \tag{A.1}$$

for spinless fermions, where $\rho_i = e\langle\hat{\rho}_i\rangle = e\langle c_i^\dagger c_i\rangle$ is the charge density at the lattice site i. The current J_i is defined as the average of the currents $J_{i-1,1}$ and $J_{i,i+1}$ defined on the two neighboring bonds of the lattice site i:

$$J_i = \frac{1}{2}\left(J_{i-1,i} + J_{i,i+1}\right) = -\frac{1}{2}\left(J_{i,i-1} - J_{i,i+1}\right). \tag{A.2}$$

In the same way, the discrete derivative of the current is defined as the difference of the two bond currents $J_{i-1,i}$ and $J_{i,i+1}$

$$\nabla_i J_i = \frac{1}{2}\left(J_{i-1,i} - J_{i,i+1}\right) = -\frac{1}{2}\left(J_{i,i-1} + J_{i,i+1}\right). \tag{A.3}$$

The time derivative of $\hat{\rho}_i$ is given by the commutator of $\hat{\rho}_i$ and and the kinetic energy $\mathcal{H}_0$. The electron-electron interaction term $\mathcal{H}_\mathrm{I}$ commutes with $\hat{\rho}_i$ and does not contribute to the current. It follows that

$$\frac{d}{dt}\hat{\rho}_i = \frac{i}{\hbar}\left[\mathcal{H}_0, c_i^\dagger c_i\right] = \frac{i}{\hbar}\left[\mathcal{H}_0, c_i^\dagger\right]c_i + \frac{i}{\hbar}c_i^\dagger\left[\mathcal{H}_0, c_i\right]. \tag{A.4}$$

Using the identities $\left[c_i^\dagger c_j, c_k^\dagger\right] = \delta_{jk}c_i^\dagger$ and $\left[c_i^\dagger c_j, c_k\right] = -\delta_{ik}c_j$, we find for the commutators

$$\begin{aligned}\left[\mathcal{H}_0, c_i^\dagger\right] &= -t\sum_j\left[e^{i\varphi_{j,j+1}}c_j^\dagger c_{j+1} + e^{i\varphi_{j,j-1}}c_j^\dagger c_{j-1}, c_i^\dagger\right] \\ &= -t\left(e^{i\varphi_{i-1,i}}c_{i-1}^\dagger + e^{i\varphi_{i+1,i}}c_{i+1}^\dagger,\right)\end{aligned} \tag{A.5}$$

and in the same way

$$[\mathcal{H}_0, c_i] = t\left(e^{i\varphi_{i,i+1}}c_{i+1} + e^{i\varphi_{i,i-1}}c_{i-1}\right). \tag{A.6}$$

Inserting these results into the continuity equation (A.1), we get a defining equation for the current J_i:

$$\begin{aligned}\frac{d}{dt}\rho_i &= \frac{et}{\hbar}\left\langle\left(e^{-i\varphi_{i-1,i}}c_i^\dagger c_{i-1} - e^{-i\varphi_{i,i-1}}c_{i-1}^\dagger c_i\right) - \left(e^{-i\varphi_{i,i+1}}c_{i+1}^\dagger c_i - e^{-i\varphi_{i+1,i}}c_i^\dagger c_{i+1}\right)\right\rangle \\ &= -J_{i-1,i} + J_{i,i+1} = -\nabla_i J_i \end{aligned} \tag{A.7}$$

where the current J_{ij} per bond is given by

$$J_{ij} = -\frac{et}{\hbar}\left(e^{-i\varphi_{ij}}\langle c_j^\dagger c_i\rangle - e^{-i\varphi_{ji}}\langle c_i^\dagger c_j\rangle\right). \tag{A.8}$$

A.2 Current in Momentum Space

Inserting equation (A.8) into equation (A.2) gives

$$J_i = \frac{et}{\hbar}\left(e^{i\varphi}\langle c_i^\dagger c_{i+1}\rangle - e^{-i\varphi}\langle c_{i+1}^\dagger c_i\rangle + e^{-i\varphi}\langle c_i^\dagger c_{i-1}\rangle - e^{i\varphi}\langle c_{i-1}^\dagger c_i\rangle\right) \tag{A.9}$$

$$\begin{aligned} &= \frac{et}{\hbar}\left[\left(\nabla_i\langle c_i^\dagger c_j\rangle\right)e^{i\varphi} - \left(\nabla_j\langle c_i^\dagger c_j\rangle\right)e^{-i\varphi}\right]\Big|_{i=j} \\ &= -\frac{et}{\hbar}\left[(\nabla_i - \nabla_j)G(i,j)\right]e^{i\varphi_{ij}}\Big|_{i=j}, \end{aligned} \tag{A.10}$$

where $\varphi = \varphi_{i,i+1} = \phi/R$ for a one dimensional ring with radius R, threaded by a magnetic flux ϕ. $G(i,j) = \langle c_i c_j^\dagger\rangle$ is the time independent Green's function in real space. In a homogeneous system, as the one dimensional ring, $G(i,j) \equiv G(i-j)$ depends only on the difference of i and j, thus J_i becomes space independent:

$$J_i = -t\frac{e}{\hbar}\big[G(1)e^{i\varphi} - G(-1)e^{-i\varphi}\big], \tag{A.11}$$

In momentum space, this equation becomes

$$\begin{aligned} J &= -T\frac{et}{hR}\sum_n\sum_k\left[\mathcal{G}(k,\omega_n)e^{-i(k-\phi)/R} - \mathcal{G}(k,\omega_n)e^{i(k-\phi)/R}\right] \\ &= -T\frac{e}{h}\sum_n\sum_k\frac{-2t}{R}\sin\left[\frac{k-\phi}{R}\right]\mathcal{G}(k,\omega_n) \\ &= T\frac{e}{h}\sum_n\sum_k\frac{\partial\varepsilon_k}{\partial k}\mathcal{G}(k,\omega_n) = \frac{e}{h}\sum_k\frac{\partial\varepsilon_k}{\partial k}n_k. \end{aligned} \tag{A.12}$$

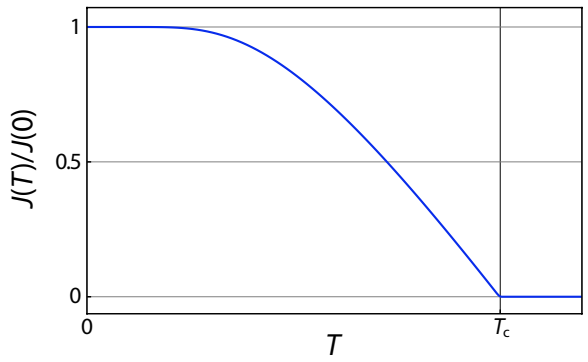

Figure A.1: Supercurrent $J(T)$ as a function of temperature T. For $T \ll T_c$, $J(T)$ is constant, then decays linearly to almost zero at T_c, where it changes to an exponential decay in T.

A.3 Free Energy

In the main part of this work we determined the groundstate by minimizing the internal energy $E = \langle \mathcal{H} \rangle$ with respect to the pair momentum q. This formalism is ideally suited to obtain the groundstate pair momentum q at $T = 0$, but for $T > 0$ we actually have to minimize the free energy F, or rather the grand potential Ω in the grand canonical ensemble. Would this modify the analysis of the flux periodicity of the supercurrent? In fact, not for $T \ll T_c$ or for T close to T_c, as we show below.

In the formalism of the second quantization, the current is given by $J = et/\hbar \langle \hat{J} \rangle$, where $\hat{J}$ is the (unitless) current operator. With the Hamiltonian $\mathcal{H} = \sum_{\mathbf{k}} \varepsilon_{\mathbf{k}} \hat{n}_{\mathbf{k}} + \mathcal{H}_I$, where the interaction term $\mathcal{H}_I$ is flux independent, and $\hat{J} = -\sum_{\mathbf{k}} (\partial \varepsilon_{\mathbf{k}} / \partial \phi) \hat{n}_{\mathbf{k}}$, the thermal average becomes

$$J = \langle \hat{J} \rangle = \frac{\mathrm{Tr}\left(\hat{J} e^{-\beta \mathcal{H}}\right)}{\mathrm{Tr}\left(e^{-\beta \mathcal{H}}\right)} = -\frac{\sum_{\mathbf{k}} \sum_{n_{\mathbf{k}}} \left(\frac{\partial \varepsilon_{\mathbf{k}}}{\partial \phi} n_{\mathbf{k}} e^{-\beta \mathcal{H}}\right)}{\sum_{\mathbf{k}} \sum_{n_{\mathbf{k}}} e^{-\beta \mathcal{H}}} = -\frac{\partial \Omega}{\partial \phi} \tag{A.13}$$

with $\beta = 1/T$ and the grand potential $\Omega = -1/\beta \ln\left(\sum_{\mathbf{k}} \sum_{n_{\mathbf{k}}} e^{-\beta \mathcal{H}}\right)$. Using the thermodynamical relation $TS = \beta \partial \Omega / \partial \beta$ for the entropy S, we obtain the correct relation between the internal energy E and J for $T > 0$:

$$\frac{\partial E}{\partial \phi} = \frac{\partial}{\partial \phi} (\Omega + TS) = -J + \beta \frac{\partial}{\partial \beta} \frac{\partial \Omega}{\partial \phi} = -J - T \frac{\partial J}{\partial T}. \tag{A.14}$$

The general dependence of $J(T)$ in the superconducting state is known [67] and shown in figure A.1. We consider the two limits:
$T \ll T_c$: In this regime, $\partial J / \partial T = 0$ and it follows that $\partial E / \partial \phi = -J$, as for $T = 0$.
$T \approx T_c$: In this regime, $J(T)$ decays exponentially in t: $J(T, \phi) = T e^{(T_c - T)/\alpha} \tilde{J}(\phi)$, where

the flux dependence is contained in $\tilde{J}(\phi)$ and α is a characteristic decay constant. It follows that

$$\frac{\partial E}{\partial \phi} = -\tilde{J}\left(1 + T\frac{\partial}{\partial T}\right) e^{(T_c - T)/\alpha} \propto -J. \tag{A.15}$$

In these two limits, the kinks of $E(\phi)$ are therefore at the same values of ϕ where $J(\phi)$ has discontinuities, which means that the periodicity of $E(\phi)$ and $J(\phi)$ is the same. In the temperature range where $J(T)$ decays linearly, $E(\phi)$ and $J(\phi)$ [or $\Omega(\phi)$] can have a different flux dependence.

B Doppler Shift and Nodes of the Hankel Function Ansatz

The ansatz for $u_{\mathbf{n}}(r)$ and $v_{\mathbf{n}}(r)$ with two Hankel functions (equations (2.13) and (2.14)) solves the normal state Schrödinger equation for the annulus as well as the BdG equations in the superconducting state with integer and half-integer flux values. In this appendix we show that it is not possible to construct an approximate analytic solution for the superconducting annulus that includes the effect of the Doppler shift. In this case $u_{\mathbf{n}}(r)$ and $v_{\mathbf{n}}(r)$ have the independent eigenenergies $(\hbar^2/2m)\,(\gamma_{\mathbf{n}}^u)^2$ and $(\hbar^2/2m)\,(\gamma_{\mathbf{n}}^v)^2$.

For this purpose we analyze the relation between the Doppler shift of the eigenfunctions of the annulus in the normal state ($\Delta = 0$) and the shift of their nodes with respect to the radial coordinate, using the following asymptotic form for the Hankel functions [118]:

$$H_l^{(1,2)}\left(\frac{l}{\cos x}\right) = \sqrt{\frac{2}{\pi\, l \tan x}}\exp\left[\pm i\left(l\tan x - l\,x - \frac{\pi}{4}\right)\right], \tag{B.1}$$

which approximates $H_l^{(1)/(2)}$ for $l \gg 1$. Choosing $x = \arccos(l/\gamma r)$ leads with $\tan(\arccos\, x) = \sqrt{1-x^2}/x$ to

$$H_l^{(1,2)}(\gamma r) = \sqrt{\frac{2}{\pi l}}\left[\left(\frac{\gamma r}{l}\right)^2 - 1\right]^{-1/4} \times \exp\left[\pm i\left(r\sqrt{\gamma^2 - \frac{l^2}{r^2}} - l\,\arccos\,\frac{l}{\gamma r} - \frac{\pi}{4}\right)\right]. \tag{B.2}$$

Thus equation (B.2) approximates $H_l^{(1,2)}(\gamma r)$ for $\gamma r \gg 1$. Inserting equation (B.2) into the boundary conditions (2.16) determines the constants $c_{\mathbf{n}}^{\alpha}$ and $\gamma_{\mathbf{n}}^{\alpha}$:

$$c_{\mathbf{n}}^{\alpha} = \exp\left[2i\left(D_{\mathbf{n}}^{\alpha}(R_1) - \frac{\pi}{4}\right)\right] = \exp\left[2i\left(D_{\mathbf{n}}^{\alpha}(R_2) - \frac{\pi}{4}\right)\right], \tag{B.3}$$

with

$$D_{\mathbf{n}}^{\alpha}(r) = r\sqrt{\left(\gamma_{\mathbf{n}}^{\alpha}\right)^2 - \frac{l_\alpha^2}{r^2}} - l_\alpha\,\arccos\,\frac{l_\alpha}{\gamma_{\mathbf{n}}^{\alpha} r}. \tag{B.4}$$

The wave functions $u_{\mathbf{n}}(r)$ and $v_{\mathbf{n}}(r)$ (equations (2.13,2.14)) become

$$u_{\mathbf{n}}(r) = u_{\mathbf{n}}\sqrt{\frac{8}{\pi l_u}}\left[\left(\frac{\gamma^u_{\mathbf{n}} r}{l_u}\right)^2 - 1\right]^{-1/4} e^{i\left[D^u_{\mathbf{n}}(R_1)+\frac{\pi}{4}\right]} \sin\left[D^u_{\mathbf{n}}(r) - D^u_{\mathbf{n}}(R_1)\right], \tag{B.5}$$

$$v_{\mathbf{n}}(r) = v_{\mathbf{n}}\sqrt{\frac{8}{\pi l_v}}\left[\left(\frac{\gamma^v_{\mathbf{n}} r}{l_v}\right)^2 - 1\right]^{-1/4} e^{i\left[D^v_{\mathbf{n}}(R_1)+\frac{\pi}{4}\right]} \sin\left[D^v_{\mathbf{n}}(r) - D^v_{\mathbf{n}}(R_1)\right]. \tag{B.6}$$

The vanishing of the wavefunction for $r = R_2$ therefore implies that

$$D^\alpha_{\mathbf{n}}(R_2) - D^\alpha_{\mathbf{n}}(R_1) = -\pi\rho \tag{B.7}$$

for an integer ρ, which determines $\gamma^\alpha_{\mathbf{n}}$. In the limit of a thin annulus ($R_1 \gg R_2 - R_1$), we expand $D^\alpha_{\mathbf{n}}(r)$ in $1/r$ and find

$$D^\alpha_{\mathbf{n}}(r) - D^\alpha_{\mathbf{n}}(R_1) \approx (r - R_1)\left[\gamma^\alpha_{\mathbf{n}} - \frac{l_\alpha^2}{2\gamma^\alpha_{\mathbf{n}} r R_1}\right]. \tag{B.8}$$

With this asymptotic form the boundary condition (B.7) becomes a quadratic equation in $\gamma^\alpha_{\mathbf{n}}$:

$$(\gamma^\alpha_{\mathbf{n}})^2 - \frac{\pi\rho}{R_1 - R_2}\gamma^\alpha_{\mathbf{n}} - \frac{l_\alpha^2}{2R_1R_2} = 0, \tag{B.9}$$

which has the positive solution

$$\gamma^\alpha_{\mathbf{n}} = \frac{1}{2}\left[\frac{\pi\rho}{R_1 - R_2} + \sqrt{\left(\frac{\pi\rho}{R_1 - R_2}\right)^2 + \frac{l_\alpha^2}{2R_1R_2}}\right]. \tag{B.10}$$

This is the simplest possible approximation for the eigenenergies of the uncoupled equations ($\Delta = 0$) of the annulus containing the Doppler shift, which is controlled by l_α^2. The flux ϕ enters $l_u$and l_v with different signs (see equation 2.11)). Thus, if $\gamma^u_{\mathbf{n}}$ decreases as a function of ϕ, $\gamma^v_{\mathbf{n}}$ increases. Since $q - 2\phi < 1$ in the groundstate, the Doppler shift $(\hbar^2/2m)[(\gamma^\alpha_{\mathbf{n}})^2(q - 2\phi) - (\gamma^\alpha_{\mathbf{n}})^2(0)]$ is linear in leading order in $(q - 2\phi)/\sqrt{R_1}$.

We further find the nodes $r_{\mathbf{n}m}$ of $u_{\mathbf{n}}(r)$ and $v_{\mathbf{n}}(r)$ by setting expression (B.8) equal to πm, where m is a positive integer, and solving it for $r > 0$:

$$r_{\mathbf{n}m} = \frac{1}{2}\left[R_1 + \frac{l_\alpha^2}{2(\gamma^\alpha_{\mathbf{n}})^2 R_1} - \frac{\pi m}{\gamma^\alpha_{\mathbf{n}}} + \sqrt{\left(R_1 + \frac{l_\alpha^2}{2(\gamma^\alpha_{\mathbf{n}})^2 R_1} - \frac{\pi m}{\gamma^\alpha_{\mathbf{n}}}\right)^2 - \frac{2l_\alpha^2}{(\gamma^\alpha_{\mathbf{n}})^2}}\right]. \tag{B.11}$$

The shift of the nodes $r_{\mathbf{n}m}(q - 2\phi) - r_{\mathbf{n}m}(0)$ as a function of flux is again linear in $(q - 2\phi)/\sqrt{R_1}$ to leading order. Thus both the Doppler shift and the nodes of $u_{\mathbf{n}}(r)$ shift

linearly with ϕ and conversely when compared with the Doppler shift and the nodes of $v_{\mathbf{n}}(r)$.

The coupled equations (2.15) for $\Delta \neq 0$ resulting from the ansatz (2.13,2.14) with non integer (or non half-integer) flux can be solved only by wave functions $u_{\mathbf{n}}(r)$ and $v_{\mathbf{n}}(r)$ with the same r-dependence. To obtain a solution of this problem, one can expand the wave functions as a sum of Hankel functions and numerically solve for the coefficients or directly solve the coupled differential equations numerically.

C The Bogoliubov - de Gennes Equations

C.1 Magnetic Field in Discrete Lattices

To describe a magnetic field in a discrete discrete system, it is necessary to clarify some definitions regarding field and vector potential. We are dealing here with a two dimensional square lattice and a magnetic field $B_z(\mathbf{r})$ perpendicular to the lattice plane. The vector potential $\mathbf{A}(\mathbf{r})$ generating $B_z(\mathbf{r})$ is a vector field in the plane. Both quantities have to be replaced by discrete objects.

The straight forward discretization scheme would be the replacements $B_z(\mathbf{r}_i) \to B_i$ and $\mathbf{A}(\mathbf{r}_i) \to (A_i^x, A_i^y)$. With the discrete derivation $\nabla_{i_x} f_i = 1/2(f_{i-\hat{x}} - f_{i+\hat{x}})$, the field B_i is given by

$$B_i = \nabla_{i_x} A_i^y - \nabla_{i_y} A_i^x = \frac{1}{2}\left[A_{i-\hat{x}}^y - A_{i+\hat{x}}^y - A_{i-\hat{y}}^x + A_{i+\hat{y}}^y\right]. \tag{C.1}$$

This definition is not ideal for our purpose, because we identify the magnetic field on site i by the non-local object on the right hand side of equation (C.1). What is more, the vector potential in the form (A_i^x, A_i^y) does not enter the Hamiltonian in real space directly. A more suitable way to define a discrete vector field is to integrate it along a line connecting two arbitrary lattice sites i and j, as is done for the Peierls phase factor, and express it through

$$\varphi_{ij} = \frac{e}{\hbar c}\int_i^j \mathrm{d}\mathbf{r}\cdot\mathbf{A}(\mathbf{r}). \tag{C.2}$$

The phase factors φ_{ij} can be understood as a kind of "super potential" in the lattice, from which we derive the vector potential by a discrete derivative: $A_i^x = 1/2(\varphi_{i,i-\hat{x}} - \varphi_{i,i+\hat{x}})$ and $A_i^y = 1/2(\varphi_{i,i-\hat{y}} - \varphi_{i,i+\hat{y}})$. Inserting these into (C.2) gives

$$\begin{aligned} B_i = \frac{1}{4}\big[&\varphi_{i-\hat{x},i-\hat{x}-\hat{y}} - \varphi_{i-\hat{x},i-\hat{x}+\hat{y}} - \varphi_{i+\hat{x},i+\hat{x}-\hat{y}} + \varphi_{i-\hat{x},i-\hat{x}+\hat{y}} \\ &-\varphi_{i-\hat{y},i-\hat{y}-\hat{x}} + \varphi_{i-\hat{y},i-\hat{y}+\hat{x}} + \varphi_{i+\hat{y},i+\hat{y}-\hat{x}} - \varphi_{i+\hat{y},i+\hat{y}+\hat{x}}\big] \end{aligned} \tag{C.3}$$

$$\begin{aligned} = \frac{1}{4}\big[&\varphi_{i-\hat{x},i-\hat{x}-\hat{y}} + \varphi_{i-\hat{x}-\hat{y},i-\hat{y}} + \varphi_{i-\hat{y},i-\hat{y}+\hat{x}} + \varphi_{i-\hat{y}+\hat{x},i+\hat{x}} \\ &+\varphi_{i+\hat{x},i+\hat{x}+\hat{y}} + \varphi_{i+\hat{x}+\hat{y},i+\hat{y}} + \varphi_{i+\hat{y},i+\hat{y}-\hat{x}} + \varphi_{i+\hat{y}-\hat{x},i-\hat{x}}\big] \end{aligned} \tag{C.4}$$

$$= \frac{1}{4}\sum_{\partial S}\varphi_{ij}, \tag{C.5}$$

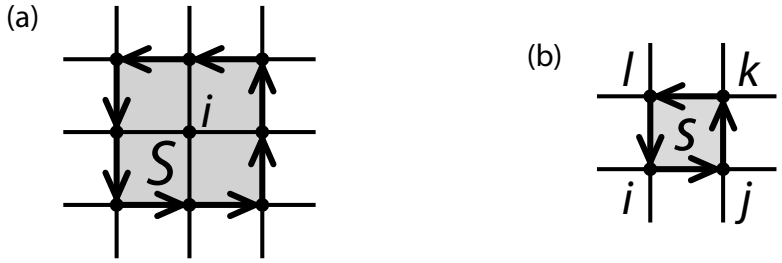

Figure C.1: On a discrete square lattice, the magnetic field perpendicular to the lattice plane can either be defined (a) on a site i as the average of magnetic flux threading the surface S containing the four neighboring plaquettes, or (b) on a single plaquette as the flux threading the surface s of the plaquette.

where ∂S contains all pairs of nearest neighbor lattice sites which lie on the boundary of the surface S constituted by the four neighboring plaquettes of site i [figure C.1 (a)]. In this sceme, B_i is given by the magnetic flux through the area S divided by four.

The definition above of the magnetic field is obviously not the best possible. The best resolution of the field is achieved if we define it not on lattice sites, but on single plaquettes as the magnetic flux threading each plaquette:

$$B_l = \sum_{\partial s_l} \varphi_{ij}, \tag{C.6}$$

where s_l is the area of the l-st. plaquette. We therefore obtain a consistent vector arithmetic in a discrete two dimensional lattice by identifying a vector field in the plane by the objects φ_{ij}, the rotation of φ_{ij} by summing it over the boundary of a plaquette, and the field perpendicular to the lattice plane by B_l define on plaquette l as the rotation of φ_{ij}.

The strength of this discrete formulation is that one can easily derive the "super potential" φ_{ij} for arbitrary field distributions B_l. A typical situation is a field $B_l = B$ which is constant on all plaquettes. In analogy to the Landau gauge for a constant field B_z: $\mathbf{A}(\mathbf{r}) = (0, -B_z, 0)$, φ_{ij} can be written in the form $\varphi_{ij} = 2\pi B(j_y - i_y)i_x$. This choice has been used widely to study vortex lattices [74, 77, 79–81], but it is problematic in connection with open boundary conditions because the Landau gauge describes a constant field infinite in all directions. Cutting the system at its boundaries generates additional fields on the boundary of the system.

A different ansatz allowing for the description of arbitrary field distributions solves this problem. A vector potential of the from $\mathbf{A}(\mathbf{r}) = 2\pi B/|\mathbf{r}|^2(y, -x, 0)$ generates a singular magnetic flux B concentrated at $\mathbf{r} = \mathbf{0}$. The discrete analogon is

$$\varphi_{ij}^{l} = B_l \arctan\left[\frac{\hat{\imath}_\mathrm{x}\hat{\jmath}_\mathrm{y} - \hat{\jmath}_\mathrm{x}\hat{\imath}_\mathrm{y}}{\hat{\imath}_\mathrm{x}\hat{\jmath}_\mathrm{x} + \hat{\imath}_\mathrm{y}\hat{\jmath}_\mathrm{y}}\right], \tag{C.7}$$

where $\hat{\imath} = i - l - \hat{x}/2 - \hat{y}/2$, which generates a flux B_l through the plaquette l centered half a lattice constant to the right and above the site l. The phase factor $\varphi_{ij} = \sum_l \varphi_{ij}^l$ generates therefore a magnetic field distribution with flux B_l through each plaquette.

C.2 Mean-Field Hamiltonian in Real Space

We define the Hamiltonian $\mathcal{H}$ in the tight binding model on a square lattice with N lattice sites, including a kinetic energy $\mathcal{H}_0$ and a spin singlet interaction term: $\mathcal{H}_\mathrm{I}$:

$$\mathcal{H}_0 = \sum_{\langle i,j\rangle,s} t_{ij} c_{is}^\dagger c_{js}, \tag{C.8}$$

and

$$\begin{aligned}\mathcal{H}_\mathrm{I} = {} & V_0 \sum_i c_{i\uparrow}^\dagger c_{i\downarrow}^\dagger c_{i\downarrow} c_{i\uparrow} \\ & + \frac{V_1}{4} \sum_{\langle i,j\rangle} \left[c_{i\uparrow}^\dagger c_{j\downarrow}^\dagger c_{j\downarrow} c_{i\uparrow} + c_{i\downarrow}^\dagger c_{j\uparrow}^\dagger c_{j\uparrow} c_{i\downarrow} - c_{i\uparrow}^\dagger c_{j\downarrow}^\dagger c_{j\uparrow} c_{i\downarrow} - c_{i\downarrow}^\dagger c_{j\uparrow}^\dagger c_{j\downarrow} c_{i\uparrow} \right],\end{aligned} \tag{C.9}$$

with an on-site interaction of strength V_0 and a nearest-neighbor interaction of strength V_1, $t_{ij} = te^{i\varphi_{ij}}$ and φ_{ij} the Peierls phase factor for the vector potential.

To obtain an effective mean-field Hamiltonian, we insert the replacement

$$c_{is} c_{js'} \longrightarrow \langle c_{is} c_{js'} \rangle + \left(c_{is} c_{js'} - \langle c_{is} c_{js'} \rangle \right), \tag{C.10}$$

$$c_{is}^\dagger c_{js'}^\dagger \longrightarrow \langle c_{is}^\dagger c_{js'}^\dagger \rangle + \left(c_{is}^\dagger c_{js'}^\dagger - \langle c_{is}^\dagger c_{js'}^\dagger \rangle \right), \tag{C.11}$$

into the interaction term $\mathcal{H}_\mathrm{I}$ and assume that the deviation $\delta = \langle c_{is} c_{js'} - \langle c_{is} c_{js'} \rangle \rangle$ from the mean-field value is small. Keeping only terns linear in δ, we obtain

$$\begin{aligned} V_0 \sum_i c_{i\uparrow}^\dagger c_{i\downarrow}^\dagger c_{i\downarrow} c_{i\uparrow} &= V_0 \sum_i \left[\langle c_{i\uparrow}^\dagger c_{i\downarrow}^\dagger \rangle c_{i\downarrow} c_{i\uparrow} + \langle c_{i\downarrow} c_{i\uparrow} \rangle c_{i\uparrow}^\dagger c_{i\downarrow}^\dagger - \langle c_{i\uparrow}^\dagger c_{i\downarrow}^\dagger \rangle \langle c_{i\downarrow} c_{i\uparrow} \rangle \right] \\ &= \sum_i \left[\Delta_i^* c_{i\downarrow} c_{i\uparrow} + \Delta_i c_{i\uparrow}^\dagger c_{i\downarrow}^\dagger - \frac{1}{V_0} \Delta_i^* \Delta_i \right], \end{aligned} \tag{C.12}$$

and

$$\begin{aligned}
&\frac{V_1}{4}\sum_{\langle i,j\rangle}\left[c^\dagger_{i\uparrow}c^\dagger_{j\downarrow}c_{j\downarrow}c_{i\uparrow}+c^\dagger_{i\downarrow}c^\dagger_{j\uparrow}c_{j\uparrow}c_{i\downarrow}-c^\dagger_{i\uparrow}c^\dagger_{j\downarrow}c_{j\uparrow}c_{i\downarrow}-c^\dagger_{i\downarrow}c^\dagger_{j\uparrow}c_{j\downarrow}c_{i\uparrow}\right]\\
&\quad=\frac{V_1}{4}\sum_{\langle i,j\rangle}\Big[\langle c^\dagger_{i\uparrow}c^\dagger_{j\downarrow}\rangle c_{j\downarrow}c_{i\uparrow}+\langle c_{j\downarrow}c_{i\uparrow}\rangle c^\dagger_{i\uparrow}c^\dagger_{j\downarrow}-\langle c^\dagger_{i\uparrow}c^\dagger_{j\downarrow}\rangle\langle c_{j\downarrow}c_{i\uparrow}\rangle\\
&\qquad+\langle c^\dagger_{i\downarrow}c^\dagger_{j\uparrow}\rangle c_{j\uparrow}c_{i\downarrow}+\langle c_{j\uparrow}c_{i\downarrow}\rangle c^\dagger_{i\downarrow}c^\dagger_{j\uparrow}-\langle c^\dagger_{i\downarrow}c^\dagger_{j\uparrow}\rangle\langle c_{j\uparrow}c_{i\downarrow}\rangle\\
&\qquad-\langle c^\dagger_{i\uparrow}c^\dagger_{j\downarrow}\rangle c_{j\uparrow}c_{i\downarrow}-\langle c_{j\uparrow}c_{i\downarrow}\rangle c^\dagger_{i\uparrow}c^\dagger_{j\downarrow}+\langle c^\dagger_{i\uparrow}c^\dagger_{j\downarrow}\rangle\langle c_{j\uparrow}c_{i\downarrow}\rangle\\
&\qquad-\langle c^\dagger_{i\downarrow}c^\dagger_{j\uparrow}\rangle c_{j\downarrow}c_{i\uparrow}-\langle c_{j\downarrow}c_{i\uparrow}\rangle c^\dagger_{i\downarrow}c^\dagger_{j\uparrow}+\langle c^\dagger_{i\downarrow}c^\dagger_{j\uparrow}\rangle\langle c_{j\downarrow}c_{i\uparrow}\rangle\Big]\\
&\quad=\frac{V_1}{2}\sum_{\langle i,j\rangle}\Big[\Big(\langle c^\dagger_{i\uparrow}c^\dagger_{j\downarrow}\rangle-\langle c^\dagger_{i\downarrow}c^\dagger_{j\uparrow}\rangle\Big)c_{i\downarrow}c_{i\uparrow}+\Big(\langle c_{j\downarrow}c_{i\uparrow}\rangle-\langle c_{j\uparrow}c_{i\downarrow}\rangle\Big)c^\dagger_{i\uparrow}c^\dagger_{j\downarrow}\\
&\qquad-\frac{1}{2}\Big(\langle c^\dagger_{i\uparrow}c^\dagger_{j\downarrow}\rangle-\langle c^\dagger_{i\downarrow}c^\dagger_{j\uparrow}\rangle\Big)\Big(\langle c_{j\downarrow}c_{i\uparrow}\rangle-\langle c_{j\uparrow}c_{i\downarrow}\rangle\Big)\Big]\\
&\quad=\sum_{\langle i,j\rangle}\left[\Delta^*_{ij}c_{j\downarrow}c_{i\uparrow}+\Delta_{ij}c^\dagger_{i\uparrow}c^\dagger_{j\downarrow}-\frac{1}{V_1}\Delta^*_{ij}\Delta_{ij}\right],
\end{aligned}\tag{C.13}$$

with the mean field order parameters

$$\Delta_i=V\langle c_{i\downarrow}c_{i\uparrow}\rangle,\qquad \Delta^*_i=V\langle c^\dagger_{i\uparrow}c^\dagger_{i\downarrow}\rangle \tag{C.14}$$

and

$$\Delta_{ij}=\frac{V_1}{2}\Big(\langle c_{j\downarrow}c_{i\uparrow}\rangle-\langle c_{j\uparrow}c_{i\downarrow}\rangle\Big),\qquad \Delta^*_{ij}=\frac{V_1}{2}\Big(\langle c^\dagger_{i\uparrow}c^\dagger_{j\downarrow}\rangle-\langle c^\dagger_{i\downarrow}c^\dagger_{j\uparrow}\rangle\Big). \tag{C.15}$$

The resulting mean-fieled Hamiltonian takes the form

$$\begin{aligned}
\mathcal{H}=\sum_{\langle ij\rangle,s}t_{ij}c^\dagger_{is}c_{js}+\sum_i\left[\Delta^*_ic_{i\downarrow}c_{i\uparrow}+\Delta_ic^\dagger_{i\uparrow}c^\dagger_{i\downarrow}\right]+\sum_{\langle i,j\rangle}\left[\Delta^*_{ij}c_{j\downarrow}c_{i\uparrow}+\Delta_{ij}c^\dagger_{i\uparrow}c^\dagger_{j\downarrow}\right]\\
-\frac{1}{V_0}\sum_i\Delta^*_i\Delta_i-\frac{1}{V_0}\sum_{\langle i,j\rangle}\Delta^*_{ij}\Delta_{ij}.
\end{aligned}\tag{C.16}$$

C.3 Bogoliubov - de Gennes Equations

C.3.1 Diagonalization

The Bogoliubov - de Gennes equations incorporate an equation defining the Bogoliubov transformation which diagonalizes $\mathcal{H}$, and a self-consistency equation for Δ_i and Δ_{ij}, respectively. For their derivation, the constant terms $1/V_0\sum_i\Delta^*_i\Delta_i$ and $1/V_1\sum_{\langle i,j\rangle}\Delta^*_{ij}\Delta_{ij}$

in (C.16) are unimportant. We therefore continue with the Hamiltonian $\mathcal{H}'$ which does not include these terms.

Defining the vectors $\mathbf{c}_\uparrow$, $\mathbf{c}_\downarrow$, $\mathbf{c}_\uparrow^\dagger$ and $\mathbf{c}_\downarrow^\dagger$ as

$$\mathbf{c}_\uparrow = \begin{pmatrix} c_{1\uparrow} \\ \vdots \\ c_{N\uparrow} \end{pmatrix}, \qquad \mathbf{c}_\downarrow = \begin{pmatrix} c_{1\downarrow} \\ \vdots \\ c_{N\downarrow} \end{pmatrix}, \tag{C.17}$$

$$\mathbf{c}_\uparrow^\dagger = \left(c_{1\uparrow}^\dagger, \cdots, c_{N\uparrow}^\dagger\right), \qquad \mathbf{c}_\downarrow^\dagger = \left(c_{1\downarrow}^\dagger, \cdots, c_{N\downarrow}^\dagger\right), \tag{C.18}$$

and the matrices $\hat{t}$, $\hat{\Delta}$ and $\hat{\Delta}^\dagger$ as $\left(\hat{t}\right)_{ij} = t_{ij}$, $\left(\hat{\Delta}\right)_{ij} = \Delta_{ij}$ and $\left(\hat{\Delta}^\dagger\right)_{ij} = \Delta_{ij}^*$, the Hamiltonian $\mathcal{H}'$ takes the form

$$\mathcal{H}' = \mathbf{c}_\uparrow^\dagger \hat{t} \mathbf{c}_\uparrow - \mathbf{c}_\downarrow \hat{t}^\dagger \mathbf{c}^\dagger{}_\downarrow + \mathbf{c}_\downarrow \hat{\Delta}^\dagger \mathbf{c}_\uparrow + \mathbf{c}_\downarrow^\dagger \hat{\Delta} \mathbf{c}^\dagger{}_\downarrow = \left(\mathbf{c}_\uparrow^\dagger, \mathbf{c}_\downarrow^\top\right) \begin{pmatrix} \hat{t} & \hat{\Delta} \\ \hat{\Delta}^\dagger & -\hat{t}^\dagger \end{pmatrix} \begin{pmatrix} \mathbf{c}_\uparrow \\ \mathbf{c}^\dagger{}_\downarrow \end{pmatrix}. \tag{C.19}$$

We diagonalize $\mathcal{H}'$ using the unitary $2N \times 2N$-matrix $\hat{U}$ defined by the eigenvalue equation

$$\begin{pmatrix} \hat{t} & \hat{\Delta} \\ \hat{\Delta}^\dagger & -\hat{t}^\dagger \end{pmatrix} \begin{pmatrix} \mathbf{u}_n \\ \mathbf{v}_n \end{pmatrix} = E_n \begin{pmatrix} \mathbf{u}_n \\ \mathbf{v}_n \end{pmatrix}. \tag{C.20}$$

The matrices $\hat{u}$ and $\hat{v}$ are given by the first N eigenvectors: $(\hat{u})_{ni} = u_{ni}$, $(\hat{v})_{ni} = v_{ni}$. This transformation defines the fermionic quasi-particle operators a_{ns} and $a_{as}^\dagger$ through

$$\begin{pmatrix} \mathbf{a}_\uparrow \\ \mathbf{a}^\dagger{}_\downarrow \end{pmatrix} = \hat{U}^\dagger \begin{pmatrix} \mathbf{c}_\uparrow \\ \mathbf{c}^\dagger{}_\downarrow{}^\top \end{pmatrix} = \begin{pmatrix} \hat{u}^\dagger \mathbf{c}_\uparrow + \hat{v}^\dagger \mathbf{c}^\dagger{}_\downarrow \\ -\hat{v} \mathbf{c}_\uparrow + \hat{u} \mathbf{c}^\dagger{}_\downarrow{}^\top \end{pmatrix} \tag{C.21}$$

in which the Hamiltonian is diagonal:

$$\mathcal{H}' = \left(\mathbf{a}_\uparrow^\dagger, \mathbf{a}_\downarrow^\top\right) \begin{pmatrix} \hat{E} & 0 \\ 0 & -\hat{E} \end{pmatrix} \begin{pmatrix} \mathbf{a}_\uparrow \\ \mathbf{a}^\dagger{}_\downarrow{}^\top \end{pmatrix} = \sum_n E_n \left[a_{n\uparrow}^\dagger a_{n\uparrow} - a_{n\downarrow} a_{n\downarrow}^\dagger\right], \tag{C.22}$$

where $\hat{E}$ is diagonal. The inverse transformation is

$$\begin{pmatrix} \mathbf{c}_\uparrow \\ \mathbf{c}^\dagger{}_\downarrow \end{pmatrix} = \hat{U} \begin{pmatrix} \mathbf{a}_\uparrow \\ \mathbf{a}^\dagger{}_\downarrow \end{pmatrix} = \begin{pmatrix} \hat{u} \mathbf{a}_\uparrow - \hat{v}^\dagger \mathbf{a}^\dagger{}_\downarrow \\ \hat{v} \mathbf{a}_\uparrow + \hat{u}^\dagger \mathbf{a}^\dagger{}_\downarrow \end{pmatrix}, \tag{C.23}$$

leading finally to the transformation for the operators $c_{i,s}$:

$$c_{i\uparrow} = \sum_n \left[u_{ni} a_{n\uparrow} - v_{ni}^* a_{n\downarrow}^\dagger\right], \tag{C.24}$$

$$c_{i\downarrow} = \sum_n \left[u_{ni} a_{n\downarrow} + v_{ni}^* a_{n\uparrow}^\dagger\right], \tag{C.25}$$

where the sum runs over the first N eigenvectors of $\mathcal{H}'$, corresponding to positive eigenenergies E_n.

C.3.2 Self-Consistency Equation

We insert now the transformations (C.24) and (C.25) into the defining equations for the order parameters Δ_i and Δ_{ij}, which constitute together with the eigenvalue equation (C.20) the Bogoliubov - de Gennes equations. For the on-site order parameter we find

$$\begin{aligned}\Delta_i &= V_o\langle c_{i\downarrow}c_{i\uparrow}\rangle \\ &= V_0\sum_{nn'}\left[u_{ni}u_{n'i}\langle a_{n\downarrow}a_{n'\uparrow}\rangle - v^*_{ni}v^*_{n'i}\langle a^\dagger_{n\uparrow}a^\dagger_{n'\downarrow}\rangle + u_{ni}v^*_{n'i}\langle a_{n\downarrow}a^\dagger_{n'\downarrow}\rangle - u_{ni}v^*_{n'i}\langle a^\dagger_{n\uparrow}a_{n'\uparrow}\rangle\right]\end{aligned} \tag{C.26}$$

Using the known expectation values for fermionic operators within a diagonal Hamiltonian $\langle a^\dagger_{as}a_{n's'}\rangle = \delta_{nn'}\delta_{ss'}f(E_n)$, $\langle a_{ns}a^\dagger_{n's'}\rangle = \delta_{nn'}\delta_{ss'}[1-f(E_n)]$ and $\langle a_{ns}a_{n's'}\rangle = \langle a^\dagger_{as}a^\dagger_{n's'}\rangle = 0$, we obtain

$$\Delta_i = V_0\sum_n u_{ni}v^*_{ni}\left[1-2f(E_n)\right] = V_0\sum_n u_{ni}v^*_{ni}\tanh(E_n), \tag{C.27}$$

where we used that if $(\mathbf{u}_n, \mathbf{v}_n)$ is an eigenvector for the eigenvalue E_n, then $(-\mathbf{v}^\dagger_n, \mathbf{u}^\dagger_n)$ is the eigenvector for the eigenvalue $-E_n$, and that $1-2f(E) = 2\tanh(E)$. For the d-wave order parameter we find

$$\begin{aligned}\Delta_{ij} &= \frac{V_1}{2}\left(\langle c_{j\downarrow}c_{i\uparrow}\rangle - \langle c_{j\uparrow}c_{i\downarrow}\rangle\right) \\ &= \frac{V_1}{2}\sum_{nn'}\Big[u_{nj}u_{n'i}\langle a_{n\downarrow}a_{n'\uparrow}\rangle - v^*_{nj}v^*_{n'i}\langle a^\dagger_{n\uparrow}a^\dagger_{n'\downarrow}\rangle - u_{nj}v^*_{n'i}\langle a_{n\downarrow}a^\dagger_{n'\downarrow}\rangle + v^*_{nj}u_{n'i}\langle a^\dagger_{n\uparrow}a_{n'\uparrow}\rangle \\ &\qquad - u_{nj}u_{n'i}\langle a_{n\uparrow}a_{n'\downarrow}\rangle + v^*_{nj}v^*_{n'i}\langle a^\dagger_{n\downarrow}a^\dagger_{n'\uparrow}\rangle - u_{nj}v^*_{n'i}\langle a_{n\uparrow}a^\dagger_{n'\uparrow}\rangle + v^*_{nj}u_{n'i}\langle a^\dagger_{n\downarrow}a_{n'\downarrow}\rangle\Big] \\ &= V_1\sum_n\left[u_{ni}v^*_{nj}f(E_n) - u_{nj}v^*_{ni}[1-f(E_n)]\right] \\ &= 2V_1\sum_{n,E_n>0}\left[u_{ni}v^*_{nj} + u_{nj}v^*_{ni}\right]\tanh(E_n).\end{aligned} \tag{C.28}$$

The Hamiltonian (C.16) gives finite pairing amplitudes only for spin singlet pairing. The nearest-neighbor order parameter can therefore alternatively be defined as $\Delta_{ij} = V_1\langle c_{j\downarrow}c_{i\uparrow}\rangle$, since the spin-triplet component drops out on inserting the Bogoliubov transformation (C.23).

C.4 Current

In appendix A we have found the current J_{ij} per bond to be

$$J_{ij} = -\frac{et}{\hbar}\sum_s\left(e^{-i\varphi_{ij}}c^\dagger_{js}c_{is} - e^{-i\varphi_{ji}}c^\dagger_{is}c_{js}\right), \tag{C.29}$$

where i and j are nearest neighbor sites.

To calculate the expectation value of the current operator, we insert the Bogoliubov transformation [equation (C.23)] into (C.29) and obtain

$$\begin{aligned}
\langle J_{ij}\rangle = -\frac{et}{\hbar}\sum_{nn'}\Big[& e^{-i\varphi_{ij}}\Big(u_{nj}u^*_{in'}\langle a^\dagger_{n\uparrow}a_{n'\uparrow}\rangle + v^*_{nj}v_{in'}\langle a_{n\downarrow}a^\dagger_{n'\downarrow}\rangle \\
& \qquad + u_{nj}u^*_{in'}\langle a^\dagger_{n\downarrow}a_{n'\downarrow}\rangle + v^*_{jn}v_{in'}\langle a_{n\uparrow}a^\dagger_{n'\uparrow}\rangle\Big) \\
& - e^{-i\varphi_{ji}}\Big(u_{ni}u^*_{jn'}\langle a^\dagger_{n\uparrow}a_{n'\uparrow}\rangle + v^*_{ni}v_{jn'}\langle a_{n\downarrow}a^\dagger_{n'\downarrow}\rangle \\
& \qquad + u_{ni}u^*_{jn'}\langle a^\dagger_{n\downarrow}a_{n'\downarrow}\rangle + v^*_{in}v_{jn'}\langle a_{n\uparrow}a^\dagger_{n'\uparrow}\rangle\Big)\Big] \\
= -2\frac{et}{\hbar}\sum_n\Big[& e^{-i\varphi_{ij}}\left(u_{nj}u^*_{ni}f(E_n) + v^*_{jn}v_{in}\left(1-f(E_n)\right)\right) \\
& - e^{-i\varphi_{ij}}\left(u_{ni}u^*_{nj}f(E_n) + v^*_{in}v_{jn}\left(1-f(E_n)\right)\right)\Big] \\
= -4\frac{et}{\hbar}\sum_n \mathrm{Im}\Big[& \left(u_{nj}u^*_{in}f(E_n) + v^*_{nj}v_{in}\left(1-f(E_n)\right)\right)e^{-i\varphi_{ij}}\Big] \\
= -8\frac{et}{\hbar}\sum_n \mathrm{Im}\left(u_{nj}u^*_{in}e^{-i\varphi_{ij}}\right)f(E_n), &
\end{aligned} \tag{C.30}$$

where we again used that $(-\mathbf{v}^\dagger_n, \mathbf{u}^\dagger_n)$ are the eigenvectors corresponding to the eigenvalues $-E_n$.

C.5 Internal Energy

The internal energy $E = \langle\mathcal{H}\rangle$ is the expectation value of the Hamiltonian in (C.16). Using the diagonalized form of $\mathcal{H}'$ [equation (C.22)], one finds

$$\begin{aligned}
E &= \langle\mathcal{H}'\rangle - \frac{1}{V_0}\sum_i \Delta^*_i\Delta_i - \frac{1}{V_1}\sum_{\langle i,j\rangle}\Delta^*_{ij}\Delta_{ij} \\
&= \sum_n E_n f(E_n) - \frac{1}{V_0}\sum_i \Delta^*_i\Delta_i - \frac{1}{V_1}\sum_{\langle i,j\rangle}\Delta^*_{ij}\Delta_{ij}.
\end{aligned} \tag{C.31}$$

D Formalism of the Extended BCS Theory

D.1 Nearest-Neighbor Pairing Interaction

D.1.1 Pairing Interaction in Momentum Space

The interaction between electrons is naturally defined in real space by the interaction Hamiltonian

$$\mathcal{H}_\mathrm{I} = \sum_{\langle i,j\rangle} V_{ij} c_i^\dagger c_j^\dagger c_j c_i, \tag{D.1}$$

where the sum $\sum_{\langle i,j\rangle}$ contains all pairs of lattice sites, between which there is a finite interaction V_{ij}. In our case, i and j are either equal, leading to conventional s-wave pairing, or nearest neighbor lattice sites, which leads to

$$\mathcal{H}_\mathrm{I} = \frac{V_1}{2} \sum_i \left[c_i^\dagger c_{i+\hat{x}}^\dagger c_{i+\hat{x}} c_i + c_i^\dagger c_{i-\hat{x}}^\dagger c_{i-\hat{x}} c_i + c_i^\dagger c_{i+\hat{y}}^\dagger c_{i+\hat{y}} c_i + c_i^\dagger c_{i-\hat{y}}^\dagger c_{i-\hat{y}} c_i \right], \tag{D.2}$$

with an attractive interaction strength $V_1 < 0$ and where $\hat{x}$ and $\hat{y}$ are unit vectors in x- and y-direction, respectively. The Fourier transformation of the first term in equation (D.2) gives

$$\sum_i c_i^\dagger c_{i+\hat{x}}^\dagger c_{i+\hat{x}} c_i = \frac{1}{N^2} \sum_i \sum_{\mathbf{k}_1,\ldots,\mathbf{k}_4} e^{i(\mathbf{k}_1+\mathbf{k}_2-\mathbf{k}_3-\mathbf{k}_4)i} e^{i(\mathbf{k}_2-\mathbf{k}_3)\hat{x}} c_{\mathbf{k}_1}^\dagger c_{\mathbf{k}_2}^\dagger c_{\mathbf{k}_3} c_{\mathbf{k}_4} \tag{D.3}$$

$$= \frac{1}{N} \sum_{\mathbf{k}_1,\mathbf{k}_2,\mathbf{k}_3} e^{i(\mathbf{k}_2-\mathbf{k}_3)\hat{x}} c_{\mathbf{k}_1}^\dagger c_{\mathbf{k}_2}^\dagger c_{\mathbf{k}_3} c_{\mathbf{k}_1+\mathbf{k}_2-\mathbf{k}_3} \tag{D.4}$$

$$= \frac{1}{N} \sum_{\mathbf{k},\mathbf{k}'} \sum_{\mathbf{q}} e^{i(\mathbf{k}-\mathbf{k}')\hat{x}} c_{\mathbf{k}}^\dagger c_{-\mathbf{k}+\mathbf{q}}^\dagger c_{-\mathbf{k}'+\mathbf{q}} c_{\mathbf{k}'}, \tag{D.5}$$

where we used that $1/N \sum_i e^{i\mathbf{k}i} = \delta_{i0}$ and the substitutions $\mathbf{k}_1 = \mathbf{k}$, $\mathbf{k}_2 = -\mathbf{k} + \mathbf{q}$ and $\mathbf{k}_3 = -\mathbf{k}' + \mathbf{q}$. With analogous transformations of the remaining three terms of equation (D.2), we obtain the interaction Hamiltonian in momentum space:

$$\mathcal{H}_\mathrm{I} = \frac{1}{N} \sum_{\mathbf{k},\mathbf{k}'} \sum_{\mathbf{q}} V(\mathbf{k},\mathbf{k}') c_{\mathbf{k}}^\dagger c_{-\mathbf{k}+\mathbf{q}}^\dagger c_{-\mathbf{k}'+\mathbf{q}} c_{\mathbf{k}'} \tag{D.6}$$

with

$$V(\mathbf{k},\mathbf{k}') = V_1\left[\cos(k_x - k_x') + \cos(k_y - k_y')\right]. \tag{D.7}$$

In standard BCS theory, $V(\mathbf{k},\mathbf{k}')$ is decomposed into product form with a symmetric and an antisymmetric contribution:

$$V(\mathbf{k},\mathbf{k}') = V_1\left[\cos k_x \cos k_x' + \cos k_y \cos k_y' + \sin k_x \sin k_x' + \sin k_y \sin k_y'\right]. \tag{D.8}$$

The symmetric cos-terms are associated with spin-singlet pairing and d-wave symmetry, whereas the antisymmetric sin-terms represent spin-triplet pairing with p-wave symmetry. Here we consider only singlet pairing, for which the antisymmetric terms don't contribute, and obtain the interaction in product form

$$V(\mathbf{k},\mathbf{k}') = V_1\left[\cos k_x \cos k_x' + \cos k_y \cos k_y'\right]. \tag{D.9}$$

D.1.2 Gauge invariance

The decomposition of $V(\mathbf{k},\mathbf{k}')$ in equation (D.8) is not unique. Adding a constant vector $\mathbf{q}'$ to both $\mathbf{k}$ and $\mathbf{k}'$ leaves $V(\mathbf{k},\mathbf{k}')$ invariant. A more general decomposition is

$$V(\mathbf{k},\mathbf{k}') \to V(\mathbf{k},\mathbf{k}',\mathbf{q}') = \left[\cos(k_x - q_x')\cos(k_x' - q_x') + \cos(k_y - q_y')\cos(k_y' - q_y')\right]. \tag{D.10}$$

In a BCS like mean-field theory, this vector $\mathbf{q}'$ cannot be chosen arbitrarily, but it is locked by gauge invariance to the center of mass momentum $\mathbf{q}$ of the pair amplitude $\langle c_{-\mathbf{k}+\mathbf{q}} c_{\mathbf{k}}\rangle$ with lowest energy.

For our purpose, it is easiest to discuss gauge invariance in a one dimensional ring, as in chapter 1. Gauge invariance demands that this system is invariant upon replacing the magnetic flux threading the ring by $\phi \to \phi \pm 1$ and the pair momentum by $q_x \to q_x \pm 2$. One finds that the self-consistency equation [see appendix D.2.2] is invariant under the replacement above only if the order parameter $\Delta(\mathbf{k},\mathbf{q})$ depends on $\mathbf{k}$ and $\mathbf{q}$ as $\Delta(\mathbf{k}-\mathbf{q}/2)$. This requires that $\mathbf{q}' = \mathbf{q}/2$ in equation (D.10) above.

Finally we decompose the interaction as

$$V(\mathbf{k},\mathbf{k}',\mathbf{q}) = V_s(\mathbf{k},\mathbf{k}',\mathbf{q}) + V_d(\mathbf{k},\mathbf{k}',\mathbf{q}) \tag{D.11}$$

with an extended s-wave component $V_s(\mathbf{k},\mathbf{k}',\mathbf{q})$ without sign change in real space, and a d-wave component $V_d(\mathbf{k},\mathbf{k}',\mathbf{q})$:

$$V_{s,d}(\mathbf{k},\mathbf{k}',\mathbf{q}) = V_{0,1} g_{s,d}(\mathbf{k}-\mathbf{q}/2) g_{s,d}(\mathbf{k}'-\mathbf{q}/2). \tag{D.12}$$

with $g_s(\mathbf{k}) = \cos k_x + \cos k_y$ and $g_d(\mathbf{k}) = \cos k_x - \cos k_y$.

D.2 Gor'kov Equations

D.2.1 Equations of Motion

We start from the tight-binding interaction Hamiltonian on a square lattice with N sites and periodic boundary conditions used in chapter 10:

$$\mathcal{H} = \sum_{\mathbf{k},s} \varepsilon_{\mathbf{k}} c^{\dagger}_{\mathbf{k}s} c_{\mathbf{k}s} + \frac{1}{N} \sum_{\mathbf{q}} \sum_{\mathbf{k},\mathbf{k}'} \sum_{s,s'} V(\mathbf{k},\mathbf{k}',\mathbf{q}) c^{\dagger}_{\mathbf{k}s} c^{\dagger}_{-\mathbf{k}+\mathbf{q}s'} c_{-\mathbf{k}'+\mathbf{q}s'} c_{\mathbf{k}'s}. \tag{D.13}$$

In the Heisenberg picture, the creation and annihilation operators depend on the imaginary time $\tau = iT$ as $c_{\mathbf{k}s}(\tau) = e^{\tau\mathcal{H}} c_{\mathbf{k}s} e^{-\tau\mathcal{H}}$. With the help of this definition, we define the Green's function of the superconducting state as follows:

$$G(\mathbf{k},\mathbf{k}',\tau) = -\langle T_\tau c_{\mathbf{k}s}(\tau) c^{\dagger}_{\mathbf{k}'s}(0)\rangle. \tag{D.14}$$

For complete characterization of the superconductor, we need additionally the two anomalous Green's functions

$$F(\mathbf{k},\mathbf{k}',\tau) = \langle T_\tau c_{\mathbf{k}s}(\tau) c_{-\mathbf{k}'s'}(0)\rangle, \tag{D.15}$$

$$F^*(\mathbf{k},\mathbf{k}',\tau) = \langle T_\tau c^{\dagger}_{-\mathbf{k}s}(\tau) c^{\dagger}_{\mathbf{k}'s'}(0)\rangle \tag{D.16}$$

for $s \neq s'$. To derive a self consistent set of equations for $G(\mathbf{k},\mathbf{k}',\tau)$, $F(\mathbf{k},\mathbf{k}',\tau)$ and $F^*(\mathbf{k},\mathbf{k}',\tau)$, we use the Heisenberg equation of motion for the operators $c_{\mathbf{k}s}$: $\partial c_{\mathbf{k}s}(\tau)/\partial\tau = [\mathcal{H}(\tau), c_{\mathbf{k}s}(\tau)]$. Applying this on $G(\mathbf{k},\mathbf{k}',\tau)$, we find

$$\frac{\partial}{\partial\tau} G(\mathbf{k},\mathbf{k}',\tau) = -\langle [\mathcal{H}(\tau), c_{\mathbf{k}s}(\tau)]\, c^{\dagger}_{\mathbf{k}'s}(0)\rangle - \delta(0)\delta_{\mathbf{k}\mathbf{k}'} \tag{D.17}$$

$$\begin{aligned} &= -\varepsilon_{\mathbf{k}} G(\mathbf{k},\mathbf{k}',\tau) \\ &\quad - \sum_{\mathbf{q}} \sum_{\mathbf{k}''} V(\mathbf{k},\mathbf{k}',\mathbf{q}) \langle c^{\dagger}_{-\mathbf{k}+\mathbf{q}s'}(\tau) c_{\mathbf{k}''s}(\tau) c_{-\mathbf{k}+\mathbf{q}s'}(\tau) c^{\dagger}_{\mathbf{k}'s}(0)\rangle - \delta(0)\delta_{\mathbf{k}\mathbf{k}'} \end{aligned} \tag{D.18}$$

For the superconducting state with singlet pairing, we use the BCS type mean-field decoupling scheme and approximate

$$\langle c^{\dagger}_{\mathbf{k}\uparrow}(\tau) c_{-\mathbf{k}'+\mathbf{q}\downarrow}(\tau) c_{\mathbf{k}'\uparrow}(\tau) c^{\dagger}_{-\mathbf{k}+\mathbf{q}\downarrow}(0)\rangle \to \langle c^{\dagger}_{-\mathbf{k}+\mathbf{q}\downarrow}(\tau) c^{\dagger}_{\mathbf{k}\uparrow}(0)\rangle \langle c_{-\mathbf{k}'+\mathbf{q}\downarrow}(\tau) c_{\mathbf{k}'\uparrow}(\tau)\rangle. \tag{D.19}$$

Here we introduce now the superconducting order parameter

$$\Delta(\mathbf{k},\mathbf{q}) = -\frac{1}{N} \sum_{\mathbf{k}'} V(\mathbf{k},\mathbf{k}',\mathbf{q}) F(\mathbf{k}',\mathbf{k}'-\mathbf{q},0), \tag{D.20}$$

$$\Delta^*(\mathbf{k},\mathbf{q}) = -\frac{1}{N} \sum_{\mathbf{k}'} V(\mathbf{k},\mathbf{k}',\mathbf{q}) F^*(\mathbf{k}'-\mathbf{q},\mathbf{k}',0). \tag{D.21}$$

Inserting the decoupling scheme from equation (D.19) and $\Delta(\mathbf{k},\mathbf{q})$ into equation (D.18), we obtain the Gor'kov equation for the Green's function:

$$\frac{\partial}{\partial\tau}G(\mathbf{k},\mathbf{k}',\tau) = -\varepsilon_{\mathbf{k}}G(\mathbf{k},\mathbf{k}',\tau) - \sum_{\mathbf{q}}\Delta(\mathbf{k},\mathbf{q})F^{*}(\mathbf{k}-\mathbf{q},\mathbf{k}',\tau) - \delta(0)\delta_{\mathbf{k}\mathbf{k}'}. \tag{D.22}$$

To solve equation (D.22), it is convenient to change to frequency space through the Fourier transformation

$$G(\mathbf{k},\mathbf{k}',\tau) = T\sum_{n}\mathcal{G}(\mathbf{k},\mathbf{k}',\omega_n)e^{-i\omega_n\tau}, \tag{D.23}$$

where $\omega_n = (2n-1)\pi T$ is the Matsubara frequency for the finite temperature T. With analogous Fourier transformations, the order parameters in frequency space become

$$\Delta(\mathbf{k},\mathbf{q}) = -\frac{T}{N}\sum_{n}\sum_{\mathbf{k}'}V(\mathbf{k},\mathbf{k}',\mathbf{q})\mathcal{F}(\mathbf{k}',\mathbf{k}'-\mathbf{q},\omega_n), \tag{D.24}$$

$$\Delta^{*}(\mathbf{k},\mathbf{q}) = -\frac{T}{N}\sum_{n}\sum_{\mathbf{k}'}V(\mathbf{k},\mathbf{k}',\mathbf{q})\mathcal{F}^{*}(\mathbf{k}'-\mathbf{q},\mathbf{k}',\omega_n), \tag{D.25}$$

which leads to the final form of the Gor'kov equation for the Green's function:

$$\mathcal{G}(\mathbf{k},\mathbf{k}',\omega_n) = \mathcal{G}_0^{-1}(\mathbf{k},\omega_n)\left[\delta_{\mathbf{k}\mathbf{k}'} - \sum_{\mathbf{q}}\Delta(\mathbf{k},\mathbf{q})\mathcal{F}^{*}(\mathbf{k}-\mathbf{q},\mathbf{k}',\omega_n)\right], \tag{D.26}$$

where $\mathcal{G}_0(\mathbf{k},\omega_n) = \left[i\omega_n - \varepsilon_{\mathbf{k}}\right]^{-1}$ is the Green's function in the normal state. With the same procedure we find the Gor'kov equations for $\mathcal{F}(\mathbf{k},\mathbf{k}',\omega_n)$ and $\mathcal{F}^{*}(\mathbf{k},\mathbf{k}',\omega_n)$ in frequency space:

$$\mathcal{F}(\mathbf{k},\mathbf{k}',\omega_n) = \mathcal{G}_0(\mathbf{k},\omega_n)\sum_{\mathbf{q}}\Delta(\mathbf{k},\mathbf{q})\mathcal{G}(-\mathbf{k}',-\mathbf{k}+\mathbf{q},-\omega_n), \tag{D.27}$$

$$\mathcal{F}^{*}(\mathbf{k},\mathbf{k}',\omega_n) = -\mathcal{G}_0(-\mathbf{k},-\omega_n)\sum_{\mathbf{q}}\Delta^{*}(\mathbf{k},\mathbf{q})\mathcal{G}(\mathbf{k}+\mathbf{q},\mathbf{k}',\omega_n). \tag{D.28}$$

D.2.2 Self-Consistency Equation

Solution of the Gor'kov equations in frequency space:

For the nearest neighbor interaction from appendix D.1.2 the order parameter has the structure

$$\Delta(\mathbf{k},\mathbf{q}) = \Delta_s(\mathbf{q})g_s(\mathbf{k}-\mathbf{q}/2) + \Delta_d(\mathbf{q})g_d(\mathbf{k}-\mathbf{q}/2), \tag{D.29}$$

$$\Delta^{*}(\mathbf{k},\mathbf{q}) = \Delta_s(\mathbf{q})g_s(\mathbf{k}+\mathbf{q}/2) + \Delta_d(\mathbf{q})g_d(\mathbf{k}+\mathbf{q}/2), \tag{D.30}$$

with a component $\Delta_s(\mathbf{q})$ for extended s-wave pairing and a d-wave component $\Delta_d(\mathbf{q})$; for an on-sight interaction one obtains the $\mathbf{k}$-independent s-wave order parameter $\Delta(\mathbf{q})$. The vector $\mathbf{q}$ labels mean-field solutions which correspond to order parameters in real space with phase winding numbers q_x and q_y in x- and y-direction, respectively.

The normal and anomalous Green's functions have finite values only under the following conditions for $\mathbf{k}$ and $\mathbf{k}'$:

$$\begin{aligned}
\mathcal{G}(\mathbf{k},\mathbf{k}',\omega_n) \neq 0 \text{ if } &\begin{cases} \mathbf{k}' = \mathbf{k}, \\ \mathbf{k}' = \mathbf{k}+\mathbf{q}-\mathbf{q}' \text{ and } \Delta(\mathbf{k},\mathbf{q}) \neq 0,\ \Delta(\mathbf{k}',\mathbf{q}') \neq 0 \end{cases} \\
\mathcal{F}(\mathbf{k},\mathbf{k}',\omega_n) \neq 0 \text{ if } &\ \mathbf{k}' = \mathbf{k}-\mathbf{q} \text{ and } \Delta(\mathbf{k},\mathbf{q}) \neq 0 \\
\mathcal{F}^*(\mathbf{k},\mathbf{k}',\omega_n) \neq 0 \text{ if } &\ \mathbf{k}' = \mathbf{k}+\mathbf{q} \text{ and } \Delta(\mathbf{k},\mathbf{q}) \neq 0
\end{aligned}$$

Inserting Eq. (D.27) into Eq. (D.26) leads to a system of coupled equations for the Green's function $\mathcal{G}(\mathbf{k},\mathbf{k}',\omega_n)$:

$$\begin{aligned}
\mathcal{G}(\mathbf{k}+\mathbf{q}_1,\mathbf{k}+\mathbf{q}_2,\omega_n) &= \mathcal{G}_0(\mathbf{k}+\mathbf{q}_1,\omega_n)\Delta(\mathbf{k}+\mathbf{q}_1,\mathbf{q}_1)\mathcal{G}_0(-\mathbf{k},-\omega_n) \\
&\times \left[\Delta^*(\mathbf{k},\mathbf{q}_1)\mathcal{G}(\mathbf{k}+\mathbf{q}_1,\mathbf{k}+\mathbf{q}_2,\omega_n) + \Delta^*(\mathbf{k},\mathbf{q}_2)\mathcal{G}(\mathbf{k}+\mathbf{q}_2,\mathbf{k}+\mathbf{q}_2,\omega_n)\right]^{-1}. \quad \text{(D.31)}
\end{aligned}$$

In principle, equation (D.31) can be solved numerically for all $\mathbf{k}$ and ω_n to obtain exact solutions of Gor'kov's equations, but this is a rather extensive task. Reinserting $\mathcal{F}^*(\mathbf{k},\mathbf{k}',\omega_n)$ and $\mathcal{G}(\mathbf{k},\mathbf{k}',\omega_n)$ iteratively into equation (D.31) leads to a powerseries in $\Delta(\mathbf{k},\mathbf{q})\mathcal{G}(\mathbf{k}+\mathbf{q},\omega_n)$ times the diagonal Green's function $\mathcal{G}(\mathbf{k},\mathbf{k},\omega_n)$. For $Q = 1$, only the zeroth order exists. For $Q \geq 2$, the first order corresponds to charge order in real space and all higher orders to higher orders of the amplitude of the charge oscillations. This amplitude is typically much smaller than the mean charge density ρ, as we have shown in section 11.2. It is therefore a good approximation to keeponly the first order terms equation (D.31), which is equivalent to reinsert only the diagonal Green's function $\mathcal{G}(\mathbf{k},\mathbf{k},\omega_n)$ into (D.32) for $f^*(\mathbf{k},\mathbf{k}',\omega_n)$ and skip the sum over $\mathbf{q}$ otherwise. Within this approximation the Gor'kov equations are solved analytically, as shown below.

Inserting equation (D.32) into equation (D.26) leads to an explicit expression for the diagonal part of the Green's function

$$\begin{aligned}
\mathcal{G}(\mathbf{k},\mathbf{k},\omega_n) &= \left[\mathcal{G}_0^{-1}(\mathbf{k},\omega_n) + \sum_{\mathbf{q}} \Delta(\mathbf{k},\mathbf{q})\mathcal{F}^*(\mathbf{k}-\mathbf{q},\mathbf{k},\omega_n)\mathcal{G}^{-1}(\mathbf{k},\mathbf{k},\omega_n)\right]^{-1} \\
&= \left[\mathcal{G}_0^{-1}(\mathbf{k},\omega_n) + \sum_{\mathbf{q}} \Delta(\mathbf{k},\mathbf{q})\Delta^*(\mathbf{k}-\mathbf{q},\mathbf{q})\mathcal{G}_0(-\mathbf{k}+\mathbf{q},-\omega_n)\right]^{-1} \\
&= \left[i\omega_n - \varepsilon_{\mathbf{k}} + \sum_{\mathbf{q}} \frac{\Delta(\mathbf{k},\mathbf{q})\Delta^*(\mathbf{k}-\mathbf{q},\mathbf{q})}{-i\omega_n - \varepsilon_{-\mathbf{k}+\mathbf{q}}}\right]^{-1}. \quad \text{(D.32)}
\end{aligned}$$

Inserting (D.32) into equations (D.26) and (D.27), we obtain the approximate anomalous Green's functions

$$\begin{aligned}\mathcal{F}(\mathbf{k},\mathbf{k}-\mathbf{q},\omega_n) &= \mathcal{G}_0(\mathbf{k},\omega_n)\Delta(\mathbf{k},\mathbf{q})\mathcal{G}(-\mathbf{k}+\mathbf{q},-\mathbf{k}+\mathbf{q},-\omega_n)\\ &= \frac{\Delta(\mathbf{k},\mathbf{q})}{i\omega_n-\varepsilon_{\mathbf{k}}}\left[-i\omega_n-\varepsilon_{-\mathbf{k}+\mathbf{q}}+\sum_{\mathbf{q}'}\frac{\Delta(-\mathbf{k}+\mathbf{q},\mathbf{q}')\Delta^*(-\mathbf{k}+\mathbf{q}-\mathbf{q}',\mathbf{q}')}{i\omega_n-\varepsilon_{\mathbf{k}-\mathbf{q}+\mathbf{q}'}}\right]^{-1},\end{aligned} \tag{D.33}$$

$$\begin{aligned}\mathcal{F}^*(\mathbf{k}-\mathbf{q},\mathbf{k},\omega_n) &= -\mathcal{G}_0(-\mathbf{k}+\mathbf{q},-\omega_n)\Delta^*(\mathbf{k}-\mathbf{q},\mathbf{q})\mathcal{G}(\mathbf{k},\mathbf{k},\omega_n)\\ &= \frac{\Delta^*(\mathbf{k}-\mathbf{q},\mathbf{q})}{-i\omega_n-\varepsilon_{-\mathbf{k}+\mathbf{q}}}\left[i\omega_n-\varepsilon_{\mathbf{k}}+\sum_{\mathbf{q}'}\frac{\Delta(\mathbf{k},\mathbf{q}')\Delta^*(\mathbf{k}-\mathbf{q}',\mathbf{q}')}{-i\omega_n-\varepsilon_{-\mathbf{k}+\mathbf{q}'}}\right]^{-1}.\end{aligned} \tag{D.34}$$

Inserting equations (D.33) and (D.34) into equations (D.24) and (D.25) yields the self-consistency equations for $\Delta(\mathbf{k},\mathbf{q})$ and $\Delta^*(\mathbf{k},\mathbf{q})$:

$$\begin{aligned}\Delta(\mathbf{k},\mathbf{q}) &= -\sum_{\mathbf{k}'}V(\mathbf{k},\mathbf{k}',\mathbf{q})\Delta(\mathbf{k}',\mathbf{q})\\ &\quad\times T\sum_n\frac{1}{i\omega_n-\varepsilon_{\mathbf{k}'}}\left[-i\omega_n-\varepsilon_{-\mathbf{k}'+\mathbf{q}}+\sum_{\mathbf{q}'}\frac{\Delta(-\mathbf{k}'+\mathbf{q},\mathbf{q}')\Delta^*(-\mathbf{k}'+\mathbf{q}-\mathbf{q}',\mathbf{q}')}{i\omega_n-\varepsilon_{\mathbf{k}'+\mathbf{q}'-\mathbf{q}}}\right]^{-1},\end{aligned} \tag{D.35}$$

$$\Delta^*(\mathbf{k},\mathbf{q}) = -T\sum_n\sum_{\mathbf{k}'}V(\mathbf{k},-\mathbf{k}'+\mathbf{q},\mathbf{q})F^*(-\mathbf{k}',-\mathbf{k}'+\mathbf{q},-\omega_n) \tag{D.36}$$

$$\begin{aligned}&= -\sum_{\mathbf{k}'}V(\mathbf{k},-\mathbf{k}'+\mathbf{q},\mathbf{q})\Delta^*(\mathbf{k}',\mathbf{q})\\ &\quad\times T\sum_n\frac{1}{i\omega_n-\varepsilon_{\mathbf{k}'}}\left[-i\omega_n-\varepsilon_{-\mathbf{k}'+\mathbf{q}}+\sum_{\mathbf{q}'}\frac{\Delta(-\mathbf{k}'+\mathbf{q},\mathbf{q}')\Delta^*(-\mathbf{k}'+\mathbf{q}-\mathbf{q}',\mathbf{q}')}{i\omega_n-\varepsilon_{\mathbf{k}'+\mathbf{q}'-\mathbf{q}}}\right]^{-1},\end{aligned} \tag{D.37}$$

where we replaced $\mathbf{k}\to-\mathbf{k}+\mathbf{q}$ and $\omega_n\to-\omega_n$ in (D.41) for $\Delta^*(\mathbf{k},\mathbf{q})$. With the pairing interaction $V(\mathbf{k},\mathbf{k}',\mathbf{q})$ defined above, the equations for $\Delta(\mathbf{k},\mathbf{q})$ and $\Delta^*(\mathbf{k},\mathbf{q})$ become identical, which leads to the simplified self-consistency equation

$$\frac{1}{V_1} = -\sum_{\mathbf{k}}g_{s,d}^2(\mathbf{k}-\mathbf{q}/2)T\sum_n\frac{1}{i\omega_n-\varepsilon_{\mathbf{k}}}\left[-i\omega_n-\varepsilon_{-\mathbf{k}+\mathbf{q}}+\sum_{\mathbf{q}'}\frac{\Delta^2(-\mathbf{k}+\mathbf{q},\mathbf{q}')}{i\omega_n-\varepsilon_{\mathbf{k}+\mathbf{q}'-\mathbf{q}}}\right]^{-1}. \tag{D.38}$$

Analytic summation over ω_n:

To find explicit solutions of the Gor'kov equations we choose an ansatz for a self consistent solution consisting of Q trial pair momenta $\mathbf{q}_1, \ldots, \mathbf{q}_Q$ and set $\Delta(\mathbf{k}, \mathbf{q}) = 0$ for all other values of $\mathbf{q} \neq \mathbf{q}_i$. Thereby we test selected combinations of $\mathbf{q}$-vectors for self consistent solutions. The Green's function can then be rearranged as

$$\mathcal{G}(\mathbf{k},\mathbf{k},\omega_n) = \frac{\prod_i (-i\omega_n - \varepsilon_{-\mathbf{k}+\mathbf{q}_i})}{(i\omega_n - \varepsilon_{\mathbf{k}}) \prod_i (-i\omega_n - \varepsilon_{-\mathbf{k}+\mathbf{q}_i}) + \sum_i \Delta(\mathbf{k}, \mathbf{q}_i) \Delta^*(\mathbf{k} - \mathbf{q}_i, \mathbf{q}_i) \prod_{j \neq i} (-i\omega_n - \varepsilon_{-\mathbf{k}+\mathbf{q}_j})}, \tag{D.39}$$

where the products and sums over i and j run from 1 to Q. The denominator of $G(\mathbf{k}, \mathbf{k}, \omega_n)$ is a polynomial in ω_n of degree $Q + 1$, whose zeros $E_\alpha(\mathbf{k})$, $\alpha = 0, \ldots, Q$, constitute the energy spectrum of the system. If $Q \leq 3$, one can obtain algebraic expressions for $E_\alpha(\mathbf{k})$, which are given in appendix D.2.4 for $Q = 2$. One obtains the momentum occupation probability function $n(\mathbf{k})$ by summing over ω_n, which leads to

$$n(\mathbf{k}) = 2T \sum_n \mathcal{G}(\mathbf{k}, \mathbf{k}, \omega_n) = 2 \sum_\alpha u_\alpha^2(\mathbf{k}) f(E_\alpha(\mathbf{k})) \tag{D.40}$$

where

$$u_\alpha^2(\mathbf{k}) = \frac{\prod_i [E_\alpha(\mathbf{k}) - \varepsilon_{-\mathbf{k}+\mathbf{q}_i}]}{\prod_{\beta \neq \alpha} [E_\alpha(\mathbf{k}) - E_\beta(\mathbf{k})]}. \tag{D.41}$$

and the products and sums over α and β run from 0 to Q. The factor 2 in Eq. (D.40) comes from the sum over spin up and down. Analogously one finds the anomalous distribution

$$\tilde{n}(\mathbf{k}, \mathbf{q}_i) = T \sum_n \mathcal{F}(\mathbf{k}, \mathbf{k} - \mathbf{q}_i, \omega_n) = \Delta(\mathbf{k}, \mathbf{q}_i) \sum_\alpha w_\alpha^2(\mathbf{k}, \mathbf{q}_i) f(E_\alpha(-\mathbf{k} + \mathbf{q}_i)) \tag{D.42}$$

with

$$w_\alpha^2(\mathbf{k}, \mathbf{q}_i) = -\frac{\prod_{j \neq i} [E_\alpha(-\mathbf{k} + \mathbf{q}_i) + \varepsilon_{-\mathbf{k}+\mathbf{q}_i-\mathbf{q}_j}]}{\prod_{\beta \neq \alpha} [E_\alpha(-\mathbf{k} + \mathbf{q}_i) - E_\beta(-\mathbf{k} + \mathbf{q}_i)]}. \tag{D.43}$$

The conventional BCS solution is realized for $Q = 1$ with just two quasiparticle bands and $\mathbf{q} = \mathbf{0}$. Generally, one obtains a set of $2Q$ coupled self-consistency equations for $\Delta_s(\mathbf{q}_i)$ and $\Delta_d(\mathbf{q}_i)$:

$$\frac{\Delta_{s,d}(\mathbf{q}_i)}{V_1} = -\frac{T}{N} \sum_{\mathbf{k}'} g_{s,d}(\mathbf{k}' - \mathbf{q}_i/2) \tilde{n}(\mathbf{k}, \mathbf{k} - \mathbf{q}_i), \tag{D.44}$$

or for the conventional s-wave order parameter

$$\frac{\Delta(\mathbf{q}_i)}{V_0} = -\frac{T}{N}\sum_{\mathbf{k}'}\tilde{n}(\mathbf{k},\mathbf{k}-\mathbf{q}_i). \tag{D.45}$$

D.2.3 Solution with Two Finite Order Parameters

The content of this appendix is of course fully contained in the general formulation above. It is meant as a collection of formulae and examples useful for calculations involving the most common PDW state with $Q = 2$ and the pair momenta $\mathbf{q}_1$ and $\mathbf{q}_2$. The Green's function (D.39) then becomes

$$\begin{aligned}\mathcal{G}(\mathbf{k},\mathbf{k},\omega_n) = \frac{(-i\omega_n-\varepsilon_{-\mathbf{k}+\mathbf{q}_1})(-i\omega_n-\varepsilon_{-\mathbf{k}+\mathbf{q}_2})}{\big[(i\omega_n-\varepsilon_{\mathbf{k}})(-i\omega_n-\varepsilon_{-\mathbf{k}+\mathbf{q}_1})(-i\omega_n-\varepsilon_{-\mathbf{k}+\mathbf{q}_2})\\ +\Delta^2(\mathbf{k},\mathbf{q}_1)(-i\omega_n-\varepsilon_{-\mathbf{k}+\mathbf{q}_2})+\Delta^2(\mathbf{k},\mathbf{q}_2)(-i\omega_n-\varepsilon_{-\mathbf{k}+\mathbf{q}_1})\big]}\end{aligned} \tag{D.46}$$

$$= \frac{(-i\omega_n-\varepsilon_{-\mathbf{k}+\mathbf{q}_1})(-i\omega_n-\varepsilon_{-\mathbf{k}+\mathbf{q}_2})}{[i\omega_n-E_1(\mathbf{k},\mathbf{q}_1,\mathbf{q}_2)][i\omega_n-E_2(\mathbf{k},\mathbf{q}_1,\mathbf{q}_2)][i\omega_n-E_3(\mathbf{k},\mathbf{q}_1,\mathbf{q}_2)]}, \tag{D.47}$$

where $E_\alpha(\mathbf{k},\mathbf{q}_1,\mathbf{q}_2)$ are the zeros of the denominator in equation (D.46), given in appendix D.2.4. In the following, we will use the abbreviation $E_\alpha(\mathbf{k}) \equiv E_\alpha(\mathbf{k},\mathbf{q}_1,\mathbf{q}_2)$. Summing over ω_n, we find

$$\begin{aligned}n(\mathbf{k}) &= T\sum_n \mathcal{G}(\mathbf{k},\mathbf{k}',\omega_n)\\ &= u_1^2(\mathbf{k},\mathbf{q}_1,\mathbf{q}_2)f(E_1(\mathbf{k})) + u_2^2(\mathbf{k},\mathbf{q}_1,\mathbf{q}_2)f(E_2(\mathbf{k})) + u_3^2(\mathbf{k},\mathbf{q}_1,\mathbf{q}_2)f(E_3(\mathbf{k})).\end{aligned} \tag{D.48}$$

where

$$u_\alpha^2(\mathbf{k},\mathbf{q}_1,\mathbf{q}_2) = \frac{[E_\alpha(\mathbf{k})+\varepsilon_{-\mathbf{k}+\mathbf{q}_1}][E_\alpha(\mathbf{k})+\varepsilon_{-\mathbf{k}+\mathbf{q}_2}]}{\prod_{\beta\neq\alpha}[E_\alpha(\mathbf{k})-E_\beta(\mathbf{k})]}, \tag{D.49}$$

From equation (D.47), the anomalous Green's function is found to be

$$\mathcal{F}(\mathbf{k},\mathbf{k}-\mathbf{q}_1,\omega_n) = \frac{\Delta(\mathbf{k},\mathbf{q}_1)(i\omega_n-\varepsilon_{\mathbf{k}-\mathbf{q}_1+\mathbf{q}_2})}{[-i\omega_n-E_1(-\mathbf{k}+\mathbf{q}_1)][-i\omega_n-E_2(-\mathbf{k}+\mathbf{q}_1)][-i\omega_n-E_3(-\mathbf{k}+\mathbf{q}_1)]}, \tag{D.50}$$

$$\mathcal{F}(\mathbf{k},\mathbf{k}-\mathbf{q}_2,\omega_n) = \frac{\Delta(\mathbf{k},\mathbf{q}_2)(i\omega_n-\varepsilon_{\mathbf{k}-\mathbf{q}_2+\mathbf{q}_1})}{[-i\omega_n-E_1(-\mathbf{k}+\mathbf{q}_2)][-i\omega_n-E_2(-\mathbf{k}+\mathbf{q}_2)][-i\omega_n-E_3(-\mathbf{k}+\mathbf{q}_2)]}. \tag{D.51}$$

Summation over ω_n leads to

$$\tilde{n}(\mathbf{k},\mathbf{q}_1) = \Delta(\mathbf{k},\mathbf{q}_1)\Big[w_1^2(\mathbf{k},\mathbf{q}_1,\mathbf{q}_2)f(E_1(-\mathbf{k}+\mathbf{q}_1)) + w_2^2(\mathbf{k},\mathbf{q}_1,\mathbf{q}_2)f(E_2(-\mathbf{k}+\mathbf{q}_1)) + w_3^2(\mathbf{k},\mathbf{q}_1,\mathbf{q}_2)f(E_3(-\mathbf{k}+\mathbf{q}_1))\Big], \quad \text{(D.52)}$$

$$\tilde{n}(\mathbf{k},\mathbf{q}_2) = \Delta(\mathbf{k},\mathbf{q}_2)\Big[w_1^2(\mathbf{k},\mathbf{q}_2,\mathbf{q}_1)f(E_1(-\mathbf{k}+\mathbf{q}_2)) + w_2^2(\mathbf{k},\mathbf{q}_2,\mathbf{q}_1)f(E_2(-\mathbf{k}+\mathbf{q}_2)) + w_3^2(\mathbf{k},\mathbf{q}_2,\mathbf{q}_1)f(E_3(-\mathbf{k}+\mathbf{q}_2))\Big] \quad \text{(D.53)}$$

where

$$w_\alpha^2(\mathbf{k},\mathbf{q}_1,\mathbf{q}_2) = -\frac{E_\alpha(-\mathbf{k}+\mathbf{q}_1)+\varepsilon_{-\mathbf{k}+\mathbf{q}_1-\mathbf{q}_2}}{\prod_{\beta\neq\alpha}[E_\alpha(-\mathbf{k}+\mathbf{q}_1)-E_\beta(-\mathbf{k}+\mathbf{q}_1)]}. \quad \text{(D.54)}$$

D.2.4 The Zeros of the Green's Function in the Two-q State

The denominator of the Green's function $G(\mathbf{k},\omega_n)$ in the state with finite order parameters $\Delta(\mathbf{k},\mathbf{q}_1)$ and $\Delta(\mathbf{k},\mathbf{q}_2)$ is given by the polynomial

$$P(z) = (z-\varepsilon_0)(-z-\varepsilon_1)(-z-\varepsilon_2) + \Delta_1^2(-z-\varepsilon_2) + \Delta_2^2(-z-\varepsilon_1), \quad \text{(D.55)}$$

where

$$z = i\omega_n, \qquad \varepsilon_0 = \varepsilon_{\mathbf{k}}, \qquad \varepsilon_{1,2} = \varepsilon_{-\mathbf{k}+\mathbf{q}_{1,2}}, \qquad \Delta_{1,2} = \Delta(\mathbf{k},\mathbf{q}_{1,2})\Delta^*(\mathbf{k}-\mathbf{q}_{1,2},\mathbf{q}_{1,2}).$$

$P(z)$ has the three real zeros

$$E_1 = \frac{1}{12}\left[a + 2\frac{b}{c} + 2c\right], \quad \text{(D.56)}$$

$$E_2 = \frac{1}{12}\left[a - \left(1+i\sqrt{3}\right)\frac{b}{c} - \left(1-i\sqrt{3}\right)2^{2/3}c\right], \quad \text{(D.57)}$$

$$E_3 = \frac{1}{12}\left[a - \left(1-i\sqrt{3}\right)\frac{b}{c} - \left(1+i\sqrt{3}\right)2^{2/3}c\right], \quad \text{(D.58)}$$

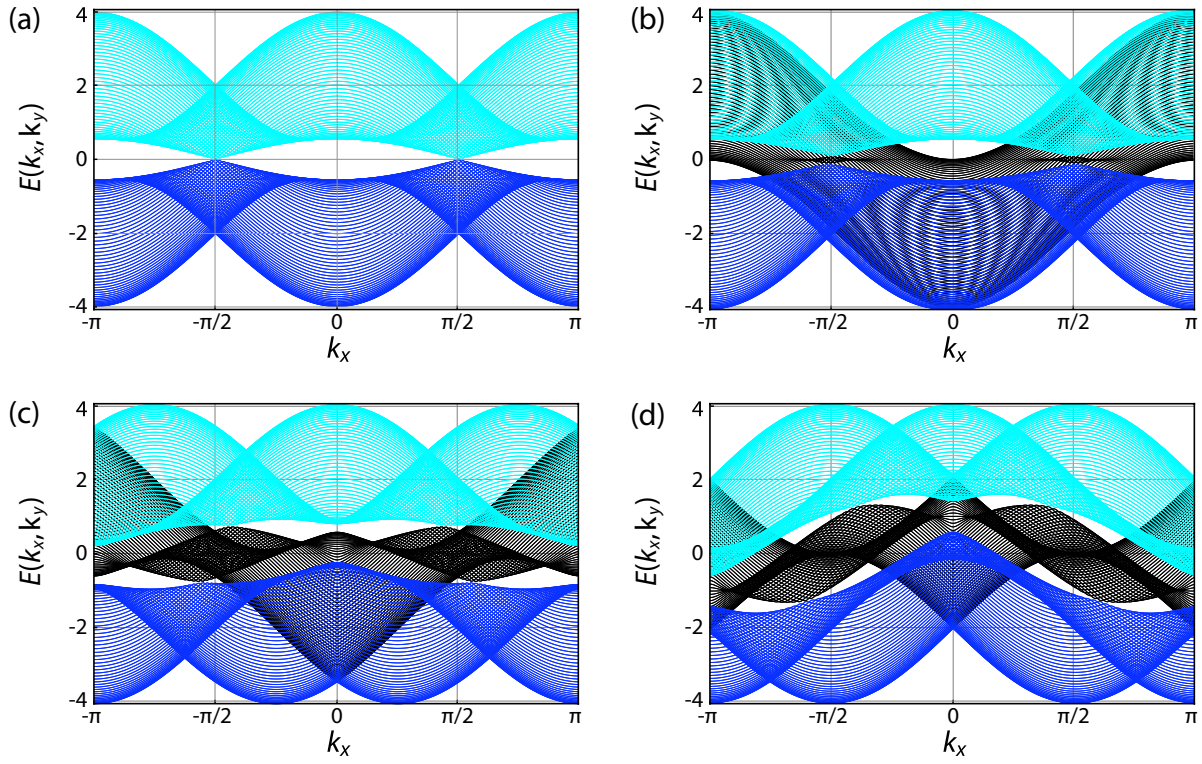

Figure D.1: (a) Upper (turquoise) and lower (blue) energy band in a *d*-wave superconductors with $Q = 1$ and pair momentum $q = 0$ for a particle-hole symmetric system with $\mu = 0$ and $t' = 0$ and fixed order parameter $\Delta_d = 0.2t$. The energy spectrum of the same system in the PDW state is shown in (b) for $q = \pi/20$, in (c) for $q = \pi/4$ and in (d) for $q = \pi/2$ with (blue) $E_0(\mathbf{k})$, (black) $E_1(\mathbf{k})$ and (turquoise) $E_2(\mathbf{k})$.

where

$$a = 4(\varepsilon_0 - \varepsilon_1 - \varepsilon_2) \tag{D.59}$$

$$b = 2^{4/3}\left[\varepsilon_0^2 + \varepsilon_1^2 + \varepsilon_3^2 + \varepsilon_0\varepsilon_1 + \varepsilon_0\varepsilon_2 - \varepsilon_1\varepsilon_2 + 3\left(\Delta_1^2 + \Delta_2^2\right)\right] \tag{D.60}$$

$$\begin{aligned} c = \Bigg\{ & 2\left(\varepsilon_0^3 - \varepsilon_1^3 - \varepsilon_2^3\right) + 3\left(\varepsilon_0^2\varepsilon_1 + \varepsilon_0^2\varepsilon_2 - \varepsilon_0\varepsilon_1^2 - \varepsilon_0\varepsilon_2^2 + \varepsilon_1^2\varepsilon_2 + \varepsilon_1\varepsilon_2^2\right) + 12\varepsilon_0\varepsilon_1\varepsilon_2 \\ & + 9\varepsilon_0\left(\Delta_1^2 + \Delta_2^2\right) - 9\left(\varepsilon_1\Delta_1^2 + \varepsilon_2\Delta_2^2\right) + 18\left(\varepsilon_1\Delta_2^2 + \varepsilon_2\Delta_1^2\right) \\ & + \Bigg[-\frac{b^3}{4} + \Big[9\Delta_1^2(\varepsilon_0 - \varepsilon_1 + 2\varepsilon_2) \\ & + (\varepsilon_0 + 2\varepsilon_1 - \varepsilon_2)\left(9\Delta_2^2 + 2\varepsilon_0^2 - \varepsilon_0\varepsilon_1 - \varepsilon_1^2 + 5\varepsilon_0\varepsilon_2 + \varepsilon_1\varepsilon_2 + 2\varepsilon_2\right)\Big]^2\Bigg]^{1/2}\Bigg\}^{1/3}. \end{aligned} \tag{D.61}$$

The resulting energy spectrum is shown in figure D.1 for different pair momenta

$\mathbf{q}_1 = -\mathbf{q}_2 = (q, 0)$ for a particle-hole symmetric system with $\mu = 0$ and next-nearest neighbor hopping $t' = 0$ (compare to figure 10.1 in section 10.2), and a fixed order parameter $\Delta_d(\mathbf{q}_{1,2}) = 0.2t$. (a) shows the spectrum of a standard d-wave superconductor with $q = 0$ and bands $E_0(\mathbf{k})$ and $E_2(\mathbf{k})$ identical to the upper and lower bands obtained from conventional BCS theory with $Q = 1$, and the unoccupied band $E_1(\mathbf{k}) = \varepsilon_{\mathbf{k}}$ is not shown. (b) - (d) show the mixing if the bands around E_F for $q \neq 0$, which is most pronounced for $q = \pi/2$.

D.3 Bogoliubov Transformation Method

D.3.1 Hamiltonian

We start again with the generalized interaction Hamiltonian (D.13) which reduces to the BCS type mean field Hamiltonian

$$\mathcal{H} = \sum_{\mathbf{k},s} \varepsilon_{\mathbf{k}} c^\dagger_{\mathbf{k}s} c_{\mathbf{k}s} + \sum_{\mathbf{k}} \sum_{\mathbf{q}} \left[\Delta^*(\mathbf{k},\mathbf{q}) c_{-\mathbf{k}+\mathbf{q}\downarrow} c_{\mathbf{k}\uparrow} + \Delta(\mathbf{k},\mathbf{q}) c^\dagger_{\mathbf{k}\uparrow} c^\dagger_{-\mathbf{k}+\mathbf{q}\downarrow} \right] - \sum_{\mathbf{k}} \sum_{\mathbf{q}} V(\mathbf{k},\mathbf{k}',\mathbf{q}) \langle c^\dagger_{\mathbf{k}\uparrow} c^\dagger_{-\mathbf{k}+\mathbf{q}\downarrow} \rangle \langle c_{\mathbf{k}+\mathbf{q}\downarrow} c_{\mathbf{k}\uparrow} \rangle, \quad \text{(D.62)}$$

with the order parameters

$$\Delta(\mathbf{k},\mathbf{q}) = \sum_{\mathbf{k}'} V(\mathbf{k},\mathbf{k}',\mathbf{q}) \langle c_{-\mathbf{k}+\mathbf{q}\downarrow} c_{\mathbf{k}\uparrow} \rangle, \quad \text{(D.63)}$$

$$\Delta^*(\mathbf{k},\mathbf{q}) = \sum_{\mathbf{k}'} V(\mathbf{k},\mathbf{k}',\mathbf{q}) \langle c^\dagger_{\mathbf{k}\uparrow} c_{-\mathbf{k}+\mathbf{q}\downarrow} \rangle \quad \text{(D.64)}$$

and a pairing interaction as defined in appendix D.1. The constant terms on the second line of (D.62) is again irrelevant in the process of diagonalization. We proceed therefore with the Hamiltonian $\mathcal{H}'$ which does not include these terms.

Taking the same ansatz for Q trial pair momenta $\mathbf{q}_1, \ldots, \mathbf{q}_Q$ as in appendix D.2.2 and setting $\Delta_{s,d}(\mathbf{k},\mathbf{q}) = 0$ (or $\Delta(\mathbf{q}) = 0$, respectively) for all other values of $\mathbf{q}$, the Hamiltonian $\mathcal{H}'$ can be written in matrix form as

$$\mathcal{H}' = \frac{1}{Q+1} \sum_{\mathbf{k}} \mathbf{c}^\dagger(\mathbf{k}) H(\mathbf{k}) \, \mathbf{c}(\mathbf{k}), \quad \text{(D.65)}$$

where the vector $\mathbf{c}(\mathbf{k})$ is defined through

$$c_0(\mathbf{k}) = c_{\mathbf{k}\uparrow}, \quad \text{(D.66)}$$

$$c_i(\mathbf{k}) = c^\dagger_{-\mathbf{k}+\mathbf{q}_i\downarrow} \quad \text{for} \quad i = 1, \ldots, Q \quad \text{(D.67)}$$

and the matrix $H(\mathbf{k})$ is

$$H(\mathbf{k}) = \begin{pmatrix} \varepsilon_{\mathbf{k}} & \Delta_1(\mathbf{k}) & \cdots & \Delta_Q(\mathbf{k}) \\ \Delta_1^*(\mathbf{k}) & -\varepsilon_{-\mathbf{k}+\mathbf{q}_1} & \cdots & 0 \\ \vdots & \vdots & \ddots & \vdots \\ \Delta_Q^*(\mathbf{k}) & 0 & \cdots & -\varepsilon_{-\mathbf{k}+\mathbf{q}_Q} \end{pmatrix}. \tag{D.68}$$

Here, the order parameters are defined as $\Delta_i(\mathbf{k}) = (Q+1)\Delta(\mathbf{k}, \mathbf{q}_i)$ and $\Delta_i^*(\mathbf{k}) = (Q+1)\Delta^*(\mathbf{k}, \mathbf{q}_i)$.

Diagonalization of $H(\mathbf{k})$ using the unitary transformation matrix $U(\mathbf{k})$ leads to the diagonal Hamiltonian

$$\mathcal{H}' = \frac{1}{Q+1} \sum_{\mathbf{k}} \sum_{\alpha} E_\alpha(\mathbf{k}) a_\alpha^\dagger(\mathbf{k}) a_\alpha(\mathbf{k}), \tag{D.69}$$

where $\alpha \in \{0, \ldots, Q\}$ and the vector $\mathbf{a}(\mathbf{k})$ contains the fermionic operators obtained through the Bogoliubov transformation

$$\mathbf{a}(\mathbf{k}) = U^\dagger(\mathbf{k})\mathbf{c}(\mathbf{k}) \qquad \Longleftrightarrow \qquad \mathbf{c}(\mathbf{k}) = U(\mathbf{k})\mathbf{a}(\mathbf{k}). \tag{D.70}$$

D.3.2 Expectation Values

In general, the eigenvalues $E_\alpha(\mathbf{k})$ and the eigenvectors $\mathbf{u}_\alpha(\mathbf{k})$ of the matrix $H(\mathbf{k})$ can not be obtained analytically, but they can be calculated easily by numerical diagonalization of $H(\mathbf{k})$. Using the Bogoliubov trnasformation $U(\mathbf{k})$, it is straight forward to calculate all desired physical quantities. The products of the fermionic operators with finite expectation value seem to be the following the following:

$$\begin{aligned} \langle c_{\mathbf{k}\uparrow}^\dagger c_{\mathbf{k}\uparrow} \rangle = \langle c_0^\dagger(\mathbf{k}) c_0(\mathbf{k}) \rangle &= \frac{1}{Q+1} \sum_{\alpha\beta} u_{0\alpha}(\mathbf{k}) u_{0\beta}(\mathbf{k}) \langle a_\alpha^\dagger(\mathbf{k}) a_\beta(\mathbf{k}) \rangle \\ &= \frac{1}{Q+1} \sum_{\alpha} u_{0\alpha}^2(\mathbf{k}) f(E_\alpha(\mathbf{k})). \end{aligned} \tag{D.71}$$

In the same way we find

$$\langle c_{-\mathbf{k}+\mathbf{q}_i\downarrow}^\dagger c_{-\mathbf{k}+\mathbf{q}_i\downarrow} \rangle = \langle c_i(\mathbf{k}) c_i^\dagger(\mathbf{k}) \rangle = \frac{1}{Q+1} \sum_{\alpha} u_{i\alpha}^2(\mathbf{k}) f(-E_\alpha(\mathbf{k})), \tag{D.72}$$

$$\langle c_{-\mathbf{k}+\mathbf{q}_i\downarrow}^\dagger c_{-\mathbf{k}+\mathbf{q}_j\downarrow} \rangle = \langle c_i(\mathbf{k}) c_j^\dagger(\mathbf{k}) \rangle = \frac{1}{Q+1} \sum_{\alpha} u_{i\alpha} u_{j\alpha}(\mathbf{k}) f(-E_\alpha(\mathbf{k})) \tag{D.73}$$

and

$$\langle c_{-\mathbf{k}+\mathbf{q}_i\downarrow} c_{\mathbf{k}\uparrow}\rangle = \langle c_i^\dagger(\mathbf{k}) c_0(\mathbf{k})\rangle = \frac{1}{Q+1}\sum_\alpha u_{i\alpha}u_{0\alpha}(\mathbf{k}) f(E_\alpha(\mathbf{k})), \tag{D.74}$$

$$\langle c_{\mathbf{k}\uparrow}^\dagger c_{-\mathbf{k}+\mathbf{q}_j\downarrow}^\dagger\rangle = \langle c_0^\dagger(\mathbf{k}) c_i(\mathbf{k})\rangle = \frac{1}{Q+1}\sum_\alpha u_{0\alpha}u_{i\alpha}(\mathbf{k}) f(E_\alpha(\mathbf{k})) \tag{D.75}$$

for $i, j \in \{1, \ldots, Q\}$. The self-consisteny equation for the Q order parameters becomes

$$\Delta_i(\mathbf{k}) = \sum_{\mathbf{k}'} V(\mathbf{k}, \mathbf{k}', \mathbf{q}) \sum_\alpha u_{i\alpha}(\mathbf{k}') u_{0\alpha}(\mathbf{k}') f(E_\alpha(\mathbf{k}')). \tag{D.76}$$

We can identify $u_\alpha(\mathbf{k}) = u_{0\alpha}(\mathbf{k})$ and $w_\alpha^2(\mathbf{k}, \mathbf{q}_i) = u_{i\alpha}(\mathbf{k}) u_{0\alpha}(\mathbf{k})$, which shows that the above expectation values derived from the mean-field Hamiltonian (D.62) using a Bogoliubov transformation is indeed identical to the solutions of the approximated Gor'kov equations. Because the two formulations of the extended BCS theory must be mathematically identical, the existence of higher order terms in $\mathcal{G}(\mathbf{k}, \mathbf{k}', \mathbf{q})$ proves that there exist more combinations of the creation and annihilation operators which have finite expectation values. These occur because the quasi-particle operators $a_\alpha(\mathbf{k})$ and $a_\beta(\mathbf{k}')$ can create quasi-particles with identical spin and momentum even for $\mathbf{k} \neq \mathbf{k}'$, if $Q \geq 2$ and $\mathbf{q}_1 \neq \mathbf{q}_2$. How the detect such expectation values and how to calculate them remains unclear in this formulation, but they can be computed from the Gor'kov equations if necessary.

Charge Density and Density of States:
Because the Hamiltonian (D.65) can be formulated equivalently with inverted spins, the expectation values $\langle c_{\mathbf{k}\downarrow}^\dagger c_{\mathbf{k}\downarrow}\rangle$ and $\langle c_{\mathbf{k}\uparrow}^\dagger c_{\mathbf{k}\uparrow}\rangle$ have to be equal. The momentum distribution function is therefore given by

$$n(\mathbf{k}) = \sum_s \langle c_{\mathbf{k}s}^\dagger c_{\mathbf{k}s}\rangle = 2\sum_\alpha u_{0\alpha}^2(\mathbf{k}) f(E_\alpha(\mathbf{k})) \tag{D.77}$$

from which follows the charge density in real space

$$\begin{aligned}\rho(\mathbf{r}) &= \frac{1}{N}\sum_{\mathbf{k},\mathbf{k}',s} e^{i(\mathbf{k}-\mathbf{k}')\mathbf{r}} \langle c_{\mathbf{k}s}^\dagger c_{\mathbf{k}'s}\rangle \\ &= \frac{1}{N}\sum_{\mathbf{k}}\sum_\alpha \left[u_{0\alpha}^2(\mathbf{k}) f(E_\alpha(\mathbf{k})) + \sum_{i\neq j} e^{i(\mathbf{q}_i-\mathbf{q}_j)\mathbf{r}} u_{i\alpha}(\mathbf{k}) u_{j\alpha}(\mathbf{k}) f(-E_\alpha(\mathbf{k})) \right].\end{aligned} \tag{D.78}$$

The differential density of states becomes

$$D(E) = 2\sum_{\mathbf{k}}\sum_\alpha u_{0\alpha}^2(\mathbf{k}) f'(E - E_\alpha(\mathbf{k})). \tag{D.79}$$

Pair Density:
We define the density of paired electrons by

$$P^2(\mathbf{k},\mathbf{k}') = \langle c^\dagger_{\mathbf{k}} c_{\mathbf{k}} c^\dagger_{-\mathbf{k}'} c_{-\mathbf{k}'}\rangle - \langle c^\dagger_{\mathbf{k}} c_{\mathbf{k}}\rangle\langle c^\dagger_{-\mathbf{k}'} c_{-\mathbf{k}'}\rangle, \tag{D.80}$$

which is the difference of the probability that a Cooper pair with total momentum $\mathbf{k} - \mathbf{k}'$ is occupied and the probability that the free electron states $\mathbf{k}$ and $\mathbf{k}'$ are occupied, but not correlated. Using the mean-field decomposition

$$\langle c^\dagger_{\mathbf{k}} c_{\mathbf{k}} c^\dagger_{-\mathbf{k}'} c_{-\mathbf{k}'}\rangle \longrightarrow \langle c^\dagger_{\mathbf{k}} c_{\mathbf{k}}\rangle\langle c^\dagger_{-\mathbf{k}'} c_{-\mathbf{k}'}\rangle + \langle c^\dagger_{\mathbf{k}} c^\dagger_{-\mathbf{k}'}\rangle\langle c_{-\mathbf{k}'} c_{\mathbf{k}}\rangle, \tag{D.81}$$

we find

$$P^2(\mathbf{k},\mathbf{k}') = \langle c^\dagger_{\mathbf{k}} c^\dagger_{-\mathbf{k}'}\rangle\langle c_{-\mathbf{k}'} c_{\mathbf{k}}\rangle = \begin{cases} \langle c_{-\mathbf{k}+\mathbf{q}_i} c_{\mathbf{k}}\rangle\langle c^\dagger_{\mathbf{k}} c^\dagger_{-\mathbf{k}+\mathbf{q}_i}\rangle, & \mathbf{k}' = \mathbf{k} - \mathbf{q}_i \\ 0, & \text{otherwise} \end{cases}, \tag{D.82}$$

thus

$$P^2(\mathbf{k},\mathbf{k}-\mathbf{q}_i) = \left[\frac{1}{Q+1}\sum_\alpha u_{i\alpha}(\mathbf{k}) u_{0\alpha}(\mathbf{k}) f(E_\alpha(\mathbf{k}))\right]^2. \tag{D.83}$$

The total pair density in momentum space is obtained by summing $P^2(\mathbf{k},\mathbf{k}')$ over $\mathbf{k}'$:

$$P^2(\mathbf{k}) = \left[\sum_i P(\mathbf{k},\mathbf{k}-\mathbf{q}_i)\right]^2 = \left[\frac{1}{Q+1}\sum_i\sum_\alpha u_{i\alpha}(\mathbf{k}) u_{0\alpha}(\mathbf{k}) f(E_\alpha(\mathbf{k}))\right]^2. \tag{D.84}$$

Internal Energy and Supercurrent:
The inner energy E of the superconducting state is the thermal average $E = \langle\mathcal{H}\rangle$ of the Hamiltonian (D.62):

$$\begin{aligned} E = \langle\mathcal{H}\rangle &= \sum_{\mathbf{k}} \varepsilon_{\mathbf{k}} n(\mathbf{k}) - \sum_{\mathbf{k}}\sum_{\mathbf{q}} V(\mathbf{k},\mathbf{k}',\mathbf{q})\langle c^\dagger_{\mathbf{k}\uparrow} c^\dagger_{-\mathbf{k}+\mathbf{q}\downarrow}\rangle\langle c_{\mathbf{k}+\mathbf{q}\downarrow} c_{\mathbf{k}\uparrow}\rangle \\ &= \sum_{\mathbf{k}} \varepsilon_{\mathbf{k}} n(\mathbf{k}) - \sum_{\mathbf{k}}\sum_{\mathbf{q}}\left[\frac{\Delta_s^2(\mathbf{q}) + \Delta_d^2(\mathbf{q})}{V_1} + \frac{\Delta^2(\mathbf{q})}{V_0}\right]. \end{aligned} \tag{D.85}$$

The expression for the supercurrent $\mathbf{J}$ in two dimensions is the analogous to appendix A.2:

$$J = \frac{e}{\hbar}\sum_{\mathbf{k}} n(\mathbf{k}) \nabla_{\mathbf{k}} \varepsilon_{\mathbf{k}} \tag{D.86}$$

D.3.3 Charge Order Parameter

In the mean-field decoupling of the interaction Hamiltonian (D.13) we so far included only the BCS type pairing order parameters. For a charge ordered system, as the finite momentum pairing state with $Q = 2$, there are more possibilities for finite mean-field terms, corresponding to charge order. These terms are

$$\mathcal{H}_{\mathrm{C}} = \sum_{\mathbf{k},\mathbf{k}'} \sum_{\mathbf{q}} V(\mathbf{k},\mathbf{k}',\mathbf{q}) \left[c^{\dagger}_{\mathbf{k}\uparrow} c_{\mathbf{k}'\uparrow} \langle c^{\dagger}_{-\mathbf{k}+\mathbf{q}\downarrow} c_{-\mathbf{k}'+\mathbf{q}\downarrow} \rangle + c^{\dagger}_{-\mathbf{k}+\mathbf{q}\downarrow} c_{-\mathbf{k}'+\mathbf{q}\downarrow} \langle c^{\dagger}_{\mathbf{k}\uparrow} c_{\mathbf{k}'\uparrow} \rangle \right]. \tag{D.87}$$

The expectation values $\langle c^{\dagger}_{\mathbf{k}\uparrow} c_{\mathbf{k}'\uparrow} \rangle$ and $\langle c^{\dagger}_{-\mathbf{k}+\mathbf{q}} c_{-\mathbf{k}'+\mathbf{q}} \rangle$ are finite only if $\mathbf{k}' = \mathbf{k}$, or is $\mathbf{k}' = \mathbf{k} + \mathbf{q} - \mathbf{q}'$ and both $\Delta(\mathbf{k},\mathbf{q})$ and $\Delta(\mathbf{k},\mathbf{q}')$ are finite. Because of the symmetry in the spins both terms in (D.87) contribute equally to the charge density, thus $\mathcal{H}_{\mathrm{C}}$ becomes

$$\mathcal{H}_{\mathrm{C}} = \sum_{\mathbf{k},\mathbf{k}'} \sum_{\mathbf{q}} V(\mathbf{k},\mathbf{k}',\mathbf{q}) c^{\dagger}_{\mathbf{k}\uparrow} c_{\mathbf{k}'\uparrow} \langle c^{\dagger}_{-\mathbf{k}+\mathbf{q}\downarrow} c_{-\mathbf{k}'+\mathbf{q}\downarrow} \rangle \tag{D.88}$$

$$= \sum_{\mathbf{k}} \sum_{\mathbf{q}} \left[V(\mathbf{k},\mathbf{k},\mathbf{q}) + V(\mathbf{k},-\mathbf{k}+\mathbf{q},\mathbf{q}) \right] c^{\dagger}_{\mathbf{k}\uparrow} c_{\mathbf{k}\uparrow} \langle c^{\dagger}_{-\mathbf{k}+\mathbf{q}\downarrow} c_{-\mathbf{k}+\mathbf{q}\downarrow} \rangle \tag{D.89}$$

The first line of (D.89) contains terms diagonal in momentum space. These do nothing more that renormalize the chemical potential μ and are not relevant for charge order; we therefore neglect them. Thus the charge order Hamiltonian can finally be written as

$$\mathcal{H}_{\mathrm{C}} = \sum_{\mathbf{k}} \sum_{i \neq j} \eta_{ij}(-\mathbf{k}+\mathbf{q}_i) c^{\dagger}_{\mathbf{k}} c_{\mathbf{k}+\mathbf{q}_i-\mathbf{q}_j} = \sum_{\mathbf{k}} \sum_{i \neq j} \eta_{ij}(\mathbf{k}) c^{\dagger}_{-\mathbf{k}+\mathbf{q}_i} c_{-\mathbf{k}+\mathbf{q}_j} \tag{D.90}$$

with the charge order parameter

$$\eta_{ij}(\mathbf{k}) = \left[V(-\mathbf{k}+\mathbf{q}_i,\mathbf{k},\mathbf{q}_i) + V(-\mathbf{k}+\mathbf{q}_i,\mathbf{k}-\mathbf{q}_j,\mathbf{q}_i) \right] \langle c^{\dagger}_{-\mathbf{k}+\mathbf{q}_i} c_{-\mathbf{k}+\mathbf{q}_j} \rangle \tag{D.91}$$

$$= \left[V(-\mathbf{k}+\mathbf{q}_i,\mathbf{k},\mathbf{q}_i) + V(-\mathbf{k}+\mathbf{q}_i,\mathbf{k}-\mathbf{q}_j,\mathbf{q}_i) \right] \sum_{\alpha} u_{i\alpha}(\mathbf{k}) u_{j\alpha}(\mathbf{k}) f(-E_{\alpha}(\mathbf{k})). \tag{D.92}$$

The order parameters $\eta_{ij}(\mathbf{k})$ have to be solved self consistently for all $\mathbf{k}$, whereat they enter into the matrix $H(\mathbf{k})$ at the positions where the form (D.68) has zeros. We give here as an example the 3×3 matrix for $Q = 2$:

$$H(\mathbf{k}) = \begin{pmatrix} \varepsilon_{\mathbf{k}} & \Delta_1(\mathbf{k}) & \Delta_2(\mathbf{k}) \\ \Delta_1^*(\mathbf{k}) & -\varepsilon_{-\mathbf{k}+\mathbf{q}_1} & \eta_{12}(-\mathbf{k}+\mathbf{q}_1) \\ \Delta_2^*(\mathbf{k}) & \eta_{21}(-\mathbf{k}+\mathbf{q}_2) & -\varepsilon_{-\mathbf{k}+\mathbf{q}_2} \end{pmatrix}. \tag{D.93}$$

D.4 Real Space: Extended Bogoliubov de Gennes Equations

The pairing Hamiltonian (D.13) with nearest-neighbor interaction is the Fourier transform the real space pairing Hamiltonian

$$\mathcal{H}' = \sum_{\langle i,j\rangle,s} t_{ij} c_{is}^\dagger c_{js} + V_1 \sum_{\langle i,j\rangle} \sum_{s,s'} c_{is}^\dagger c_{js'}^\dagger c_{js'} c_{is}. \tag{D.94}$$

Using the usual BCS mean-field decoupling for the spin singlet interaction terms gives the real space BCS Hamiltonian

$$\mathcal{H}' = \sum_{\langle i,j\rangle,s} t_{ij} c_{is}^\dagger c_{js} + \sum_{\langle i,j\rangle} \left[\Delta_{ij} c_{i\uparrow}^\dagger c_{j\downarrow}^\dagger + \Delta_{ij}^* c_{j\downarrow} c_{i\uparrow} \right]. \tag{D.95}$$

with the bond order parameter $\Delta_{ij} = V_1 \langle c_{j\downarrow} c_{i\uparrow} \rangle$. Equation (D.31) can be written in the usual matrix form

$$\mathcal{H} = (\mathbf{c}_\uparrow^\dagger, \mathbf{c}_\downarrow) \begin{pmatrix} \hat{t} & \hat{\Delta} \\ \hat{\Delta}^* & -\hat{t}^* \end{pmatrix} \begin{pmatrix} \mathbf{c}_\uparrow \\ \mathbf{c}_\downarrow^\dagger \end{pmatrix}, \tag{D.96}$$

as defined in appendix C.3.1. This 2×2 matrix structure is however not unique. We can expand it to a $(Q+1) \times (Q+1)$ matrix structure analogous to the momentum space formulation of equation (D.68):

$$\mathcal{H} = (\mathbf{c}_0^\dagger, \mathbf{c}_1^\dagger, \ldots, \mathbf{c}_Q^\dagger) \begin{pmatrix} \frac{2}{Q+1}\hat{t} & \hat{\Delta}_1 & \cdots & \hat{\Delta}_Q \\ \hat{\Delta}_1^* & -\frac{2}{Q+1}\hat{t}^* & \cdots & 0 \\ \vdots & \vdots & \ddots & \vdots \\ \hat{\Delta}_Q^* & 0 & \cdots & -\frac{2}{Q+1}\hat{t}^* \end{pmatrix} \begin{pmatrix} \mathbf{c}_0 \\ \mathbf{c}_1 \\ \vdots \\ \mathbf{c}_Q \end{pmatrix} \tag{D.97}$$

with arbitrary matrices $\hat{\Delta}_l$ fulfilling the condition $\sum_l \hat{\Delta}_l = \hat{\Delta}$, and $\mathbf{c}_{0i} = c_{i\uparrow}$ and $\mathbf{c}_{li} = c_{i\downarrow}^\dagger$ for $l = 1, \ldots, Q$. This ansatz leads to an extended version of the Bogoliubov - de Gennes equations with a Bogoliubov transformation of the form

$$c_{i\uparrow} = \sum_n \sum_\alpha u_{0\alpha ni} a_{\alpha ni}, \tag{D.98}$$

$$c_{i\downarrow} = \sum_n \sum_\alpha u_{l\alpha ni}^* a_{\alpha ni}^\dagger \tag{D.99}$$

for any $l \in \{1, \ldots, Q\}$ and $\alpha \in \{0, \ldots, Q\}$. The coefficients $u_{\beta\alpha ni}$ are given by the eigenvalue equation

$$\begin{pmatrix} \frac{2}{Q+1}\hat{t} & \hat{\Delta}_1 & \cdots & \hat{\Delta}_Q \\ \hat{\Delta}_1^* & -\frac{2}{Q+1}\hat{t}^* & \cdots & 0 \\ \vdots & \vdots & \ddots & \vdots \\ \hat{\Delta}_Q^* & 0 & \cdots & -\frac{2}{Q+1}\hat{t}^* \end{pmatrix} \begin{pmatrix} \mathbf{u}_{0\alpha n} \\ \mathbf{u}_{1\alpha n} \\ \vdots \\ \mathbf{u}_{Q\alpha n} \end{pmatrix} = E_{\alpha n} \begin{pmatrix} \mathbf{u}_{0\alpha n} \\ \mathbf{u}_{1\alpha n} \\ \vdots \\ \mathbf{u}_{Q\alpha n} \end{pmatrix} \tag{D.100}$$

With the transformations (D.98) and (D.99) we obtain the self-consistency equation

$$\Delta_{l,ij} = V_1 \langle c^\dagger_{lj} c_{0i} \rangle = V_1 \sum_n \sum_\alpha u_{l\alpha ni} u^*_{0\alpha nj} f(E_{\alpha n}) \tag{D.101}$$

for the elements of $\hat{\Delta}_l$. We further obtain the spin or charge densities

$$n_{i\uparrow} = \langle c^\dagger_{i\uparrow} c_{i\uparrow} \rangle = \langle c^\dagger_{0i} c_{0i} \rangle = \sum_n \sum_\alpha |u_{0\alpha ni}|^2 f(E_{\alpha n}), \tag{D.102}$$

$$n_{i\downarrow} = \langle c^\dagger_{i\downarrow} c_{i\downarrow} \rangle = \langle c^\dagger_{li} c_{li} \rangle = \sum_n \sum_\alpha |u_{l\alpha ni}|^2 f(E_{\alpha n}). \tag{D.103}$$

To describe the finite momentum pairing solution found in section 11, we solve the Bogoliubov - de Gennes equation on a $N \times M$ lattice with periodic boundary conditions for $Q = 2$. We start the self-consistency loop with initial order parameters of the form

$$\Delta_{1,ij} = \Delta_{ij} e^{2\pi i q (x_i + x_j)/2N} \tag{D.104}$$

$$\Delta_{2,ij} = \Delta_{ij} e^{-2\pi i q (x_i + x_j)/2N} \tag{D.105}$$

with constant order parameters Δ_{ij} with d-wave symmetry and phase gradients in x-direction such that the phase shift over the whole system is a multiple of 2π, corresponding to a pair momentum q. Then let's hope that the system indeed converges into a superconducting state with order parameters with phase gradients as chosen above...

E Solutions of the Laplace Equation in a Square Frame

Here follows a selection of the most esthetic eigenfunctions of the free Schrödinger equation (Laplace equation) for a particle confined in a square frame geometry. Shown is the probability density (absolute square of the wave functions) in different multi-valued color codes designed to reproduce most clearly the special structures to the eigenfunctions.

Page 157 & 160: Solutions in a 208 × 208 frame with a centered 72 × 72 square with enhanced chemical potential (which reduces the probability density) and a 6× square hole at the center.

Page 158 & 159: Solutions in a 204 × 204 frame with a 32 × 32 hole in the center.

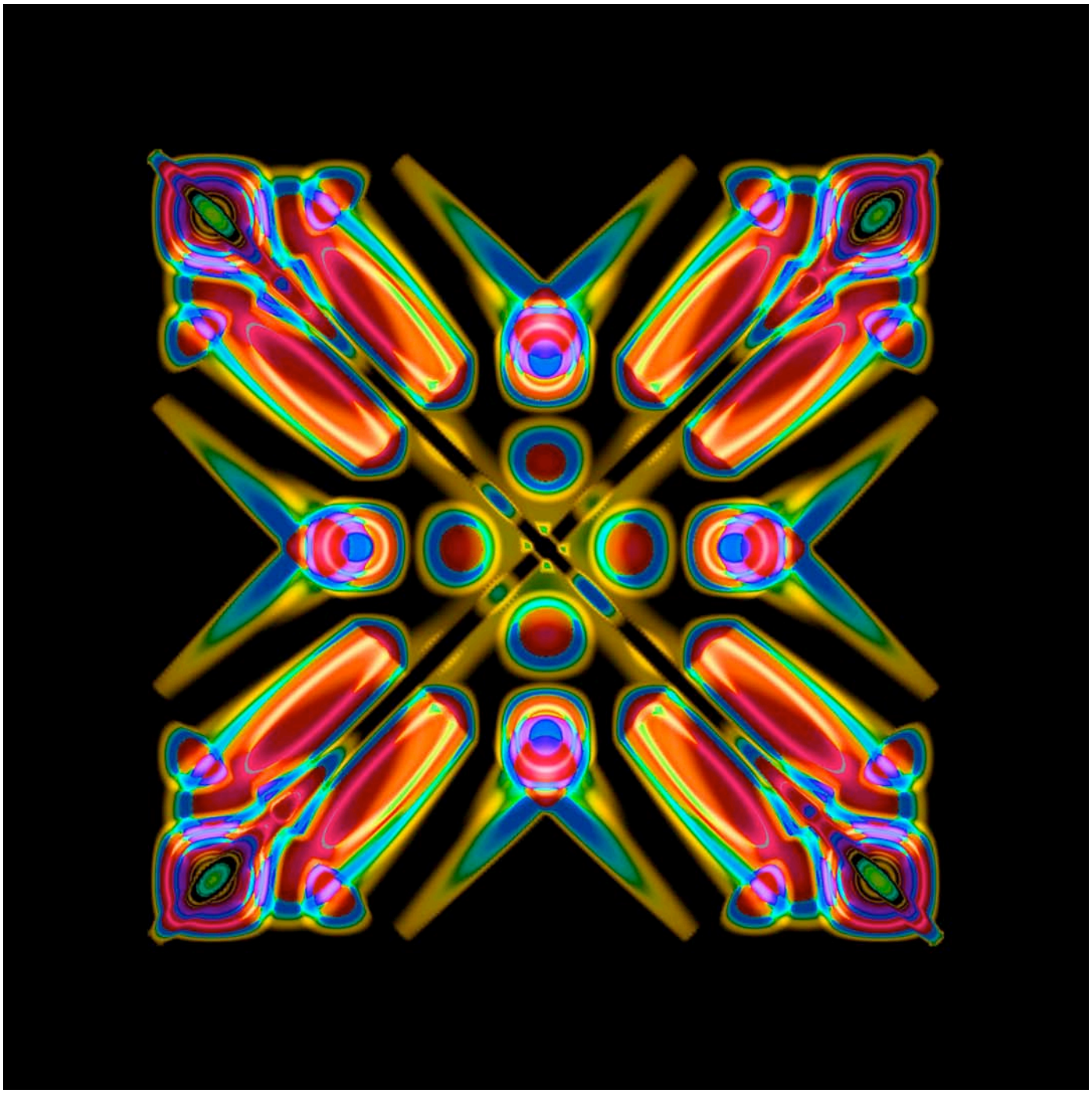

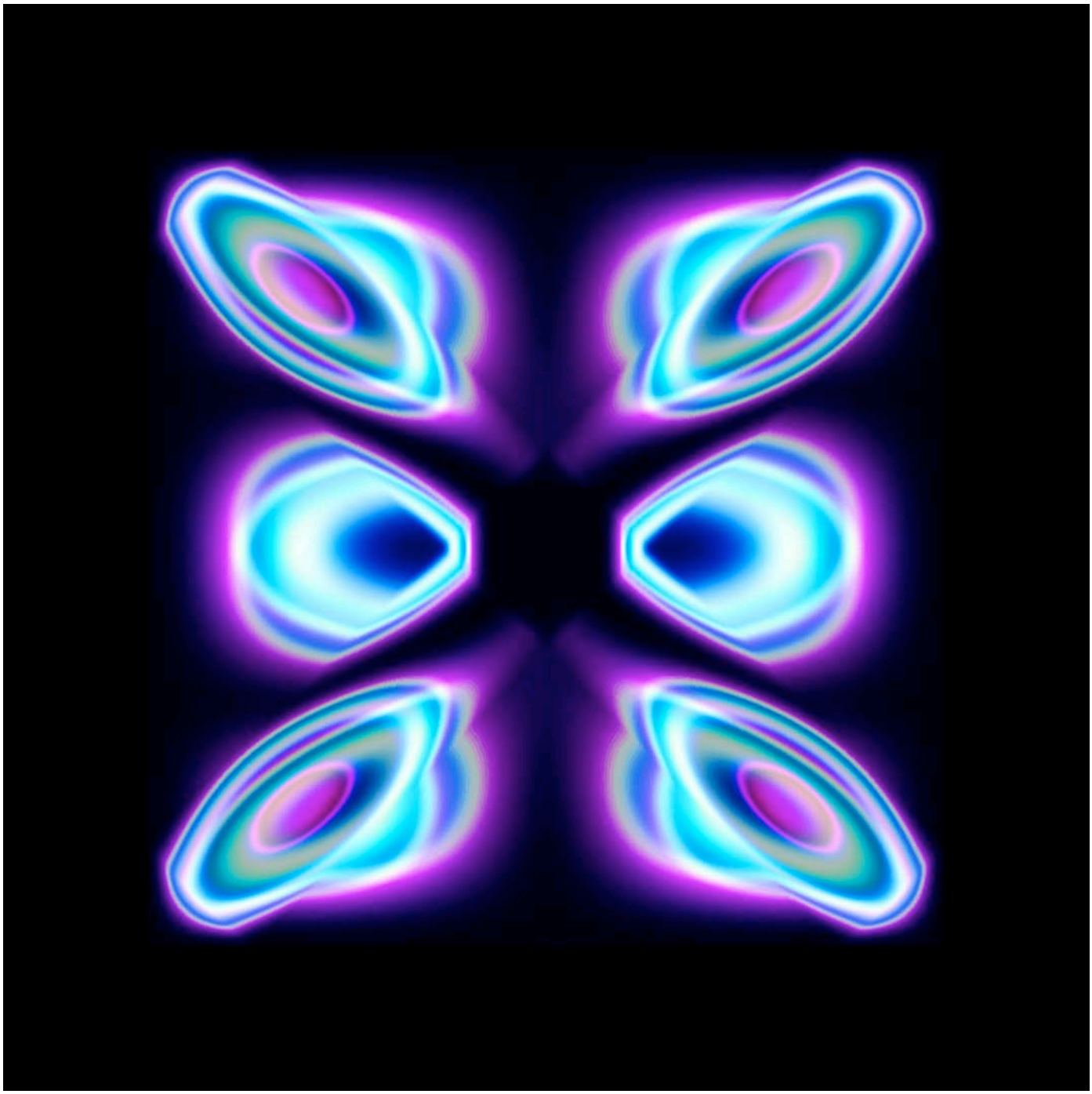

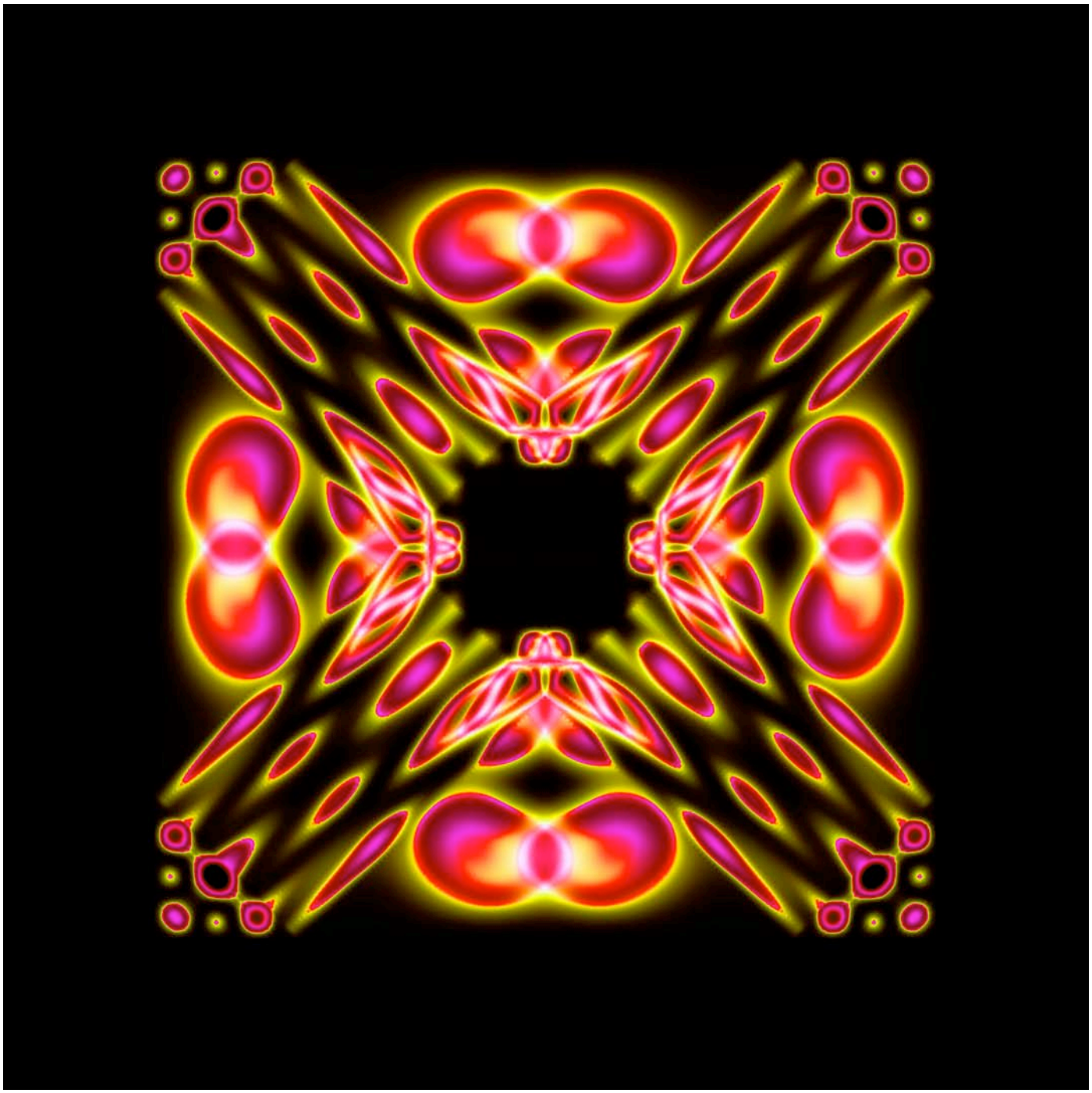

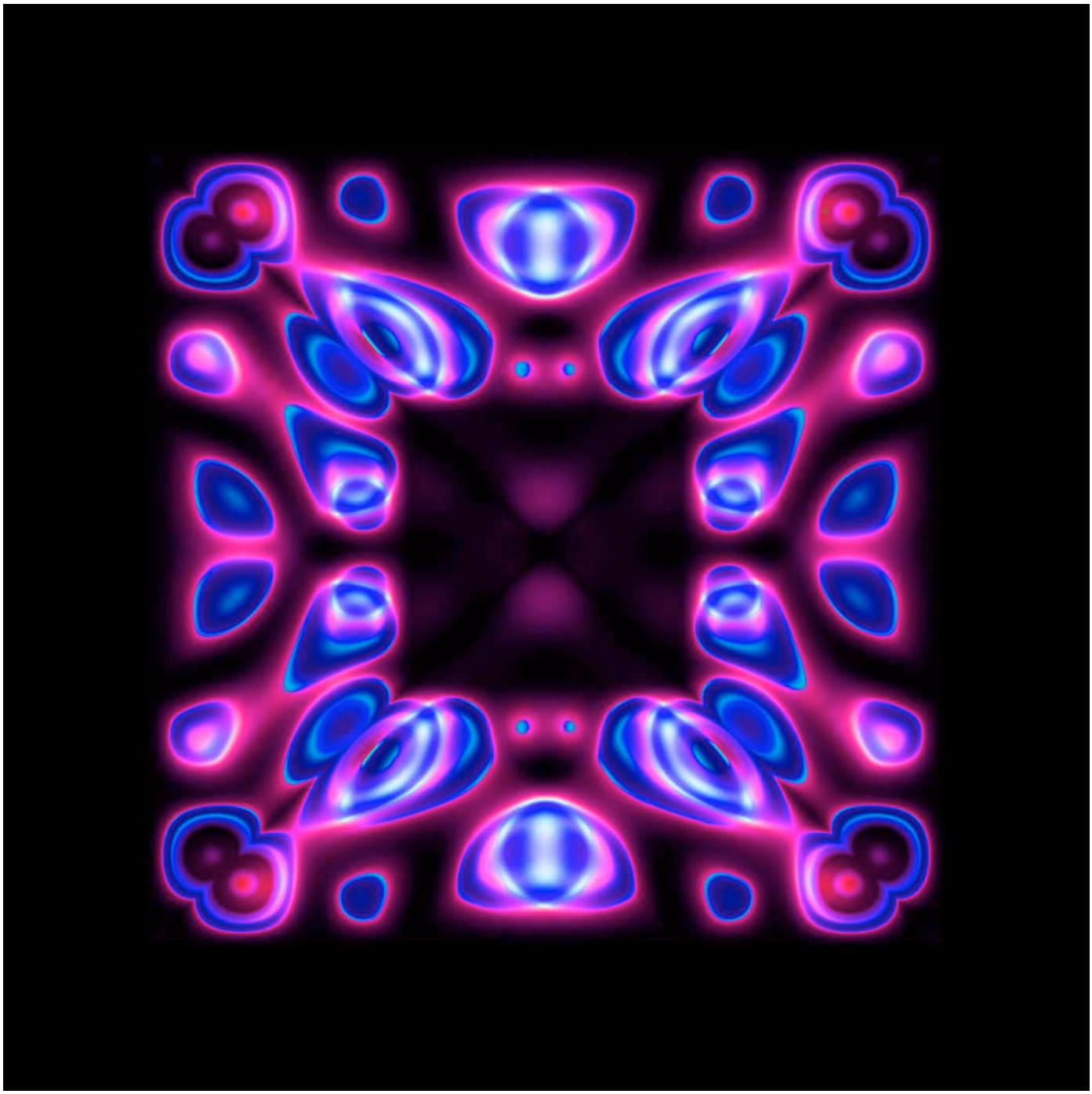

Publications

- F. Loder, A. P. Kampf, T. Kopp, J. Mannhart, C. W. Schneider and Y. S. Barash. *Magnetic flux periodicity of h/e in superconducting loops.* Nat. Phys. **4**, 112 (2008).
- F. Loder, A. P. Kampf and T. Kopp. *Crossover from hc/e to $hc/2e$ current oscillations in rings of s-wave superconductors.* Phys. Rev. B **78**, 174526 (2008).
- F. Loder, A. P. Kampf, T. Kopp and J. Mannhart. *Flux periodicities in loops of nodal superconductors.* New J. Phys. **11**, 075005 (2009).
- F. Loder, A. P. Kampf and T. Kopp. *hc/e Periodicity in loops of nodal superconductors.* Physica C (2009), doi:10.1016/j.physc.2009.12.014.
- F. Loder, A. P. Kampf and T. Kopp. *Superconducting state with a finite-momentum pairing mechanism in zero external magnetic field.* Phys. Rev. B **81**, (R)020511 (2010).
- F. Loder, A. P. Kampf and T. Kopp. *Flux periodicities in loops and junctions with d-wave superconductors.* Eur. Phys. J. Special Topics **180**, 191 (2010).

Some parts of the articles listed above, containing longer calculations and discussions of numerical results, are included in this thesis without major revisions. These are:

- The discussion of the periodicity crossover in a multi-channel s-wave ring in Phys. Rev. B **78**, 174526 (2008).
  [Part I, Chapter 2.2]
- The derivation of an analytical description of the supercurrent in a d-wave loop and the comparison to numeric results in New J. Phys. **11**, 075005 (2009).
  [Part I, Chapter 3]
- Parts of the discussion of the properties of the striped "pair density wave" state in Phys. Rev. B **81**, (R)020511 (2010).
  [Part III, Chapter 11.2]

Bibliography

[1] W. Ehrenberg and R. E. Siday. *The refractive index in electron optics and the principles of dynamics.* Proc. Phys. Soc. B **62**, 8 (1949).

[2] Y. Aharonov and D. Bohm. *Significance of electromagnetic potentials in the quantum theory.* Phys. Rev. **115**, 485 (1959).

[3] F. London. *Superfluids.* John Wiley & Sons, New York (1950).

[4] J. Bardeen, L. N. Cooper and J. R. Schrieffer. *Theory of superconductivity.* Phys. Rev. **108**, 1175 (1957).

[5] R. Doll and M. Näbauer. *Experimental proof of magnetic flux quantization in a superconducting ring.* Phys. Rev. Lett. **7**, 51 (1961).

[6] B. S. Deaver and W. M. Fairbank. *Experimental evidence for quantized flux in superconducting cylinders.* Phys. Rev. Lett. **7**, 43 (1961).

[7] A. A. Abrikosov. *On the magnetic properties of superconductors of the second group.* Soviet Physics – JETP **5**, 1174 (1957).

[8] U. Essmann and H. Träuble. *The direct observation of individual flux lines in type II superconductors.* Phys. Lett. A **24**, 526 (1967).

[9] J. R. Schrieffer. *Theory of Superconductivity*, chapter 8. Addison Wesley Publishing Company (1964).

[10] N. Byers and C. N. Yang. *Theoretical considerations concerning quantized magnetic flux in superconducting cylinders.* Phys. Rev. Lett. **7**, 46 (1961).

[11] L. Onsager. *Magnetic flux through a superconducting ring.* Phys. Rev. Lett. **7**, 50 (1961).

[12] W. Brenig. *Remark concerning quantized magnetic flux in superconductors.* Phys. Rev. Lett. **7**, 337 (1961).

[13] M. Tinkham. *Effect of fluxoid quantization on transitions of superconducting films.* Phys. Rev. **129**, 2413 (1963).

[14] W. A. Little and R. D. Parks. *Observation of quantum periodicity in the transition temperature of a superconducting cylinder.* Phys. Rev. Lett. **9**, 9 (1962).

[15] R. D. Parks and W. A. Little. *Fluxoid quantization in a multiply-connected superconductor.* Phys. Rev. **133**, A97 (1964).

[16] W. A. Little. *Long-range correlations in superconductivity.* Rev. Mod. Phys. **36**, 264 (1964).

[17] D. H. Douglass. *Properties of a thin hollow superconducting cylinder.* Rev. Rev. **132**, 513 (1963).

[18] M. Peshkin. *Fluxoid quantization, pair symmetry, and the gap energy in the current carrying Bardeen-Cooper-Schrieffer state.* Phys. Rev. **132**, 14 (1963).

[19] C. N. Yang. *Concept of off-diagonal long range order and the quantum phases of liquid He and of superconductors.* Rev. Mod. Phys. **34**, 694 (1962).

[20] L. P. Gorkov. *On the energy spectrum of superconductors.* Sov. Phys. JETP **9**, 505 (1958).

[21] E. N. Bogachek, G. A. Gogadze and I. O. Kulik. *Doubling of the period of flux quantization in hollow superconducting cylinders due to quantum effects in the normal state.* Phys. Stat. Sol. (b) **67**, 287 (1975).

[22] T. Lindström *et al. Dynamical effects of an unconventional current-phase relation in YBCO dc SQUIDs.* Phys. Rev. Lett. **90**, 117002 (2003).

[23] C. Schneider *et al. Half-$h/2e$ critical current-oscillations of SQUIDs.* Europhys. Lett. **72**, 68 (2004).

[24] C. Schneider Conference on "*Superconductivity and Magnetism in the Perovskites and Other Novel Materials*", Tel Aviv 2007, unpublished.

[25] C. H. Gough *et al. Flux quantization in a high-T_c superconductor.* Nature **326**, 855 (1987).

[26] F. Loder, A. P. Kampf, T. Kopp, J. Mannhart, C. Schneider and Y. Barash. *Magnetic ux periodicity of h/e in superconducting loops.* Nature Phys. **4**, 112 (2008).

[27] S. Washburn and R. A. Webb. *Quantum transport in small disordered samples from the diffusive to the ballistic regime.* Rep. Prog. Phys. **55**, 1311 (1992).

[28] J. Zhu and Z. D. Wang. *Supercurrent determined from the Aharonov-Bohm effect in mesoscopic superconducting rings.* Phys. Rev. B **50**, 7207 (1994).

[29] K. Czajka, M. M. Maśka, M. Mierzejewski and Z. Śledź. *Interplay between impurities and correlations in superconducting nanorings.* Phys. Rev. B **72**, 035320 (2005).

[30] T.-C. Wei and P. M. Goldbart. *Emergence of h/e-period oscillations in the critical temperature of small superconducting rings threaded by magnetic ux.* Phys. Rev. B **77**, 224512 (2008).

[31] V. Vakaryuk. *Universal mechanism for breaking the $hc/2e$ periodicity of flux-induced oscillations in small superconducting rings.* Phys. Rev. Lett. **101**, 167002 (2008).

[32] F. Loder, A. P. Kampf and T. Kopp. *Crossover from hc/e to $hc/2e$ current oscillations in rings of s-wave superconductors.* Phys. Rev. B **78**, 174526 (2008).

[33] F. Loder, A. P. Kampf and T. Kopp. *Flux periodicities in loops of nodal superconductors.* New J. Phys. **11**, 075005 (2009).

[34] Y. S. Barash. *Low-energy subgap states and the magnetic flux periodicity in d-wave superconducting rings.* Phys. Rev. Lett. **100**, 177003 (2008).

[35] V. Juričić, I. F. Herbut and Z. Tešanović. *Restoration of the magnetic hc/e-periodicity in unconventional superconductors.* Phys. Rev. Lett. **100**, 187006 (2008).

[36] J.-X. Zhu. *Restoration of $hc/2e$ magnetic flux periodicity in a hollow d-wave superconducting cylinder.* Preprint **arXiv:0806.1084** (2008).

[37] I. G. Kaplan and O. Navarro. *Statistics and properties of coupled hole pairs in superconducting ceramics.* Physica C **341**, 217 (2000).

[38] I. G. Kaplan, O. Navarro and J. A. Sánchez. *Exact commutation relations for the Cooper pair operators and the problem of two interacting Cooper's pairs.* Physica C **419**, 13 (2005).

[39] G. Röpke, A. Schnell and P. Schuck. *Four-particle condensate in strongly coupled fermion systems.* Phys. Rev. Lett. **80**, 3177 (1998).

[40] S. Koh. *Thermodynamics of uperconductivity beyond the Gorkov decoupling.* Phys. Rev. B **49**, 8983 (1994).

[41] J. Maćkoviak and P. Tarasewicz. *An extension of the Bardeen-Cooper-Schrieffer model of suerconductivity*. Physica C **331**, 25 (1999).

[42] P. Tarasewicz and J. Maćkoviak. *Thermodynamic functions of Fermi gas with quadruple BCS-type binding potential.* Physica C **329**, 130 (2000).

[43] P. Tarasewicz. *Thermodynamic functions of Fermi gas with quadruple BCS-type binding potential with $d_{x^2-y^2}$-wave-pairing symmetry*. J. Supercond. **17**, 431 (2004).

[44] U. Eckern and P. Schwab. *Normal persistent currents.* Adv. in Physics **44**, 387 (1995).

[45] K. A. Mateev, A. I. Larkin and L. I. Glazman. *Persistent current in superconducting nanorings.* Phys. Rev. Lett. **89**, 096802 (2002).

[46] C. C. Gerry and A. V. Singh. *Feynman path-integral approach to the Aharonov-Bohm effect*. Rev. Rev. D **20**, 2550 (1979).

[47] M. Büttiker, Y. Imry and R. Landauer. *Josephson behavior in small normal one-dimensional rings.* Phys. Lett. A **96**, 365 (1983).

[48] R. Landauer and M. Büttiker. *Resistance of small metallic loops.* Phys. Rev. Lett. **54**, 2049 (1985).

[49] H. Cheung, Y. Gefen, E. K. Riedel and W. Shih. *Persistent currents in small one-dimensional metal rings.* Phys. Rev. B **37**, 6050 (1988).

[50] R. M. Fye, M. J. Martins, D. J. Scalapino, J. Wagner and H. W. *Drude weight, optical conductivity, and flux properties of one-dimensional Hubbard rings.* Phys. Rev. B **44**, 6909 (1991).

[51] R. M. Fye, M. J. Martins, D. J. Scalapino, J. Wagner and H. W. *Optical-conductivity properties of one-dimensional Hubbard rings: Repulsive-U and attractive-U cases.* Phys. Rev. B **45**, 7311 (1992).

[52] X. Waintal, G. Fleury, K. Kazymyrenko, M. Houzet, P. Schmitteckert and D. Weinamm. *Persistent currents in one dimension: The counterpart of Leggett's theorem*. Rev. Rev. Lett. **101**, 106804 (2008).

[53] M. Sigrist. *Quantenmechanik I*, chapter 2 (2003). Lecture Notes.

[54] P. G. de Gennes. *Superconductivity of Metals and Alloys*, chapter 5. Addison Wesley Publishing Company (1966).

[55] M. Tinkham. *Superconductivity*, chapter 3. McGraw-Hill Internation Editions (1996).

[56] V. P. Mineev and K. V. Samokhin. *Introduction to Unconventional Superconductivity*, chapter 5. Gordon and Breach science publishers (1999).

[57] A. A. Abrikosov, L. P. Gorkov and I. E. Dzyaloshinski. *Methods of Quantum Field Theory in Statistical Physics*, chapter 7. Dover (1963). For the general formalism see:
V. V. Mineev and K. V. Samokhin, *Introduction to Unconventional Superconductivity* (Gordon and Breach, 1999), chap. 17.

[58] V. P. Mineev and K. V. Samokhin. *Introduction to Unconventional Superconductivity*, chapter 17. Gordon and Breach science publishers (1999).

[59] P. Fulde and R. A. Ferrell. *Superconductivity in a strong spin-exchange field.* Phys. Rev. **135**, A550 (1964).

[60] P. F. Bagwell. *Critical current of a one-dimensional superconductor.* Phys. Rev. B **49**, 6841 (1994).

[61] J. Bardeen. *Critical Fields and Currents in Superconductors.* Rev. Mod. Phys. **34**, 667 (1962).

[62] A. M. Zagoskin. *Quantum Theory of Many-Body Systems*, chapter 4. Springer (1998).

[63] S. V. Sharov and A. D. Zaikin. *Influence of parity on the persistent currents of superconducting nanorings.* Phys. Rev. B **71**, 014518 (2005).

[64] V. P. Mineev and K. V. Samokhin. *Introduction to Unconventional Superconductivity*, chapter 8. Gordon and Breach science publishers (1999).

[65] D. J. Scalapino, S. R. White and S. Zhang. *Insulator, metal, or superconductor: The ctriteria.* Phys. Rev. B **47**, 7995 (1993).

[66] C. J. Pethick and H. Smith. *Relaxation and collective motion in superconductors: a two-fluid description.* Annals of Physics **119**, 133 (1979).

[67] F. von Oppen and E. K. Riedel. *Flux-periodic persistent current in mesoscopic superconducting rings close to T_c.* Phys. Rev. B **46**, 3203 (1992).

[68] I. Khavkine, H.-Y. Kee and K. Maki. *Supercurrent in nodal superconductors.* Phys. Rev. B. **70**, 184521 (2004).

[69] A. Damascelli, Z. Hussain and Z.-X. Shen. *Angle-resolved photoemission studies of the cuprate superconductors.* Rev. Mod. Phys. **75**, 473 (2003).

[70] O. Fischer, M. Kugler, I. Maggio-Aprile and C. Berthod. *Scanning tunneling spectroscopy of high-temperature superconductors.* Rev. Mod. Phys. **79**, 353 (2007).

[71] M. Sigrist. *Unkonventionelle Supraleitung*, chapter 2 (2006). Lecture Notes.

[72] M. Büttiker and T. M. Klapwijk. *Flux sensitivity of a piecewise normal and superconducting metal loop.* Phys. Rev. B **33**, 5114 (1986).

[73] J. Cayssol, T. Kontos and G. Montambaux. *Isolated hybrid normal/superconducting ring in a magnetic flux: From persistent current to Josephson current*. Phys. Rev. B **67**, 184508 (2003).

[74] P. I. Soininen, C. Kallin and A. J. Berlinsky. *Structure of a vortex line in a $d_{x^2-y^2}$ superconductor.* Phys. Rev. B **50**, 13883 (1994).

[75] Y. Wang and A. H. MacDonald. *Mixed-state quasiparticle spectrum for d-wave superconductors.* Phys. Rev. B **55**, R3876 (1995).

[76] M. Franz, C. Kallin and A. J. Berlinsky. *Impurity scattering and localization in d-wave superconductors.* Phys. Rev. B **54**, R6897 (1996).

[77] M. Takigawa, M. Ichioka and M. Kazushige. *Theory of vortex excitation imaging via an NMR relaxation measurement.* Phys. Rev. Lett. **83**, 3057 (1999).

[78] J.-X. Zhu, T. K. Lee, C. S. Ting and C.-R. Hu. *Quasiparticle resonant states induced by a unitary impurity in a d-wave superconductor.* Phys. Rev. B **61**, 8667 (2000).

[79] J.-X. Zhu and C. S. Ting. *Quasiparticle states in a d-wave vortex core in high-T_c superconductors: Induction of local spin density wave order.* Phys. Rev. Lett. **87**, 147002 (2001).

[80] A. Ghosal, C. Kallin and A. J. Berlinsky. *Competition of superconductivity and antiferromagnetism in a d-wave vortex lattice.* Phys. Rev. B **66**, 214502 (2002).

[81] Y. Chen, Z. D. Wang and C. S. Ting. *Temperature dependence of vortex charges in high-temperature superconductors.* Phys. Rev. B **67**, 220501 (2003).

[82] S. Datta and P. F. Bagwell. *Can the Bogoluibov - de Gennes equations be interpreted as a 'one particle' wave function?* Superlattices & Microstructures **25**, 1233 (1999).

[83] K. Ziegler, W. A. Atkinson and P. J. Hirschfeld. *Density of states width-prity effect in d-wave superconducting quantum wires.* Phys. Rev. B **64**, 054512 (2001).

[84] A. M. Bobkov *et al. Density of states width-prity effect in d-wave superconducting quantum wires.* Phys. Rev. B **64**, 054512 (2001).

[85] M. Tinkham. *Superconductivity*, chapter 4. McGraw-Hill Internation Editions (1996).

[86] F. Gygi and M. Schlüter. *Self-consistent electronic structure of a vortex line in a type-II superconductor.* Phys. Rev. B **43**, 7609 (1990).

[87] D. B. Josephson. *Possible new effects in superconductive tunnelling.* Phys. Lett **1**, 251 (1962).

[88] M. Tinkham. *Superconductivity*, chapter 6. McGraw-Hill Internation Editions (1996).

[89] A. A. Golubov, M. Y. Kupriyanov and E. Il'ichev. *The current-phase relation in Josephson junctions.* Rev. Mod Phys. **76**, 411 (2004).

[90] B. M. Andersen, I. V. Bobkova, P. J. Hirschfeld and Y. S. Barash. *Bound states at the interface between antiferromagnets and superconductors.* Phys. Rev. B **72**, 184510 (2005).

[91] B. M. Andersen, I. V. Bobkova, P. J. Hirschfeld and Y. S. Barash. $0 - \pi$ *transitions in Josephson junctions with antiferromagnetic interlayers.* Phys. Rev. Lett **96**, 117005 (2006).

[92] A. I. Larkin and Y. N. Ovchinnikov. Zh. Eksp. Teor. Fiz. **47**, 1136 (1964). [Sov. Phys. JETP **20**, 762 (1965)].

[93] B. Büchner, M. Breuer, A. Freimuth and A. P. Kampf. *Critical Buckling for the disappearance of superconductivity in rare-earth-doped* $La_{2-x}Sr_xCuO_4$. Phys. Rev. Lett. **73**, 1841 (1994).

[94] J. M. Tranquada *et al. Evidence for stripe correlations of spins and holes in copper oxide superconductors.* Nature (London) **375**, 561 (1995).

[95] M. Fujita *et al. Stripe order, depinning, and fluctuations in* $La_{1.875}Ba_{0.125}CuO_4$ *and* $La_{1.875}Ba_{0.075}Sr_{0.050}CuO_4$. Phys. Rev. B **70**, 104517 (2004).

[96] P. Abbamonte *et al. Spatially modulated 'Mottness' in* $La_{2-x}Ba_xCuO_4$. Nat. Phys. **1**, 155 (2005).

[97] E. Berg *et al. Dynamical layer decoupling in a stripe-ordered high-T_c superconductor.* Phys. Rev. Lett. **99**, 127003 (2007).

[98] J. M. Tranquada *et al. Evidence for unusual superconducting correlations coexisting with stripe order in $La_{1.875}Ba_{0.125}$ CuO_4.* Phys. Rev. B **78**, 174529 (2008).

[99] R.-H. He *et al. Energy gaps in the failed hight-T_c superconductor $La_{1.875}Ba_{0.125}$ CuO_4.* Nat. Phys. **5**, 119 (2009).

[100] D. F. Agterberg, Z. Zheng and S. Mukherjee. *Spatial line nodes and fractional vortex lines in the Fulde-Ferrel-Larkin-Ovchinnikov vortex state of spin-singlet superconductors.* Phys. Rev. Lett. **100**, 017001 (2008).

[101] D. F. Agterberg and H. Tsunetsugu. *Dislocations and vortices in pair-density-wave superconductors.* Nat. Phys. **4**, 639 (2008).

[102] D. F. Agterberg, M. Sigrist and H. Tsunetsugu. *Order parameter and vortices in the superconducting Q phase of $CeCoIn_5$.* Phys. Rev. Lett. **102**, 207004 (2009).

[103] E. Berg, E. Fradkin and S. A. Kivelson. *Theory of the striped superconductor.* Phys. Rev. B **79**, 064515 (2009).

[104] E. Berg, E. Fradkin and S. A. Kivelson. *Charge-4e superconductivity from pair-density-wave order in certain high-temperature superconductors.* Nat. Phys. (2009). Advance Online Publication.

[105] S. Baruch and D. Orgad. *Spectral signatures of modulated d-wave superconducting phases.* Phys. Rev. B **77**, 174502 (2008).

[106] A. B. Vorontsov. *Broken Translational and time-reversal symmetry in unconventional superconducting films.* Phys. Rev. Lett. **102**, 177001 (2009).

[107] A. Ptok, M. M. Maśka and M. Mierzejewski. *The Fulde-Ferrel-Larkin-Ovchinnikov phase in the presence of pair hopping interaction.* J. Phys. Condens. Matter **21**, 295601 (2009).

[108] P. Nikolić, A. A. Burkov and A. Paramekanti. *Pair density wave instability of cold fermionic atoms in an optical lattice.* arXiv:0906.2202 (2009). Unpublished.

[109] A. Himeda, T. Kato and M. Ogata. *Stripe states with spatially oscillating d-wave superconductivity in the two-dimensional $t - t' - J$ model.* Phys. Rev. Lett. **88**, 117001 (2002).

[110] M. Vojta and T. Ulbrecht. *Magnetic excitations in a bond-centered stripe phase: spin waves far from the semiclassical limit.* Phys. Rev. Lett. **93**, 127002 (2004).

[111] G. S. Uhrig, K. P. Schmidt and M. Grüninger. *Unifying magnons and triplons in stripe-ordered cuprate superconductors.* Phys. Rev. Lett. **93**, 267003 (2004).

[112] S. Komiya, H.-D. Chen, S. Zhang and Y. Ando. *Magic doping fractions for high-temperature superconductors.* Phys. Rev. Lett. **94**, 207004 (2005).

[113] M. Raczkovski, M. Capello, D. Poilblanc, R. Frésard and A. M. Oleś. *Unidirectional d-wave superconducting domains in the two-dimesional t – J model.* Phys. Rev. B **76**, 140505(R) (2007).

[114] S. R. White and D. J. Scalapino. *Pairing on striped t – t′ – J lattices.* Phys. Rev. B **79**, 220504(R) (2009).

[115] B. Andersen, P. J. Hirschfeld, A. P. Kampf and M. Schmid. *Disorder-induced static antiferromagnetism in cuprate superconductors.* Phys. Ref. Lett. **99**, 147002 (2007).

[116] F. Braun and J. von Delft. *Fixed-N superconductivity: the crossover from the bulk to the few-electron limit.* Phys. Ref. Lett. **81**, 4712 (1998).

[117] F. Braun and J. von Delft. *Superconductivity in ultrasmall metallic grains.* Phys. Ref. B. **59**, 5527 (1999).

[118] M. Abramowitz and A. Stegun. *Pocketbook of Mathematical Functions.* Verlag Harri Deutsch, Thun (1984).

Thanks to ...

... all the many people who were around during the time of my thesis and helped in some way to successfully conclude all this work.

At the very first place, I have to thank Thilo Kopp and Arno Kampf, who were the tutors of my PhD. They spent a great amount of time discussing physics, from which many of the ideas presented in this thesis originate, and many other things. In particular, I appreciate the great work they invested in correcting and improving my writings for publication. This was certainly not much fun, but always proved necessary.

More people contributed considerably to the success of this thesis. In a number of discussions, Jochen Mannhart provided an intuitive understanding of connections that seemed to me rather complex and intransparent. They really helped a lot in advancing this work. Christof Schneider was the initiator of the whole story, with his amazing variety of SQUID experiments and ideas for their interpretation. There was not a single article in this field that missed his attention. Especially in the beginnings of this work, Yuri Barash was essentially involved in pointing out the novelty of our results and in working out of some of the theoretical concepts. A great help in pointing out the truly important aspects of this work was Dieter Vollhardt.
Thank you all very much for your help!

Special thanks go also to Raymond Frésard, who introduced the "pair density wave" state to me and thereby provided the basis for the theory of finite momentum pairing in part III of this thesis.

I would like to thank all our group at the chair for experimental physics VI. Some of you were a big help in the organization of the larger and smaller things to do. And all of you were, and are, responsible for the comfortable life in this group. These same thanks go to the group of Dieter Vollhardt and Arno Kampf.

I thank especially my long-term office mates Cyril Stephanos and Iris Xhango for the nice time we had so far. Cyril has been around for a very long time and is still a major help in whatever has to be done...

Finally, I thank the experts Thilo Kopp, Dieter Vollhardt, and Raymond Frésard for taking the time to write the reports needed for this thesis.

Curriculum Vitae

Name: Florian Loder
Geburtstag: 13. Februar 1979
Geburtsort: Zürich, Schweiz

Schulausbildung:

05/1986 - 07/1992:	Primarschule Bonstetten, Schweiz
08/1992 - 02/1999:	Kantonsschule Limmattal in Urdorf, Schweiz
02/1999:	Matura Typus B an der Kantonsschule Limmattal

Studium:

10/1999 - 11/2004:	Studium an der ETH Zürich, Schweiz
10/2000:	1. Vordiplom
10/2001:	2. Vordiplom
03/2004:	Schlussdiplom
05/2004 - 10/2004:	Diplomarbeit an Institut für theoretische Physik bei Prof. M. Sigrist Titel: “Superconductivity In A 2D-Lattice With Alternating Spin-Orbit Coupling”
01/2005 - 08/2005:	wiss. Mitarbeiter an der ETH Zürich in der Theoriegruppe von Prof. M. Sigrist

Promotion:

09/2005 - 12/2009:	Doktorarbeit und Anstellung als wiss. Mitarbeiter an der Universität Augsburg am Lehrstuhl für Experimentalphysik VI Doktorprüfung am 22/12/2009